Abstracts of Papers

CONTENTS

§ *L*. General lectures

L·1. D. Hodgkin. *Towards the X-ray analysis of proteins.*

The last few years have seen very striking advances towards the X-ray analysis of proteins, from the deduction of the α helix structure for peptide chains to the calculation of direct, sign determined, electron-density projections, first for haemoglobin and now for several other proteins. We have to consider how best the different lines of approach can meet in the evaluation of the electron-density distribution in three dimensions in any protein and its interpretation in chemical terms.

Some of the experience gained in the study of vitamin B_{12} may be useful here. Although smaller than any protein—about one-quarter the size of insulin, one-tenth that of ribonuclease—it is probably large enough to be a reasonable model. Its X-ray analysis has provided evidence not only of the detailed arrangement of the atoms within the molecule but also of the nature of the intermolecular contacts, the distribution of water molecules between the B_{12} molecules and the changes that occur both on removing crystals from their mother liquor and on substituting selenocyanate groups for cyanide groups in the molecule.

In the course of this analysis it was not found possible to use direct isomorphous-replacement methods of phase-angle determination except for a few low-angle reflexions. Instead, a detailed study was made of Patterson superposition methods and of imperfect electron-density distributions based on phases derived from the calculated contributions of varying numbers of other atoms. Observations were also made on intensity differences due to anomalous dispersion. One can now see many ways in which the course of the X-ray analysis actually taken could have been improved and difficulties of interpretation originally encountered might have been avoided. Already some of these points can be illustrated by recent studies of heavy-atom derivatives of proteins.

L·2. G. S. Žданov. *Crystal chemistry.*

The study of the structure of crystalline substances supplemented by the results of other methods of investigation, presents important information for the understanding of the nature of the chemical bond and the molecular interaction. The data of crystal chemistry comprise both the chemistry of small molecules and the chemistry of endless molecules, metals, semiconductors and dielectrics. The qualitatively different and isolated types of chemical bonds (covalent, metallic, ionic) and molecular interactions (van der Waals forces) were established historically. The progress of crystal chemistry, and the evolution of electronic theory and quantum mechanics permitted the development of a consistent picture of chemical and molecular interactions.

The structure and the properties of molecules and crystals are predetermined by the electronic structure of atoms of which they are composed.—The peculiarity of the electronic structure of the atoms of chemically active and chemically inert elements.—The structural characteristics of the bonds in crystals of simple substances in the Mendeleev periodic system.—Some data on the crystal chemistry of the simple and complex compounds.—Crystallochemical evidence on the differences of the electronegativity in the components of the compounds.—Some results in the crystal chemistry of molecular interaction.—The application of the crystallochemical rules for the creation of new substances with definite physical properties.

L·3. D. G. Jenkin, J. S. Taylor & L. E. Sutton. *Some remarks about our present knowledge of interatomic distances and molecular configurations.*

The compilation of interatomic distances and molecular configurations for gaseous molecules, published in 1949 by P. W. Allen & L. E. Sutton (*Acta Cryst.*, (1950), **3**, 46), has been extended and greatly enlarged in scope by H. J. M. Bowen, J. Donohue, D. G. Jenkin, Olga Kennard, P. J. Wheatley and D. H. Whiffen. It now contains a comprehensive but critical collection of such determinations on molecules and on ions in the vapour and in the solid phase, made by any of the spectroscopic or the diffraction methods. Values from ionic lattices and from adamantine lattices are included when useful for comparison. It is expected to form an octavo book of 700–900 pages.

The demands of editing have prevented the present authors from giving much attention as yet to the general analysis of the great mass of results for about 2,000 substances, now brought together. Nevertheless, from the preparation of a list of selected interatomic distances, good to ± 0.02 Å, some remarks can be made about our present knowledge.

It appears that there are as yet not many X-ray crystallographic determinations, other than those on simple lattices, which yield as accurate interatomic distances as do the average electron-diffraction gas determinations; and there are not many of the latter which are as good in this respect as the average micro-wave spectroscopic determination. X-ray crystallographic analysis can, however, be applied successfully to vastly more complicated structures than can these other methods.

The distribution of information over the elements is extremely uneven. Carbon-containing bonds, especially C–C bonds, have been investigated very intensively. There is considerable information also for bonds containing N, O, P, or S. For those containing As, B, Ge, or Si there is a moderate amount. For most metals there are now very good values. For many elements the only values good within $\pm 0{\cdot}02$ Å are those for diatomic species observed in discharge-tube spectra. Much of the early electron diffraction work has been excluded from the select list.

There is not yet much precise information about distances in complex ions, nor is it often possible to make significant comparisons of molecular dimensions in the vapour and in the solid phases.

Statistical averaging has been applied when appropriate. An attempt has been made to check the assumptions implied in such averaging by developing a continuous probability function to be plotted against interatomic distance. As yet this has been calculated only for C–C and for C–H distances. For the former it confirms current chemical ideas rather than suggests new ones; but at least it provides a convenient graphical summary of present knowledge. For the latter distances some rather more novel ideas emerge.

L·4. G. W. Brindley. *Clay minerals.*

Clay minerals can be defined as silicates with a particle size less than 1 micron which develop plastic properties in association with water. The size limitation restricts diffraction analysis to X-ray powder techniques, but single-crystal data are obtainable by electron diffraction. The platy character of most clay particles restricts the electron diffraction data to *hk*0 reflections, which are the least informative. Electron microscopy combined with single-crystal diffraction study enables morphology to be correlated with structure.

The small particle size of clay minerals and their usual lack of strict regularity make high precision structure analysis virtually impossible. These minerals therefore tend to have little interest for pure crystallographers but considerable interest for those who incline towards solid-state studies.

The following are the main objectives in the diffraction study of clays:

(1) *Structure analysis*: This seldom goes beyond the stage of determining an idealized structure.

(2) *Analysis of structural imperfections*: These include lattice irregularities arising from displaced layers, curved layers, and irregular sequences of layers.

(3) *Identification of clay minerals*: X-ray diffraction is the principal method for identification of clays, but thermal, chemical, and other techniques are generally used in conjunction with X-ray diffraction in order to obtain more precise identification than is possible with any one technique alone.

Associated with this objective is the search for new clay minerals and new structural varieties.

Many attempts have been made to obtain quantitative mineralogical analyses on the basis of X-ray intensity measurements, but many difficulties remain to be solved.

(4) *Structural study of clay mineral reactions*: Diffraction analysis is used to follow thermal reactions of clays, their behavior in water and humid atmospheres, and the formation of organic complexes.

The diffraction study of clay minerals has been greatly facilitated by the study of analogous macrocrystalline minerals. Thus, among the kaolin clays, dickite and nacrite occur in sizes suitable for single-crystal study, and a detailed analysis of dickite has recently been completed. The repercussions of this work on the study of kaolinite will be considered.

The clay micas (essentially non-swelling) and the montmorillonites and vermiculites (essentially swelling minerals) are closely related to macrocrystalline micas. The identification of different mica polymorphs by X-ray powder analysis makes possible their identification also among clay-grade minerals. Vermiculite occurs in both macro- and microcrystalline forms; a single-crystal study of the former material has provided detailed information on the nature of the water layers in the hydrated forms of this mineral, and their relation to interlayer cations.

Investigations of chrysotile and halloysite have given rise to basic studies of diffraction by cylindrical lattices, and thus opened the way to a more detailed analysis of these structures. It still remains difficult, however, to reconcile the observed density of chrysotile with a tubular morphology. New data on the superlattice *a* parameter of antigorite will be presented.

The widespread occurrence of mixed-layer clay minerals is becoming increasingly well known. Powder diagrams of these minerals show non-integral basal reflections and lines of variable profiles. MacEwan has suggested a Patterson-type analysis to determine the nature of the component layers and their frequency of occurrence.

Studies of synthetic clay minerals, prepared by hydrothermal methods, are aimed mainly at determining the stability relations of clay minerals (composition, temperature and pressure relations), but in addition they provide evidence of new crystalline varieties. They also provide evidence for new crystalline transformations. The 7 Å to 14 Å layer transformation, in particular, has been studied by Roy and his co-workers.

In conclusion it can be said that the structural study of clay minerals advances hand-in-hand with other investigations of these materials and cannot be divorced from these other fields of work. Progress takes place mainly on a broad front rather than by intensive efforts on special minerals.

L·5. P. B. Hirsch. *Imperfect structures.*

The perfection of crystalline materials varies over a wide range, from that of highly perfect 'whiskers' or crystals of germanium or calcite, to that of certain polymers, 'amorphous' carbons, or glasses. In the case of 'nearly perfect crystals' the atomic arrangement can be described in terms of the regular lattice plus certain well-defined imperfections, such as impurities, vacancies, interstitial atoms, dislocations and stacking faults. These defects influence profoundly many of the physical and

chemical properties of crystals. Each defect has associated with it a certain energy, and several defects in the same crystal interact and may move to take up positions of minimum potential energy. An example of this is the formation of low-angle boundaries between crystals, by the movement of dislocations into plane arrays. The forces between defects are complex, and theory has predicted many different interactions, which have been invoked to explain many of the plastic properties of crystals.

Recently, methods have been developed for observing dislocations and faults in crystals. For example, by 'decorating' the dislocations it has been possible to observe their arrangement in crystals such as AgBr, NaCl and Si. Networks, low-angle boundaries and dislocation sources predicted theoretically have all been observed. The 'mosaic structure' of crystals is now interpreted in terms of distributions of dislocations.

By using transmission electron microscopy it has been possible to observe directly dislocations and faults in thin metal foils. The arrangement of the dislocations can be studied as a function of deformation and other treatments of the crystals, and their movement can be observed directly in the electron microscope. By using ciné techniques the motion of dislocations has been recorded, and their interaction followed. The results obtained so far include observations on pile-ups, networks, the splitting of dislocations to form stacking faults, the interaction of dislocations with boundaries or with the surface, and the nucleation of dislocations. Already many theoretical predictions have been confirmed.

Studies such as these should lead to a better knowledge of the nature and arrangement of defects in crystals, and to a better understanding of the complex interactions of defects and of the effect of defects on the physical and chemical properties of crystals.

§ 1(i). Apparatus

1(i)·1. D. P. Riley & J. R. Stansfield. *A new microfocus and semi-microfocus X-ray generator.*

In all X-ray diffraction techniques, intensity of radiation is a most important factor, especially when studying weakly diffracting specimens which normally demand long exposure times. In addition, when high resolution is required, the collimating system necessarily restricts the width of focus which can be effectively used, so that the prime requirement is that the target loading should be high, giving the highest possible brilliance at the focus. It has been shown that the specific loading on a line focus can be markedly increased as the width of the focus is reduced, and the X-ray tube described in this paper has been developed on this basis. On the other hand, particularly when making use of a diffractometer, the total energy received by the detector is of importance, as distinct from the energy density at the film which determines the exposure required in a photographic recording. There is, therefore, an optimum focal width to give high brilliance and high total power, and, although the optimum depends upon the particular problem under investigation, a useful general-purpose value of about 0·1 mm. has been established.

The advantages of working with a fine-focus X-ray source with a line width of the order of 0·1 mm. are nullified if the focus is of irregular shape or uneven brilliance. If the loading is uneven, a 'hot spot' results and this limits the mean brilliance at which it is safe to operate. Uniformity in this respect is more difficult to achieve than with a circular focus, but a simple form of electron gun has been developed meeting these requirements.

A tungsten filament 0·18 mm. in diameter is held 1·0 mm. behind the surface of a plane focusing cap in which a simple slot is cut to accommodate the filament; the dimensions of the slot are 6·2 mm. × 2·0 mm. with rounded ends. The face of the focusing cap is 7·0 mm. from the anode, and the cylindrical body of the X-ray tube has an internal diameter of 25 mm. Positive rectified high tension of up to 50 kV. d.c. is applied to the anode, which is oil cooled. The tube casing and the focusing cap are at earth potential, while the filament is given a positive bias by means of a biassing resistance of the order of 0·5 megohms.

It is found that it is essential to operate the tube in the saturated condition. This means that for a given anode voltage and emission current, the bias potential should be adjusted so that further heating of the filament causes no increase in tube current, the emission being then limited by the space charge. Under these conditions, not only do any 'wings' on either side of the line focus disappear, but the focus itself is evenly loaded across its breadth. It will not necessarily be evenly brilliant along its length. A straight filament with sharply bent ends produces end loading of the focus, the so called 'dumb-bell effect'; this can be obviated by a more gradual bend at either end of the straight filament.

Under the conditions described, a focus of approximately 0·1 mm. × 1·4 mm. is obtained, and a copper target will safely withstand a current of 3·5 mA. at 45 kV. d.c., a total loading of 160 W. Compared with a conventional tube of focal area 1·0 mm. × 10·0 mm. operated at 1 kW., the loading per unit area is 1·1 kW.mm.$^{-2}$ compared with 0·1 kW.mm.$^{-2}$, and the loading per unit length of the focal line is 110 W.mm.$^{-1}$ compared with 100 W.mm.$^{-1}$.

A complete X-ray generator incorporating this tube has been developed with a view to great versatility. The tube itself is made of non-tarnishable Monel metal. It is of small dimensions, the diameter of the cylindrical stem (38 mm.) having been reduced to the minimum compatible with sound vacuum engineering. At the top of the stem a rectangular Monel metal block 38 mm. square by about 60 mm. long houses the cathode gun and the target and is fitted with windows 26·7 cm. above the working table top. Two versions of the tube have been developed, one in which the block is vertical, and one in which it is horizontal. In the first the electron beam is projected horizontally to strike a vertical target face; two X-ray beams emerge in the same horizontal plane from opposite sides of the block, each at a nominal angle of 6° to the target face. A cathode gun with a vertical filament and slot gives a vertical line focus, made apparently narrower by the angle of viewing, and this is eminently suited to horizontal Debye–Scherrer cameras and diffractometers. Alternatively, a horizontal cathode gives a focus foreshortened in length and is of use when a high-intensity spot is required. In the other form of the tube, the Monel metal block is vertical and the electron beam is projected vertically downwards on to the horizontal face of the

anode; three beams emerge, each making a nominal angle of 6° upwards from the horizontal. This form of the tube is to be preferred when horizontal slit systems are used. As a further alternative, an adjustable micro-focus gun can be fitted following the focusing system developed by Ehrenberg & Spear and providing a 0·04 mm.-diameter focus of exceptionally high brilliance. Although the total power permissible on a copper target is only 25 W., this is equivalent to a loading of 15 kW.mm.$^{-1}$.

A particularly striking and important feature of the X-ray generator is that the slim X-ray tube itself is the only projection above the table top provided by the control cubicle. This allows the unimpeded mounting of cameras or diffractometers. Furthermore, the X-ray tube is rigidly clamped to the table top, which is an aluminium alloy casting of ample strength and rigidity, and the anode rod is firmly located with the body of the tube. It is therefore possible to maintain precise and constant alignment of instruments relative to the focus and the particularly stringent needs of work with miniature cameras can be fully met by clamping to the stem of the X-ray tube.

During the presentation of this paper, photographs showing the quality of the focus will be shown, and also a selection of diffraction-pattern photographs and recordings illustrating the type of work in which the performance of this tube confers particular advantages.

1(i)·2. N. KATO. *A study on lattice distortion by an X-ray diffraction technique.*

The author has already presented an X-ray diffraction technique to study lattice distortion (*Acta Metallurg.* (1957), in the Press). In the present paper thorough considerations about the resolution and instrumental errors will be reported, as well as some results of study on crystal textures.

(A) *Resolution of distance and angle*

The general principle of the present technique is similar to that of H. Lambot *et al.* (*Acta Metallurg.* (1953), **1**, 711; (1955), **3**, 150). The main difference is that the convergent X-ray beam was made by a transmission-(or Cauchois-)type monochromater and, accordingly, the X-ray target was placed in an horizontal plane (we take the focused X-ray line as the vertical direction). By this means the linear resolution on the specimen along the vertical direction could be increased significantly.

Notation.

f: Resolvable distance along horizontal direction.
g: Resolvable distance along vertical direction.
$\Delta\theta_v$: Resolvable rotation angle about the vertical axis.
$\Delta\theta_h$: Resolvable rotation angle about the horizontal axis lying in the reflexion net plane.
a: The height of X-ray source projected on to the direction of the X-ray beam.
b: The line breadth of focused X-ray line.
Z: The distance between the X-ray source and the monochromator.
R': The distance between the monochromator and the specimen.
L: The distance between the specimen and the recording film.
θ: Bragg angle of specimen.
r: Resolvable distance on the recording film.
E: Effective thickness of specimen.

Results.—

	Formula	No. 1	No. 2
f	$\propto b$ and E	$b = 37\mu$	$b \lesssim 20\mu$
g	$= aL/(Z+R'+L)$	20μ	20μ
$\Delta\theta_v$	$= r/L$	2″	2″*
$\Delta\theta_h$	$= g/2(2L \sin\theta)$†	40″‡	20″§

* $r = 5\mu$. † $h = aL/(Z+R')$. ‡ $\sin\theta = 0{\cdot}1$. § $\sin\theta = 0{\cdot}2$.

No. 1 is the apparatus for study by Laue diffraction; Mo $K\alpha_1$ radiation; $L = 50$ cm., $Z = 13$ cm., $R' = 20$ cm. No. 2 is the apparatus for study by Bragg diffraction; Cu $K\alpha_1$ radiation; $L = 50$ cm., $Z = 23$ cm., $R' = 10$ cm.

(B) *Discussion of the instrumental errors in obtaining the angular range of reflexion*

Experiments showed that the angular range of reflexion became negative in very good crystals if it was corrected according to the treatments of Lambot *et al.* It seems that there are two points to be revised in their treatments. First, the correction due to the thickness of specimens must be treated on the basis of the dynamical theory of diffraction. Broadly speaking, the magnitude to be corrected for an ideally perfect crystal is about 70% of the value estimated by the kinematical theory of diffraction. Secondly, the causes of instrumental line-broadening must be treated on the basis of the X-ray paths for a combination of curved crystal and plane crystal (specimen), as has been done in the theory of double-crystal spectrometer. The present treatments show that Lambot *et al.*'s treatments bring about a slight over-correction. Unfortunately, however, the true angular range of reflexion cannot be given without any ambiguity, since it depends upon some unknown characteristics of bent-crystal monochromator.

The consideration of the X-ray paths shows that the monochromator and the specimen must be placed in the following arrangement to eliminate the errors due to natural breadth of X-ray line as far as possible:

Laue case: parallel (or −) setting;
Bragg case: anti-parallel (or +) setting.

(C) *Experimental results*

(i) *Quartz and* $NaClO_3$.—The angular breadths of reflexion were less than 4·9″ and 5·6″ for good regions of quartz and $NaClO_3$ crystals respectively. In $NaClO_3$ straight reflexion lines are put out of joint at several points by an order of $16'' \sim 13''$, where the intensity is increased remarkably. This is probably due to the reduction of extinction effects. A random distribution model of the dislocations is not a good approximation for these substances.

(ii) KCl.—Several specimens prepared by the Kyropoulos method were investigated before and after annealing. Diffraction patterns show that distortions in crystals are very different from position to position. After sufficient annealing, polygonization in the continuously twisting region was observed as well as the usual polygonization in bending regions (R. W. Cahn, *J. Inst. Metals* (1949), **76**, 121). The changes in diffraction patterns become detectable after annealing of several hours at a temperature higher than 400° C. At $450 \sim 550$° C. continuously distorted regions are divided into crystallites of $30 \sim 70\ \mu$, each of which is misorientated by an

angle of about $60 \sim 30''$. At the higher temperatures some crystallites disappear and the others grow.

1(i)·3. R. PEPINSKY, K. DRENCK, H. DIAMANT, S. HOSHINO, T. MITSUI & F. JONA. *Instrumentation for diffraction, micro-optical, morphological and dielectric investigations of crystals.*

The following new instruments are described: a miniaturized Weissenberg camera, permitting a focal-spot–film distance of 4·3 cm., for use with our microfocus X-ray tube; a new Weissenberg camera for studies at liquid-helium temperature; a new heating camera for the Unicam and Supper Weissenberg cameras; a new heating chamber for powder and single-crystal studies on the G. E. XRD-3 instrument; a new servo-controlled miniaturized X-ray and neutron single-crystal counter goniometer; several new microscope stages for observations at liquid-helium and liquid-nitrogen temperatures, and a liquid-nitrogen dewar for studies on the Waldmann chemists' microscope; a new two-circle photoelectric optical goniometer for morphological measurements, which automatically records stereographic projections; a new instrument for single-crystal piezoelectric measurements; new multiple-crystal holders for dielectric measurements at low and high temperatures; a self-balancing bridge and servo-driven recorder for automatic measurement and plotting of dielectric constants versus temperature; a new type of temperature controller and indicator, for use in thermostats at temperatures from −196° C. to +500° C., with a control accuracy of ±0·05° C.; a system for electrode evaporative coating of hydroscopic crystals, for dielectric studies; and a new string saw for oriented crystal cutting.

1(i)·4. P. A. AGRON, M. D. DANFORD, M. A. BREDIG, H. A. LEVY & P. C. SHARRAH. *Apparatus, techniques and methods in molten-salt diffraction studies.*

An X-ray diffractometer designed specifically for studies on the structure of liquids will be described. The diffraction pattern from the horizontal surface of the liquid sample is obtained with a divergent-beam technique similar to the Bragg–Brentano flat system. For unambiguity in the patterns, monochromatic X-radiation is obtained through the use of a bent and ground sodium chloride monochromater. The instrument provides for a stationary flat sample which is scanned by the simultaneous angular motion of the X-ray tube and detector on arms moving about a horizontal axis lying in the liquid surface. A scintillation detector and step-scan counting to a desired accuracy are an aid in giving high precision to the diffraction data.

The molten salt is enclosed under a partial atmosphere of helium in a gasketed beryllium cup. Experiences in uses of gasketing materials up to 665° C. will be described. Welding attempts of beryllium to other metals will be illustrated.

1(i)·5. L. GRÉGOIRE & M. ROUAULT. *Optique du diffracteur électronique de l'Université de Montréal.*

L'appareil comprend deux lentilles magnétiques L_1 et L_2. L_1 forme un faisceau parallèle d'électrons qui est diffracté par la préparation, solide ou jet moléculaire de gaz; L_2 focalise le phénomène de diffraction sur l'émulsion photographique placée dans son plan focal; le spot central a un diamètre de 0,03 mm. environ et le phénomène de diffraction est indépendant de la position de la préparation, donc de la dimension du faisceau de gaz. L'étalonnage de l'appareil et son application à la structure d'au moins une molécule seront donnés.

1(i)·6. C. A. TAYLOR & H. LIPSON. *Experiences with a large optical diffractometer.*

An optical diffractometer with lenses 15 in. in diameter and of 30 ft. focal length has been constructed, primarily for the study of optical Fourier synthesis. The method of optical Fourier synthesis already developed (A. W. Hanson, C. A. Taylor & H. Lipson, *Nature, Lond.* (1951), **168**, 160); A. W. Hanson & H. Lipson, *Acta Cryst.* (1952), **5**, 362) is not easy to use because in order to include an appreciable number of terms, the plugs which have to be adjusted to control the phase and amplitude of the various terms have to be made very small; the operation requires considerable manipulative skill. With the new instrument a much larger number of terms—probably up to $h = k = \pm 30$—will be included and, in addition, the plugs will be large enough to make the operation comparatively simple.

The optical system has now been successfully completed; the lenses—which are single components with aspheric surfaces and are remarkably free from bubbles and inclusions—are mounted near the middle of a steel tube which is constructed like an aircraft fuselage and is 70 ft. long and 3 ft. 6 in. in diameter. The tube is suspended horizontally on twelve springs just below the ceiling and passes through seven rooms. At the middle, between the lenses, the tube has an opening so that, when adjustments are being made, the operator may stand on a platform with his head and shoulders in between the lenses. So far, no trouble has been experienced from vibration or from convection currents—although, of course, it is necessary for the opening between the lenses to be covered during observation or photography.

Television equipment (A. W. Hanson, C. A. Taylor & H. Lipson, *Proceedings of Symposium on Astronomical Optics and Related Subjects*, (1956). Amsterdam: North-Holland) is being developed so that the final image may be presented on a large scale on a cathode ray tube close to the operating position at the centre of the tube without intermediate photography and enlargement.

The necessary equipment for Fourier synthesis has not yet been completed but a number of optical transform projects, impracticable with the standard instrument, are being attempted. For example, well resolved diffraction patterns from cross gratings with a primitive translation of 4 or 5 cm. can be obtained and it is practicable to study the effect of small, accurately known displacements from the true lattice positions and various other imperfection problems. Studies are also being made of analogues of the fringe systems observed recently in electron-microscope studies (J. W. Menter, *Proc. Roy. Soc.* A, (1956), **236**, 119).

It is hoped to devote the lecture time available to an up-to-date presentation of the results and experience obtained.

1(i)·7. J. M. Cowley & A. F. Moodie. *ISAAC—An image-seeking computer using contoured Patterson maps.*

A computer has been built to carry out automatically the process of image seeking by use of Buerger's minimum function. It is designed to use Patterson maps in contoured form since such maps are more readily prepared from calculated data than are intensity-modulated maps. The contoured maps, suitably coded, are wrapped on an internally illuminated perspex cylinder which is rotated at 50 cycles per sec. and translated at a rate of 1 in. per sec. past a set of light-sensitive probes, so mounted that their positions may be adjusted readily. The sensitive element in each probe is a phototransistor. From the signals given by each probe the voltage proportional to the value of the Patterson function at the corresponding point is generated. The instantaneous minimum of all such voltage is found and displayed in a contoured form on a cathode ray tube with two-dimensional scans synchronized with the motions of the cylinder.

The coding system consists in making the spaces between the contour lines of the Patterson map either *A* (black), *B* (striped black and transparent), or *C* (all transparent). The corresponding signals given by the probes are then, *A* (zero), B (short pulses), or *C* (continuous signal). The electronic circuits distinguish between these three types of signal and feed either a positive or a negative unit pulse into an integrator at each change of signal type. The sequence *ABCABC*..., representing an increase in voltage, is distinguished from the sequence *ACBACB*..., representing a decrease. The fact that the origin of a Patterson map is always the highest point allows a simple zero-setting device to establish automatically the correct d.c. level for the output voltage from each probe circuit, and also allows an indication of the probe positions on the output tube. By the use of pulse techniques throughout, the usual difficulties and inaccuracies of analogue computation have been largely avoided.

Some idea of the range and accuracy of the computer may be gained from the fact that the minimum spacing between contour lines which can be used is about 1/150 of the unit cell dimensions. The time taken to scan a complete unit cell is 10 sec. or less. Provision has been made for the use of up to 24 probes simultaneously.

The process of image seeking on a two-dimensional Patterson map is then reduced to observing the changes in the contoured map in the output cathode ray tube as the number of probes used and their positions are adjusted. The number of probes used is increased as atomic positions are progressively determined.

Examples will be shown of preliminary results obtained using a small number of probes.

1(i)·8. V. I. Vlasenko & G. S. Žđanov. *Automatic synthesis of two-dimensional crystal structure patterns.*

1. The application of high-speed digital computers for summation of the Fourier series results in obtaining large numerical tables in a short time. The further working up of these large tables requires much time, thus considerably reducing the effect of the application of the high-speed computers. This is why the use of an automatic machine for working up these tables is necessary.

2. The first problem of automatization is to convert the numerical tables to a more readily surveyable form.

3. The simplest method of this synthesis is the construction of a mosaic image. In this case each number in the table is replaced by a round or a square spot with the colour corresponding to this number. The whole of the colour spots gives a visual mosaic image of the electron density. This is due to the ability of the eye to integrate discrete elements in smooth forms.

4. The model section method is a better but more difficult one. In this case it is necessary to construct a model of the two-dimensional function of the electron density, then to dissect the model with a series of planes parallel to *XY* on different levels and to register on a flat screen the intersection lines.

5. The model is constructed by two-dimensional interpolation first along the *X* axis, secondly along the *Y* axis. The results of the first (*X*-axis) interpolation is registered in a special storage device and represents the initial data for the second (*Y*-axis) interpolation.

6. The first interpolation is performed by electronic circuits, the results being recorded in parallel circular tracks on a rotation magnetic drum. The second (*Y*-axis) interpolation of these results along the drum axis as well as all other operations are also made by the electronic equipment.

The results of the second interpolation may be thought of as a curve, representing the distribution of electronic density along the *Y* axis (drum axis). An amplitude discriminator automatically dissects this curve parallel to the *Y* axis by a series of straight lines, representing the given set of electron-density values. The intersection points are registered as light spots on a screen of a cathode-ray tube, the coordinates of these spots corresponding to the position of the intersection points. Thus during one revolution of the magnetic drum the light spots form dotted lines, representing the whole electron-density map.

7. The use of the magnetic drum and electronic circuits for the above mentioned purposes allows one to obtain an electron-density map on a cathode-ray tube screen in a few seconds after the summation of the Fourier series on the high-speed computer has been ended.

1(i)·9. E. Hellner. *Über eine Analog-Maschine zur Berechnung von Strukturfaktoren mit Hilfe von Drehtransformatoren.*

Bei einer angegebenen Primärspannung *A* ergibt ein Drehtransformator eine Sekundärspannung *A* cos α bzw. *A* sin α; die Werte der Funktionen sind abhängig von der Winkel-Stellung (α) der Sekundärspulen. Die α-Werte werden über selbstkonstruierte Schaltklinkenräder an den Drehtransformatoren eingestellt.

Für eine Maschine zur Berechnung von Strukturfaktoren ist es wünschenswert, folgende Formel berechnen zu können:

$$F_{hkl} = \sum_{i=1}^{10} f_i \begin{Bmatrix} \cos \\ \sin \end{Bmatrix} 2\pi h x_i \begin{Bmatrix} \cos \\ \sin \end{Bmatrix} 2\pi k y_i \begin{Bmatrix} \cos \\ \sin \end{Bmatrix} 2\pi l z_i \ .$$

An die je drei Drehtransformatoren werden spezielle Anforderungen gestellt, wenn die Multiplikation *ohne* zwischengeschaltete Verstärker vorgenommen werden soll:

Bezüglich der Genauigkeit der Endwerte soll die Maschine folgendes leisten:

(1) Das Verhältnis von Eingangs- und Endspannung an einem 'Dreierrechenelement' ($\cos\alpha \cos\beta \cos\gamma$ bzw. $\sin\alpha \sin\beta \sin\gamma$) muss konstant sein.
(2) Die cos- bzw. sin-Funktionen müssen von allen drei Drehtransformatoren (I, II, III) in dem Dreierrechenelement exakt wiedergegeben werden.
(3) Während der Rechenoperation darf keine Phasenverschiebung der Endspannungen eintreten, damit die Addition der zehn Endspannungen durchgeführt werden kann.

Die Messungen ergeben zu

(1) Abweichungen der Endspannung treten bis zu 1,5% als relativer Fehler auf. Bei der Einstellung der Spannungswerte (Atomformfaktoren f_1) kann dieser Fehler bis auf 0,5% verringert werden.
(2) Die cos- bzw. sin-Funktion wird vom dritten Drehtransformator (III) des Dreierrechenelements ideal wiedergegeben, für die Drehtransformatoren I und II treten bei kleinen Funktionswerten eine relative Abweichung von 1,5% bzw. 0,6% auf. Durch variable Einstellung der ohmschen Belastung in der zweiten Sekundärspule des jeweiligen Drehtransformators gelingt es, den systematischen Fehler für den Drehtransformator II auszuschalten; für den Drehtransformator I bleibt eine Abweichung von 0,6% als relativer Fehler.
(3) Phasenverschiebungen der Endspannungen zu einander wurden durch Parallelkondensatoren ausgeschaltet. Die addierten Werte der Endspannung lagen bezüglich ihrer Abweichungen innerhalb der Fehlergrenze des Messinstruments. Das Vorzeichen des F-Wertes wird mit dem Zweiweg-Oszillographen bestimmt.

Alle 10 Sekunden kann ein F_{hkl}-Wert für 30 Parameter gefunden werden.

§ 1. (ii) Techniques and methods

1(ii)·1. W. Parrish & J. Taylor. *The precision diffractometer measurement of lattice parameters.*

The theory and technique of precision lattice-parameter measurements with the counter-tube diffractometer will be illustrated with several examples. Instrumentation and methods for temperature control ($\approx$ 0·1° C. up to about 300° C.), location of the specimen surface, precise zero-angle calibration, goniometer alignment, determining and centering intensity distribution of the primary beam, etc., will be described. Procedures to minimize the effects of various sources of non-systematic errors such as electronic circuit operation, resolving time, misalignments, etc., will be discussed. Since the diffraction angles are derived from a series of intensity measurements, the role of peak intensity, peak-to-background ratio, angular increment, and measurement technique (fixed count, rate-meter, etc.) in determining the precision of the angular measurements will be described.

The use of the center-of-gravity, peak position and other methods of obtaining the diffraction angles will be related to the precision of the measurements and the systematic errors. Procedures for calculating and plotting the lattice parameter will be shown for several types of typical conditions. The magnitude and angle-dependence of practically all the geometrical aberrations such as flat specimen, transparency, specimen surface displacement (A. J. C. Wilson), etc., are now known quantitatively in terms of the center-of-gravity of the diffraction line, and hence high precision absolute measurements may be made with the diffractometer with greater confidence than by other methods.

1(ii)·2. K. W. Andrews & W. Johnson. *A new method for the determination of grain or crystallite size from spotty diffraction rings.*

The method employs a thin section and a transmitted beam in contrast to the more usual back-reflexion arrangements. This removes the uncertainty about the depth of penetration of the X-rays but introduces new possible sources of error which can, however, be allowed for. The angular divergence of the beam Δ is effectively increased by oscillating the specimen through an angle ψ. The probability of reflection is then given by $P = [\psi/\pi + \frac{1}{2}\Delta] \cos\theta$.

The number of spots on any diffraction ring at Bragg angle θ is given by $Y = (Atp./v)P$. By altering the specimen thickness, t, the collinator area A, or the angle of oscillation ψ it is possible to obtain a suitable number of spots on a chosen ring from a wide range of crystal sizes. The number of spots should be large enough to give a good measure of the average grain volume v but not too large to give appreciable overlapping of spots. Laue spots are eliminated by the oscillation.

Errors arise from uncertainty in the beam divergence Δ and from the loss of weak reflexions from crystals on the side of the specimen away from the film. The error due to Δ is greatly reduced by the overriding effect of the angle of oscillation ψ, and the weak reflexions can be detected by increased exposure. In obtaining a mean linear dimension from the cube-root of v, errors arise in coarse-grained specimens if the linear dimension is not small compared with the specimen thickness. The choice of thicker specimens and hence shorter wavelengths for these cases enables this effect to be taken into account. Some examples of applications are given.

1(ii)·3. W. L. Bond. *Absorption, Lorentz and double polarization corrections for the equi-inclination Weissenberg.*

New absorption tables are presented; polarization corrections using a monochromator are given, also Lorentz–Tunnel factors. These are all applied to zero and upper levels.

1(ii)·4. M. J. Buerger. *Reduced cells.*

Several authors have erroneously stated that the end-point of the Delaunay reduction is the reduced cell, although Delaunay himself was well aware of the literature on reduced cells and avoided using the term in connection with his reduction. The nature of the reduced cell and the cell resulting from the Delaunay reduction are discussed. There are several reasons for preferring the reduced cell. The popularity which the cell resulting from the Delaunay reduction has achieved appears to be due to the fact that no one has made a point of developing methods for finding the reduced cell. In this paper the following three methods of finding the reduced cell from

an arbitrary primitive cell are presented: (1) a simple graphical method; (2) an analytical method suitable for digital computers; and (3) an algorithm which is not only simpler, but which converges to its result more rapidly than the Delaunay reduction.

Niggli has already prepared the ground for identifying the crystal system and lattice type from the scalar representation of the reduced cell. Some of his results are presented in more convenient tabular form.

1(ii)·5. V. Luzzati. *Diffusion centrale multiple des rayons X par la matière hétérogène.*

Un faisceau de rayons X qui traverse un échantillon de matière hétérogène perd une partie de son énergie selon deux mécanismes différents: diffusion en dehors de sa direction de propagation (on suppose ici que cette diffusion est limitée à la région centrale) et absorption ordinaire par la même matière à l'état compact. Le rapport entre l'énergie diffusée aux petits angles et l'énergie dissipée par absorption augmente avec la masse de l'échantillon par unité de surface: si la masse est suffisante le résidu du faisceau direct peut disparaître complètement. Simultanément la diffusion aux petits angles s'élargit. En principe, il s'agit d'un phénomène général qu'on ne peut toutefois observer expérimentalement qu'au cas où l'énergie diffusée par un échantillon de masse petite (où la diffusion multiple est négligeable) n'est pas trop petite par rapport à l'énergie dissipée par absorption.

Ce problème a été étudié par plusieurs auteurs, qui ont calculé la diffusion multiple par un système de sphères identiques, distributées au hasard, en admettant que l'intensité diffusée par une sphère suit une loi de Gauss. La première hypothèse restreint considérablement le domaine de validité de la théorie; la deuxième, celle d'admettre une loi de diffusion ayant la forme d'une fonction de Gauss, équivaut à admettre implicitement que la loi de la diffusion multiple ne dépend que de la forme de la diffusion simple aux angles très petits. Cette hypothèse est en fait incorrecte.

On tache de développer la théorie de la diffusion centrale d'un faisceau de rayons X par un échantillon de n'importe quelle masse, sans choisir au préalable un modèle de structure: on cherche au contraire à déterminer la relation générale qui existe entre la forme du faisceau transmis et la structure de l'échantillon.

On utilise dans la suite la notation suivante:

- $\mathbf{r}$ est le vecteur qui mesure la position d'un point de l'échantillon, par rapport à l'origine: sont unité est 1 Å.
- $0z$ est la direction de propagation du faisceau incident.
- $\mathbf{t}$ est la composante vectorielle de $\mathbf{r}$ contenue dans le plan perpendiculaire à $0z$.
- $\mathbf{s}$ est le vecteur qui mesure la position d'un point de l'espace réciproque par rapport à l'origine ($|s| = 2 \sin\theta/\lambda$).
- τ est la composante de $\mathbf{s}$ contenue dans le plan perpendiculaire à $0z$.
- $\nu d\gamma_\tau = \lambda^2 \times 7{,}9 \times 10^{-26} d\gamma_\tau$ est l'énergie cohérente, reçue par un élément de surface $d\gamma_\tau$ diffusée par un électron se trouvant dans un faisceau de rayons X d'intensité (flux d'énergie par cm.²) unitaire.
- η est la masse de l'échantillon par unité de surface, mesuré en électrons par cm.².
- μ est le coefficient d'absorption de la matière dont est formé l'échantillon, à l'état compacte.
- $\chi(\tau)$ est l'intensité diffusée par un échantillon de masse unitaire (1 électron).
- $q(\mathbf{t})$ est la transformée de Fourier de $\chi(\tau)$. On peut interpréter $q(\mathbf{t})$ comme la projection sur le plan de $\mathbf{t}$ de la fonction de Patterson d'un échantillon de masse unitaire.
- $*$ indique l'opération produit de composition.
- $\mathfrak{T}$ indique l'opération transformation de Fourier.

Un faisceau de rayons X monochromatique, dont la direction de propagation est $0z$, éclaire un échantillon uniforme, limité par deux surfaces planes perpendiculaires à $0z$, qui contient η électrons par cm.²; le faisceau transmis est reçu dans un plan perpendiculaire à $0z$, à une grande distance de l'échantillon. On suppose en première approximation que toute l'énergie diffusée par l'échantillon soit contenue dans la région de l'espace réciproque voisine de l'origine, où sont valables les approximations $\sin 2\theta = 2\theta$, $\cos 2\theta = 1$. On mesure la distribution de l'intensité du rayonnement en flux d'énergie par élément de surface $d\gamma_\tau$ du plan du récepteur.

On décompose l'échantillon en un grand nombre n de tranches élémentaires, comprises entre des plans équidistants, perpendiculaires à $0z$. Si $\mathscr{I}_0(\tau)$ est la forme du faisceau incident, la forme du faisceau qui sort de la première tranche $\mathscr{I}_1(\tau)$ est:

$$\mathscr{I}_1(\tau) = \mathscr{I}_0(\tau) * \{[1-(\eta/n)(\mu+\nu q(0))]\delta(\tau) + (\eta/n)\nu\chi(\tau)\} .$$

Le terme $[1-(\eta/n)(\mu+\nu q(0))]$ représente le résidu de faisceau direct: $(\eta/n)\mu$ tient compte de l'absorption massive, $(\eta/n)\nu q(0)$ représente l'énergie diffusée. Le faisceau diffusé apparaît dans le terme $(\eta/n)\nu\chi(\tau)$.

Si on appelle

$$W(\tau) = [1-(\eta/n)(\mu+\nu q(0))]\delta(\tau) + (\eta/n)\nu\chi(\tau)$$

le faisceau qui sort de la deuxième tranche a la forme

$$\mathscr{I}_2(\tau) = \mathscr{I}_1(\tau) * W(\tau)$$

et le faisceau qui sort de la $n$ième tranche

$$\mathscr{I}_n(\tau) = \mathscr{I}_{n-1}(\tau) * W(\tau) .$$

En appliquant à chacune de ces équations le théorème de réciprocité entre produit et produit de composition, on obtient

$$\mathscr{I}_n(\tau\mathfrak{T}) j_0(\mathbf{t}) [\omega(\mathbf{t})]^n ,$$

où

$$j_0(\mathbf{t})\,\mathfrak{T}\,\mathscr{I}_0(\tau), \quad \omega(\mathbf{t})\,\mathfrak{T}\,W(\tau) .$$

En effectuant le calcul on a

$$\mathscr{I}_n(\tau)\,\mathfrak{T}\, j_0(\mathbf{t}) \exp(-\eta\mu) \exp\{\eta\nu[q(\mathbf{t})-q(0)]\} . \qquad (1)$$

La fonction (1) est la loi générale qu'on cherche à établir. Pour en discuter les propriétés il convient de considérer le cas simple où le faisceau incident est très étroit: $j(\mathbf{t}) \equiv 1$. Le terme $\exp(-\mu\eta)$ tient compte de l'absorption ordinaire: on le néglige dans la suite, car il atténue uniformément tout le faisceau transmis par l'échantillon, sans en modifier la forme. Après ces simplifications, la fonction (1) devient:

$$\exp\{\eta\nu[q(\mathbf{t})-q(0)]\} . \qquad (2)$$

Pour les grandes valeurs de t, $q(\mathbf{t})$ tend vers zéro, et

l'équation (2) tend vers $\exp[-\eta v q(0)]$. Il convient de séparer (2) en deux parties:

$$\exp\{\eta v[q(\mathbf{t})-q(0)]\} = \exp[-\eta v q(0)] + \exp[-\eta v q(0)]\{\exp[\eta v q(\mathbf{t})]-1\}. \quad (3)$$

Le premier terme de (3) est constant: sa transformée de Fourier est une fonction δ

$$\exp[-\eta v q(0)]\mathfrak{T}\exp[-\eta v q(0)]\delta(\boldsymbol{\tau})$$

qui représente l'intensité du résidu du faisceau incident transmis par l'échantillon. Le deuxième terme représente le faisceau diffusé. Le rapport entre l'énergie des deux faisceaux est

$$\exp[-\eta v q(0)]/\{1-\exp[-\eta v q(0)]\} = \beta.$$

La loi (2) rend bien compte des observations expérimentales. Si la masse η de l'échantillon est très petite, on a la loi:

$$\exp\{\eta v[q(\mathbf{t})-q(0)]\} \simeq 1+\eta v[q(\mathbf{t})-q(0)]$$

qui correspond à la diffusion par un échantillon de petite masse, cas où les phénomènes de diffusion multiple sont négligeables. A mesure que la masse de l'échantillon augmente le rapport β diminue, et le deuxième terme de (3) représente une courbe de plus en plus aiguë autour de l'origine, ce qui traduit l'élargissement du faisceau diffusé: β tend finalement vers zéro, lorsque l'énergie du résidu du faisceau transmis devient négligeable en comparaison de celle du faisceau diffusé.

Si $\eta v q(0)$ est très grand la fonction (2) est non-nulle seulement aux points où la différence $q(\mathbf{t})-q(0)$ est voisine de zéro: cela se produit près de l'origine, car $q(\mathbf{t})$ est en général une fonction monotone. Donc la forme du faisceau transmis par un échantillon de grande masse ne dépend que de la forme de $q(\mathbf{t})$ près de l'origine.

Ce dernier cas est particulièrement important lorsque l'échantillon est formé de grains d'une matière de densité électronique uniforme, immergés dans un milieu de densité électronique également uniforme. En effet la forme de $q(\mathbf{t})$ à l'origine ne dépend dans ce cas que de l'étendue de la surface de séparation entre les deux milieux:

$$q(\mathbf{t})-q(0) = \frac{1}{4}\frac{\varrho S}{V}t^2 \lg\left(\frac{1{,}08}{8}\frac{tS}{V}\right), \quad \frac{tS}{V} \to 0.$$

ϱ est la différence entre les densités électroniques des deux milieux, S l'étendue de l'interface, V le volume occupé par la matière la plus dense.

Donc la forme de toute la courbe de diffusion multiple ne dépend que de ϱ et S/V, lorsque la masse de l'échantillon est grande.

La diffusion centrale par un échantillon de grande masse présente sur la diffusion par un échantillon de petite masse l'avantage de permettre de déterminer la fonction $q(\mathbf{t})$ en *valeur absolue*, tout en mesurant les intensités en valeur relative. En effet, si l'échantillon a une masse suffisante, l'énergie du résidu de faisceau direct qui est transmis devient comparable à l'énergie du faisceau diffusé; on peut alors déterminer la valeur de $q(0)$, calculer la transformée de Fourier de l'ensemble du faisceau transmis (1) et obtenir ainsi, après normation, la fonction $q(\mathbf{t})-q(0)$ correspondant à une masse donnée.

A mesure que la masse de l'échantillon augmente, la forme du faisceau transmis est définie par la forme de $q(\mathbf{t})$ d'une région de plus en plus petite, autour de l'origine: à cet égard, la technique de la diffusion centrale par des échantillons de masses différentes peut se comparer à l'examen de la matière par un microscope à grossissement variable.

Dans le cas, important dans la pratique, où l'échantillon est formé de deux régions de densité électronique constante, la diffusion centrale ne dépend que de la différence ϱ des deux densités électroniques et de la surface spécifique de la région de densité élevée. On peut donc envisager la détermination expérimentale de ces paramètres, dont l'importance pratique (surtout la surface spécifique) est considérable.

La théorie exposée ici peut être étendue à d'autres phénomènes physiques.

On discute l'aspect expérimental de la diffusion centrale des rayons X par des échantillons de grande masse; les résultats théoriques sont étayés sur quelques exemples expérimentaux.

1(ii)·6. P. HARRISON, G. A. JEFFREY & J. TOWNSEND. *An experimental study of the anomalous dispersion effect in* ZnO *with* Mo $K\alpha$ *radiation.*

The effect of anomalous dispersion in the non-centrosymmetrical ZnO structure should useful in determining the u parameter, since

$$\Delta|F| = |F^{\text{calc.}}_{hkl}| - |F^{\text{calc.}}_{\overline{hkl}}| = \frac{4}{|F|}f_0\left[1+(-1)^l\cos 2\pi\left(\frac{h+2k}{3}\right)\right]\Delta f''_{\text{Zn}}\sin 2\pi lu,$$

where $|F|$ is the structure amplitude without anomalous dispersion, and $\Delta f''$ is the imaginary part of the atomic scattering factor.

An experimental study of this predicted $\Delta|F|$ was carried out as a function of 2θ for $hk6$, $hk8$, $hk10$ using Mo $K\alpha$ radiation. Theoretical values of C. H. Dauden & D. H. Templeton (*Acta Cryst.* (1955), **8**, 841) give values of the right order of magnitude for $2\theta < 80°$ and suggest a u parameter in excess of 0·375. However, for $2\theta > 80°$ the theoretical angular dependence of $\Delta|F|$ is not verified and disagreement between theory and experiment of as much as 100% is encountered.

1(ii)·7. R. MASON. *The value of photographic methods for accurate single-crystal analysis.*

Photographic data have been used for the analysis of several aromatic hydrocarbons and heterocyclics. High internal consistency of the observed data is achieved, and final reliability factors (3·5–6·0%) suggest good absolute accuracy. Choice of crystal, scaling of data, and 'patchiness' in the experimental observations are discussed.

1(ii)·8. O. KENNARD. *Radioactive tracer method for the measurement of film densities.*

The method to be described represents an attempt to measure the integrated intensity of crystal-diffracted X-ray beams by a combination of photographic and ionization methods.

The diffraction pattern is recorded photographically in the conventional way on a stationary- or moving-film

apparatus. The developed film is treated with a solution containing a suitable radioactive tracer so that the silver grains in the diffraction spots are quantitatively labelled. The integrated intensity of the diffracted beam will then be proportional to the total radioactivity of the recorded spot, which can be measured directly with a suitable counter.

A. E. Ballard, G. W. Zuehlke & G. W. W. Stevens (*Radioisotope Techniques*, (1951). London: Stationery Office), using I^{131} as tracer, were the first to apply this method to the determination of silver in photographic images. Their technique was adapted for use with X-ray diffraction patterns, and modified to enable adequate and reproducible activation of the very small areas to be measured.

In the preliminary experiments constant areas of film were punched out from an activated step-wedge of intensities. The film samples were counted with a commercial-type Geiger–Müller counter and the relation between count rate, silver content, optical density and X-ray exposure was established for the different types of X-ray film in common use. A straight-line relationship was found between count rate and X-ray exposure up to about an optical density of 1·0—about three times the range covered by visual comparison or by direct photometry of an X-ray negative (G. Kaan & W. F. Cole, *Acta Cryst.* (1949), **2**, 38).

Since it would not be practicable to punch out all the individual diffraction spots given by a crystal of even moderate complexity an apparatus called a 'spot densitometer' (British Patent Application No. 21209/56) was designed to enable the direct measurement of activated diffraction photographs. The apparatus consists essentially of a drum, carrying the activated film as well as a non-active duplicate copy made by contact printing or X-rays. A specially constructed miniature Geiger–Müller counter and a pair of cross-wires are mounted in the same relationship to each other for traverse relative to the film carrier so that the radioactive film can be scanned accurately by the Geiger-counter by scanning the diffraction pattern on the control film with the eyepiece. This method also allows the assignment of indices to individual diffraction spots, using Weissenberg or precession charts. The Geiger–Müller counter carries a platinum collimator large enough to isolate the individual diffraction spots and operates with standard counting equipment. Appropriate corrections are made for background effects.

Typical results obtained with this apparatus will be presented and the advantages and disadvantages compared with other techniques will be discussed.

1(ii)·9. U. W. Arndt & D. C. Phillips. *The collection of single-crystal intensity data by means of a counter diffractometer.*

For the gathering of three-dimensional intensity data a diffractometer is required which possesses three independent degrees of freedom corresponding to the three reciprocal-lattice co-ordinates of a general reflexion. The necessary movements may be divided between crystal and counter axes in a variety of different ways; one of the most convenient of these geometries is that of the cone-diffractometer due to T. C. Furnas & D. Harker (*Rev. Sci. Instrum.* (1955), **26**, 449). An instrument of this type has been constructed in this laboratory. It was found desirable for the diffractometer to be usable with a variety of different X-ray tubes affording the choice of stationary and moving anodes with different target materials. Accordingly, monitoring the incident beam by means of a proportional counter was chosen in preference to stabilization of the X-ray tube power supply; the monitoring arrangement is an integral part of the incident-beam collimator so as to make the diffractometer self-contained and independent of any particular generator. It was further desirable for there to be no specific restrictions on the shape or uniformity of the X-ray tube focal spot and the rocking-crystal method was thus preferred to the stationary-crystal technique (W. Cochran, *Acta Cryst.* (1950), **3**, 268). Even though the counting statistics of the former method is inferior, it lends itself to the greater precision since somewhat less accuracy is required in the setting of the instrument (U. W. Arndt & D. C. Phillips, to be published) and since sources of error such as the broadening of some reflexions and the non-uniformity of the background are more easily detected and allowed for. The actual measurement of a reflexion is slower, but during data collection more time is generally spent on setting than on counting. The angular positions of crystal and counter are either calculated or derived on a simple analogue computer; once the instrument is set for the reflexion the sequence of measuring the integrated intensity under the rocking curve and correcting it for background is semi-automatic and it is readily made completely automatic. Some illustrations of the performance of the instrument will be given.

1(ii)·10. T. C. Furnas, Jr. *Pitfalls in the measurement of integrated intensities.*

This work is to be published as part of a Monograph, Catalog No. A4967 E, *Single Crystal Orienter Instruction Manual*, (1957), General Electric Company, Milwaukee, Wisconsin, U.S.A.

Modern determinations of fine details of structure require increasingly accurate three-dimensional sets of self-consistent integrated intensity measurements.

A set of integrated intensity measurements is not self consistent unless (1) the same volume of specimen is illuminated in each measurement, and (2) each element of the crystal is illuminated by the same incident intensity. For instance, a set of equi-inclination Weissenberg films are not self consistent if a long cylindrical specimen is used, since different layer lines are produced by different volumes of crystal.

The nature of the source, i.e. whether or not it is directed, whether or not it is uniform, and whether or not its intensity fluctuates with time, primarily determines the techniques by which self-consistent sets of integrated intensity measurements can be obtained. It will be shown why no one technique is universally applicable, why illumination of the specimen by crystal-monochromatized radiation is almost never satisfactory, and how any of the usual direct radiation sources may be utilized.

Irrespective of the measurement technique used, the response of the detector must be uniform over the entire area that is capable of receiving diffracted X-rays. This is particularly important with counters, since the collec-

tion of large numbers of quanta may be falsely interpreted as providing accurate measurements.

The manner in which background corrections are made, and indeed the solid angle included in a measurement, affects the accuracy of the results. The use of balanced filters gives the best results, but is extremely inconvenient with film methods.

Finally, the specimen itself must be of quality capable of giving the desired accuracy of data while using the measurement technique appropriate to the available equipment. A suitable quality concerns not only the perfection and size of the specimen, but also its reproducibility and stability during the measurements.

1(ii)·11. W. C. HAMILTON. *The effect of crystal shape and setting on secondary extinction.*

The problem of secondary extinction in diffraction experiments has been treated by several authors (G. E. Bacon & R. D. Lowde, *Acta Cryst.* (1948), **1**, 303; R. W. James, *The Optical Principles of the Diffraction of X-rays*, (1950). London: Bell; W. H. Zachariasen, *Theory of X-ray Diffraction in Crystals*, (1945). New York: Wiley). These authors have generally confined their theoretical treatments to infinite flat plates and their empirical corrections to one-parameter functions. Because of the increasing use in structure refinements of very accurate intensity measurements on single crystals, it seems of interest to examine the effect of crystal shape on the secondary extinction coefficient. This is of particular importance in neutron-diffraction studies, where corrections for secondary extinction are generally far more important than those for absorption.

The following differential equations may be written for a crystal of uniform cross-section:

$$\partial P_H/\partial m = -(\mu+\sigma)P_H+\sigma P_0 ,$$
$$\partial P_0/\partial n = -(\mu+\sigma)P_0+\sigma P_H ,$$

where P_H is the power in the primary beam at the point (n, m), P_0 is the power in the reflected beam at the point (n, m), n and m being the directions of the incident and reflected beams, μ is the linear coefficient of true absorption, and σ, the reflectivity, is proportional to F^2 modified by a correction for primary extinction if present. These differential equations are in general difficult to solve, and they have been replaced by the corresponding difference equations on a Cartesian coordinate grid. These are readily solved by numerical procedures. To obtain the integrated intensity, one integrates P_H over the exit surface of the crystal. The secondary extinction coefficient is defined as the integrated intensity divided by the integrated intensity which would have been obtained had there been only primary extinction and true absorption present to reduce the value of the intensity.

Calculations have been carried out for a number of crystal shapes, Bragg angles, and crystal setting angles. The more interesting results may be summarized as follows:

(1) If the extinction coefficient is less than 0·70, it becomes quite dependent on the Bragg angle of the reflection. For example, at the point where E_s is 0·20 for a 0° reflection, it is 0·30 for a 180° reflection (cylindrical crystal).

(2) For a cylindrical crystal, with $E_s > 0{\cdot}70$, the following approximation is valid to 5% for all Bragg angles:

$$E_s \approx \exp(-8\sigma D/3\pi) ,$$

where D is the diameter of the crystal.

(3) However, crystals with rectangular cross sections (4×1, for example) can have E_s values of from 0·50 to 0·80 for the same volume of crystal which gives $E_s=0{\cdot}70$ for the cylindrical crystal.

(4) As σD becomes large, the intensities approach limiting values (the limiting value at 180° being twice that at 0° Bragg angle). From these limiting values, one may derive good estimates of the mosaic-spread parameter.

One may conclude that for accurate intensity measurement, it is preferable to use a cylindrical crystal (spherical if higher layer lines are to be observed). Furthermore, a one-parameter extinction correction is not valid unless the extinction is not severe ($E_s > 0{\cdot}70$). Ideally, curves should be calculated for the particular crystal shape and absorption coefficient characterizing the problem at hand.

Experimental comparison with intensities from a magnetite crystal showing particularly severe extinction (E_s as low as 0·20) have borne out the major features of this treatment. For example, the value of the mosaic-spread parameter derived from the limiting intensity is about the same as that derived from the exponential fit at low intensities.

1(ii)·12. H. J. GRENVILLE-WELLS. *Machine methods and crystal physics.*

Programmes now in use on the Ferranti PEGASUS computer use fractional co-ordinates to derive orthogonal Ångström co-ordinates, bond lengths and angles, the equation of the mean molecular plane, and the distances of atoms from it. Such data can be valuable for the compilation of reference works such as *Structure Reports*. General programmes, applicable to all space groups, produce F's, corrected for absorption, from the observed intensities; compute structure factors and diagonal least-squares refinements involving anisotropic vibrations and dispersion corrections; and evaluate Fourier syntheses. Other applications of value in crystal physics, such as the application of relaxation methods in the study of vibrating lattices, will be suggested.

1(ii)·13. A. TULINSKY. *A two-dimensional Fourier program for an IBM Type-650 magnetic-drum data-processing machine.*

The program can evaluate two-dimensional series of the form

$$\sum_{hk}\sum A(hk)\begin{matrix}\cos\\ \sin\end{matrix}[2\pi hx]\begin{matrix}\cos\\ \sin\end{matrix}[2\pi ky]$$

and

$$\sum_{hk}\sum A(hk)\begin{matrix}\cos\\ \sin\end{matrix}[2\pi hx]\begin{matrix}\sin\\ \cos\end{matrix}[2\pi ky]$$

in any combination of the four. The evaluation proceeds at increments of n/100ths of the period, where n is usually a small integer. There are seven levels of computation, four in the first dimension and three in the second. Only three of these levels are important for program speed.

The computation is performed dividing the Fourier

coefficients into even odd groups. Summations are carried out over one quarter of a period and the sub-totals are employed as input for a subsidiary program, which generates a complete period by the consideration of trigonometric identities. This latter program takes a constant 5 or 10 min., depending upon the fineness of the grid (1/50th × 1/100th or 1/100th × 1/100th).

The most important feature of the program is its 'parallel' nature of computation. Given a Fourier coefficient, the program forms the products and accumulates the partial sums,

$$B(hy) = \sum_k A(hk) \begin{matrix}\cos\\ \sin\end{matrix} [2\pi ky] ,$$

for all y (one quarter of the period). This eliminates excessive operational redundancy and creates extra storage facilities. Since the trigonometric functions and the Fourier coefficients are stored as tables, the former are located by means of variable and the latter by means of systematic address modification. Such a procedure is much faster than conventional table look-up, especially with large tables.

Another time- and space-conserving feature of the program is to ignore Fourier coefficients of zero magnitude. Such coefficients are left out of the table. The program determines whether a coefficient is zero by comparing program-generated indices with the indices corresponding to a non-zero coefficient. The latter indices are packed in the same word as the Fourier coefficient. The only program requirement is that the table of non-zero coefficients be in order of increasing magnitude of $10h+k$.

The foregoing technique is employed in the first dimension only, the assumption being made that few, if any, of the coefficients $B(hy)$ are zero. Therefore, the summation in the second dimension is 'sequential' and zero coefficients are considered when present.

Another fundamental feature is the generation of a variable termination constant in the first summation. This permits the consideration of all reflections bounded by a circle in two-dimensional reciprocal space. The radius of the circle can be given any value out to $2\theta = \pi$. This technique eliminates unnecessary consideration of impossible reflections.

The last two program capabilities arose from the fact that the program was to process data from a crystalline protein. Their consideration increases in importance as the number of reflections or the unit cell size increases.

Thus far, this program has been employed in the space groups $P1$, $P2_1$, $P2_1/c$ and $P2_12_12_1$. It has evaluated series with approximately 150 possible coefficients at 1301 points in about 10 min. and larger ones in the neighborhood of 900 possible coefficients, at the same number of points, in about 45 min.

1(ii)·14. L. H. Jensen. *The speed of the I.B.M. 650 computer in Fourier methods of refining crystal structures.*

Programs for calculating Fourier syntheses and structure factors on the I.B.M. 650 electronic data-processing machine have been written.

The Fourier program was written to evaluate the series at points of a grid that are multiples of 1/200th of the unit-cell edges. The most convenient multiples are those that result in grids of 1/200, 1/100, 1/50, 1/25 and 1/20. The time in seconds for evaluating a two-dimensional series is given roughly by the expression: $t = (g_1/20)[n+h_2g_2/2]$, where g_1 and g_2 are the number of grid points along coordinate axes corresponding to h_1, the index summed over first, and h_2, the index summed over second, and n is the total number of reflections, both observed and unobserved. Thus to evaluate $\varrho_{x,z}$ for L-cystine hydrobromide ($a_0 = 17{\cdot}85$, $c_0 = 7{\cdot}48$ Å, $P2_122_1$) over a quarter of a 100×40 grid requires about 9 min.

F_{h0l}'s for the above compound, using an overall temperature factor and excluding hydrogen atoms, may be calculated at the rate of 40 per min. Using individual atom anisotropic temperature factors, again excluding hydrogen atoms, the rate is 25 per min.

1(ii)·15. V. Vand, J. W. Turley & R. Pepinsky. *Crystallographic calculations on* IBM 704 *and* 604 *machines.*

A program has been designed for computation, on the IBM 704 machine, of all interatomic distances below ~ 4 Å, and corresponding bond angles, on the IBM 704 machine. This has been successfully tested on structures up to 35 atoms in the asymmetric unit. Data for all published structures for which three-dimensional coordinates are available are being transferred to punched cards, and distances (to ~ 4 Å) and bond angles for all of these will be re-computed and statistically analyzed.

Sayre's least-squares refinement program for the IBM 704 machine has been slightly modified and extended to a large number of space groups. It has been applied in more than a dozen crystal analyses from this laboratory.

Efficient routines are described for various simpler crystallographic calculations on the IBM 604 machine.

1(ii)·16. W. N. Lipscomb, R. E. Dickerson & F. L. Hirshfeld. *Procedures made possible by high speed computers.*

Some 200 hr. of experience in the use of the Remington Rand UNIVAC SCIENTIFIC 1103 Computer have led to general programs for structure factor, Fourier series and least-squares procedures. The scaling down of indicated atomic shifts is usually necessary in least squares if convergence is to be obtained. The use of a large number of iterations often results in cumulative atomic shifts which are very large compared with standard deviations and shifts in a single cycle of refinement, especially for light atoms in the presence of heavy atoms. Some conditions under which trial structures refine either to incorrect structures or to correct structures will be described for hydrogen in the presence of boron.

A comparison of R with $r = \Sigma w_i(F_o^2-F_c^2)_i^2 \div \Sigma w_i(F_o^4)_i$, the normalized function minimized in the least-squares treatment, will be given. A partial summary is as follows for final structures obtained after a large number of iterations:

	R	r
B_4H_{10}	0·090	0·037
B_5H_{11}	0·106	0·048
B_9H_{15} (borons only)	0·21	0·24
B_9H_{15} (one H incorrect)	0·167	0·144
B_9H_{15}	0·155	0·075
B_6H_{10} (borons only)	0·156	0·124
B_6H_{10} (6 H's included)	0·138	0·098
B_6H_{10} (3-bridge hydrogen model)	0·120	0·075
B_6H_{10} (4-bridge hydrogen model)	0·117	0·068

The value of r is a much more sensitive criterion of the correctness of the structure than R, a result which is even more apparent when earlier stages of refinement are considered. Finally, the use of r or R for various classes of planes will be discussed in terms of the removal of ambiguities in pseudo-homometric projections and structures.

1(ii)·17. D. W. J. CRUICKSHANK. *Further crystallographic calculations on the Manchester University electronic computer.*

In the last five years the crystallographic computing group at Leeds University have worked on 37 crystal structures, using over 1,500 hr. computing time on the Manchester University electronic computer. About 150 cycles of three-dimensional refinement have been carried out, 35 of these allowing for the full anisotropic thermal motion. A description will be given of some of the computer programmes used in these detailed refinements. Very efficient programmes have had to be devised for the enormous calculations on wet B_{12} (2600 A's and B's, 105 atoms) in order for the work to be practical on this now relatively slow computer.

1(ii)·18. F. R. AHMED. *Programmes applicable to all space groups for computation on FERUT.*

Until recently, programmes for performing crystallographic computations on high-speed automatic digital computers have been prepared for specific space groups. Generalized programmes were first reported by Fowweather (1955) for two-dimensional calculations in the triclinic, monoclinic, and orthorhombic systems and by Sparks, Prosen, Kruse & Trueblood (1956) for calculations in all space groups. The latter programmes, however, deal explicitly with the structure factors for the (hkl), $(\bar{h}kl)$, $(h\bar{k}l)$ and $(hk\bar{l})$ reflexions, and with all the atoms in the unit cell regardless of the space-group symmetry elements, other than a centre.

The following generalized programmes, applicable to all space groups without modification, have now been prepared for use on FERUT: the calculation of structure factors; Patterson and Fourier syntheses at intervals of 1/120 of the cell edges or at any multiple of 1/120 either throughout the asymmetric part of the unit cell or in selected patches; observed and calculated differential syntheses, including correction of finite summation errors by Booth's back-shift method; the estimation of the scale factor, the discrepancy factor, and the standard deviations of the atomic co-ordinates. The programmes are designed to take advantage of the symmetry characteristics of the space group under consideration by employing the corresponding equations given in the *International Tables for X-ray Crystallography*, thus avoiding wasteful repetition of the calculations for crystallographically equivalent atoms and reflexions. The equations are expressed in terms of a simple pseudo code which is stored in the machine with the master programme and the experimental data. As a new group of reflexions is sensed by the machine, the pseudo code of the corresponding equation causes specific instructions to be planted in certain vacant lines of the programme. The machine then proceeds to evaluate this equation for the data within the group. In this way the programmes are capable of computing different equations for the different space groups as well as for the different groups of reflexions within the data. No storage space is wasted by the unobserved reflexions due to systematic or non-systematic absences, or by the special planes (having one or more zero indices) which are equivalently related to other reflexions. Intermediate checks are included in order to minimize loss of machine time due to machine errors or derails and to permit stopping the computation at any stage without loss of previous results. Short tests have demonstrated the applicability of these programmes to all crystal systems, and they are now in routine use for the determination and refinement of actual crystal structures. Their generality has not involved any additional computation time compared with the programmes for the space group $P2_1/a$ reported by Ahmed & Cruickshank (1953), on which the present programmes are based.

§ 2. Recent progress in structure determination

2·1. M. ATOJI. *On the electron density of atoms in the X-ray Fourier method.*

The analytical formulae for the electron distribution in all atoms have been obtained from the Fourier, Hankel and Gauss transformations of the atomic scattering factors modified by the Debye–Waller temperature factor. All atomic scattering factors are expressed in analytical forms using either the electronic wave functions or the Thomas–Fermi method. The agreement between the calculated values and the observed data in the X-ray Fourier map is quite reasonable (M. Atoji, *Acta Cryst.* (1957), in the Press). The peak heights $\varrho_n(0)$ of atoms under any experimental condition may be approximated by

$$\varrho_n(0) = k_n(a_n+b_nB)^{-\nu_n},$$

where k_n, a_n, b_n and ν_n are numerical constants and B is the isotropic temperature-factor coefficient, n being 2 for a two-dimensional and 3 for a three-dimensional synthesis. From these numerical results, it is found that the iso-electronic atoms such as F^-, Mg^{2+}, Al^{3+} and Si^{4+} can well be distinguishable from the peak values in most of the experimental conditions. The peak curvature, $\varrho_n''(0)$, can be obtained from $\varrho_n(0)$ using the relation (Atoji, *loc. cit.*)

$$\frac{16\pi^2}{n}\frac{\partial\varrho_n(0)}{\partial B} = \varrho_n''(0).$$

If we know $\varrho_n(r)$ and $\varrho_n''(0)$ in parts of the unit cell, some new relations for the sign determination of the structure factor can be derived, using the Herglotz theorem. The general formulae for the peak shape in the generalized Fourier synthesis are also derived and are compared with those discussed above. An application of these equations has been shown in the case of the Magnus green salt (M. Atoji *et al.*, *J. Amer. Chem. Soc.* (1957), to be published).

A simple but useful relation between the orthogonal curvatures in the Fourier map $\partial^2\varrho/\partial x^2$ etc. and B is obtained, namely

$$\partial\varrho/\partial B = (1/16\pi^2)\{\partial^2\varrho/\partial x^2+\partial^2\varrho/\partial y^2+\partial^2\varrho/\partial z^2\}.$$

The equations in the case of the general anisotropic temperature-factor are similarly discussed. The electron

densities of atoms in thermal vibrations are calculated, using the electronic wave functions, the molecular orbital method and the Thomas–Fermi distribution. It is again emphasized that the Thomas–Fermi method is a satisfactory approximation even for the light atoms in appreciably large thermal motion. The effect of the outer electronic distribution to the atomic scattering factor is discussed using the Thomas–Fermi method in connection with the results given above.

2·2. R. CALDER, W. COCHRAN & S. DARLOW. *Recent work on electron distributions in crystals.*

Some improvements in the technique of measurement of the X-ray intensities required for accurate electron-density determinations have been made. A comparison of calculated with observed electron distributions in LiH has been completed. The electron distribution in potassium hydrogen maleate is being determined accurately, and is of interest because the molecule contains a short O–H–O bond in which the proton may be symmetrically placed between the oxygens.

2·3. H. J. GRENVILLE-WELLS & R. MASON. *A new refinement of anthracene and naphthalene at* 290° K. *and* 90° K.

New two-dimensional photographic data, having high internal consistency, have been used in the refinement of B factors and atomic co-ordinates in naphthalene and anthracene at different temperatures. A single cycle of refinement leads to reliability factors of approx 7%, and further refinement is possible. Theoretical techniques used to shorten the work will be briefly discussed, and the results compared with those obtained from three-dimensional data.

2·4. A. TULINSKY & C. R. WORTHINGTON. *An accurate analysis of basic beryllium acetate by three-dimensional Fourier methods.*

A detailed structure of basic beryllium acetate, $(Be_4O(CH_3CO_2)_6$, $Fd3$, $a = 15{\cdot}74$ Å, $Z = 8)$ has been obtained, employing three-dimensional Fourier methods. The intensity data were collected with an Eulerian cradle Geiger-counter spectrometer. Peak intensities were measured to a constant count of 1024 and the peak height was taken to be proportional to the integrated intensity. $K\alpha_1$ and $K\alpha_2$ splitting was corrected for empirically. All the independent reflections (370) out to $2\theta = 164°$ (Cu $K\alpha$) were observed. In general, the accuracy of the data is better than 10% in intensity.

The molecules posses 23 symmetry and lie at the points of a diamond structure. Space-group requirements fix:

(i) O_I at 0, 0, 0 .
(ii) Be at u, u, u; $\bar{u}, \bar{u}, u$; $\bar{u}, u, \bar{u}$; $u, \bar{u}, \bar{u}$.
(iii) C_I at $\pm v, 0, 0$; ↻.
(iv) C_{II} at $\pm w, 0, 0$; ↻.
(v) O_{II} at $x, \pm y, z$; ↻; and $\bar{x}, \pm y, \bar{z}$; ↻.

The hydrogen atoms are in general positions but require twofold symmetry since the methyl carbon atom lies on a twofold axis. A total of thirteen positional parameters describes the structure. Seven of these fix the simplest hydrogen atom arrangement (coplanarity being assumed).

Space-group requirements are also encountered in the consideration of general harmonic thermal vibrations. These are:

(i) O_I: $\delta_1 = \delta_2 = \delta_3$, three principal directions coincident with three twofold axes.
(ii) Be: $\delta_1 = \delta_2 = \delta_3$, δ_1 direction coincident with a threefold axis.
(iii) C_I and C_{II}: $\delta_1 \neq \delta_2 \neq \delta_3$, one principal direction coincident with a twofold axis.
(iv) O_{II} and H: $\delta_1 \neq \delta_2 \neq \delta_3$, principal directions general.

The δ's are directly related to the three principal mean square displacements. The hydrogen atoms were considered to be isotropic so that eighteen parameters describe the thermal vibrations in a general way. Including a scale constant, thirty-two independent atomic parameters fix the structure completely. Since there are 370 observed reflections (approximately 12 per parameter), this structure presents a particularly good example for the investigation of fine detail in electron density.

In order not to bias the calculated electron density between bonded atoms and leave open the possibility of differentiating between the charge density of a bonded atom and that of an isolated one, vibrational amplitudes were fixed by examining electron and difference densities in non-bonding directions. The simplest way to adjust the principal vibrations and their directions is from the tensor components B_{ij}. The latter are obtained directly from three electron and difference density sections through the center of an atom.

Refinement of the structure began with a trial based upon atomic coordinates proposed by Pauling & Sherman. After four cycles of refinement, it became quite apparent that the difference densities in the vicinity of atoms could not be reduced to zero by merely considering general harmonic vibrations. Therefore, the degrees of ionization of the various atoms were investigated by counting the number of electrons associated with each atom. This treatment revealed that all the atoms except the methyl carbon are partially ionized, beryllium donating to the central oxygen and the carboxyl carbon donating to the carboxyl oxygen.

During the course of analysis, it was observed that the charge density of the various atoms differs in bonding and non-bonding directions. This effect is most pronounced in the central oxygen atom and the beryllium atoms. Both possess tetrahedral charge distributions. The tetrahedral directions of the central oxygen atom are directed to its four neighboring beryllium atoms. One of the beryllium tetrahedral directions is to the central oxygen atom while the other three are directed toward the carboxyl oxygen atoms. This type of behavior can be interpreted as being due to bonding if it is assumed that any anharmonicity of thermal motion is small. Such effects are much smaller in the other atoms.

Six 'partial' hydrogen atoms have been located. They originally appeared in difference densities, where they were not included. Later, they were observed in the electron density. At present, it is not yet clear whether they are half-electron atoms or smaller. If the former, the methyl groups must possess an orientational disorder, where the methyl group is in one of two orientations separated by $\frac{1}{3}\pi$. If the latter, the methyl groups must

possess a certain amount of hindered rotation superimposed upon an orientational disorder. Further work is now in progress.

2·5. J. A. Ibers & D. T. Cromer. *The effects of weighting and of the number of data on the least-squares refinement of the structure of ceric iodate monohydrate.*

The crystal structure of ceric iodate monohydrate (J. A. Ibers, *Acta Cryst.* (1956), **9**, 225) has been refined by the least-squares method with a view to learning more about the effects of weighting and of the number of data on the accuracy with which parameters may be determined in a light-atom–heavy-atom structure. The problems of the effects of other variations, such as in the form factors or in the form of the temperature factor, were not considered. An individual isotropic temperature factor was assigned to each of the eighteen atoms (excluding hydrogen) which are in the asymmetric quarter cell ($P2_1/n$). The refinements were carried out on the following sets of data: All data used and weighted inversely proportional to the estimated variance due to observational error (J. A. Ibers, *Acta Cryst.* (1956), **9**, 967) (*W*Mo); all data used and weighted equally (*U*Mo); only data within the copper limit used and weighted as above (*W*Cu); only copper data used and weighted equally (*U*Cu). For *W*Mo and *U*Mo the number of input data was 6,254; for *W*Cu and *U*Cu it was 2,190.

A number of interesting features were noted in the results of these refinements. For example, the parameters determined from the four sets of refinements exhibit no differences which are more than possibly significant on the basis of the usual statistical tests. The standard deviations of the heavy-atom parameters increased in the expected order *W*Mo, *U*Mo, *W*Cu, *U*Cu, while the standard deviations of a typical oxygen increased in the order *W*Mo, *W*Cu, *U*Mo, *U*Cu. These and other trends in the refinements will be described and discussed in detail.

2·6. C. A. Taylor. *A method for locating molecules of known orientation.*

The method described earlier (C. A. Taylor, *Acta Cryst.* (1954), **7**, 757) has now been systematized so that the results are expressed as a contour map, the position of the molecule being indicated by the deepest minimum.

The basis of the method, which can be applied to any kind of molecule—planar or non-planar—and to any two-dimensional space group, can best be explained in terms of structure-factor graphs. W. L. Bragg & H. Lipson (*Z. Kristallogr.* (1936), **95**, 323) describe the use of contoured graphs showing the combined contribution to a particular reflexion of a particular atom with its symmetrically-related partners as it is moved about the unit cell. A similar graph could be prepared to show the combined contribution to a particular reflexion of a molecule and its symmetrically-related partners. If such a graph were prepared for a reflexion with an observed intensity zero, then the locus of possible positions of the molecule —defined in terms of some arbitrary point chosen within the molecule and used in calculating the graph—would be the zero contour of the graph. If the graphs for about 6–8 zero or weak reflexions were prepared and superimposed and a new graph was prepared with contours representing the sum of the moduli of the separate graphs, the position of the molecule most nearly satisfying *all* reflexions would be indicated as the minimum point on this map. A simple technique, using Beevers–Lipson strips and closely resembling a Fourier synthesis for a simple structure, has been derived for producing this final graph directly.

The method is not intended to be completely objective; the choice of reflexions used is important and, with care in this choice, the method can be used to fix the positions of portions—a benzene ring for example—of a molecule when the remainder is unknown. The choice of reflexions is simplified if the method is used in conjunction with optical-transform methods—although this is by no means essential.

The advantages of the method are that the final result shows the 'pseudo-homometric' solutions as well, the deepest minimum being the correct one. Non-zero reflexions if necessary may be used but this is rarely necessary. Applications to known and unknown structures will be described.

The method recently described by V. Vand & R. Pepinsky (*Z. Kristallogr.* (1956), **108**, 1), although superficially similar, has a different range of applications. Use is made of all reflexions and the method is completely objective. The method now described may be of greater use in the early stages when the precise shape of the molecule has not been defined; the method of Vand & Pepinsky may be of greater use in the later stages.

2·7. L. V. Azároff. *The effect of substructure in crystals on their Fourier transforms and Patterson representations.*

If the atoms in a crystal are arranged on the points of a sublattice of the true lattice, then the Fourier transform of such a crystal structure can be represented by the product of the transform of the sublattice with the transform of the substructure. The effect of the sublattice is to impose a limitation on the *magnitude* of the Fourier transform that varies cosinusoidally in reciprocal space.

The consequence of this is that the first zone of the Fourier transform, bounded in reciprocal space by the node occurring halfway between the first two maxima of the sublattice transform, is the transform of the substructure multiplied by a constant which can be thought of as the 'zero order' transform of the sublattice. The second zone of the Fourier transform, bounded by the nodes occurring halfway between the first and second maxima, and the second and third maxima of the sublattice transform, is the transform of the substructure multiplied by the first-order transform of the sublattice. Since this is the same as the Fourier transform of the crystal structure, except for scale, a Fourier series, using the reciprocal lattice point sampling of this zone of the transform for coefficients, is proportional to the crystal structure.

The effect of a substructure on the Fourier transform of a crystal is illustrated by means of one-dimensional analogues and two-dimensional projections of real crystal structures. It can be shown that the crystal structure need not conform to the sublattice exactly, i.e. the part of the structure associated with each sublattice point can be different, and the periodicity of the sublattice need not be exact. It is possible, therefore, to observe this effect in both ionic and molecular crystals.

The Patterson representation of a crystal structure that is based on a substructure is characterized by the

presence of relatively high maxima corresponding to the periods of the substructure. The presence of these maxima is undesirable since they tend to mask the maxima representing individual interatomic vectors. The presence of a substructure in a crystal also can be recognized directly by inspection of the weighted reciprocal lattice, which shows a damped cosinusoidal variation emanating radially from the origin. It is possible, therefore, to divide the reciprocal lattice into zones bounded by the nodes between adjacent maxima in this cosinusoidal envelope.

It can be shown that if, instead of the autocorrelation function suggested by Patterson, we use a cross-correlation function,

$$A(X, Y, Z) = \iiint \varrho_{\mathrm{II}}(x, y, z)\varrho(x+X, y+Y, z+Z)\,dx\,dy\,dz\,,$$

where $\varrho_{\mathrm{II}}(x, y, z) = \varrho(x, y, z) - \varrho_{\mathrm{I}}(x, y, z)$, and the subscripts denote the different zones in the Fourier transform, then the undesirable maxima are removed. It is easy to show that

$$A(X, Y, Z) = P(X, Y, Z) - P_{\mathrm{I}}(X, Y, Z)\,,$$

where $P(X, Y, Z)$ is the normal Patterson autocorrelation function and $P_{\mathrm{I}}(X, Y, Z)$ is a Patterson series containing only the terms lying in the first zone.

The cross-correlation function $A(X, Y, Z)$ contains all the maxima corresponding to interatomic vectors present in the autocorrelation function, except that they are modified in scale. Since the successful interpretation of the Patterson representation requires that these maxima can be readily recognized, the slight alteration of their magnitudes is not a serious objection.

A one-dimensional analogue of a crystal structure is first used to demonstrate the principles of this method. Several examples using known crystal structures are also given. Using the cross-correlation function, crystal structures can be deduced directly from their Patterson representations with the aid of the Buerger minimum function.

2·8. W. Hoppe. *Die 'Faltmolekülmethode' — eine neue Methode zur Bestimmung der Kristallstruktur bei ganz oder teilweise bekannter Molekülstruktur.*

Bei bekannter Molekülstruktur hat sich die Fouriertransformmethode als schnelle und anschauliche Methode sehr bewährt. Es liegt ihr der Gedanke zu Grunde, 'moleküleigene' (gegen Translationen und Rotationen im Kristallgitter invariante) Funktionen im reziproken Raume aufzubauen und diese (wegen der bekannten Molekülstruktur bekannten) Funktionen als 'Bausteine' für den Aufbau der Gewichtsverteilung im reziproken Raume zu benutzen. Leider hat die Fouriertransformmethode eine Reihe prinzipieller Nachteile:

(1) Die Fouriertransforme sind komplexe Funktionen; ihre Überlagerung muss daher vektoriell erfolgen, was selbst im zentrosymmetrischen Fall zumindest die Berücksichtigung des Vorzeichens erforderlich macht.

(2) Translationen von Molekülen werden als Modulationen der Fouriertransforme mit Sinuswellen in unübersichtlicher Weise abgebildet.

(3) Ist die Molekülstruktur nicht genau bekannt — sodass mehrere Molekülmodelle zur Diskussion stehen — so müssen von jedem Modell neue Fouriertransforme berechnet werden, was langwierig und umständlich ist, wenn nicht spezielle Geräte (z. B. optische Interferometer nach Lipson–Taylor) zur Verfügung stehen.

Wir haben daher eine neue Methode ausgearbeitet, welche auf eine Auswertung von Pattersondiagrammen hinausgeht, wobei jedoch analog wie bei der Fouriertransformmethode kristallinvariante 'moleküleigene' Funktionen im Kristallraum (Faltmoleküle) als Bausteine zur Zusammensetzung der — nur einmal zu berechnenden — Pattersonstruktur benutzt werden. Ihr Vorteil ist:

1. Die Faltmoleküle sind reell und positiv, ihre Überlagerung ist daher rein additiv.
2. Translationen werden wieder als Translationen abgebildet.
3. Die Faltmolekülkonstruktion ist — ähnlich wie die Konstruktion einer Patterson — sehr einfach und kann schnell auch für mehrere Molekülmodelle durchgeführt werden.

Die Faltmolekülmethode hat sich bei der Bestimmung einer Kristallstruktur eines Moleküls unbekannter Konstitution (Biflorin, $C_{20}H_{20}O_3$) bereits gut bewährt.

Gegeben sei die Elektronendichte eines Molekülkristalles mit n Molekülen $\varrho(x, y, z)$. Wir zerlegen nun die Elektronendichte in n Bestandteile $\varrho_k(x, y, z)$, welche den einzelnen Molekülen entsprechen, wobei wir jedem Molekül einen eigenen Molekülursprung (x_k, y_k, z_k) zuordnen:

$$\varrho(x, y, z) = \sum_{k=1}^{n} \varrho_k(x-x_k, y-y_k, z-z_k)\,.$$

Dann ist bekanntlich die Pattersonfunktion gleich dem Faltungsprodukt von $\varrho(x, y, z)$ mit $\varrho^*(x, y, z)$

$$\varrho^*(x, y, z) = \varrho(\bar{x}, \bar{y}, \bar{z})\,.$$

Dieses errechnet sich in unserem Fall zu

$$\widehat{\varrho\varrho^*} = \sum_{k=1}^{n} \sum_{k'=1}^{n} \widehat{\varrho_{k(x-x_k,\, y-y_k,\, z-z_k)}\varrho^*_{k'}}$$

$$\widehat{\varrho\varrho^*} = \sum_{\substack{k=1 \\ k=k'}}^{n} \sum_{k'=1}^{n} u_{kk'(x,y,z)} + \sum_{\substack{k=1 \\ k\neq k'}}^{n} \sum_{k'=1}^{n} v_{kk'(x-x_k+x_{k'},\, y-y_k+y_{k'},\, z-z_k+z_{k'})}$$

mit

$$u_{kk'} = \widehat{\varrho_{k(x,y,z)}\varrho^*_{k(x,y,z)}} \text{ für } k = k'\,,$$

$$v_{kk'} = \widehat{\varrho_{k(x,y,z)}\varrho^*_{k'(x,y,z)}} \text{ für } k \neq k'\,.$$

Das Resultat hat, wie hier nicht weiter gezeigt werden kann, eine sehr anschauliche Bedeutung. Es beschreibt eine Patterson der Molekülursprungsstruktur im Kristall, in welcher jedoch statt der Pattersonpunkte die Faltungsprodukte $\widehat{\varrho_{k(x,y,z)}\varrho^*_{k'(x,y,z)}}$ der zu den entsprechenden Molekülursprungsvektoren gehörenden Molekülpaare aufgehängt sind. Die erste Teilsumme entspricht hierbei dem Nullmaximum der Molekülursprungspatterson.

Wir bezeichnen nun das Faltprodukt von zwei Molekülen als 'Faltmolekül'. Die erste Teilsumme enthält n Faltmoleküle, welche durch Faltung jedes Moleküls mit seinem, durch eine Symmetriezentrum erzeugten Abbild entstehen. Sie sind also nichts anderes als die Pattersonstrukturen der einzelnen Moleküle. Wir bezeichnen diese Strukturen als Faltmoleküle erster Art. Sie sind invariant gegen Translationen im Kristallgitter und werden daher im Anfangstadium der Analyse zur Bestimmung der

Rotationsparameter der Moleküle verwendet. (Diese Arte der Auswertung entspricht bis zu einem gewissen Grade der bekannten Diskussion des inneren Bereiches einer Pattersonsynthese.) Wesentlich für die neue Methode sind die n^2-n Faltungsprodukte zwischen *verschiedenen* Molekülen, welche als Faltmoleküle zweiter Art bezeichnet werden sollen. Sie können erst nach Bestimmung der Orientierung der Moleküle konstruiert werden. Sie liefern aber dann durch einfache translatorische Verschiebung in der Pattersonstruktur direkt die Pattersonvektoren der Molekülursprünge. Da die Zahl der Moleküle in der Elementarzelle selten vier übersteigt, ist die Ursprungspattersonstruktur meist sehr einfach.

Die Faltmolekülmethode lässt sich auch als eine 'Schweratomtechnik ohne schwere Atome' verwenden. Enthält ein unbekanntes Molekül eine grössere bekannte Gruppe, so kann nach dem oben angegebenen Verfahren diese Gruppe als 'schweres Atom' verwendet werden. Man hat als ersten Schritt der Analyse nur statt der Orte der Pattersonmaxima der schweren Atome zunächst die Orientierung der Faltmoleküle erster Art der bekannten Gruppe und anschliessend die Orte der Faltmoleküle zweiter Art in der Pattersonstruktur aufzusuchen. Hierbei ist es — im Gegensatz zu den Superpositionsmethoden — besonders günstig, wenn die verwendete Gruppe möglichst viele zufällige Koinzidenzen in den Faltungsprodukten aufweist (also z. B. ein aromatisches System darstellt), da die dann auftretenden sehr charakteristischen Faltmoleküle mit Mehrfachmaximus hohen Gewichtes ihr Auffinden im Pattersondiagramm sehr erleichtert.

2·9. W. Hoppe. *Strukturanalyse über drei- und zwei-dimensionale Schnitte aus doppelten Pattersonfunktionen.*

D. Sayre (*Acta Cryst.* (1953), **6**, 430) hat eine Verallgemeinerung der Pattersonsynthese abgeleitet (doppelte Patterson)

$$\mathrm{DP} = V^2 \sum_H \sum_{H'} U_H U_{H'} U_{(-H-H')} \exp 2\pi i (SR)$$

(U unitäre Strukturfaktoren, H, H' zwei reziproke Gittervektoren, S sechsdimensionaler Gittervektor im reziproken Raum der DP mit den Komponenten von H und H', R sechsdimensionaler Ortsvektor in der DP) in welcher ein Maximum

$$\mathrm{DP}_{(x_{j'}-x_{j''},\, y_{j'}-y_{j''},\, z_{j'}-z_{j''},\, x_j-x_{j''},\, y_j-y_{j''},\, z_j-z_{j''})}$$

anzeigt, dass irgendein Atom $I''_{(x_{j''} y_{j''} z_{j''})}$ von einem Atom $I'_{(x_{j'}, y_{j'}, z_{j'})}$ um einen Vektor $(x_{j'}-x_{j''},\, y_{j'}-y_{j''},\, z_{j'}-z_{j''})$ und gleichzeitig von einem Atom $I_{(x_j, y_j, z_j)}$ um einen Vektor $(x_{j'}-x_{j''},\, y_{j'}-y_{j''},\, z_{j'}-z_{j''})$ entfernt ist. Die DP kann im Gegensatz zur einfachen Patterson nicht exakt berechnet werden, da die Phasen der Produkte $U_H U_{H'} U_{(-H-H')}$ unbekannt sind; doch gelten für zentrosymmetrische Strukturen die bekannten Wahrscheinlichkeitrelationen von Sayre–Cochran–Zachariasen, sodass eine Berechnung der DP mit durchwegs positivem Vorzeichen zur näherungsweisen Berechnung der DP führen muss.

Wir haben nun gezeigt, dass die DP bereits die Lösung der Kristallstruktur in sich enthält und dass diese Lösung gewonnen werden kann, ohne dass vollständige sechsdimensionale (oder vier-dimensionale) Reihen berechnet werden müssen, sodass die Anwendung der DP in der praktischen Strukturanalyse entgegen einer von Sayre geäusserten Vermutung als nützlich erscheint. Legt man nämlich einen dreidimensionalen Schnitt in der 'Höhe' $(x_{j'}-x_{j''},\, y_{j'}-y_{j''},\, z_{j'}-z_{j''})$ durch die sechs-dimensionale DP, so erhält man unmittelbar die Kristallstruktur mit dem Atom J'' als Ursprung, vorausgesetzt, dass der so gewählte Vektor $J'-J''$ singulär ist. In der praktischen Durchführung muss man also analog wie bei den Superpositionsmethoden mit der Auswahl eines singulären Maximums in einer Pattersonsynthese beginnen.

Bei Verwendung n-zähliger Pattersonmaxima erhält man n-fache Überlagerungen der Struktur. Besonders aussichtsreich dürfte sich das Verfahren bei Vorliegen von wenigen schweren Atomen gestalten, da einerseits das Auffinden von singulären Schweratommaxima einfach ist und da andererseits das Gewicht der Atombilder im entsprechenden DP-Schnitt besonders gross ist (das Quadrat der Elektronenzahl des schweren Atoms tritt als Faktor auf). Die Anwendung der Methode mit schweren Atomen besitzt grundsätzliche Vorteile gegenüber der gebräuchlichen Schweratomtechnik, da Vorzeichenrelationen zusätzlich eingehen.

In einer empfehlenswerten Variante werden die (auf das Symmetriezentrum als Ursprung transformierten) Phasen eines DP-Schnittes, und die direkt gemessenen Absolutwerte der Strukturfaktoren für die erste Fouriersynthese benutzt.

Die Berechnung der Fourierkoeffizienten des DP-Schnittes kann leicht automatisiert werden; die Anzahl der Glieder, welche einen Koeffizienten des Schnittes additiv zusammensetzen, ist von der Grössenordnung des Strukturfaktorenkörpers. Da jedoch die Vorzeichenrelationen nur bei den grösseren Strukturfaktorenprodukten mit ausreichender Wahrscheinlichkeit gelten, kann die Zahl der Glieder der DP sehr stark reduziert werden.

Es existieren auch 'gemischte Schnitte' der DP, welche ebenfalls die Struktur direkt wiedergeben.

2·10. M. G. Rossmann & H. M. M. Shearer. *Some improvements on the method of generalized projections.*

A technique known variously as a 'generalized projection' or a 'weighted density' method has been developed in recent years. The three-dimensional electron density is weighted by an arbitrary function in such a manner as to make most terms in a three dimensional summation disappear (C. J. B. Clews & W. Cochran, *Acta Cryst.* (1949), **2**, 46; R. F. Raeuchle & R. E. Rundle, *Acta Cryst.* (1952), **5**, 85; W. Cochran & H. B. Dyer, *Acta Cryst.* (1952), **5**, 634; R. M. Curtis & R. A. Pasternak, *Acta Cryst.* (1955), **8**, 675). This reduces the calculations to manageable size on desk calculating machines, while at the same time some of the three-dimensional character is maintained. The weighting function which has so far been used exclusively has the effect of producing a summation over all structure factors in one layer line. There are in general always two possible generalized projections of, say, the (hKl) planes, K being constant: the cosine and the sine series. These are so called because the *generalized density* of atoms, σ_K, is multiplied by $\cos 2\pi Ky$ or $\sin 2\pi Ky$, respectively. The product $\sigma_K \cos 2\pi Ky$ or $\sigma_K \sin 2\pi Ky$ will be termed the *weighted generalized density*.

Generalized projections have been employed on a number of occasions but have never been utilized to obtain an *accurate* measure of the co-ordinate parallel

to the direction of projection (H. B. Dyer, *Acta Cryst.* (1951), **4**, 42; J. Zussman, *Acta Cryst.* (1953), **6**, 504; J. C. Speakman, *Acta Cryst.* (1953), **6**, 784; W. H. Zachariasen, *Acta Cryst.* (1954), **7**, 305; J. Fidrichsons & A. McL. Mathieson, *Acta Cryst.* (1955), **8**, 761; D. C. Phillips, *Acta Cryst.* (1956), **9**, 237). The heights of the peaks from which the y co-ordinates have to be calculated in the case of an (hKl) generalized projection are effected by, in order of magnitude: (i) variation of $\cos 2\pi Ky$ and $\sin 2\pi Ky$; (ii) termination-of-series error; (iii) temperature factor of atoms; (iv) random errors in structure factors.

Nothing but greater accuracy in intensity measurements can reduce (iv). A 'difference' technique can virtually eliminate (ii), and a simultaneous employment of the cosine and sine projections can separate out the variables of (i) and (ii). Thus a fairly precise determination of the mean spherical temperature factor and the co-ordinate parallel to the direction of projection for each atom can be made.

If the terms

$$\left[\{|F_o|-|F_c|\}\begin{matrix}\cos\\ \sin\end{matrix}\alpha\right]$$

are used as coefficients in the generalized projection Fourier summations, then the difference D between the observed and calculated weighted generalized densities will be, for the Kth layer,

$D^{SK} = \sigma_{K,o}\sin 2\pi Ky_o - \sigma_{K,c}\sin 2\pi Ky_c$ for the sine series,

and

$D^{CK} = \sigma_{K,o}\cos 2\pi Ky_o - \sigma_{K,c}\cos 2\pi Ky_c$ for the cosine series.

Should the temperature factors for all atoms be known to a fair degree of accuracy, it may be assumed that $\sigma_{K,o} = \sigma_{K,c}$. Hence y_o can be found for each atom by application of usual refinement methods to the generalized projections, when one of the two equations above is used to analyse the weighted generalized density. The choice of the equation is determined by the value of the angle $2\pi Ky$. For $2\pi Ky$ near 0 or π sine varies rapidly with y, hence the first equation has greater sensitivity. On the other hand, if the temperature factor is not known accurately, then $\sigma_{K,o}$ will not be known accurately either. By using the above two equations simultaneously both $\sigma_{K,o}$ and y_o can be found.

The above considerations necessitate the determination of the quantities D^S and D^C at atomic sites. Therefore the calculations can be simplified by computing the difference densities at atomic centers only, thus reducing to less than one quarter of the time taken to determine D^C and D^S with either Beevers–Lipson strips or Robertson masks. However, the computation of these functions over the whole asymmetric unit permits the simultaneous refinement of the x and z as well as the y co-ordinate and temperature factor for each atom. It can be shown that the gradient of the function $(D^{SK}\sin 2\pi Ky_c + D^{CK}\cos 2\pi Ky_c)$ is proportional to the required shift of an atom in any given direction, while its magnitude is proportional to $(\sigma_{K,o}-\sigma_{K,c})$, which is a measure of the temperature-factor adjustment necessary for each atom. This treatment of the (hKl) planes is analogous to a least-squares refinement of the same terms when all observed structure factors are given a weight proportional to the reciprocal of their scattering factors, and all unobserved terms are taken to have zero weight.

The above equations have been used for the refinement of the overcrowded aromatic hydrocarbons 1:9—5:10 di*peri*naphthylyne anthracene and dinaphtho (7′:1′—1:13)(1″:7″—6:8) peropyrene (M. G. Rossmann, (1956), PhD. Thesis, University of Glasgow; J. M. Robertson *et al.* (1957), § 7, No. 23). Projections down the a or c crystallographic axes would view these roughly planar molecules lying on their edge. The generalized projections of the $(h1l)$ reflections showed the nature and magnitude of the buckling caused by overcrowding in both cases. The method has also been applied to determine the degree of planarity of the hydrocarbon 2:3—8:9 dibenz perylene (Rossmann, *loc. cit.*; Robertson *et al.*, *loc. cit.*). The $(h0l)$ and $(h1l)$ planes were used. Thus the amount of experimental data was very considerably increased over that available in the $(hk0)$ and $(0kl)$ zones; and, since the b axis was short, resolution was good. The estimated standard deviation of the y co-ordinates was 0·025 Å. Agreement of bond lengths with molecular-orbital calculations (D. Watson, (1956), B. Sc. Thesis, University of Glasgow) was within experimental error. A generalized-projection refinement of some upper layer lines is in progress for the compound azulene (J. M. Robertson & H. M. M. Shearer, (1957), § 7, No. 27).

2·11. J. M. Cowley & A. F. Moodie. *Possibilities for the direct observation of crystal structures.*

The recent development of a new theoretical approach to problems of the physical optics of light and electrons (Cowley & Moodie, in the Press) has allowed the examination and evaluation of several schemes whereby information on the structure of crystals may be derived from an examination of images formed in an electron microscope. The theoretical results have been confirmed by experiments with visible light.

A very thin crystal is, in effect, a phase grating for electrons. An in-focus image of it obtained with an ideal electron microscope would have almost zero contrast. If the crystal were illuminated by a point source of electrons a set of 'Fourier images' identical with the normal 'in-focus' image, and so having zero contrast, would be observed at positions on either side of the crystal given by $1/Rq + 1/R = \nu a^2/\lambda$, where Rq and R are the distances of the source and the plane of observation from the crystal, a is the lattice constant and ν is an integer. For ν non-integral, amplitude-contrast images occur with intensity distributions related to, but not identical with, the phase distribution due to the crystal. For example, for ν nearly integral the intensity distribution corresponds to the second differential of the phase distribution; for ν half-integral the intensity distribution corresponds to the phase distribution with even-numbered Fourier components suppressed.

The magnification of the Fourier images, $(Rq+R)/Rq$, may be made quite large by placing the source close to the crystal. The possibility therefore exists of obtaining intensity-modulated images of known relation to the crystal lattice on a magnified scale. These images may then be further magnified with a normal electron microscope. Nor is a point source of electrons necessary. High-resolution magnified images may be obtained from sources very much larger than the unit-cell dimensions, provided that the edges of the source are sharply defined.

These effects will be illustrated by photographs of Fourier images of a phase grating, using visible light.

If two very thin crystals are superimposed so that their unit-cell axes differ slightly in magnitude or direction, a further effect of interest occurs. Although both crystal lattices, acting as phase gratings, would be invisible in an ideal electron microscope, it can be shown that scattering of electrons in first one crystal and then the other will give rise to a periodic intensity modulation with unit-cell dimensions very much larger than those of the crystals. The intensity distribution is given by the square of the convolution of one crystal lattice with the centro-inversion of the other crystal lattice. In particular, if the crystals are identical, the intensity distribution corresponds to the square of the Patterson function. If one of the crystals is of unknown structure and the other of known structure, it may be possible to deduce the unknown structure by a process of image seeking on the convolution function.

The effect is similar to the production of moiré fringes using two optical phase grating. At least a partial confirmation that it occurs with crystals is provided by the observation of fringes in electron microscope images of superimposed crystals, e.g. by Farrant & Rees (in the Press) using molybdenum oxide.

2·12. E. F. Bertaut. *Méthode statistique et probabilité élémentaire en cristallographie.*

Formulation générale du problème: la probabilité élémentaire des positions atomiques est modifiée au fur et à mesure que l'information sur la structure augmente. Des exemples pratiques sont donnés.

2·13. A. I. Kitajgorodskij. *Théorie de corrélation entre les facteurs de structure et les méthodes directes de l'analyse de structure.*

On peut obtenir expérimentalement une très intéressante règle: le produit structural $X_{HK} = \hat{F}_H\hat{F}_K\hat{F}_{H+K}$ est positif dans la plupart des cas; et plus grande est la valeur absolue du produit structural, plus grande est la part de X_{HK} positif. Une première définition de cette loi a été donnée par moi en 1953 (une même explication est donnée dans le travail de Karle & Hauptman de la même année); nous avons montré qu'une loi pouvait être déduite si on suppose une distribution uniforme des arguments de fonctions trigonométriques qui entrent dans les formules des facteurs de structure.

Cette supposition faite permet de trouver la fonction de probabilité de la valeur X_{HK} et ensuite de montrer qu'elle a un maximum dans le rayon positif.

Dans le travail cité de 1953 j'ai montré que la possibilité de signe positif du produit structural peut être donnée par l'expression $W_+ = (1+\exp[-2NX_{HK}])^{-1}$, où N est le nombre effectif des atomes dans la maille.

On appelle statistiques les théories de cette sorte.

L'opinion a été émise qu'avec les théories statistiques il est possible d'expliquer la loi de prédominance de la valeur positive de X_{HK} et que les idées statistiques doivent faire le fond de la méthode directe de l'analyse de structure.

Des considérations plus approfondies nous montrent que cette opinion est erronée. Les théories statistiques ont un rôle prépondérant seulement dans le cas de petits X_{HK}. En ce qui concerne les grandes valeurs absolues de X_{HK} (et on doit souligner que seulement les grands X_{HK} ont un intérêt pratique), la loi de prédominance de la valeur positive de X_{HK} a une explication très différente et de plus une explication stricte, qui ne demande aucune proposition ou hypothèse.

Particulièrement, la loi de prédominance est juste dans le cas où tous les atomes sont dans des positions spéciales et quand les arguments (**Hr**) peuvent prendre un tout petit nombre de valeurs discrètes.

Dans un travail précédent j'ai montré que le produit structural est incontestablement positif si $|X_{HK}| > \frac{1}{8}$. Mais dans des conditions moins rigides il y a aussi une tendance qui n'a pas de nature statistique (c'est-à-dire qu'elle n'a pas de corrélation avec le caractère de distribution des coordonnées des atomes dans la maille) qui mène à la loi de prédominance de la valeur positive de X_{HK}.

La corrélation la plus générale entre les facteurs structuraux est atteinte dans la condition que la déterminante D_m soit positive:

$$D_m = \begin{vmatrix} 1 & \ldots & & \\ F_H & 1 & \ldots & \\ F_K & F_{K-H} & 1 & \ldots \\ F_L & F_{L-H} & F_{L-K} & 1 \ \ldots \\ . & . & . & . \\ . & . & . & . \\ . & . & . & . \\ . & . & . & . \\ . & . & . & . \end{vmatrix} > 0 .$$

La déterminante peut être écrite dans la forme d'une série bien connue. On a donc

$$1 - \sum_H \hat{F}_H^2 + \sum_{H,K} \hat{F}_H\hat{F}_K\hat{F}_{H+K} - \ldots > 0 .$$

Les termes écrits sont les plus essentiels pour la somme. Il est clair que la positivité de la somme peut être obtenue seulement si la plupart des produits structuraux sont positifs. Et encore, on trouve d'après cette formule que tous les produits structuraux sans exception seront positifs si les valeurs de $\hat{F}$ qui composent la déterminante dépassent une certaine limite δ.

Ainsi la méthode directe de détermination des signes des facteurs de structure a pour base les propriétés de la déterminante D_m mais non les idées statistiques sur la distribution des coordonnées atomiques dans la maille.

Nous posons: *la prédominance des valeurs positives des grands produits structuraux n'a aucune correspondance avec les théories statistiques quelles qu'elles soient.*

Si le produit structural n'est pas absolument positif, nous pouvons discuter la question de probabilité de son signe positif.

La question posée d'une façon peu nette et la manière de *laisser de côté* les corrélations absolues entre les facteurs a amené divers auteurs à calculer la densité de probabilité de la valeur du produit structural, au lieu de calculer la probabilité de structure pour qui le produit structural a une valeur donnée.

Les expressions pour la probabilité de signe positif de X_{HK} déduites dans les précédents travaux ne montraient pas qu'il y a une valeur critique de X quand la probabilité se réduit à un.

L'expression correcte pour la probabilité du signe positif du produit structural est $W_+ = 1/(1+\varepsilon)$, où

$$\varepsilon = \sqrt{\left\{\frac{1-\hat{F}_H^2-\hat{F}_K^2-\hat{F}_{K+H}^2-2\hat{F}_H\hat{F}_K\hat{F}_{K+H}}{1-\hat{F}_H^2-\hat{F}_K^2-\hat{F}_{K+H}^2+2\hat{F}_H\hat{F}_K\hat{F}_{K+H}}\right\}} \times \exp\left[-2N.\hat{F}_H\hat{F}_K\hat{F}_{K+H}\right].$$

Vraies ou fausses, malgré tout les formules d'origine statistique ont, pensons-nous, une importance secondaire.

Les méthodes directes avec lesquelles on peut chercher les signes des facteurs de structure sont effectives seulement dans le cas où un grand nombre de produits structuraux ont incontestablement des signes positifs.

Les bons résultats donnés par la méthode directe ne sont aucunement liés aux théories statistiques.

A mon avis, le travail avec méthodes directes doit être accompli par composition des déterminantes D_m de toutes sortes. Les signes justes des facteurs de structure ne doivent pas donner une valeur négative à des déterminantes quelconques.

J'ai montré que la règle $X_{HK} > 0$ si $|X_{HK}| > \frac{1}{8}$ peut être élargie aux déterminantes de n'importe quel rang. Si la déterminante de rang m est composée avec F pour qui $|F| > \delta_m$, alors tous les produits structuraux qui n'entrent pas dans la déterminante sont incontestablement positifs.

Les grandeurs δ_m diminuent avec la croissance de m. L'analyse de déterminantes de hauts rangs nous permet de juger de la positivité d'un produit structural cent fois plus petit que $\frac{1}{8}$.

Nous pensons que les méthodes qui permettent de déterminer directement les signes des facteurs de structure joueront un grand rôle dans l'analyse de structure par rayons X, mais l'emploi de machines à calculer électroniques est indispensable.

2·14. I. L. KARLE. *Application of probability methods to p, p'-dimethoxybenzophenone.*

The structure of $(CH_3OC_6H_4)_2CO$ has been investigated by means of the probability methods described by H. Hauptman & J. Karle (*Solution of the Phase Problem.* I. (1953). A. C. A. Monograph). The crystal is monoclinic with $a = 16{\cdot}43$, $b = 16{\cdot}03$, $c = 9{\cdot}62$ Å, $\beta = 100°\ 15'$; $Z = 8$; space group $P2_1/a$, with 30 C, 6 O, and 28 H atoms per asymmetric unit. Copper radiation was used and 5527 independent reflections were measured of which 1261 were assigned zero intensity. The F_o^2 were corrected for vibrational motion and placed on an absolute scale by means of a K curve (J. Karle & H. Hauptman, *Acta Cryst.* (1953), **6**, 473). E values were then obtained from the corrected F_o^2 (J. Karle & H. Hauptman, *Acta Cryst.* (1956), **9**, 635, equation (3·12)).

To facilitate the determination of the phases by probability methods, the E_{hkl} were arranged in order of descending E magnitudes in groups where the indices were *g*0*g*, 0*g*0, *ggg*, *ggu*, *guu*, *gug*, *ugg*, *ugu*, *uug*, *uuu* (g = even, u = uneven). It was immediately apparent from the E values that the reflections with l even were considerably stronger than those with l odd. Furthermore, in the groups *ggg* and *ugu* the reflections with $k = 4, 8, 12, \ldots$ were very much stronger than those with $k = 2, 6, 10, \ldots$ and in the groups *ugg* and *ggu* all the strong reflections had $k = 2, 6, 10, \ldots$. There was no particular pattern for k odd. Since there was this ordered distribution of normalized intensities (E) with respect to the k index, the Σ_1 phase-determining formula for $P2_1/a$ could not be used reliably and the crystal was treated as if it were in $P\bar{1}$.

Using Σ_1 formula for $P\bar{1}$, five *ggg* phases were assigned. No information other than the magnitudes of all the intensities were used to assign these phases. Using the initial five phases and Σ_2 and Σ_3, about 50 additional strong *ggg* phases ($|E| > 2$) were assigned. Three phases were arbitrarily assigned to the largest $|E_{hkl}|$ in *ugg*, *ggu*, and *guu* (see Invariants and Seminvariants (Hauptman & Karle, 1953)). With the 50 known *ggg* phases and the three assigned phases used in Σ_2 and Σ_3, it was possible to assign nearly 220 additional phases from all groups of reflections (with $|E| > 1{\cdot}8$). If machine computing had been available to us it would have been possible to cross-check each of the 270 phases and in addition to assign many more.

A three-dimensional Fourier (with E instead of F_o) was computed using the 270 reflections for which phases were assigned. Even though there was no damping (effects of crystal vibrations are removed from E values) and the sample of data involved only certain of the largest E values, it was quite easy to find the two molecules in the map. The coordinates for the C and O atoms as taken from the map were subjected to a preliminary least-square refinement, using the first 1143 reflections (in increasing order of s) and including all the zero reflections. One vibrational parameter per atom was included. The R factor at present is 0·26. Further refinements are in progress.

The molecules lie near the 202 planes with the benzene rings twisted considerably out of the plane containing the three oxygen atoms. One molecule in the asymmetric unit is approximately related to the other by a shift of $z+\frac{1}{2}$ and a reflection through $y = \frac{1}{8}$.

2·15. J. KARLE. *The phase problem for space group P*1.

The problem of phase determination in space group $P1$ has two main parts. The first is to derive formulas which yield values of the magnitude of the structure invariants (H. Hauptman & J. Karle, *Acta Cryst.* (1956), **9**, 45), i.e. values for special linear combinations of phases which are determined by the intensities alone. The second part involves the determination of the individual phases from the values of the magnitudes of the invariants by means of a procedure which requires the specification of the sign of an invariant in order to choose an enantiomorph, and the specification of the values of three phases, whose indices form a suitable primitive triple, in order to choose an origin.

Formulas for the determination of the magnitudes of structure invariants have been derived by algebraic means (J. Karle & H. Hauptman, *Acta Cryst.* (1957), in the Press) which yield values for $\cos(\varphi_{\mathbf{h}_1}+\varphi_{\mathbf{h}_2}+\varphi_{-\mathbf{h}_1-\mathbf{h}_2})$ directly from the measured X-ray intensities. If a large number of such functions are computed, it is clear that individual phases will occur many times.

The first step after obtaining values for $|\varphi_{\mathbf{h}_1}+\varphi_{\mathbf{h}_2}+\varphi_{-\mathbf{h}_1-\mathbf{h}_2}|$ is to arrange the invariants in groups of four, such as

$$\left.\begin{array}{llllll} \varphi_\alpha & + & \varphi_\beta & + & \varphi_{-\alpha-\beta}, \\ \varphi_{-\alpha} & + & \varphi_\gamma & + & \varphi_{\alpha-\gamma}, \\ \varphi_{-\beta} & + & \varphi_{-\gamma} & + & \varphi_{\beta+\gamma}, \\ \varphi_{\alpha+\beta} & + & \varphi_{-\alpha+\gamma} & + & \varphi_{-\beta-\gamma}. \end{array}\right\}$$

It is seen that the sum of the values for these four must

be zero since $\varphi_\alpha = -\varphi_{-\alpha}$. It turns out that ten such groups of four, involving nineteen different invariants, form a very useful set for carrying out the specifications of enantiomorph and origin, for the determination of the values of the individual phases, and for the improvement of these values by means of least-squares adjustments (Karle & Hauptman, *loc. cit.*).

The formulas for computing invariants and the phase-determining procedure were applied to a theoretical test model consisting of ten atoms per unit cell of space group $P1$. With only a limited calculation involving nineteen invariants composed of twelve different phases, the phases were determined with an average error of about 0·06 radians.

The main formulae used in this computation have been coded for SEAC (digital computer at the National Bureau of Standards) by Mr Peter O'Hara, to whom we are indebted.

2·16. H. HAUPTMAN. *A unified algebraic approach to the phase problem: space group* $P\bar{1}$.

For space group $P\bar{1}$ the normalized structure factor $E_{\mathbf{h}_1}$ is the special case $q = 1$ of the more general definition

$$E_{\mathbf{h}_1\mathbf{h}_2\ldots\mathbf{h}_q} = \frac{2^q}{N^{q/2}} \sum_{j_1 \neq j_2 \neq \ldots \neq j_q}^{N/2} \prod_{i=1}^{q} \cos 2\pi \mathbf{h}_i \cdot \mathbf{r}_{j_i}, \quad (1)$$

where $\mathbf{r}_{j_i}$ is the position vector of the j_ith atom and it is assumed that the structure consists of N identical point atoms per unit cell. By computing $\prod_{i=1}^{2} E_{\mathbf{h}_i}$ we readily express $E_{\mathbf{h}_1\mathbf{h}_2\ldots\mathbf{h}_q}$ in terms of normalized structure factors, e.g.

$$E_{\mathbf{h}_1\mathbf{h}_2} = E_{\mathbf{h}_1}E_{\mathbf{h}_2} - \frac{1}{N^{1/2}}(E_{\mathbf{h}_1+\mathbf{h}_2} + E_{\mathbf{h}_1-\mathbf{h}_2}). \quad (2)$$

Next, we employ (1) with $q = 1$ to obtain

$$\prod_{i=1}^{4} E_{\mathbf{h}_i} = R_1 + R_2 + R_2^1 + R_3 + R_4, \quad (3)$$

where the R's are first-, second-, third- or fourth-order sums. Replacing $\mathbf{h}_1$ by $\mathbf{h}-\mathbf{k}$, $\mathbf{h}_2$ by $\mathbf{h}_1-\mathbf{k}$, $\mathbf{h}_3$ by $\mathbf{k}$ and $\mathbf{h}_4$ by $\mathbf{k}$, and averaging over all vectors $\mathbf{k}$, we find

$$\langle R_2\rangle_{\mathbf{k}} = \langle R_3\rangle_{\mathbf{k}} = \langle R_4\rangle_{\mathbf{k}} = 0, \quad (4)$$

and (using (2)) obtain expressions for $\langle R_1\rangle_{\mathbf{k}}$ and $\langle R_2^1\rangle_{\mathbf{k}}$ in terms of normalized structure factors. Substituting into (3) we finally obtain

$$E_{\mathbf{h}}E_{\mathbf{h}_1} = \frac{N}{2}\langle E_{\mathbf{h}+\mathbf{k}}E_{\mathbf{h}_1+\mathbf{k}}(E_{\mathbf{k}}^2-1)\rangle_{\mathbf{k}} + \frac{1}{2N^{1/2}}E_{\mathbf{h}+\mathbf{h}_1} + \frac{1}{N^{1/2}}E_{\mathbf{h}-\mathbf{h}_1}, \quad (5)$$

and a similar formula with $\mathbf{h}_1$ replaced by $-\mathbf{h}_1$.

If $E_{\mathbf{h}_1}$ is linearly independent modulo 2 its sign may be specified arbitrarily. Then (5) enables us to obtain the signs of all normalized structure factors $E_{\mathbf{h}}$ which are linearly dependent modulo 2 on $E_{\mathbf{h}_1}$ provided that the average in (5) is taken over all vectors $\mathbf{k}$ linearly dependent modulo 2 on $\mathbf{h}_1$ and provided that the signs of all structure factors which are linearly dependent modulo 2 have already been found. The signs of the latter are obtainable from

$$\left(E_{\mathbf{h}}^2 - \frac{1}{2} + \frac{2}{N}\right)E_{2\mathbf{h}} = \frac{N^{3/2}}{8}\langle (E_{\mathbf{k}}^2-1)(E_{\mathbf{h}+\mathbf{k}}^2-1)(E_{\mathbf{h}-\mathbf{k}}^2-1)\rangle_{\mathbf{k}} + \frac{1}{N^{1/2}}(2E_{\mathbf{h}}^2 + E_{2\mathbf{h}}^2 - 2) + \frac{1}{N^{1/2}}E_{\mathbf{h}}E_{3\mathbf{h}} - \frac{1}{N}E_{4\mathbf{h}}, \quad (6)$$

an equation derivable from $\prod_{i=1}^{6} E_{\mathbf{h}_i}$ by an analysis similar to that used in deriving (5).

Several other formulas are readily obtained in the same way, e.g., the well known

$$E_{\mathbf{h}} = N^{1/2}\langle E_{\mathbf{k}}E_{\mathbf{h}+\mathbf{k}}\rangle_{\mathbf{k}}, \quad (7)$$

from which the sign of a structure factor $E_{\mathbf{h}}$, linearly dependent modulo 2 on the pair $E_{\mathbf{h}_1}$, $E_{\mathbf{h}_2}$, may be obtained provided that the signs of $E_{\mathbf{h}_1}$ and $E_{\mathbf{h}_2}$ have been arbitrarily specified (which is permitted if this pair is linearly independent modulo 2), or previously determined.

We conclude that for a structure consisting of N identical point atoms in space group $P\bar{1}$, (5), (6), and (7) enable us to determine the signs of all the structure factors directly from their magnitudes provided that enough of the latter are known to permit the computation of the three averages in (5), (6), and (7) with sufficient precision.

The formulas obtained by the present method duplicate and supplement those derived by probability methods. The supplementary formulas are quite powerful and can be expected to facilitate the determination of phases. Furthermore these equations show that many of the formulas previously obtained have, under certain circumstances, exact, rather than merely probable validity.

2·17. G. VON ELLER. *Recherche systématique des signes des facteurs de structure par les inégalités angulaires.*

Ayant remplacé le déterminant général de Karle & Hauptman (d'éléments U_{ij} précédés des signes arbitraires) par le tableau des arccos U_{ij}, on 'condense' l'espace proprement euclidien ainsi défini en se servant d'un réseau stéréographique.

Après chaque incompatibilité on change un signe.

Description du procédé; technique d'économie de calculs; détermination immédiate des éléments responsables de chaque incompatibilité; possibilités d'adaptation au calcul électronique.

2·18. A. KLUG. *Joint probability distribution of structure factors and the phase problem.*

The probability distribution of a structure factor may be calculated by making use of a relatively simple and powerful statistical method for expressing the probability distribution of a sum of random variables in terms of the cumulants of the distribution of one random variable. This method has been extended to develop formulae for the multivariate case, and these may then be used to obtain expressions for the joint probability distribution

of any desired set of structure factors. The work thus represents an extension of that of Karle & Hauptman, Cochran & Woolfson and Bertaut. The expressions are obtained in the form of a strictly asymptotic series in powers of $1/N^{\frac{1}{2}}$ (where N is the number of atoms in the unit cell) in the case of equal atoms, and in terms of related quantities in the general case. In this way the physical content of the statistical approach to the phase problem, and the range of validity of the methods that have been used is clearly brought out.

In the course of the work a new inequality relating U_h, $U_{h'}$ and $U_{h+h'}$ was obtained.

2·19. C. M. Mitchell. *Phase determination in noncentric crystals by the two-wavelength method.*

In a recent paper Y. Okaya & R. Pepinsky (*Phys. Rev.* (1956), **103**, 1645) have shown that, in a noncentric crystal, using radiation scattered anomalously by one or more atoms in the unit cell, two possible solutions are obtained for the components of the structure amplitude of the normal scattering atoms, provided the positions of the anomalously scattering atoms are known. Several methods of choosing one solution are proposed, including the use of a second incident wavelength producing normal scattering for all atoms.

In the present communication the method of using two incident radiations, producing anomalous scattering, is examined. Linear equations are obtained in $A^{\text{n.s.}}$ and $B^{\text{n.s.}}$, the components of the structure amplitude for normal scattering by all atoms in the crystal; these equations give a single valued solution for $A^{\text{n.s.}}$ and $B^{\text{n.s.}}$, where the positions of the anomalous scattering atoms are known, in terms of sums and differences of the observed structure factors $F^2_{\mathbf{h}}$ and $F^2_{-\mathbf{h}}$ for the reflections $\mathbf{h}(hkl)$ and $-\mathbf{h}(\bar{h}\bar{k}\bar{l})$. Criteria for the choice of optimum wavelengths for any crystal can be set up from these relations.

The method is most powerful either when two radiations exist which will excite only one atom in the unit cell; or when one radiation producing normal scattering by all atoms can be combined with one exciting a single atom in the cell. In both cases a direct solution of the phase of the reflection is obtained. Considering the anomalous scattering atom as the cell origin, the components of the structure amplitude are:

$$B^{\text{n.s.}}_{\mathbf{h}} = \frac{F^2_{\mathbf{h}} - F^2_{-\mathbf{h}}}{4f''_a}$$

$$A^{\text{n.s.}}_{\mathbf{h}} = \frac{\overline{F}^2_{\mathbf{h}\lambda_1} - \overline{F}^2_{\mathbf{h}\lambda_2} + (\Delta f'_a)^2_{\lambda_2} - (\Delta f'_a)^2_{\lambda_1} + (f''_a)^2_{\lambda_2} - (f''_a)^2_{\lambda_1}}{2(\Delta f'_{a\lambda_1} - \Delta f'_{a\lambda_2})}$$

where $\overline{F}^2_{\mathbf{h}\lambda_j}$ is the mean square value:

$$\overline{F}^2_{\mathbf{h}\lambda_j} = \tfrac{1}{2}(F^2_{\mathbf{h}\lambda_j} + F^2_{-\mathbf{h}\lambda_j}) ,$$

and $\Delta f'_{a\lambda_j}$ and $f''_{a\lambda_j}$ are the in-phase and out-of-phase anomalous scattering increments to the normal atomic scattering factor f^0_a, for wavelength λ_j.

The conditions for optimum values of the two incident wavelengths are that the out-of-phase component f''_a be large for one wavelength, and that the difference in in-phase components $(\Delta f'_{a\lambda_1} - \Delta f'_{a\lambda_2})$ be a maximum.

2·20. R. Pepinsky, Y. Okaya & Y. Takeuchi. *Theory and application of the $P_s(\mathbf{u})$ function and anomalous dispersion in direct determination of structures and absolute configuration in non-centric crystals.*

The use of the $P_s(\mathbf{u})$ function (R. Pepinsky & Y. Okaya, *Proc. Nat. Acad. Sci. U.S.* (1956), **42**, 286) for direct determination of the structures and absolute configurations of non-centric crystals is illustrated by the analysis of zinc and cobaltous L-aspartate trihydrates, cobaltous L-glutamate, 2*d*-$[Co(en)_3]Cl_3.NaCl.6H_2O$, *d*-$[Co(en)_3]Cl.$*d*-tartrate$.5H_2O$, and Ba glycerophosphate. The method does not require the preliminary analysis of the structure except for hand, in contrast with the techniques of Bijvoet *et al.* (cf. A. F. Peerdeman & J. M. Bijvoet, *Acta Cryst.* (1956), **9**, 1012). Use of the $P_s(\mathbf{u})$ function is compared with the more recent method of phase determination of individual structure factor pairs as introduced by Y. Okaya & R. Pepinsky (*Phys. Rev.* (1956), **103**, 1645). Since all pairs $|F_H|^2 - |F_{\bar{H}}|^2$ are used at once in the synthesis, use is immediately made of the over-determination inherent in the Fourier method.

In the usual case of one anomalous scatterer per asymmetric unit, the $P_s(\mathbf{u})$ function corresponds to a Patterson map which has been extensively deconvoluted by a powerful image-seeking technique, to the extent that only peaks corresponding to vectors between anomalous scatterers and normal scatterers appear. The only remaining problem in the reduction of such a map to the equivalent of a density function is that of elimination of the effects of rotational and translational symmetry. This can be accomplished by a final image-seeking operation, which corresponds to application of a simple symmetry operation. Examples of such complete deconvolution are presented.

W. J. Taylor (*J. Appl. Phys.* (1953), **24**, 262) showed that Buerger's minimum function $M(\mathbf{r})$ can be expressed as the difference between a 'sum' function $S(\mathbf{r})$ and the absolute magnitude of a difference function $D(\mathbf{r})$:

$$M(\mathbf{r}) = S(\mathbf{r}) - |D(\mathbf{r})| .$$

Taylor's expressions for $S(\mathbf{r})$ and $D(\mathbf{r})$ must be modified, for the $P_s(\mathbf{u})$ function, to become

$$S_u(\mathbf{r}) = \sum_H [\Delta F^2_H . \sum \cos 2\pi \mathbf{H}.\mathbf{u}_n] \sin 2\pi \mathbf{H}.\mathbf{r} ,$$

and

$$D_u(\mathbf{r}) = \sum_H [\Delta F^2_H . \sum \sin 2\pi \mathbf{H}.\mathbf{u}_n] \cos 2\pi \mathbf{H}.\mathbf{r} ,$$

where $\Delta F_H = |F_H|^2 - |F_{\bar{H}}|^2$, and $\mathbf{u}_n$ is the vector from the origin to an anomalous scatterer. Here $D_u(\mathbf{r})$ is an even function of $\mathbf{r}$. Hence subtraction of $D_u(\mathbf{r})$ from $S_u(\mathbf{r})$ reveals the minimum value of $M_u(\mathbf{r})$ immediately, whatever the sign of $D_u(\mathbf{r})$.

Thus for a non-centric structure the completely deconvoluted function derivable from $P_s(\mathbf{u})$ can be directly computed and contoured on a machine such as X-RAC.

2·21. G. N. Ramachandran. *Determination of phase from anomalous dispersion.*

The paper deals with a new method of determining the phases of reflexions from a non-centrosymmetric crystal, making use of the difference in intensities of the hkl and $\bar{h}\bar{k}\bar{l}$ reflexions. The method can be used provided

the positions of the anomalously scattering atoms can first be determined to a good degree of accuracy. The problems connected with the application of the method are critically discussed and results are presented of its test in one case where the structure is known and another in which it is unknown. The method appears to be highly promising, particularly when it is combined with the isomorphous-replacement method, for the ambiguity in phase determination can then be eliminated.

2·22. G. B. MITRA & G. SANYAL. *A microwave analogue method for the solution of the phase problem.*

A hypothetical model of the atomic structure of the crystal under study is made with microwave antennae simulating the atoms. The polar diagram of each antenna is the same as given by the atomic structure factor at various angles of the atom it simulates. This antenna array is flooded with a beam of microwaves and the diffraction pattern is studied. Coordinates of the antennae are changed till a diffraction pattern identical with the corresponding X-ray diffraction pattern of the crystal under study is obtained. Thus, a trial structure is obtained very quickly. The superiority of this method over other methods lies in that the effects of defects and lattice vibrations can be studied by this method. Structures of aluminium, copper and graphite have been determined by this method.

§ 3. Minerals

3·1. N. V. BELOV. *New silicate structures.*

The epoch-making book in mineralogy by W. L. Bragg on the structure of silicates was entirely absorbed in textbooks on crystal chemistry and mineralogy immediately after its publication. But the contents of corresponding chapters of these books remained unchanged in the following 25 years and particularly do not reflect the big changes in this branch of science made during the last 5–7 years. One of the reasons is that the considerable part of this work on silicate structures has been carried out in USSR and therefore finds its way into the international market with difficulty.

Some of these new silicate structures make some of the classical structures not so unique as they appear in textbooks. Dioptase, $Cu_6[Si_6O_{18}].6\,H_2O$, is, after beryl, another instance of a silicate with sixfold rings of Si tetrahedra. Katapleite, $Na_2Zr[Si_3O_9].2\,H_2O$, is also, after benitoite, the second instance of a silicate with threefold rings $[Si_3O_9]$.

Another representative of silicates with endless chains $[SiO_3]_\infty$ in every respect similar to those in pyroxenes is ramsayite, $Na_2Ti_2Si_2O_9$. Instead of the metasilicate ratio Si:O = 1:3, which is characteristic for pyroxenes, we have in ramsayite Si:O = $1:4\frac{1}{2}$. Three oxygen atoms out of every nine do not participate in the Si–O radical, and the correct formula is $Na_2Ti_2O_3[Si_2O_6]$.

Important is the discovery of another Si–O radical with hexagonal symmetry, which is two-storeyed $[Si_{12}O_{30}]$, in the rare Swiss mineral milarite, $KCa_2(Al_2Be)[Si_{12}O_{30}]$. A reservation about the rarity of this mineral loses its significance after the discovery that similar rings $[(Si, Al)_{12}O_{30}]$ are characteristic for uniaxial (high) cordierites as compared to biaxial (low) cordierites with rings $[(Si, Al)_6O_{18}]$ of the beryl type.

The Si–O radical in orthorhombic (pseudo-hexagonal as cordierite) elpidite $Na_2ZrSi_6O_{15}.3\,H_2O$ is a result of the condensation of two (katapleite) rings $[Si_3O_9]$ into one two-storeyed $[Si_6O_{15}]$ (= $2[Si_3O_9]$–3 O) with the same (pseudo) trigonal symmetry.

'Pyrosilicate' groups Si_2O_7 have been found in a number of minerals. In some of them the existence of these radicals is suggested by the formula itself: cuspidine, $Ca_4[Si_2O_7]F_2$, tilleyite, $Ca_5[Si_2O_7](CO_3)_2$; but in such minerals as ilvaite, epidote, zoisite these groups were a surprise as the formulas of these minerals gave no reasons to suspect their ortho-properties. In ilvaite all Si atoms are in these pyrosilicate groups, but in epidote and zoisite the same structure contains two kinds of radicals: $[Si_2O_7]$ and $[SiO_4]$. The eighth atom O in ilvaite and the twelvth in epidote-zoisite do not enter the Si–O radical, and the corresponding formulas are:

$$CaFe^{\cdots}\,Fe_2^{\cdot\cdot}\,O[Si_2O_7]OH \text{ (ilvaite)}$$

and

$$Ca_2Al_2FeO[SiO_4][Si_2O_7]OH \text{ (epidote).}$$

The chains $[SiO_3]_\infty$ in pyroxenes and ramsayite are identical, but in the pyroxenoid–wollastonite, $CaSiO_3$, we have discovered a radical of the chain type with the same formula $[SiO_3]_\infty$ but with very different geometry. When doubling the pyroxene chain by a plane of symmetry we obtain a lath of amphibole with a formula $4\,SiO_3–O = [Si_4O_{11}]_\infty$, but when doubling the chain of the wollastonite type we obtain a lath of another type, $6\,SiO_3–O = [Si_6O_{17}]_\infty$, which is characteristic for xonotlite $Ca_6[Si_6O_{17}](OH)_2$.

Instead of two classical types of chains (Bragg) we distinguish now six of them (Fig. 1): three with the same formula $[SiO_3]_\infty$ but with different geometries and three doubled types (laths) with formulas: $[Si_2O_5]_\infty$ (sillimanite), $[Si_4O_{11}]_\infty$ (amphiboles), $[Si_6O_{17}]_\infty$ (xonotlite).

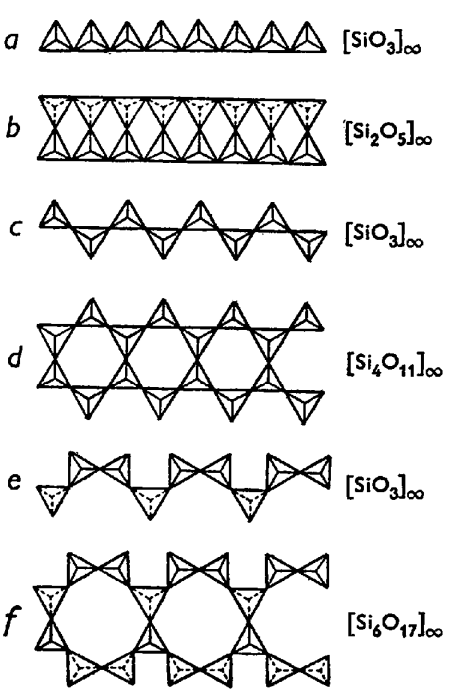

Fig. 1.

The Si–O radicals are strong but not rigid, and accordingly morphological peculiarities of silicates depend on the configurations of cations such as Mg(Fe), Al, on one side and Ca(Na) on another. In all stretched (columnar, needle-like) minerals we find endless columns of Mg(Fe), Al-octahedra or of Ca-octahedra. As a result of very different lengths of edges in these two kinds of octahedra (2·8 and 3·8 Å) different Si–O-radicals arrange themselves along the cation columns: pyroxene and amphibole chains along the edges of Mg(Fe) and Al-octahedra, wollastonite and xonotlite chains (laths) along the edges of Ca-octahedra. In silicates with groups $[Si_2O_7]$ these groups arrange themselves with their axes at right angle to the columns of Al- or Fe-octahedra (ilvaite, epidote (Fig. 2(*a*))) but parallel to the columns of Ca-octahedra (cuspidine, tilleyite (Fig. 2(*b*))).

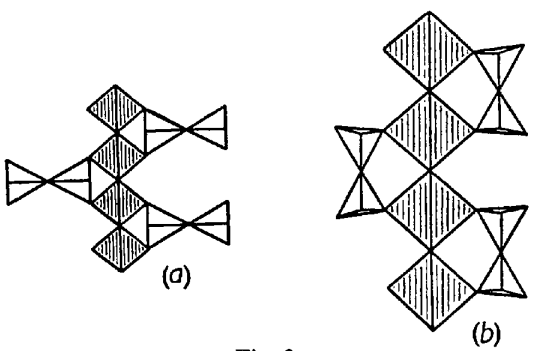

Fig. 2.

When cation-octahedra are arranged in sheets, as in micas and similar minerals, Si-tetrahedra form also sheets; but these sheets are (pseudo) hexagonal with six-fold rings when over sheets of Mg(Fe) and Al-octahedra (Fig. 3(*a*)), but tetragonal with alternating tetragonal and octagonal rings over Ca-octahedra (apophyllite (Fig. 3(*b*))).

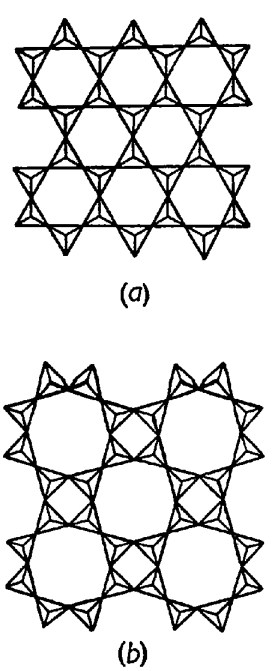

Fig. 3.

As the octagonal meshes of such a net are too large, the net shrinks, the octagonal meshes assume an elongated form, but the small tetragonal meshes do not change and the whole symmetry of the pattern remains tetragonal (Fig. 4).

The following step in Ca minerals is the association (condensation) of these sheets in three-dimensional frameworks also with tetragonal and octagonal meshes which are characteristic for felspars.

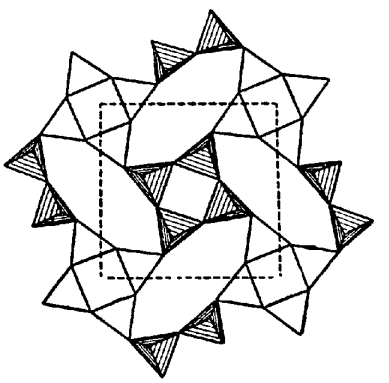

Fig. 4.

The great partition of rock silicates in two categories, melanocratic with high densities and leucocratic with low densities, is entirely determined by the size of cations and their octahedra. The small Mg and Al cations associate with close-packed (pseudo) hexagonal Si–O radicals, whereas the large Ca cations and their octahedra associate with (pseudo) tetragonal Si–O frameworks with large meshes. The size of Mg and Al cations is similar to the sizes of a great many cations, a large part of which are coloured. The (isomorphic) entrance of these cations in (Mg, Al)-minerals results in their melanocratic character. The large size of Ca cations restricts the possible isomorphic substitutions only to Na and K and hence leucocratic characteristics of felspars and a small number of similar minerals.

Two other instances which illustrate the elastic properties of Si–O frameworks are sodalite and dioptase. Sodalite is the only cubic silicate with a continuous three-dimensional framework of Si and Al tetrahedra. The nuclei of this structure are huge Cl anions with their perfect (spherical) symmetry and around them the said framework of tetrahedra forms the 'Chinese lanterns' which are so characteristic for the structure of sodalite (and the whole group of related minerals).

The rhombohedral symmetry of dioptase

$$Cu_6[Si_5O_{12}].6\,H_2O$$

depends on the fact that its nuclei are rhombohedral rings $(H_2O)_6$ which are cut out from the structure of ice (with the same distances between O atoms and with the same bond angles), and to these rings are fitted (above and below) two rings $[Si_6O_{18}]$ which assume the same rhombohedral symmetry $\bar{3}$, as compared with the symmetry $6/m$ of the rings $[Si_6O_{18}]$ in beryl.

3·2. P. Gay & M. G. Bown. *X-ray investigations of certain pyroxenes.*

All clino-pyroxenes have structures which are basi-

cally similar to that of diopside, $CaMg(SiO_3)_2$, which is monoclinic with cell dimensions $a \sim 9{\cdot}7$, $b \sim 8{\cdot}9$, $c \sim 5{\cdot}2$ Å, $\beta \sim 106°$ and space group $C2/c$. Early X-ray work suggested that apart from changes in cell dimensions, all clino-pyroxenes had similar structures based on the same space group. Very recently, it has been shown by Morimoto that a clino-pyroxene, a pigeonite of composition $(Ca_{0{\cdot}32}Mg_{0{\cdot}90}Fe_{0{\cdot}78})(SiO_3)_2$, has the space group $P2_1/c$.

We have found the same result independently for pigeonites of varying compositions, both from volcanic and plutonic rocks. Further, the distinctive reflexions having $h+k$ odd can be slightly diffuse for some specimens. Plutonic pigeonite usually occurs with a lamellar intergrowth of augite, the two phases having the (001) phase in common; for some of these unmixed specimens, the single-crystal diffraction patterns show continuous streaks between the spots from the pigeonite and augite components. Heating experiments have been carried out on some specimens, and the results of these are presented. Observations and comment upon the diffuse spots and continuous streaks will be made.

Examination of other clino-pyroxenes, both within the ternary field (Ca, Mg, Fe) and other members of the group (acmite, johannsenite, jadeite, spodumene) has been made, but no other case of a primitive lattice has so far been found.

3·3. B. Ray & E. W. Hughes. *The crystal structure of zunyite.*

The structure proposed by Pauling for the rare aluminosilicate mineral zunyite ($(OH,F)_{18}Al_{13}Si_5O_{20}Cl$) has been confirmed and refined with the use of 163 ($hk0$) reflections and 409 (hkl) reflections obtained with Mo$K\alpha$ radiation from single-crystal Weissenberg photographs. The structure is isometric (T_d^2) and is built up of Si_5O_{16} groups of linked silicon tetrahedra combined with $Al_{12}O_{16}(OH)_{30}$ groups of linked aluminum octahedra. Refinement was carried out independently for the ($hk0$) and the (hkl) data, and the final reliability factors are 0·11 and 0·10 respectively. Positional parameters were refined by the least-squares method, and isotropic temperature parameters for separate atoms were adjusted with the help of difference syntheses. Statistical estimation of parameter accuracy by three different methods indicates that Si and Al atoms are located with an estimated standard deviation of 0·003 Å and O with 0·011 Å. Positional parameters derived from the two independent sets of data are found to agree within the tolerances required by these standard deviations. A large apparent temperature parameter discrepancy between the two refinements was caused by slight variations in the contrast factor (γ) of different X-ray films. The refined structure differs from the trial structure by distortion of coordination polyhedra in a fashion similar to the distortions in related structures. The interatomic distance Al–O of $1{\cdot}82 \pm 0{\cdot}02$ Å is derived for tetrahedrally coordinated Al in a position isolated from silicon tetrahedra. The arrangement of protons in the structure is deduced from structural arguments. The proposed arrangement requires the inclusion of at least two F atoms per stoichiometric molecule, modifying the chemical formula to $(OH, F)_{16}F_2Al_{13}Si_5O_{20}Cl$ and explaining the importance of fluorine in the formation of zunyite.

3·4. G. Brunton, H. Steinfink & C. W. Beck. *The crystal structure of callaghanite.*

The crystal structure of callaghanite,

$$Cu_2Mg_2(CO_3)(OH)_6 . 2H_2O ,$$

has been determined from $0kl$, $hk0$ and $hk1$ X-ray diffraction photographs. The crystal system is monoclinic, the space group is $C2/c$ and the unit-cell dimensions are $a = 10{\cdot}05$, $b = 11{\cdot}80$, $c = 8{\cdot}24$ Å, $\beta = 107° 18'$. There are four molecules per unit cell.

The parameters of the atoms are:

	x	y	z
Cu	0·048	0·108	0·455
Mg	0·158	0·317	0·321
O	0·117	0·483	0·250
OH_1	0·017	0·267	0·105
OH_2	0·118	0·946	0·482
OH_3	0·230	0·159	0·425
H_2O	0·336	0·323	0·289
O	0	0·657	0·250
C	0	0·548	0·250

There are four OH groups arranged in a square around the Cu atom with average Cu–OH bond lengths of 2·01 Å. One O atom of the CO_3 group, together with a water molecule and four OH groups, form a distorted octahedron around the Mg atom. The average Mg–O, OH distance is 2·06 Å and the Mg–(H_2O) distance is 2·24 Å. There are two C–O bonds 1·41 Å long when the oxygens are also part of the octahedra around the Mg atoms, while the remaining C–O bond length is 1·29 Å for the oxygen which forms only a hydrogen bond with the water molecule. The length of this hydrogen bond between the O of the CO_3 group and the O of the water molecule is 2·52 Å.

3·5. R. B. Ferguson, R. J. Traill & W. H. Taylor. *The crystal structures of low-temperature and high-temperature albites.*

The crystal structures of a low and a high albite have been refined by a series of two-dimensional F_o and $(F_o - F_c)$ syntheses. The mean bond lengths within the four non-equivalent tetrahedra are, in low albite, $1{\cdot}74_2$, $1{\cdot}59_0$, $1{\cdot}63_6$ and $1{\cdot}61_6$ Å, and in high albite, $1{\cdot}65_2$, $1{\cdot}63_9$, $1{\cdot}64_2$ and $1{\cdot}64_7$ Å, with a standard deviation of 0·02 Å. It is concluded that in low albite the first site $Si_1(0)$ (Megaw notation) contains about three-quarters of the Al, and that in high albite the Al and Si atoms are randomly distributed throughout the four tetrahedral sites. The dimorphism of soda felspar is thus related to differences in the degree of Al–Si ordering. The Na atom in both albites has a temperature factor greater than that implied in the f curve of Bragg & West, and this factor is greater in high albite than in low. Further, the Na atom in both albites shows an anisotropic thermal vibration with a maximum amplitude nearly along y equivalent to an atomic separation of $\sim 0{\cdot}1$ Å in low albite, and $\sim 0{\cdot}6$ Å in high albite. A possible interpretation is that the Na atom occupies at random through the structures one or other of two positions, within the same large cavity, separated by these distances nearly along y. On this view, when the Al–Si atoms are disordered, as in high albite, the cavity available for Na is much larger than it can fill, whereas when the Al–Si atoms are largely

ordered, as in low albite, the cavity is small enough to nearly enclose the Na atom.

On the assumption that maximum stability corresponds to local balance of electrostatic charges throughout the structure, a consideration of the two albites and of sanidine and intermediate microcline leads to a number of unexpected and important conclusions: (1) In low-temperature felspars the most stable structure is not necessarily, as is widely assumed, one in which the Al–Si atoms are completely ordered, but rather one in which the best overall electrostatic charge distribution is achieved. (2) The most stable potassium felspar is not 'maximum' microcline but a monoclinic ($C2/m$) orthoclase with Al partially ordered into one half of the tetrahedra. (3) Intermediate microcline has an unstable charge distribution and all microclines lie outside the normal stability range of the potassium felspars, which runs from disordered sanidine to partially ordered orthoclase. (4) Most microclines are probably formed by the cooling, from fairly high temperatures, of alkali felspars containing an appreciable proportion of sodium which confers on the microcline its partially ordered triclinic character.

3·6. L. S. Dent. *Zeophyllite: unit cell and transformation to cuspidine.*

Zeophyllite was first described by A. Pelikan, who assigned to it the formula $Ca_4Si_3O_7(OH)_4F_2$. A new analysis by R. A. Chalmers gives the formula $Ca_4Si_3O_9F_2.3H_2O$ and is quoted below, with the original analysis for comparison.

	Pelikan	Chalmers
SiO_2	38·84	36·0
Al_2O_3	1·73	1·5
Fe_2O_3	0·10	Nil
MgO	0·17	< 0·5
CaO	44·32	46·3
Na_2O	0·38	0·48
K_2O	0·24	0·09
H_2O	8·98	11·0
F	8·23	7·49
Sum	102·99	102·86
O/F	3·47	3·15
Total	99·52	99·7

The lime and magnesia were determined by titration with EDTA. The experimental error in the calcium determination precluded the accurate determination of the small amount of Mg, which was estimated to be not more than 0·5%.

The unit cell is triclinic with $a = b = 9·34 \pm 0·05$, $c = 13·2 \pm 0·1$ Å, $\alpha = 90·0 \pm 0·1°$, $\beta = 110 \pm 1°$, $\gamma = 120·0 \pm 0·1°$, cleavage (001), $Z = 3$. This cell corresponds to a hexagonal one with a tilted c axis. It is geometrically equivalent to a C-face-centred monoclinic cell with $a = 16·2$, $b = 9·34$, $c = 13·2$ Å, $\beta = 67°$. This monoclinic cell is often more convenient to use.

Dehydration curves show a step at 300–400° C. corresponding to a loss of two-thirds of the total water. The remainder, together with some of the F, is lost between 400 and 1000° C.

Weissenberg photographs of the material heated to 450° C. show that d_{001} has shrunk from 12·1 to 11·1 Å, and that reflexions other than $00l$'s are streaked parallel to c^*. This indicates that the crystals are disordered in the plane of the flake.

On heating to 700° C., the crystals undergo ordered transformation to cuspidine, $Ca_4Si_2O_7F_2$, twinned in three orientations. The relationship of the orientations to that of the original material has been determined. The plane of the flake becomes the cuspidine (012) for all three orientations, and for each one the a axis is 19° from one of the original pseudo-hexagonal axes, so giving three orientations 120° apart. In the light of this relationship, some predictions can be made about the structure of zeophyllite.

The triclinic cell contents are $Ca_{12}Si_9O_{27}F_6 9H_2O$. If the water lost below 400° C. is assumed to be present as water molecules, and the remainder as hydroxyl, the formula can be re-written as $Ca_{12}Si_9O_{24}(OH)_6F_6 6H_2O$. The flaky nature of the material, and the manner in which it is transformed to cuspidine, strongly suggest some type of sheet structure. If the hydroxyl is not attached to silicon, the sheets would be $(Si_9O_{24})^{12-}$. A sheet of six- and nine-membered rings can be postulated to fit this formula, and gives a reasonable explanation of the transformation to cuspidine.

Zeophyllite heated to 940° C. yields a mixture consisting mainly of β-$CaSiO_3$, together with a little larnite.

3·7. M. G. Bown & P. Gay. *Further complexities in the diffraction patterns of intermediate plagioclase felspars.*

The diffraction patterns of intermediate plagioclase felspars are characterized by the replacement of the type-(b) reflexions of the anorthite structures ($h+k$ odd, l odd) by pairs of reflexions, the separation of which is continuously variable with the composition. In addition to these, extra reflexions can occur in pairs close to and symmetrical about the main type-(a) reflexions ($h+k$ even, l even).

It has now been shown that the separations of these extra satellite reflexions varies with composition, and further that their intensities are strongly dependent on composition. This is in contrast with the behaviour of the split type-(b) reflexions, whose intensities are apparently constant over most of the composition range of the intermediate structure (for low-temperature specimens). In addition, very diffuse reflexions of type (c) ($h+k$ even, l odd) are found in intermediate plagioclases more basic than An_{55}.

3·8. J. V. Smith. *The rhombic section and composition plane of pericline twins of plagioclase feldspars.*

The position of the rhombic section of plagioclase feldspars, as calculated from the measured cell dimensions, has been shown to vary with the structural state of inversion, especially for sodic plagioclases. The theoretical composition plane of pericline twins is the rhombic section. If the structural state of the feldspar changes after twinning has occurred, the cell dimensions and hence the rhombic section will change; however, the composition plane of the pericline twin will probably remain unchanged unless recrystallization occurs, or perhaps if the feldspar is subjected to strong stress. Thus the observed pericline composition plane need not coincide with the rhombic section except at the time twinning occurred. Comparison of the observed composition planes with the corresponding calculated rhombic section shows that some of them do indeed differ, and the differences have been used to provide information on the structural changes

occurring subsequent to the establishment of the pericline twins. The interpretation is complicated by the occurrence of the acline-*A* twin, whose composition plane is 001, for the rhombic section of plagioclase felspars from An_0 to An_{60} may coincide with 001 if the structural state of inversion has a particular value. When the observed composition plane would agree with both pericline and acline-*A* twinning, the new term *b-axis twin* has been used.

3·9. H. D. Megaw. *Structures and disorder in the plagioclase felspars.*

A model of a disordered structure is proposed in which 'stacking faults' are allowed to occur on three sets of planes, and are distributed statistically on each set. The intensity distribution in three dimensions is deduced by diffraction theory. It is shown that maxima can occur in non-Bragg positions for a suitable choice of 'slip vector'. The theory can be applied to the non-Bragg reflexions in the intermediate plagioclases by using a unit cell double that of primitive anorthite and a slip vector of one-quarter of the axial length. To explain the dependence on composition, it is necessary to postulate a relation between the probability of a fault and the probability of a 'site-mistake', i.e. the substitution of Na for Ca or Si for Al, and to assume that the site-mistake, or small complex of site-mistakes, propagates itself with perfect regularity as the crystal grows, thus forming the fault plane. The nature of these site-mistakes is discussed in terms of recent work on the structures of anorthite and several other plagioclases. The theoretically predicted displacements of maxima from Bragg positions are compared with Gay's experimental results, and satisfactory agreement is found.

3·10. J. V. Smith & W. S. MacKenzie. *The nature of alkali feldspars in selected igneous rocks.*

The alkali feldspars from rocks specially chosen to represent the transition from volcanic to plutonic conditions have been studied by single-crystal X-ray and optical methods. The rocks examined are: various rhyolites and trachytes; Beinn and Dubhaich granite, Isle of Skye; Slieve Gullion composite ring-dyke of porphyritic felsite and granophyre; Arran and Mourne granites; Dartmoor granite and South California batholite. The following assemblages have been found: one sanidine, one anorthoclase, two sanidines, sanidine + anorthoclase, monoclinic K-feldspar + anorthoclase + sodic plagioclase, orthoclase + sodic plagioclase, orthoclase + microcline + sodic plagioclase, microcline + sodic plagioclase.

The present assemblages are interpreted as the products of a series of reactions that have taken place in an original homogeneous feldspar. Although the volatile content and pressure of the rock undoubtedly have had important effects, there is a strong relation between the inferred rate of cooling and the nature of the products. The slower the inferred rate of cooling the further along the series of reactions. A series of phase diagrams for the different rates of cooling is given.

3·11. S. O. Agrell & J. V. Smith. *X-ray crystallography of mullite, sillimanite and praguite.*

All three minerals are orthorhombic with a pronounced pseudo-cell with $a = 7{\cdot}4$, $b = 7{\cdot}6$, $c = 2{\cdot}9$ Å. Sillimanite contains sharp reflexions which show that true $c = 2 \times$ pseudo c. Mullite contains many weak, diffuse reflexions which show that true $a = 3 \times$ pseudo a, true $b = 8 \times$ pseudo b, true $c = 6 \times$ pseudo c. Only one specimen of praguite was studied by the submission time of the abstract. It has true $c = 2 \times$ pseudo c; a and b under examination. It is not identical with sillimanite. The specimen also showed very weak, diffuse reflexions very similar and perhaps identical with those of mullite.

3·12. F. Liebau. *The crystal structures of rhodonite,* $CaMn_4[Si_5O_{15}]$, *and pyroxmangite,* $(Ca, Mg)(Mn, Fe)_6[Si_7O_{21}]$.

Rotation and Weissenberg photographs of rhodonite from Franklin, New Jersey, and of pyroxmangite from Iva, South Carolina, gave the following cell dimensions:

	Rhodonite	Pyroxmangite
a	6·68 Å	6·67 Å
b	7·66 Å	7·56 Å
c	12·20 Å	17·45 Å
α	111·1°	113·3°
β	86·0°	84·0°
γ	93·2°	94·3°

Corresponding Patterson projections of these silicates, which belong to the group of triclinic pyroxenes, are quite similar. Moreover, their $P(u, v)$ projections show a great similarity to the $P(v, w)$ projections of β-wollastonite and $(NaAsO_3)_x$ (F. Liebau, *Acta Cryst.* (1956), **9**, 811).

With the aid of minimum functions, Fourier projections, difference syntheses, and trial-and-error, the crystal structure of rhodonite was first determined. It was found that rhodonite contains chains parallel [001] with a periodicity of 5 SiO_4 tetrahedra. Like β-wollastonite, the crystals have layers of chains parallel $(1\bar{1}0)$, held together by layers of cations.

The structure determination of pyroxmangite, which we have not yet finished, is being completed by the same methods. The structure of this silicate seems to differ from that of rhodonite essentially by the fact that the chains parallel [001] have a periodicity of 7 SiO_4 tetrahedra instead of 5.

The shape of the 3-periodic chain (β-wollastonite), i.e. the chain with 3 SiO_4 tetrahedra per period, is evidently closely related to that of the 5-periodic (rhodonite) and 7-periodic (pyroxmangite) chains, but the 2-periodic chain has a quite different shape.

According to the crystal structure and chemical composition of rhodonite from different localities its formula should be given as $CaMn_4[Si_5O_{15}]$, rather than $MnSiO_3$ as usually; there is no isomorphous replacement between Mn and Ca in rhodonite.

Similarly, the formula of pyroxmangite should be given as $(Ca, Mg)(Mn, Fe)_6[Si_7O_{21}]$.

3·13. W. Nowacki & G. Bergerhoff. *Die Kristallstruktur des Zeolithes Faujasit.*

Dreh- und Weissenbergaufnahmen an natürlichen Faujasit (oktaedrische Kristalle) von Sasbach (Kaiserstuhl) ergaben die Gitterkonstante $a = 24{\cdot}74$ Å und die Raumgruppe O_h^7–$Fd3m$. Es sind 192/7 Formeleinheiten $NaCa_{0{\cdot}5}(Al_2Si_5O_{14}) \cdot 10H_2O$ in der Zelle vorhanden.

Es war das Ziel, die Struktur auf möglichst *direktem* Wege abzuleiten. Dazu wurden folgende Wege beschritten: (*a*) Methode der Ungleichungen. Da die wenigen grossen unitären Strukturamplituden $U_{hkl} = 0{,}4$, die meisten aber um 0,2 waren, erwies sich dieses Verfahren als unanwendbar; (*b*) Methode des isomorphen Ersatzes. Ein natürlicher Faujasitkristall wurde in einer $AgNO_3$-Lösung einem Ionenaustausch (Na, Ca ⟷ Ag) unterworfen und vom Ag-Faujasit alle nötigen Röntgenaufnahmen hergestellt und vermessen. Analoge Schnitte durch eine dreidimensionale Pattersonsynthese des natürliche bzw. des Ag-Faujasites zeigten aber, dass die beiden Strukturen gar nicht streng isotyp sind, indem die Ag-Ionen auch noch andere als nur die ursprünglichen Alkali-Lagen einnehmen. Dieser Weg führte daher auch nicht weiter; (*c*) Superpositions-Methode. Die eben erwähnten Schnitte liessen aber erkennen, dass die Punktlage (48(*f*)) einen beiden Faujasiten gemeinsamen Gitterkomplex darstellt. Für den Ag-Faujasit wurde nun eine *drei*dimensionale (additive) *Überlagerungssynthese* berechnet, über den Gitterkomplex (48(*f*)) superponiert. Aus dieser Synthese konnte folgende plausible Struktur des Faujasites entnommen werden: das (Si, Al)O-Gerüst besteht aus kubooktaedrischen Käfigen, wie sie in den Ultramarinen und wahrscheinlich auch im Chabasit vorkommen ((Si, Al) = Ecken eines Kubooktaeders, d. i. einer Kombination eines Würfels mit einem Oktaeder, von Quadraten und regulären Sechsecken gleicher Kantenlänge = (Si–Si)-Abstand ≈ 3,09 Å begrenzt); diese Käfige sind gegenseitig wie die C-Atome im Diamantgitter angeordnet und durch gemeinsame O-Atome, welche die Si(Al) tetraedrisch umgeben (in der Zelle sind 192 solcher über Ecken verbundene Tetraeder vorhanden), miteinander verbunden; die Alkali-Ionen und die Wassermoleküle scheinen innerhalb und an der Oberfläche der Käfige und im Innern der weiten Kanäle (von ca. 6–7 Å Durchmesser), welche || den Richtungen [110] die Struktur durchziehen und eine Erklärung für die besonderen Ionen-Austausch-Eigenschaften dieser Substanz liefern (R. M. Barrer, W. Buser & W. F. Grütter, *Helv. Chim. Acta* (1956), **39**, 518), zu sitzen.

Auf Grund der gefundenen Si- und O-Lagen alleine wurden die $\pm|F|$-Werte ermittelt; mit dem $|F|_{beob.}$ ergaben sie einen Zuverlässigkeitsindex von $R = 0{,}32$. Die erhaltenen Vorzeichen wurden zur Berechnung einer ersten dreidimensionalen Fouriersynthese verwendet, welche nur eine geringfügige Änderung der Si- und O-Lagen und weitere Maxima (Alkalien, Wasser) ergab, worauf die $\pm|F|$-Werte nochmals berechnet wurden. Die Strukturbestimmung befindet sich damit im Stadium der Verfeinerung.

3·14. J. R. Goldsmith. *Exsolution of ordered rhombohedral carbonates in the systems* $CaCO_3$–$MgCO_3$ *and* $CaCO_3$–$MnCO_3$.

The sub-solidus phase diagrams of the $CaCO_3$–$MgCO_3$ join and the $CaCO_3$–$MnCO_3$ join in the systems CaO–MgO–CO_2 and CaO–MnO–CO_2 are described. Immiscibility gaps are present in both systems, and the ordered compounds $CaMg(CO_3)_2$ and $CaMn(CO_3)_2$ are in equilibrium with disordered solid solutions in the appropriate P_{CO_2}–T–X regions. Substitutional disorder begins at 450° C. in the compound $CaMn(CO_3)_2$, but $CaMg(CO_3)_2$ remains ordered at least up to 850° C.

A number of carbonate rocks were examined in the light of the experimental systems. Calcites from a variety of marbles have been investigated by single-crystal X-ray techniques, chiefly the Buerger precession method. Most of the specimens were relatively high-temperature metamorphic carbonates. The typically milky calcite of these rocks commonly contains $CaMg(CO_3)_2$ (dolomite), revealed by the X-ray photographs, but not always observed under the microscope. This finely disseminated dolomite is in the same crystallographic orientation as the host calcite and is almost certainly an exsolution product. Similar oriented intergrowths of an ordered Ca–Mn carbonate are observed in crystals of appropriate composition.

An oriented intergrowth of dolomite in calcite was produced in the laboratory. The original material was an echinoid plate, made up of spongy, but single-crystal calcite with approximately 10% $MgCO_3$ in metastable disordered solid solution. This amount of Mg is stable in calcite at temperatures above 650° C.; therefore exsolution of some of the Mg as $CaMg(CO_3)_2$ took place when the sample was heated under CO_2 pressure at 500° C. The host magnesian calcite retained its identity as a single crystal, and the dolomite exsolved in the same crystallographic orientation as the host.

The usefulness of an X-ray method for observing the amount of Mg in solid solution in $CaCO_3$, as well as the amount of exsolved $CaMg(CO_3)_2$, is discussed in the light of geologic thermometry.

3·15. A. W. Hanson. *The crystal structure of nolanite.*

This iron vanadate is hexagonal, probably $P6_3mc$, with $a = 5{\cdot}85$, $c = 9{\cdot}29$ Å. It occurs in thin platelets normal to [0001]. Good single crystals are very scarce and the chemical composition is not precisely known. Three-dimensional intensity data were collected from integrated precession photographs, and from various types of integrated and non-integrated Weissenberg photographs taken with Mo$K\alpha$ radiation. The data can be separated into the three following groups in descending order of precision: ($hk.0$); ($h0.l$); all remaining ($hk.l$). Some data also were obtained using other radiations. Absorption corrections were made where necessary. The size and shape of the unit cell suggested a structure consisting of a close-packed hexagonal framework of 16 oxygen atoms, with a total of 10 metal ions occupying various interstices. In such a structure, all the atoms would lie on or near a few lines parallel to c ($(0, 0, ., z)$; $(\frac{1}{2}, 0, ., z)$; $(\frac{1}{3}, \frac{\bar{1}}{3}, ., z)$; $(\frac{1}{6}, \frac{\bar{1}}{6}, ., z)$). A three-dimensional Patterson synthesis, evaluated only for the appropriate lines, led to a plausible structuer. Six of the vanadium ions (V^{4+}) apparently occupy sixfold positions of octahedral coordination. The four remaining metal ions (some Fe^{2+}, some V^{3+}) lie on the two threefold axes, distributed among positions of octahedral and tetrahedral coordination. It has been possible to some extent to distinguish between Fe (atomic number 26) and V (atomic number 23) by the use of radiations with wavelengths near the absorption edges of the two metals. Refinement of the structure is proceeding satisfactorily and is expected to be completed before the Congress, at which time details of the structure will be presented.

3·16. R. Euler, H. Rosch, G. Weitz & E. Hellner. *Über ein strukturelles Bauprinzip für sulfidische Erze (Spiessglanze).*

Es gibt etwa 70–80 verschiedene sulfidische Minerale, die As_2S_3, Sb_2S_3 und Bi_2S_3 in wechselnden Mengen mit PbS, Ag_2S, FeS, Cu_2S usw. enthalten. Für einige dieser Minerale, wie z. B. Miargyrit, Berthierit, Galenobismutit, Antimonit, Aikinit, Wolfsbergit, Seligmannit usw. sind bisher die Strukturen bekannt, ohne dass ein Bauprinzip aufgezeigt werden konnte. Eigene Strukturbestimmungen wurden an den Mineralen Diaphorit, $4PbS.3Ag_2S.3Sb_2S_3$, Freieslebenit, $4PbS.2Ag_2S.2Sb_2S_3$, Andorit, $2PbS.Ag_2S.3Sb_2S_3$, Fizelyit, $5PbS.Ag_2S.2Sb_2S_3$, Cosalit, $2PbS.Bi_2S_3$, Meneghinit, $3PbS.Sb_2S_3$, Gratonit, $9PbS.2As_2S_3$, durchgeführt.

Alle diese Strukturen zeigen zusammenhängende Bereiche des PbS-(NaCl-)Typs; sie lassen sich in drei verschiedener Art und Weise vom PbS-Gitter ableiten:

1. Möglichkeit: Einige Spiessglanze wählen als ihre *c*-Richtung die (001)-Richtung des PbS-Gitters oder ein Vielfaches davon. In diese Klasse gehören die Minerale Diaphorit, Freieslebenit, Schapbachit, so wie wahrscheinlich Lengenbachit.
2. Möglichkeit: Einige Spiessglanze (vorwiegend die Sb- und Bi-haltigen) wählen als ihre *c*-Richtung die (110)-Richtung des PbS-Gitters oder ein Vielfaches; hierher gehören Miargyrit, Andorit, Ramdohrit, Fizelyit, Cosalit, Meneghinit, Berthierit, Antimonit, Wolfsbergit u. a.
3. Möglichkeit: Einige Spiessglanze (anscheinend vor allem As-Spiessglanze) wählen als ihre *c*-Richtung die (111)-Richtung des PbS-Gitters. Gratonit leitet sich vom PbS-Gitter in dieser Weise ab; er kann als deformierter 3-Schichttyp einer kubisch dichtesten Kugelpackung aufgefasst werden. Jordanit und Geocronit lassen sich wahrscheinlich als 10-Schicht-Typ auffassen.

Für die Grösse der PbS-Bereiche und der Abweichungen vom PbS-(NaCl-)Typ sind zwei Faktoren massgebend, die aus der chemischen Formel abgeleitet werden können:

$$f_1 = \frac{Ag+Pb+Sb(As, Bi)}{S} \text{ und } f_2 = \frac{Ag+Pb}{Sb(As, Bi)}.$$

$f_1 \times 100$ gibt die prozentulae Besetzung der oktaedrischen Kücken in der dichtesten Kugelpackung, aus Schwefelatomen bestehend, an. Je grösser der Wert von f_1 ist, umso grösser ist die Annäherung an das PbS-Gitter. f_2 gibt die zusätzliche Verzerrung des Gitters an, die durch die unterschiedliche Bindung der Sb(As, Bi)-Atome gegenüber Schwefel besteht (mit drei Nachbarn wird etwa eine gleichseitige Pyramide gebildet).

Eine Gruppeneinteilung der Spiessglanze auf Grund der *f*-Faktoren ist möglich. In einer beiliegenden Abbildung ist eine Gruppeneinteilung ohne Berücksichtigung der letzten Ergebnisse der Strukturbestimmungen gegeben. Für zwei Strukturen (Cosalit und Berthierit) sind Abbildungen beigefügt; in welchen die PbS-Bereiche schraffiert sind. Den 'Formel-Kriterien' werden die 'Struktur-Kriterien' gegenübergestellt. Als Strukturkriterium ist die Grösse der zusammenhängenden PbS-(NaCl-)Bereiche gewählt.

Ein Vergleich zwischen 'Formelkriterien' (f_1 und f_2-Faktoren) und Strukturkriterien (Grösse der PbS-Bereiche) zeigt gute Übereinstimmung. Die Vielzahl der Spiessglanzstrukturen, ihre Verwachsungsgesetze sowie myrmekitische Strukturbilder unter dem Auflichtmikroskop können in einfacher Weise gedeutet werden.

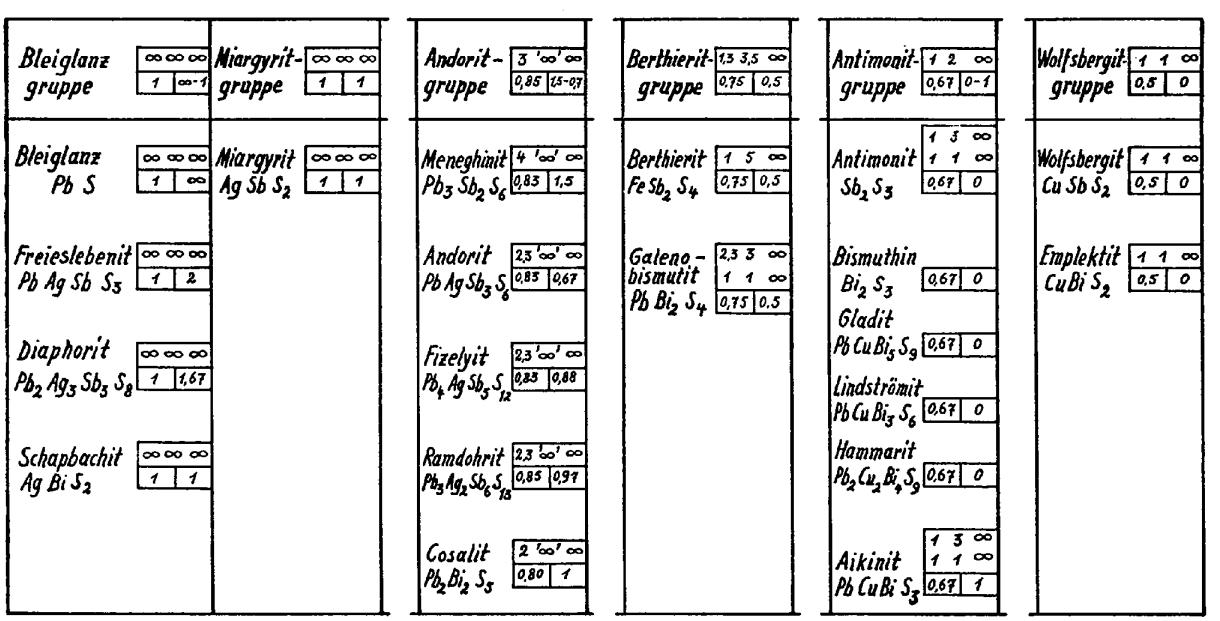

Einteilung der Antimon- und Wismut-Spiessglanze nach strukturellen Gesichtspunkten.

3·17. A. J. Frueh, Jr. *The crystal structure, polymorphism and twinning of acanthite* (Ag_2S).

The space group of a single crystal of naturally occurring acanthite (Ag_2S) from Freiberg, Saxony, was determined to be monoclinic $P2_1/n$. The cell constants were determined as $a = 4{\cdot}23$, $b = 6{\cdot}91$, $c = 7{\cdot}87$ Å; $\beta = 99°35'$. This differs in orientation from the non-primitive cell ($B2_1/c$) described by L. S. Ramsdell (*Amer. Min.* (1943), **28**, 401) by the following transformation $\frac{1}{2}\ 0\ \frac{1}{2}/0\ 1\ 0/\bar{\frac{1}{2}}\ 0\ \frac{1}{2}$. There are $4(Ag_2S)$ per unit cell and all atoms lie on the following fourfold general positions Ag(I): $x = 0{\cdot}733$, $y = 0{\cdot}018$, $z = 0{\cdot}305$; Ag(II): $x = 0{\cdot}285$, $y = 0{\cdot}317$, $z = 0{\cdot}432$; S: $x = 0{\cdot}333$, $y = 0{\cdot}233$, $z = 0{\cdot}133$.

The structure of the polymorph argentite, stable above 179° C., was determined by P. Rahlfs (*Z. phys. Chem. B* (1936), **31**, 157), and consists of a body-centered sulfur structure with the silver atoms distributed at random throughout the interstices. Acanthite is seen to retain the close-packed sulfur cell in a slightly distorted form with the three cell edges of the cube parallel to $[10\bar{3}]$, [121] and $[\bar{1}21]$ directions in the monoclinic crystal. When crystals are cooled through the transition, many small domains are formed, related to each other by having the directions $[10\bar{3}]$, [121] and $[\bar{1}21]$ in one domain parallel to another combination of these directions in the other domains.

3·18. G. Donnay, J. D. H. Donnay & G. Kullerud. *Crystal and twin structure of digenite*, Cu_9S_5.

Digenite undergoes a rapidly reversible, non-quenchable transformation between 60 and 65° C. We are reporting on the room-temperature form; previous authors (P. Rahlfs, *Z. phys. Chem. B* (1936), **31**, 157; N. W. Buerger, *Amer. Min.* (1942), **27**, 712) studied the high-temperature form.

In an investigation of the system Cu_2S–CuS carried on by one of us (G. K.), digenite was synthesized in octahedra, modified by small cube faces and ranging in size from barely visible to 2 mm. in longest dimension. Rotation, Weissenberg, and precession patterns, taken with Cu $K\alpha$ ($\lambda = 1{\cdot}5418$ Å) and Mo $K\alpha$ radiations, lead to a cubic cell whose edge has five times the length reported in the literature: $a = 5a' = 27{\cdot}71$ Å$\pm 0{\cdot}3\%$. With 100 Cu_9S_5 per cell, the density is 5·715 g.cm.$^{-3}$ (calc.), against 5·6 g.cm.$^{-3}$ (obs.). The Laue symmetry is $4/m\bar{3}2/m$, the diffraction aspect $F***$. Only reflections HKL of the type $10m\pm L$, $10n\pm L$, L (m, n integers) are observed. It proved impossible, in any acceptable space group, to find a crystal structure that would account for the numerous 'structural absences'.

Assume the octahedra to consist of four rhombohedral crystals, oriented with their hexagonal c axes along the body diagonals and their hexagonal a axes along the face diagonals of the simulated cubic cell. The transformation of indices for each crystal I to IV is given by the following matrices (cubic HKL from rhombohedral hkl): I: $7\bar{3}\bar{3}/3\,7\,\bar{3}/\bar{3}\,\bar{3}\,7$; II: $\bar{3}\,7\,\bar{3}/\bar{7}\,3\,3/\bar{3}\,\bar{3}\,7$; III: $\bar{7}\,3\,3/3\,\bar{7}\,3/\bar{3}\,\bar{3}\,7$; IV: $3\bar{7}\,3/7\,\bar{3}\,\bar{3}/\bar{3}\,\bar{3}\,7$. In cubic notation a reflection hkl of crystal I becomes $H = 10h-s$, $K = 10k-s$, $L = 10l-s$, with $s = 3(h+k+l)$, or, by eliminating s, $H = 10(h-l)+L$, $K = 10(k-l)+L$, L, which is of the form $10m+L$, $10n+L$, L. Reflections from crystals II to IV likewise obey the structural absences. The cubic symmetry of the diffraction aspect, noted in all twenty twins examined, is explained if the four crystals in a twin have equal volumes. The twin axis is $[\bar{3}\bar{3}7]$, referred to the rhombohedral axes of each crystal. The twin index is 5. The twin obliquity is zero; we are dealing with twinning by reticular merohedry (high-order merohedry?). Twinning is presumably of the intimate penetration type, for no composition surface could be observed either under the microscope or in polished sections viewed in reflected light. Twinning accompanies inversion on cooling and the twin retains the octahedral form of the high-temperature crystal; on heating, the twin changes to a crystalline powder, pseudomorph after the 'octahedron'.

The rhombohedral cell ($a = 16{\cdot}16$ Å, $\alpha = 13°56'$) contains one Cu_9S_5. The diffraction aspect is $R**$. The pronounced pseudo-cube $a' = a/5 = 5{\cdot}54$ Å, with reference to which only two lines of the powder pattern cannot be indexed ($d = 3{\cdot}05$ and 2·17 Å), is explained as follows. Only those reflections whose HKL indices are multiples of 5 receive contributions from all four crystals of the twin. They are the only reflections, moreover, to which sulfur atoms contribute. Space group $R\bar{3}m$ leads to an acceptable structure. The angle α is so small that all atoms must lie on the threefold axis, on onefold or twofold positions of type x, x, x. Sulfur atoms lie at $x = 0, \pm\frac{1}{5}, \pm\frac{2}{5}$, and lead to an S–S distance of 3·92 Å. The sulfur sites correspond to the face centers of the small cubes. One copper atom, presumably a cupric ion, is located at $x = \frac{1}{2}$, octahedrally co-ordinated to sulfur atoms. The other copper atoms, presumably cuprous, are found approximately at: $x = \pm 0{\cdot}060$, in tetrahedral co-ordination but displaced from the center toward one face of the tetrahedron; $x = \pm 0{\cdot}133$, in triangular co-ordination; $x = \pm 0{\cdot}250$ and $\pm 0{\cdot}350$, in regular tetrahedral co-ordination. The Cu–S distance ranges from 2·26 Å for the triangular co-ordination to 2·77 Å for the octahedral one. There is thus strong structural evidence that, in the low-temperature form, the digenite formula should be written $CuS.4Cu_2S$.

3·19. E. Onorato. *X-ray examination of cobaltite.*

My researches on cobaltite have established that the mineral has not the structure of ullmannite determined by Mechling, but that of pyrite with the ordered substitution of the pair As–As for the pair S–S. Such ordered substitution is manifested in that in the unit cell the series of lattice planes parallel to one of the three faces of the cube contain alternately the centres of equilibrium of the pair As–As, S–S. Therefore it is a case of a superstructure with the atoms of Co all in octahedral coordination, but for one half of which the corners of the octahedra are occupied by 4 As + 2 S and for the other half by 4 S + 2 As.

The following observations have enabled me to reach these conclusions:

(*a*) The non-equivalence of faces of the cube, with well marked differences between the planes (100) on the one hand and the planes (010) and (001) on the other. In fact, while the reflexions (h00) are present for all h values, even and odd, the reflexions (0k0) and (00l) appear only in the even orders.

(*b*) The non-equivalence of the zones [010] and [001] in that systematic extinctions which are absent in the second case are noted in the first.

(*c*) The presence of mirror planes normal to (001), (010) and (100).

(*d*) The Patterson projection is identical to that of pyrite. The coordinates of atoms in the unit cell are:

4 Co: $0, 0, 0;\ \frac{1}{2}, \frac{1}{2}, 0;\ 0, \frac{1}{2}, \frac{1}{2};\ \frac{1}{2}, 0, \frac{1}{2}$.
4 As: $x, x, x;\ \bar{x}, \bar{x}, x;\ x, \frac{1}{2}-x, \frac{1}{2}+x;\ \bar{x}, \frac{1}{2}+x, \frac{1}{2}-x$.
4 S: $\frac{1}{2}+x', \frac{1}{2}-x', \bar{x}';\ \frac{1}{2}-x', \frac{1}{2}+x', x';$
$\frac{1}{2}-x', \bar{x}', \frac{1}{2}-x';\ \frac{1}{2}+x', x', \frac{1}{2}-x'$.
$x = x' = 0{\cdot}386$.

This same result is also reached by a direct determination of the space group, which is C_{2h}^5, and confirms that cobaltite must be considered as a polysynthetic twin of monoclinic crystals.

Examining the several types of twinning proposed by Schneiderhöhn one concludes that they all are referred to a unique law, i.e. the pinacoid (100).

3·20. [Withdrawn.]

3·21. D. E. Appleman & H. T. Evans, Jr. *The crystal structure of carnotite.*

In connection with crystal chemical studies of uranium and vanadium minerals, the crystal structures of synthetic anhydrous carnotite, $K_2(UO_2)_2V_2O_8$, and of its cesium analogue have been determined by direct X-ray diffraction methods. Crystals of both compounds, suitable for X-ray and optical goniometric investigation, were synthesized by Paul Barton, U. S. Geological Survey. Synthetic potassium carnotite, yielding X-ray diffraction patterns virtually identical to those of natural carnotite, is monoclinic $P2_1/a$, $a = 10{\cdot}47\pm0{\cdot}02$, $b = 8{\cdot}41\pm0{\cdot}01$, $c = 6{\cdot}59\pm0{\cdot}01$ Å, $\beta = 103°50'\pm05'$, $Z = 2[K_2(UO_2)_2V_2O_8]$, sp. gr. (calc.) = 4·99, sp. gr. (obs.) = $4{\cdot}95\pm0{\cdot}05$. Synthetic cesium carnotite is monoclinic $P2_1/a$, $a = 10{\cdot}51\pm0{\cdot}02$, $b = 8{\cdot}45\pm0{\cdot}01$, $c = 7{\cdot}32\pm0{\cdot}01$ Å, $\beta = 106°05'\pm05'$, $Z = 2[Cs_2(UO_2)_2V_2O_8]$, sp. gr. (calc.) = 5·52, sp. gr. (obs.) = $5{\cdot}48\pm0{\cdot}05$. Both compounds form plate-like crystals parallel to (001), with {110} always present, {100} and {010} occasionally present.

Intensity data were obtained from zero-level precession photographs of the three principal zones, taken with Mo $K\alpha$ radiation. Although the physical properties of carnotite preclude artificial absorption corrections, the *hk*0 reflections can be made essentially self-correcting by using a plate-like crystal which fills the X-ray beam (G. Donnay & J. D. H. Donnay, (1955), *U. S. Geological Survey, TEIR*, **507**, 7). The angle (β–90°) between the a^*b^* net and (001) is apparently not large enough to obstruct the correction effect. The coordinates of the U, V, and alkali atoms were obtained by comparison of the Patterson projections along [001]. After refinement of their coordinates, subtraction of the heavy atoms yielded final electron-density projections along [001] in which all oxygen atoms were resolved. *Z* coordinates were obtained from 0*kl* and *h*0*l* Patterson and electron-density projections.

Comparison of the structures obtained in this study with the structure previously proposed for synthetic anhydrous carnotite (I. Sundberg & L. G. Sillén, *Ark. Kemi* (1949), **1**, 337) shows that only the U and K atoms are in agreement. The vanadium coordination, rather than being tetrahedral, is fivefold, with five oxygens forming a distorted trigonal bipyramid about each vanadium. Two such bipyramids share an edge to form a 'divanadate' ion, $V_2O_8^{-6}$, which is similar in structure to two links from the five-coordinated $V_nO_{3n}^{-n}$ chains found in $KVO_3.H_2O$ (C. L. Christ *et al.*, *Acta Cryst.* (1954), **7**, 801). The linear uranyl ion is coordinated by five oxygens from three $V_2O_8^{-6}$ groups. The structure thus consists of $[(UO_2)_2V_2O_8]_n^{-2n}$ sheets parallel to (001), with linear uranyl ions nearly normal to the sheets; interlayer alkali ions bind the sheets together. The fivefold coordination of uranyl ion has recently been found in this laboratory in the structure of johannite, $Cu(UO_2)_2(SO_4)_2(OH)_2.6H_2O$, and is reported by D. K. Smith (Ph.D. Thesis, University of Minnesota, 1956) in the structure of uranophane, $[Ca(H_3O)_2](UO_2)_2(SiO_4)_2.3H_2O$.

The residual factor *R* for the *hk*0 reflections in the present stage of refinement is 16·1% for K carnotite and 12·3% for Cs carnotite. The coordinates of the atoms are:

	K carnotite			Cs carnotite		
Atom	*x*	*y*	*z*	*x*	*y*	*z*
U	0·180	0·023	0·988	0·181	0·019	0·988
V	0·046	0·353	0·095	0·055	0·352	0·095
K	0·336	0·233	0·538	—	—	—
Cs	—	—	—	0·363	0·233	0·539
O_1	0·117	0·086	—	0·102	0·058	—
O_2	0·255	0·463	—	0·250	0·458	—
O_3	0·000	0·156	—	0·026	0·148	—
O_4	0·070	0·356	—	0·056	0·355	—
O_5	0·384	0·077	—	0·397	0·059	—
O_6	0·231	0·334	—	0·243	0·307	—

3·22. [Withdrawn.]

3·23. E. J. W. Whittaker. *Helical structures in chrysotile.*

Now that the general features of the atomic arrangements in the three varieties of chrysotile have been elucidated (E. J. W. Whittaker, *Acta Cryst.* (1956), **9**, 855, 862, 865) primary interest in this mineral centres on larger-scale textural features which are likely to have a bearing on the formation and physical properties of the fibres, especially helical and spiral structures and the incomplete cylindrical layers which are presumably responsible for filling the voids within and between the cylindrical fibrils.

The existence of a helical structure in some specimens of chrysotile, and not in others, has previously been demonstrated (H. Jagodzinski & G. Kunze, *N. Jb. Min. Mh.* (1954), **415**, p. 137; Whittaker, *Acta Cryst.* (1956), **9**, 855) from the distribution of intensity close to the origin of the 6th layer line. New and more specific information on the helical structures present in some fibrils has now been obtained from two unusual electron-diffraction photographs of single fibrils. On such photographs in general the 0*kl* reflexions (which are diffuse on X-ray diffraction photographs) are resolved into a series of closely spaced spots corresponding to the successive peaks of high-order Bessel functions. On the particular photographs under discussion this feature is maintained but each 0*kl* reflexion is split into two components flanking the layer line, the separation between the components being proportional to the *k* index. This effect is characteristic of cylindrical structures in which the *c* axis is slightly inclined to the cylinder axis. From the arrangements of the fine structure of the reflexions it can be shown that this angle varies from layer to layer within the fibre, and that the structure is based on a helical cylindrical lattice in which the *b* and *c* axes are

presumably perpendicular in every layer. In one case the order of the helix appears to be as large as about $3\frac{1}{2}$, the external radius being about 100 Å. This information is obtained from a consideration of the fine structure of the reflexions; the displacement of the reflexions from the layer line only gives the quotient of these two quantities. This is also true of the information available from X-ray photographs of the 6th layer line, and moreover the latter does not distinguish between helical structures of the type discussed above and those in which the c axis remains parallel to the cylinder axis and there is a small variable distortion of the angle β from $\frac{1}{2}\pi$.

If helical structures of the type observed by electron diffraction were of common occurrence they would lead to a spread of the $0kl$ reflexions along Debye arcs. This phenomenon is well-known to occur in all chrysotile specimens (though it occurs to different degrees in specimens from different sources) and may well be due either wholly or partly to the presence of such helical structures. However, investigation of the intensity distribution along these arcs shows that there must be a preponderance of the other type of helical structure (in which the c axis remains parallel to the cylinder axis), in some specimens at least.

3·24. V. I. Mikheev. *X-ray determinative tables for minerals.*

The idea of X-ray determinative tables for minerals was expressed by a distinguished crystallographer and mineralogist A. K. Boldirev in the 1920's.

In 1938–9 the first two publications of X-ray determinative tables for minerals appeared. They included 288 minerals. At present new X-ray determinative tables for minerals are being published, and include 905 minerals. In addition, another issue of these tables including 300 minerals is ready for publication. All the above mentioned determinative tables have been worked out in the X-ray laboratory of the Leningrad Mining Institute.

Generalization of a large amount of factual material in the field of X-ray study of minerals, while working out the new X-ray determinative tables, made it possible, to find the mathematical dependence between the chemical composition and the dimensions of the unit cells for isomorphous series of minerals.

For many isomorphous series the dimensions of the unit cells are a function of the mean radius of the cations.

At present, formulas of the dimensions of the unit cell for the following groups of minerals have been found:

(1) Nickeliferous iron (kamacite), $Fe_{1-x}Ni_x$: $a = 2{\cdot}86124 + 0{\cdot}00041x$.

(2) Pyrhotite, $(Fe''_{1-x}Fe'''_{\frac{2}{3}x})S$: $c = 9{\cdot}655 + 2{\cdot}50r$, where r is the mean radius of iron.

(3) Oxides of divalent metals with the structure of sodium chloride: $a = 2{\cdot}632 + 2{\cdot}095r''$, where r'' is the ionic radius of a divalent metal.

(4) The spinel group with the general formula $(A''_{1-x}B'''_{\frac{2}{3}x})B''_2O_4$, which takes into account a possible abundance of trivalent oxides: $a = 5{\cdot}778 + 0{\cdot}95r'' + 2{\cdot}79r'''$, where r'' is the mean radius of tetrahedral cations, and r''' is the mean radius of octahedral cations.

(5) Olivine, $(Mg_{1-x}Fe'_x)_2SiO_4$: $c = 5{\cdot}972 + 0{\cdot}100x$.

(6) Garnets, $A''_3B''_2Si_3O_{12}$: $a = 9{\cdot}125 + 1{\cdot}560r'' + 2{\cdot}000r'''$, where r'' is the mean radius of a divalent cation, and r''' is the mean radius of a trivalent cation.

(7) Micas: $d_{060} = 1{\cdot}396 + 0{\cdot}1821\ r$, where r is the mean radius of an octahedral ion.

(8) Chlorites, $Mg_{6-x-y-z}Fe''_z(Al, Fe''')_{x+\frac{2}{3}y}\{Al_x\ Si_{4-x}\ O_{10}\}[OH]_8$: $b = k.r$, where r is the radius of the octahedral cations of the talceous layer; $c = f(x)$.

(9) Ilmenite, $Fe''_{1-x}Fe'''_{2x}Ti_{1-x}O_3$: $a = 4{\cdot}356 + r$, where r is the radius of an octahedral ion.

The establishment of analytical dependence between the composition and the dimensions of the unit cell affords much wider possibilities for the X-ray determinative method in mineralogy, the objects of which are always substances of variable composition. The X-ray determinative method makes it possible to determine the composition of the mineral, even in the most complicated cases of the isomorphous series.

§ 4. Clay minerals

4·1. G. B. Mitra. *Line profiles of the X-ray reflexions of kaolinite.*

X-ray powder diffraction patterns of kaolinite under various stages of dehydration have been taken. The experimentally obtained line profiles of the various reflexions have been corrected for the geometrical factor. The particle sizes and shapes have been determined by studying the samples under an electron microscope. An expression for the line profile due to particle size of a triclinic crystal has been derived. In comparison with the theoretical line profiles thus obtained, the experimental line profiles have been corrected for the particle-size factor by a method similar to that due to Stokes for correcting for the geometrical factor. The doubly corrected line profiles thus obtained are due to defects only. A preliminary study of these line profiles has revealed a random disordering increasing with dehydration and a shift by $\frac{1}{3}b$ in the b direction. Studies are being continued.

4·2. A. Oberlin. *Détermination de la structure cristalline d'une kaolinite altérée.*

De nombreux échantillons de kaolinite en provenance du Sahara Central ont été étudiés au microscope électronique. L'étude morphologique a montré que la forme des microcristaux variait, en fonction de la position de l'échantillon dans un même gisement. Un prélévement effectué à une profondeur supérieure à un mètre n'a fourni que des plaquettes pseudo hexagonales typiques de la kaolinite; au contraire, les particules placées immédiatement à la surface du sol, se sont montrées fréquemment enroulées en forme de tube.

Cette modification de faciés a suggéré la possibilité d'une altération de surface, due au climat désertique.

Pour tenter de reproduire des conditions analogues au laboratoire un échantillon de kaolinite pure a été soumis pendant 31 jours à une alternance régulière de lessivages par l'eau (en cycle fermé) et de chauffages à 80° C.

Le changement apporté par ce traitement dans le faciès des particules a été étudié au microscope électronique; les résultats sont les suivants: Les cristaux de kaolinite en plaquettes pseudohexagonales, se clivent d'abord

suivant (001), puis les particules les plus amincies se replient et s'enroulent en tubes dont la forme est proche de celle de l'halloysite ou de la métahalloysite.

Les microcristaux altérés par percolation-dessication ont été ensuite étudié par microdiffraction électronique. Les diagrammes obtenus sont des diagrammes de cristaux uniques ne présentant que les taches (*hk*0) mais les clichés permettent après calcul des facteurs de structure, d'identifier les produits d'altération comme étant de la métahalloysite.

Le mécanisme du traitement est le suivant: les cristaux s'amincissent par clivage jusqu'à obtenir une désorganisation complète des feuillets suivant la perpendiculaire à (001), ce qui permet l'enroulement de la particule suivant les axes *a* ou *b*. Le produit obtenu est un minéral à feuillets isolés désordonnés répondant à la définition de la métahalloysite.

4·3. H. Steinfink. *The crystal structures of the monoclinic and triclinic forms of chlorite.*

A detailed investigation of the triclinic and monoclinic polymorphs of chlorite was undertaken with the following aims in mind: (1) To what extent do the atomic coordinates of these two polymorphs differ from the 'ideal' coordinates proposed by G. W. Brindley *et al.* (*Acta Cryst.* (1950), **3**, 408)? (2) Is the distribution of ions which replace part of the magnesium and silicon in the talc and brucite layers random, or is there preferential concentration of these ions in certain sites?

The monoclinic specimen used was obtained from the U.S. National Museum and was labeled 'Prochlorite # 45875'. The unit-cell dimensions are $a = 5{\cdot}37$, $b = 9{\cdot}30$, $c = 14{\cdot}25$ Å, $\beta = 96°\ 17'$; the space group is $C2$; there are two molecules of the approximate composition

$$(Mg_{2\cdot6}Fe''_{0\cdot2}Fe'''_{1\cdot5}Al_{1\cdot2})(Si_{2\cdot2}Al_{1\cdot8})O_{10}(OH)_8$$

in the unit cell. The analysis shows that the Si–O tetrahedra are rotated about an axis through the apex of the tetrahedron and perpendicular to the plane of the basal oxygens. It is found that the isomorphous replacement of the Mg and Si in the octahedral and tetrahedral sites respectively is restricted to fixed positions in the monoclinic polymorph. It is shown that the net negative charge on the talc layer in the unoxidized specimen arises from replacement of Si by Al in the tetrahedral sites and that this charge is neutralized by excess positive charge on the brucite sheet.

The triclinic specimen was a corundophillite from Mochako District, Kenya, and was obtained from the Harvard collection. The unit-cell dimensions are $a = 5{\cdot}34$, $b = 9{\cdot}27$, $c = 14{\cdot}36$ Å, $\beta = 97°\ 22'$; the space group is $P\bar{1}$; there are two molecules of the approximate composition

$$(Mg_{4\cdot9}Al_{0\cdot8}Fe'''_{0\cdot2}Fe''_{0\cdot1}Cr'''_{0\cdot2})(Si_{2\cdot6}Al_{1\cdot4})O_{10}(OH_8)$$

in the unit cell. The rotation of the Si–O tetrahedra is also observed in this structure but the isomorphous replacement of Mg and Si ions occurs randomly.

4·4. F. H. Gillery. *The X-ray study of synthetic* Mg–Al *serpentines and chlorites.*

Current interest in the two closely related mineral species chlorite and serpentine has prompted an investigation of the properties of the synthetic equivalents produced hydrothermally.

It has been found by examination of a range of composition between

$$Mg_6Si_4O_{10}(OH)_8$$

and

$$(Mg_4Al_2)(Si_2Al_2)O_{10}(OH)_8$$

that chlorites are formed at higher temperatures and pressures than serpentines.

The chlorites formed hydrothermally do not appear to differ appreciably from natural chlorites apart from a small difference in basal spacing, and a tentative explanation can be given for this.

Hydrothermal serpentines can be produced with more aluminum than has been found in natural specimens. They occur in three structural types according to the amount of aluminum they contain and the pressure at which they are formed.

4·5. M. Pezerat. *Détection des cations échangeables de la montmorillonite par l'emploi des séries différences.*

Dans un travail précédent nous avons montré que les mesures correctes effectuées sur quatorze réflexions (00*l*) produites par un échantillon orienté de montmorillonite permettent une synthèse de Fourier unidimensionnelle, de valeur comparable à celle que fournirait un cristal unique.

Nous avons perfectionné la technique en particulier en déterminant l'échelle absolue des intensités des réflexions. Nous l'avons appliquée à l'étude comparée de l'état anhydre et des états d'hydratation homogène. Les mesures sont assez précises pour permettre le calcul des séries $(F_o - F_c)$. Dans le cas du minéral anhydre on met ainsi en évidence le pic des cations échangeables sodium: ces cations se trouvent logés dans les cavités hexagonales de la surface des feuillets. Sur le minéral hydraté à une couche on isole la couche d'eau et les cations. On constate que les cations Na demeurent dans les cavités hexagonales, malgré l'hydratation du minéral.

4·6. H. F. W. Taylor. *The dehydration of tobermorite* ($Ca_5Si_6O_{22}H_{10}$) *and its conversion into* β-$CaSiO_3$ *and into xonotlite* ($Ca_6Si_6O_{17}(OH)_2$).

The behaviour of tobermorite on heating has been studied, using single crystals from Ballycraigy (N. Ireland). Two successive processes occur:

I. Unidimensional lattice shrinkage along *c* giving the lower hydrate with a basal spacing of 9·35 Å. This process appears irreversible. The 9·35 Å hydrate first appeared at 180° C. and was the only phase detected in crystals heated at 300–700° C. Its X-ray reflexions are fewer and more diffuse than those of the unheated mineral. Except for the value of *c*, the unit cell is probably similar to that of the latter, but the pseudo-cell ($a = 5{\cdot}58$, $b = 3{\cdot}66$, $c = 18{\cdot}7$ Å) is *A*-centred and not body-centred. These results confirm Megaw & Kelsey's views (1956) on the packing of the metasilicate chains in the 9·35 Å hydrate. They also suggest that H_2O:Si for this phase can vary from zero to at least 0·33, and that interlayer Si–O–Si links probably occur to an extent which increases as H_2O:Si becomes less.

II. At about 800° C., the 9·35 Å hydrate is converted

into β-$CaSiO_3$ (wollastonite or parawollastonite). There is no other detectable product, and no evidence of any intermediate phase. A single crystal of tobermorite is converted (via the 9·35 Å hydrate) into a crystal of β-$CaSiO_3$ twinned in two orientations related by reflexion across the tobermorite (100). The tobermorite *b* becomes *b* for both orientations of the β-$CaSiO_3$, and the (101) and (10$\bar{1}$) planes of the 9·35 Å hydrate become the monoclinic (201) planes for the two orientations of the β-$CaSiO_3$. The mechanism of this change is discussed.

Work done by the author in collaboration with Dr J. A. Gard and Mr J. W. Howison shows that certain tobermorite specimens of other origin behave differently on dehydration. Crystals from Loch Eynort (Scotland) change directly into β-$CaSiO_3$ without intermediate formation of the 9·35 Å hydrate. Badly-crystallized synthetic specimens undergo unidimensional lattice shrinkage, but the subsequent changes are complex. The crystals become highly disordered by about 600° C., and β-Ca_2SiO_4 (larnite) is usually the first recognizable anhydrous product to appear, at 600–700° C. The larnite tends to disappear at higher temperatures, giving mainly β-$CaSiO_3$ with low-lime preparations (Ca:Si $<$ 1·2 approximately) and rankinite ($Ca_3Si_2O_7$) with high-lime preparations (Ca:Si 1·2–1·4). β-$CaSiO_3$, when it occurs, is often predominant by 850–900° C., but rankinite is rarely detectable below 1000° C.

The related hydrothermal transformation of tobermorite into xonotlite has also been studied, using single-crystal methods. It occurs on treatment with supercritical water at 380° C., without intermediate formation of the 9·35 Å hydrate. A single crystal of tobermorite gives a crystal of xonotlite twinned in two orientations. The tobermorite *a*, *b* and *c* directions become respectively *a*, *b* and *c* for one orientation of the xonotlite and *a*, *b* and $\bar{c}$ for the other (xonotlite is monoclinic with $\beta = 90°$). The mechanism of the change is discussed.

§ 5. Metals and alloys

5·1. U. M. Martius. *The initial stages of oxidation of metals.*

A number of experimental investigations have shown that strongly crystallographic phenomena can occur in the initial stages of oxidation of a metal (J. Benard & J. Bardolle, *Rev. Métall.* (1952), **49**, 613; *C. R. Acad. Sci., Paris* (1954), **239**, 706; E. A. Gulbrausen *et al. J. Metals* (1954), **6** 1027; (1955), **7**, 701; U. Martius, *Canad. J. Phys.* (1955), **33**, 466). The oxide layers are then discontinuous and their structure is related to the crystallographic orientation of the underlying metal. The present paper discusses an investigation of this problem by means of direct microscopic observations during oxidation at high temperature, employing controlled amounts of oxygen. The dependence of the discontinuous oxidation on temperature, rate of oxidation, crystallographic orientation of the base metal and surface preparation is discussed for pure nickel.

5·2. F. W. von Batchelder & R. F. Raeuchle. *The structures of a new series of MBe_{12} compounds from the elements in groups* V–*A*, VI–*A and* VII–*A*.

The crystal structures of VBe_{12}, $NbBe_{12}$, $TaBe_{12}$, $CrBe_{12}$, WBe_{12} and $MnBe_{12}$ have been determined from X-ray single-crystal data. The crystals are isostructural and the space group is $I4/mmm$–D_{4h}^{17}, with two molecules per unit cell. These compounds are isomorphous with $MoBe_{12}$. The dimensions and calculated density of the tetragonal unit cell are:

Compound	a_0 (Å)	c_0 (Å)	c/a	D_x
VBe_{12}	7·278	4·212	0·579	2·37
$NbBe_{12}$	7·376	4·258	0·577	2·88
$TaBe_{12}$	7·334	4·267	0·582	4·18
$CrBe_{12}$	7·230	4·173	0·577	2·44
$MoBe_{12}$*	7·271	4·234	0·582	3·02
WBe_{12}	7·362	4·216	0·573	4·25
$MnBe_{12}$	7·276	4·256	0·585	2·40
$TeBe_{12}$	—	—	—	—

* R. F. Raeuchle & F. W. von Batchelder, *Acta Cryst.* (1955), **8**, 691.

5·3 K. Schübert. *On the increase of axial ratio with electron concentration in morphotropic transitions.*

It is well known that in a large class of compounds one finds a (linear) dependence of molar volume on the increments (W. Biltz) and concentrations of the ions or atoms involved. This statement generally does not depend on the structure of the compound. Structure analysis, together with density experiments, now makes it possible to measure not only the volume of a compound but also something like a morphotropic extension tensor. There are many structure families the members of which have the same structural pattern in some directions but a different building plan in the remaining directions. The question is, whether the morphotropic extension is only a secondary feature of morphotropic transitions, or whether it obeys some rules which are to a certain degree independent, on the whole, of structural data. It seems that the latter is the case. One can see an indication of this in the fact that one mostly finds an increase of axial ratio coming from a strain in one direction if the concentration of the outer electrons increases. This fact will be discussed with some examples.—A morphotropic rule emerges which allows different types of structure to be grouped into structural families, which means a step in the direction to a natural system of crystal structures.

What can be the reason for the behaviour of structures expressed in the above rule? A first way to interpret the extension rule lies in the assumption that there exists a crystalline spatial correlation of the outer electrons, and that a commensurability of an assumed electron lattice with the crystal lattice is energetically favourable. If this is the case, then one would expect crystal structures to exist which have a commensurability in two directions, whereas in the third direction the commensurability is destroyed to allow more or fewer electrons to be filled in the electron lattice relatively to (the elementary cell of) the crystal lattice. If the electron lattice has a certain spatial correlation, the crystal lattice must then be strained.

5·4. E. Parthé. *Contributions to the Nowotny phases.*

During the course of intensive investigations on the structures and properties of silicides of transition metals of the IV–VI groups, attempts have been made to prepare silicides with the formula M_5Si_3. It was noticed during

this work that different silicides of the seemingly equal composition M_5Si_3 are formed in dependence on crucible material, gas atmosphere and starting material. These results could be explained since it was shown by Nowotny *et al.* that one of these M_5Si_3 phases corresponds to a ternary silicide, which is referred to as a Nowotny phase. It could be shown that this hexagonal Nowotny phase, which crystallizes in the $D8_8$ type, can be stabilized by carbon, oxygen and nitrogen pick-up of pure M_5Si_3 phases. The amount of metalloid which is necessary to stabilize the Nowotny phase is in general small but is changing with the position of the metal component in the Periodic System. In the case of Zr_5Si_3, for example, 0·3 atomic% carbon is necessary only to prevent the formation of the pure silicides. As the commerical zirconium powder contains contaminations we will not wonder that the ternary $Zr_5Si_3(C)$ phase was till now considered as pure silicide. Additional experiments revealed that Nowotny phases are formed by silicides with boron addition too.

New experiments showed that germanides will also form Nowotny phases if carbon is available. As in the case of silicides, the necessary amount of carbon increases with the group number of the metal.

$D8_8$ phases are known, furthermore, for stannides and plumbides, but it is not known how far stabilizer atoms are necessary for the formation of this structure type.

An intensity calculation for C-stabilized Mo_5Si_3 with $D8_8$ structure showed that there is a metal deficiency in the 4(*d*) position of the structure. This led to a general formula:

$$M_{0\cdot375}M_{0\cdot25}(C, Si)_{0\cdot25(1-\alpha)}(C, Si)_{0\cdot375}, \quad \text{where} \quad \alpha \leq 1 .$$

This formula takes care of the large homogeneity range of the Nowotny phase.

A consideration of the homogeneity ranges of different C-stabilized Nowotny phases reveals that the center of this phase lies at all times about 37·4 atomic% Si. Furthermore, it was found that for the center of the homogeneity range of Nowotny phases, α equals K/N, where K is a constant for each period and N is the group number for the metal component. We therefore get a new formula for the center of the homogeneity range of different C-stabilized Nowotny phases:

$$M_{0\cdot375}M_{0\cdot25\,K/N}C_{0\cdot25(1-K/N)}Si_{0\cdot375}$$

and

$$\text{atomic\% C} = 25(1-K/N) .$$

Someone might be tempted to get from this formula a criterion for Nowotny phases: the metal electron concentration in the 4(*d*) position has to be constant for all kinds of Nowotny phases. As we do not know the electron contribution of transition metals in these compounds, it seems advisable to call the given formula an empirical one.

For the characteristics of Nowotny phases the following points may be given:

(*a*) Nowotny phases are ternary silicide or germanide phases with $D8_8$ structure which are stabilized by small amounts of metalloids like C, N, O, B.

(*b*) The composition of Nowotny phases is not constant. The amount of metalloid which is necessary for stabilization of Nowotny phases increases in each group of the Periodic System with the period number of the metal component.

(*c*) The necessary amount of metalloid increases, too, in each period with the group number of the metal component.

(*d*) Nowotny phases do not occur at all ternary system *M*–Si–C, N, O, B. The tendency to form Nowotny phases increases from O over N, B to C.

(*e*) Under impure preparative working conditions the Nowotny phases may mask pure silicides. The masking only happens by metal-rich silicides.

5·5. H. J. GOLDSCHMIDT. *Occurrence of the β-manganese structure in transition metal alloys, and some observations on χ-phase equilibria.*

Manganese occupies a unique position amongst transition metals in that each of its four allotropic forms presents a prototype to intermetallic phases, themselves not containing manganese. (This is the converse to the case of σ-phase, which, as a 'typical' binary or ternary compound between elements flanking Mn in the periodic system, occurs in a pure metal, β–U.)

A report is given on an intermetallic compound possessing the β–Mn structure and discovered in the Fe–Cr–W–C system. The phase (here denoted π) is stable only at temperatures close to the melting point, but retainable by quenching, and some of its characteristics and conditions of formation are described. It possesses an appreciable homogeneity width, the cubic lattice spacings ranging from 6·288 to 6·403 Å as against 6·302 Å for Mn. A representative composition is $Fe_{10}Cr_9W_2C$ (but the 'ideal' formula probably is $Me_{20}C$ in conformity with the 20 metals atoms per unit cell of manganese). As in manganese metal, the compound is a high-temperature allotropic form of Andrews' now well established χ-phase of α-Mn structure. Both phases, however, possess their own solubilities for further elements, in some analogy to the austenite/ferrite relationship for iron. A decomposition reaction $\pi \rightarrow \chi+\alpha$ (ferrite) was observed, and could be induced by several types of thermal treatment, as well as by cold work. The present phase contains carbon as an integral element, but its existence in carbon-free alloys (where it may not be quenchable) is not excluded. Phase assemblies in which π is associated include χ, σ austenite and ferrite, the ferrite of greatly expanded lattice. The π phase seems likely to enter significantly in certain alloy steels, when rapidly cooled.

The α-Mn structure (χ) was confirmed as prominent in the Fe–Cr–Mo, Fe–Cr–W and Fe–Cr–W–C systems, and dimensional lattice changes in χ and equilibria between 900 and 1400° C. are reported. The χ-phase possesses a considerable solubility for carbon. The phase can, in fact, assume the double role of 'a carbide' as well as of a primary carbon-solvent; the carbide aspect of the χ-phase is affirmed by the fact of its being able to replace η carbide in high-speed steels with varying chromium contents.

To complete the structure systematics, all four crystallographic forms of manganese may now be regarded as represented as it is justified to relate γ and δMn to the austenitic and ferritic constituents occurring.

5·6. D. A. EVANS & K. H. JACK. *Interstitial alloys with the structure of β-manganese.*

In the Fe–Mo–N system, a new phase (now called β^m) has the β-Mn type of metal-atom arrangement, the cubic unit cell of which (a = 6·6948–6·7020 Å) contains

ideally $Fe_7Mo_{13}N_4$. The interstitial atoms, which are essential for the occurrence of the structure, are at the fourfold sites (*a*) of space group $P4_132$ and are each surrounded by six metal atoms in (*d*) sites at distances of 2·09 Å. The nitrogen atom has an effective radius of about 0·7 Å and an environment which is mid-way between that observed in δ-MoN and that found in γ-Mo_2N and in iron nitrides.

An η_1-carbide-type structure is also found in the same system at compositions near Fe_3Mo_3N (a = 11·065–11·095 Å), and β^m occurs under conditions where the η_2-carbide-type might have been expected. The conditions necessary for the formation of η structures (K. Kuo, *Acta Metallurg.* (1953), **1**, 301) apply equally to the formation of β^m, and it is predicted that the latter will occur in a number of interstitial systems. We have found β^m phases isostructural with $Fe_7Mo_{13}N_4$ in the systems Mn–Mo–N, Co–Mo–N, Ni–Mo–N and Ni–Mo–O, and a β^m-Fe–W–C alloy of unknown composition (a = 6·395 Å) has already been reported (K. Kuo, *J. Metals, N.Y.* (1956), **8**, 97).

It is of interest that in β-manganese itself there exist interstices at sites (*a*) which are large enough to accommodate up to 16 atomic% of C, N or O without undue strain.

The relationships between interstitial and substitutional β^m structures are as yet unknown; their further examination may clarify not only the nature of the factors involved in this type of metal-atom arrangement, but it may also contribute to an understanding of the metal–non-metal bonding in interstitial alloys.

5·7. W. H. Taylor. *Structures of transition metal alloys.*

The paper reports further developments in a research aimed at determining (*a*) the systematic structural geometry, and (*b*) the detailed electron distribution for alloys rich in electrons and containing transition metals.

In these alloys the transition metal atom is surrounded by a well defined polyhedral grouping of Al atoms (or other atoms with equivalent role). From the variations in coordination number and contact distance conclusions have been drawn about the occurrence of powerful bonds between transition metal and Al atoms. Recent work on V–Al structures by P. J. Brown has supplemented published information on alloys containing Co, Mn, Cr or Fe, and in a following paper J. A. Bland describes some further systematization of the structural geometry based upon analysis of Mn–Al and W–Al alloys.

The structure of (Fe, Cu)Al_6 is a copy of $MnAl_6$, and the refinement of the former has led to a further refinement of the latter beyond the stage reached in the published analysis. A relaxation of the symmetry appears to be involved, and although at the time of writing this abstract the re-examination of this structure type is not yet completed, and it is clear that only very small variation in contact distances are involved, it seems possible that some light may be thrown on the nature of the bonding.

In the hope of removing ambiguities which arise in making electron counts when normal routines of structure analysis are followed, a technique has been devised for the absolute measurement of intensities of X-ray reflexion with small alloy crystals. It is being applied first to $MnAl_6$ and it is hoped that results may be obtained in time for presentation at the Congress: the aim is to determine the electron distribution within known limits of accuracy, and, in particular, to decide whether any electrons are absorbed from the structure by the transition metal atoms, which would thus display an effective negative valency.

5·8. J. A. Bland. *The structural geometry of the transition metal alloys* $MnAl_6$, Mn_4Al_{11}, *and* WAl_4.

The crystal structures of the intermetallic compounds Mn_4Al_{11} and WAl_4 have been determined from Weissenberg camera data.

Mn_4Al_{11} is triclinic, pseudo-monoclinic, with cell constants

$$a=5\cdot092\pm0\cdot003,\quad b=17\cdot098\pm0\cdot010,\quad c=5\cdot047\pm0\cdot003\ \text{Å};$$
$$\alpha=92°52'\pm5',\quad \beta=100°24'\pm5',\quad \gamma=88°38'\pm5';$$

and space group $C\bar{1}$. The approximate structure has been determined directly using Harker–Kasper inequalities, and the atomic parameters have been refined by two-dimensional F_o and F_o-F_c syntheses.

WAl_4 is monoclinic with cell constants

$$a=5\cdot272\pm0\cdot003,\quad b=17\cdot771\pm0\cdot010,\quad c=5\cdot218\pm0\cdot003\ \text{Å},$$
$$\beta=100°12'\pm5',$$

and the non-centrosymmetrical space group C_m. The heavy-atom method has been used to determine the structure, and F_o syntheses have been employed in the refinement of the parameters.

Both structures are related to $MnAl_6$ (A. D I. Nicol, *Acta Cryst.* (1953), **6**, 285), which is orthorhon.bic but has a corresponding monoclinic cell:

$$a = 4\cdot9811\pm0\cdot0005,\ b = \tfrac{1}{2}\ (17\cdot7406)\pm0\cdot005,$$
$$c = 4\cdot9811\pm0\cdot0005\ \text{Å},\ \beta = 98°34'.$$

The relationship is described in terms of sequences of similar nets of atoms perpendicular to the corresponding monoclinic b axes; most of the nets are distorted 5-connected nets.

The environments of the transition metal atoms are similar in the three structures. Some abnormally short contacts exist between the transition metal and Al atoms and it is possible to conclude that there are strong bonds between unlike atoms. There is evidence that some of the short bonds from the transition metal atoms in each structure are in the same orientation as the short bonds from Mn to Al in $MnAl_6$.

5·9. J. E. Noakes, A. H. Turner & R. A. Artman. *Anomalous behavior of solution of titanium in iron.*

Lattice-parameter measurements have been made on the Fe–Ti system over the range of concentrations of solubility of titanium in iron.

The lattice parameter of the Fe–Ti solution is essentially constant up to a concentration of approximately ½% titanium. Beyond this concentration, and up to the solubility limit, the lattice parameter increases linearly with a slope which is approximately that predicted by Vegard's law. These lattice parameters do not extrapolate to those of pure iron. These results extend the measurements to lower concentrations than those reported by

A. L. Sutton & W. Hume-Rothery (*Phil. Mag.* (1955), (7), **46**, 1295) and are in essential agreement with them at the higher concentrations.

Samples were prepared by filing under argon and sieving through a 325-mesh screen. The filings from the various alloys were separated into three groups which were heat treated at 900° C. for 1, 24, and 120 hr. respectively. The samples were furnace cooled. Lattice-parameter measurements were made on a diffractometer using Cr $K\beta$ radiation, and reproducibilities of 1 part in 30,000 were obtained.

Experiments have been concerned with establishing whether the parameter anomaly with low titanium concentration is a volume effect or surface effect. Samples containing greater than $\frac{1}{2}$% titanium annealed for 24 hr. or more show two sets of reflections whose separation increases with titanium content. Lattice measurements from one set of reflections were those of iron while the others were due to the solutions of titanium in iron. The extra lines are not present in the low concentration short-time-anneal samples. Chemical analyses show that the titanium is in metallic solution for all anneals. These results indicate that the anomalous lattice-parameter curve is due to a bulk effect and the formation of the iron peaks for long anneals is a surface effect.

Measurements of electrical resistivity have been made to substantiate these conclusions. Heat treatment of solid samples paralleled those of the filings. These measurements were made at liquid-helium temperature as well as room temperature. The resistivity results show an apparent departure from Matthiesen's rule. It has been shown by X-ray work on a back-reflection camera that this is due to a layer of iron on the surface of the solid samples. The electrical-resistivity and X-ray-parameter results are consistent.

5·10. Ju. S. Terminasov & E. Z. Galperin. *Structural changes in steel due to cold working and heat treatment.*

1. Changes of different structural characteristics, such as dispersity, elastic and static distortions of the α-phase lattice, characteristic temperature and carbide-phase state, were examined in the course of plastic deformation and heat treatment of silicon steel 55C2.

2. Steel samples were statically compressed, and a part of them was filed (after annealing) in order to obtain powder. The roentgenographic part included photographic and ionisation measurements of the diffraction maxima produced by Fe $K\alpha$ and Mo $K\alpha$ radiations.

3. Effects of fragmentation and elastic distortions, responsible for the diffraction-line widening, were separated analytically and by means of harmonic analysis.

4. Both methods gave a satisfactory coincidence of the elastic distortion data. The calculated crystallite dimensions depended essentially on the choice of the analytic function. The function $1/(1+K^2x^2)^2$ was found to be the most suitable.

5. Static distortions of the atomic lattice were rated according to changes in the diffraction-line intensity for the lines (110) and (220) of Fe $K\alpha$ radiation and $6 \leq \Sigma hi^2 \leq 38$ of Mo $K\alpha$ radiation. The extinction effect was taken into account and it was found that this effect is practically unimportant for Mo radiation. The extinction effect provoked a 10–15% intensity change of the (110) line of Fe $K\alpha$ radiation.

6. No regular intensity changes were found in the course of plastic deformation, which apparently proves the absence of a direct connexion between static distortions and $\sqrt{(\overline{Us^2t})}$.

7. An attempt was made to state a relationship between the structural characteristics of the samples examined and their mechanical properties, e.g. microhardness. It was found that the hardening of deformed steel is due essentially to submicroscopic structural non-uniformities appearing in the course of the α-phase fragmentation and the formation of severely distorted boundary regions.

8. An indentical method was applied to the examination of oil-hardened steel samples tempered at 200–700° C. for 1 hr. The carbide sediment from a part of the samples was obtained and examined by means of Fe $K\alpha$ radiation.

9. Maximum changes of the steel 55C2 characteristic temperature, caused by heat treatment, do not exceed 3–4%.

10. A regular diffraction intensity change is found in the course of tempering which allows static distortions to be rated according to $\sqrt{(\overline{U^2st})}$.

11. Tempering of hardened steel 55C2 at less than 400° C. causes the formation of an intermediate carbide with a hexagonal lattice ($a=2{\cdot}72$, $c=4{\cdot}35$ Å). At higher temperatures this carbide transforms actively to cementite.

12. The main effect on the tempered steel hardening has several factors: carbon state, different admixtures and their distribution, and static distortions of the α-phase lattice.

5·11. R. M. Fisher. *Crystallographic relations of carbide and ferrite in pearlite, bainite and tempered martensite.*

The crystallographic relations between carbide and ferrite have been determined for pearlite, bainite and tempered martensite. The relative orientations were determined by a combination of electron-diffraction techniques and analysis of Kossel lines resulting from reflections of X-rays produced in ferrite grains under electron bombardment.

5·12. A. Taylor & R. M. Jones. *X-ray and magnetic investigation of iron-rich iron–aluminum alloys.*

Considerable changes have been made in the constitution diagram of the iron–aluminum system as a result of the present investigation. Powder patterns of quenched iron-rich alloys have yielded lattice parameters which differ quite appreciably from those of Bradley & Jay, obtained nearly 25 years ago. These new results are more in accord with the magnetic properties of the alloys. Diffraction patterns at elevated temperatures reveal a new order–disorder transformation over the composition range $Fe_{13}Al_3$–Fe_2Al. It has been found that severe cold-working of non-magnetic α-phase alloys converts them to a ferromagnetic condition without destroying the superlattice and, at the same time, induces a volume expansion of nearly 3·0% at favored compositions.

In addition to the body-centered cubic α phase structure, a ferromagnetic face-centered cubic phase is occasionally found, which is associated with alloys over the range 18–33 atomic% aluminum. This structure is probably epitaxially related to the body-centered cubic

matrix of the α phase and seems to undergo an order–disorder transformation.

A high-temperature ε phase has been established in the region of $FeAl_2$. This phase cannot be retained on quenching. High-temperature powder patterns taken at 1150° C. are consistent with an orthorhombic unit cell.

5·13. D. Bally & C. Maris. *La dissociation de certains alliages* Cu–Ni–Fe (*étude à l'aide de rayons X*).

Interprétation théorique du phénomène

L'apparition de la structure intermédiaire dans certains alliages Cu–Fe–Ni, soumis à un traitement isothermique à une température à laquelle l'état d'équilibre est caractérisé par deux réseaux cristallins, peut être expliquée si l'on admet qu'au début de ce traitement apparaissent dans le réseau cristallin initial des domaines de concentration rapprochée de celle des phases solides, caractérisant l'état d'équilibre. La continuation du traitement isothermique conduit à l'agrandissement de ces domaines et à la variation de leur concentration, ce qui détermine ensuite l'apparition de centres de cristallisation de phases nouvelles, dont le réseau cristallin est indépendant.

L'existence de domaines de concentration différente dans le réseau cristallin conduit à sa déformation. Les travaux de V. Daniel & H. Lipson (*Proc. Roy. Soc.* A (1943), **181**, 368; (1944), **182**, 378) et de A. H. Geisler & J. B. Newkirk (*Trans Amer. Inst. Min.* (*Metall.*) *Engrs.* (1949) **180**, 101) sur les alliages Cu–Ni–Fe, conduisent à la conclusion que les directions de déformation du réseau cristallin initial coincident avec les directions des axes du cube.

Soit a, a_1 et a_2, respectivement, les paramètres du réseau de la structure cristalline initiale et des structures cristallines qui correspondent à l'état d'équilibre ($a_2 < a < a_1$).

En admettant que dès le début du traitement isothermique apparaissent dans le réseau cristallin initial des domaines dont la concentration correspond à celle des structures qui résultent du processus de la dissociation, la déformation du réseau cristallin dépendra des valeurs des différences a_1-a et $a-a_2$.

Nous allons évaluer les amplitudes et les intensités maxima de la diffraction donnée pour un réseau cristallin déformé de cette façon, si l'on suppose que le volume total reste constant au cours de la déformation du réseau. Pour simplifier, nous traiterons d'abord le cas monodimensionnel, en généralisant ensuite les résultats obtenus pour le cas tridimensionnel.

Dans ce qui suit, nous allons utiliser les notations employées par Daniel & Lipson et aussi par M. E. Hargreaves (*Acta Cryst.* (1951), **4**, 301).

Nous considérons donc une série de périodes a. Qa est la longueur des segments qui contiennent un seul centre de déformation, la dimension duquel est $ax(k+1)$, où $k+(a_1-a)/(a-a_2) = \alpha/\beta$.

La dilatation du réseau sur une longueur de x intervalles et sa compression le long de kx intervalles suivants, conduit à la définition d'une fonction $f(q)$ de la déformation de la structure (Fig. 1).

Le résultat obtenu, sans modifier la forme de l'image de diffraction prévue par les résultats obtenus antérieurement, indique néanmoins une variation des amplitudes relatives, tant en ce qui concerne la diffraction, qu'en ce qui concerne le paramètre k qui caractérise la structure ayant souffert une déformation.

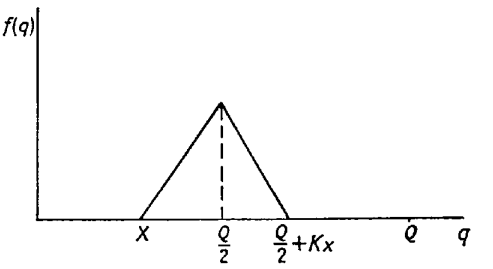

Fig. 1.

Pour obtenir, sous forme explicite, la dépendance de l'intensité des satellites des dimensions des centres de déformation, nous avons évalué les amplitudes relatives de la ligne fondamentale et des satellites dans l'hypothèse que $f(q)/Qa \ll 1$.

Dans cette hypothèse, l'intensité des satellites rapportée à l'intensité de la ligne fondamentale, donne les expressions suivantes:

$$\frac{\mathscr{I}_{l\pm 1/Q}}{\mathscr{I}_l} = 2l^2\frac{\alpha^2}{a^2}x^2\,; \qquad \frac{\mathscr{I}_{l\pm 2/Q}}{\mathscr{I}_l} = \frac{1}{4}l^2\frac{\alpha^2}{a^2}x^2\,, \tag{1}$$

où $\mathscr{I}_{l\pm 1/Q}$, $\mathscr{I}_{l\pm 2/Q}$ et $\mathscr{I}_l$ représentent les intensités des satellites de l'ordre de $l\pm 1/Q$, respectivement, $l\pm 2/Q$ et de la ligne fondamentale. La relation (1) indique une diminution de l'intensité relative des satellites par rapport à l'éloignement de la ligne fondamentale, conclusion qui découle également du mode d'interprétation employé par d'autres auteurs (Daniel & Lipson, *loc. cit.*; Hargreaves, *loc. cit.*).

Il est intéressant de noter le fait que le rapport $\mathscr{I}_{l\pm 1/Q}/\mathscr{I}_l$ est proportionnel au carré des dimensions relatives du centre de déformation et avec le rapport α/a, caractéristique pour une structure cristalline donnée.

Le résultat obtenu pour le cas monodimensionnel peut être généralisé pour le cas tridimensionnel, en admettant que dans le réseau cristallin initial apparaissent des centres de déformation de forme lamellaire avec une structure tétragonale, la direction de l'axe C coincidant avec l'un des axes du cube. Dans le cas d'images de diffraction données par des polycristaux où chaque maximum d'intensité correspond à une valeur $N = h^2+k^2+l^2$ donnée, s'accompagnera d'une série de paires de satellites. L'intensité des satellites du premier ordre, rapportée à l'intensité de la ligne fondamentale, sera:

$$\frac{\mathscr{I}}{\mathscr{I}_0} = 2N\frac{\alpha^2}{a^2}x^2\,. \tag{4}$$

Méthode de travail

On a étudié quatre alliages du système Cu–Fe–Ni dont la composition en pourcentage atomique est indiquée au-dessus:

No. de l'alliage	Cu (%)	Fe (%)	Ni (%)
1	49,43	11,92	38,65
2	53,29	9,92	36,78
4	49,05	10,57	40,38
9	51,38	29,49	20,23

L'examen aux rayons X a été effectué dans une chambre de diffraction ayant un diamètre de 14 cm. On s'est servi d'un tube à rayons X avec anode de cuivre,

la radiation produite par le tube étant filtrée par un filtre de nickel.

Le processus de déformation du réseau cristallin a été réalisé en traitant des alliages à la température de 550 C. pendant 129 hr. Les traitements ont été faits en enfermant les poudres dans des ampoules de quartz.

Pour déterminer les paramètres du réseau de la structure biphasique correspondant à l'état d'équilibre, les alliages ont été traités pendant 172 hr. à 600° C., ce qui a conduit dans tous les cas à l'apparition nette de l'image de diffraction correspondante.

Pour évaluer la largeur des lignes de diffraction on a employé la méthode de l'étalon. On a obtenu pour chaque étape de l'étude et pour chaque alliage deux images de la diffraction: l'une pour l'alliage et l'autre pour un mélange de cuivre et de l'alliage étudié.

Résultats des expériences

Déterminations des dimensions des centres de déformation. — Le traitement thermique à 550° C. conduit dans tous les cas à la modification de l'image de diffraction. Les maxima de diffraction sont encadrés d'une paire de satellites. Ainsi qu'il résulte des travaux cités ci-dessus (V. Dehlinger, *Z. Kristallogr.* (1927), **101**, 149; Hargreaves, *loc. cit.*) leur intensité baisse avec l'ordre de la ligne fondamentale. Pour évaluer les dimensions des centres de déformation, nous avons déterminé le rapport des intensités des satellites et de la ligne fondamentale pour des intervalles de temps de traitement variant entre 15 et 20 hr. Le mécanisme de la déformation du réseau cristallin reste le même dans les quatre cas étudiés, le processus étant décalé dans le temps, en fonction de la composition des alliages.

On observe que les valeurs de x, calculées avec les données des lignes de diffraction de différents ordres, coincident pratiquement. Le résultat obtenu démontre qu'une correction pour l'extinction n'est pas nécessaire, puisque le rapport $\mathscr{I}/N\mathscr{I}_0$ demeure constant avec la variation de N.

Dans la Fig. 2 est indiquée la dépendance de x du temps de traitement. Dans tous ces cas la dépendance est linéaire, indiquant un accroissement uniforme dans le temps des centres de déformation, au cours de la période pendant laquelle la cohérence du réseau initial est conservée. Ce résultat est intéressant parce qu'il peut conduire à une explication de la variation des propriétés magnétiques de ces alliages avec le temps de traitement (voir les paragraphes suivants).

Étude de l'intensité des maxima de diffraction. — L'apparition des centres de déformation et leur croissance pendant la période de conservation de la cohérence du réseau cristallin initial conduit à l'affaiblissement des intensités des maxima principaux de diffraction. Le mécanisme proposé pour expliquer le processus de la déformation conduit au déplacement des atomes dans certaines régions du réseau cristallin, par rapport à leurs positions initiales. Ce déplacement suggère l'existence de tensions de l'ordre 3, identiques à celles qui apparaissent dans le réseau cristallin dans le cas de sa déformation plastique.

L'évaluation des rapports $\dfrac{\mathscr{I}'_{h'k'l'}}{\mathscr{I}'_{hkl}} \Big/ \dfrac{\mathscr{I}_{h'k'l'}}{\mathscr{I}_{hkl}}$ où l'on a noté par $\mathscr{I}'$ les intensités des maxima de diffraction de l'alliage déformé et par $\mathscr{I}$ les intensités des mêmes maxima donnés par l'alliage non déformé, en utilisant les valeurs des intensités des lignes (420) et (331) rapportées à celles des lignes (111) conduisent aux valeurs comprises entre 0,2 et 0,3 Å pour le déplacement moyen $\sqrt{(\overline{u^2})}$, en fonction de la durée du traitement.

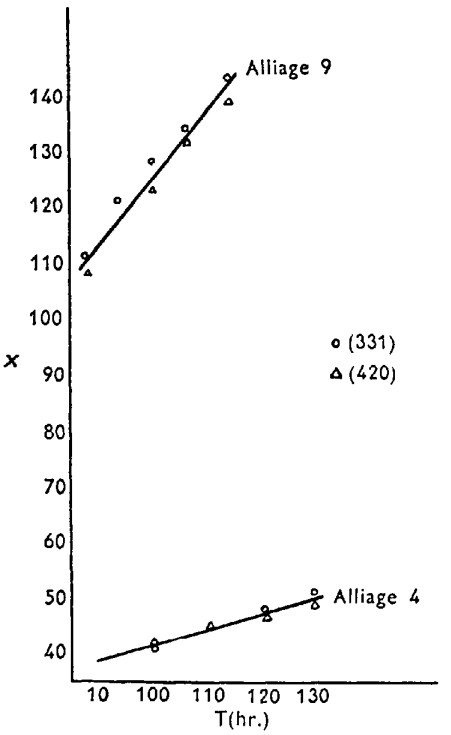

Fig. 2.

La largeur des maxima de la diffraction. — Pour déterminer la largeur des maxima de diffraction, nous avons employé la méthode proposée par L. J. Lisak.

Les mesures faites pour les lignes (311) pour lesquelles le rapport B/b (où B est la largeur de la ligne étudiée et b la largeur de la ligne de l'étalon), est compris entre les limites 1,5−2, en employant la relation $\beta = \sqrt{(B^2-b^2)}$, conduisent à un accroissement de β avec la durée du traitement à 550° C. Les valeurs β pour les alliages étudiés sont:

Alliage 1		Alliage 2	
T (hr.)	β (mm.)	T (hr.)	β (mm.)
0	0,2	0	0,2
20	0,3	90	0,3
30	0,4	110	0,4
50	0,5	129	0,5

Le phénomène observé peut être déterminé par l'existence de tensions de l'ordre 2, apparaissant dans le réseau cristallin au cours du processus de déformation et de la présence des centres de déformation, dont les dimensions sont en tous cas plus petits que 10^{-5} cm., comme il a été dit dans les paragraphes précédents et enfin par la présence des satellites dans le voisinage immédiat des maxima de diffraction.

Nous considérons que la séparation des trois facteurs mentionnés, pourrait conduire à des résultats intéressants.

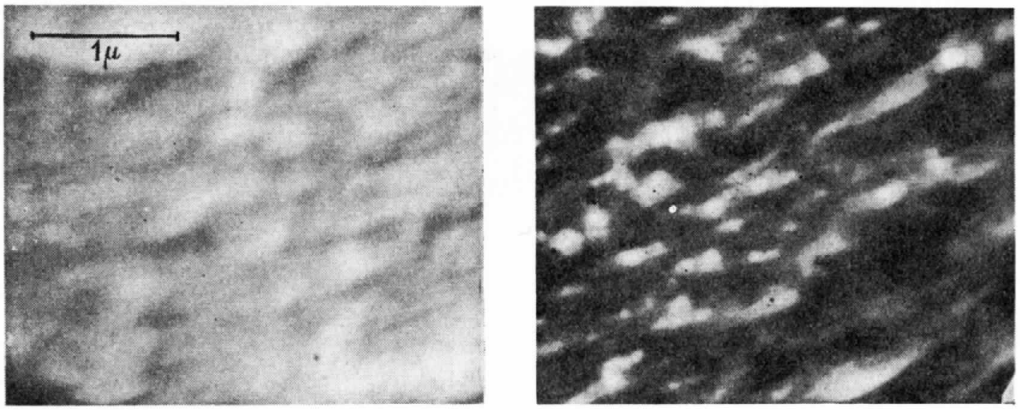

(*a*) (*b*)

Fig. 3.

Observations au microscope électronique

Les observations au microscope électronique de la structure des alliages Cu–Ni–Fe ont été effectuées avec le concours de MM. N. Croitoru et I. Teodorescu. Dans tous les cas étudiés, le traitement thermique à 1000° C. conduit à l'apparition d'une structure cristalline monophasique. Les images des surfaces, agrandies 30,000 fois, indiquent la présence de régions non-homogènes, dont les dimensions sont de l'ordre de 10^{-5} cm. (Fig. 3(*a*)).

Le traitement isothermique à 550° C. conduit dans tous les cas à l'apparition de la structure biphasique. La forme lamellaire des cristallites des nouvelles phases, apparue après la rupture du réseau cristallin initial, peut être observée dans la Fig. 3(*b*).

Propriétés magnétiques

Une étude préliminaire des propriétés magnétiques des alliages étudiés, a été faite avec le concours de M. A. Glodeanu. La mesure de la force coercitive des alliages après le traitement à 1000° C. donne des valeurs inférieures à 1 Oe. pour tous les alliages étudiés. Le traitement isothermique à 550° C. conduit dans tous les cas étudiés à l'accroissement de la force cœrcitive. L'intervalle de temps, pendant lequel on a pu déterminer la croissance linéaire des dimensions des centres de déformation avec la durée du traitement, est compris dans l'intervalle de temps pendant lequel la force cœrcitive s'accroit linéairement avec la durée du traitement. Dans cet intervalle la force cœrcitive augmente de 10 Oe. jusqu'aux valeurs comprises entre 100 et 200 Oe., en fonction de l'alliage. La continuation du traitement thermique conduit à un accroissement sensiblement plus lent de la force cœrcitive.

Conclusions

Les résultats obtenus démontrent que:

1. Pour un intervalle assez grand l'épaisseur de ces lamelles dépend linéairement de la durée de traitement de l'alliage.

2. Les intensités des maxima de diffraction baissent conformément à une loi simple, avec l'augmentation de la durée de traitement, ce qui indique la présence d'une déformation de l'ordre 3 du réseau cristallin.

3. On peut établir une corrélation entre les dimensions des centres de déformation et la force cœrcitive des alliages étudiés.

4. La largeur réelle des maxima de diffraction s'accroit sensiblement avec le degré de déformation du réseau cristallin.

5·14. Y. Komura, D.P. Shoemaker & C.B. Shoemaker. *The crystal structure of the R phase*, Mo–Co–Cr.

The *R* phase in the system Mo–Co–Cr (30·4–51·3–18·3 atomic ratio), discovered by Beck *et al.*, is one of a family of transition-group intermetallic phases of related structure which includes the σ phase, the δ phase, the μ phase, the χ phase, and the *P* phase, as well as being related to the Laves–Friauf phases. A structure for the *R* phase has been found which is rhombohedral, with space group $C_{3i}^2-R\bar{3}$, and with 53 atoms per primitive rhombohedral cell. The corresponding 159-atom hexagonal cell has lattice constants $a_0 = 10{\cdot}9$, $c_0 = 19{\cdot}4$ Å.

The structure may be constructed by linking together coordination polyhedra coaxially along the threefold axes. Per repeat on one axis there are two 16-coordination polyhedra (icosioctahedra) which share a hexagonal ring of atoms with each other, and three 12-coordination polyhedra (icosahedra) which share triangular groups with each other and with the 16-coordination polyhedra. These groupings pack together, without requiring additional atoms, to yield a structure containing eleven kinds of atoms (one 3(*b*), two 6(*c*), and eight 18(*f*)), of which six have coordination 12, two 14, one 15, and two 16. These are the same coordinations observed in the *P* phase and in the σ phase, excepting only that the σ phase does not contain coordination 16.

Pseudo-hexagonal layers strongly resembling those in the *P* phase may be seen parallel to planes $(\bar{3}45)$. By a transformation $(-\frac{1}{3}, -\frac{2}{3}, \frac{1}{3}; \frac{10}{3}, \frac{5}{3}, \frac{2}{3}; \frac{2}{3}, \frac{1}{3}, \frac{1}{3})$ from the hexagonal axes a primitive cell may be obtained the basal plane of which ($a_0' = 9{\cdot}00$, $b_0' = 34{\cdot}0$ Å, $\gamma' = 92°\ 53'$) is parallel to the planes $(\bar{3}45)$. The basal layer is roughly describable as a superstructure on that of the orthorhombic *P* phase ($a_0 = 9{\cdot}07$, $b_0 = 16{\cdot}98$ Å); much the same arrangement of hexagonal 'holes' and pentagonal 'holes' exists. As in the σ and *P* phases, a network of six-coordinated ligands is recognizable; indeed, there is only one three-dimensional network, and no independent layer

networks or row lines such as exist in the σ and P phases.

The unrefined structure gives satisfactory preliminary ($hk0$) structure-factor agreement ($R = 0{\cdot}37$) and satisfactory qualitative ($00l$) agreement. Refinement will be carried out with three-dimensional Weissenberg data.

5·15. Z. G. PINSKER. *The investigation of some carbides and nitrides of chrome, iron, tungsten and molybdenum by electron diffraction.*

1. Limitation of the data given in the reports on the structures of carbides and nitrides. 2. The new experimental techniques. 3. Results of determination of phase composition and structures of some phases. 4. Non-diffusial transformations. 5. Determination of the C and N positions in the crystal structure of carbides and nitrides.

5·16. L. D. CALVERT, H. S. DUNSMORE, L. V. KUHI & R. S. TSE. *The crystal structures of* AgCa *and* Ag_2Ca.

AgCa is stable in argon at room temperature. It decomposes to Ag and $Ca(OH)_2$ in moist air. It is orthorhombic with $a = 4{\cdot}08$, $b = 11{\cdot}48$, $c = 4{\cdot}65$ Å ($\pm 0{\cdot}5\%$), $Z = 4$, $d_{meas.} = 4{\cdot}3-4{\cdot}5$, $d_{calc.} = 4{\cdot}53$. A piezo-electric test gave a faint response from some fragments of AgCa. Precession photographs fixed the diffraction symbol as *mmmC–c–*. *Cmcm*, *Ama2*, and $Cmc2_1$ are the possible space groups. The first was ruled out by the piezo-electric test and also by packing arguments. The second was also ruled out on space considerations. The Ag and Ca atoms were located by trial and error in the fourfold positions (*a*) $0, y, z$; $0, \bar{y}, \frac{1}{2}+z$; $\frac{1}{2}, \frac{1}{2}+y, z$; $\frac{1}{2}, \frac{1}{2}-y, \frac{1}{2}+z$ of space group $Cmc2_1$, Ag having $y = 0{\cdot}425$, $z = 0$ and Ca having $y = 0{\cdot}165$, $z = 0$. These positions gave satisfactory agreement between calculated and observed F's for 38 ($h0l$) and ($0kl$) planes and reasonable agreement for 16 (hkl) planes for which only very rough intensity measurements were available. This structure is characterized by AgCa pairs with a separation of 2·99 Å. The shortest Ag–Ag distance is 2·89 Å and the corresponding Ca–Ca distance is 3·65 Å.

Ag_2Ca is stable in argon at room temperature; it decomposes slowly in moist air. It is orthorhombic with $a = 7{\cdot}26$, $b = 4{\cdot}68$, $c = 8{\cdot}14$ Å ($\pm 0{\cdot}5\%$), $Z = 4$, $d_{meas.} = 5{\cdot}8-6{\cdot}0$, $d_{calc.} = 6{\cdot}1$. Precession photographs fixed the diffraction symbol as *mmmI–a–* with space groups *Imma* and *Ima2* possible. Both space groups were considered but the atoms could be placed satisfactorily only in *Imma* with 8 Ag in positions (*i*) $x, \frac{1}{4}, z$, etc. with $x = 0{\cdot}200 \pm 0{\cdot}0025$ and $z = 0{\cdot}080 \pm 0{\cdot}025$ and 4 Ca in positions (*e*) $0, \frac{1}{4}, z$, etc. with $z = 0{\cdot}645 \pm 0{\cdot}005$. These coordinates gave satisfactory agreement between observed and calculated F's for 30 planes of the type ($h0l$) and ($hk0$) and reasonable agreement for 7 (hkl) planes for which only very rough estimates of intensity were possible.

This structure is characterized by Ag_2Ca groups with the Ag–Ca separation 2·86 Å and the angle Ag–Ca–Ag approximately 97°. The shortest Ag–Ag distance is 2·68 Å and the shortest Ca–Ca distance is 3·32 Å.

5·17. N. E. WESTON & D. P. SHOEMAKER. *The crystal structures of three phases in the* Na–Pb *system.*

The crystal structures of three closely related phases of closely similar compositions in the 'Na_2Pb' region of the Na–Pb system have been determined; as far as is known, there are no remaining phases of undetermined structure in this system. These phases, as described by Krohn, Werner & Shapiro are: (I) a phase of maximum melting composition Na_9Pb_4, which is stable only above 190° C., and at that temperature rapidly and reversibly transforms to a phase (II) of presumably the same composition; and (III) a phase of composition Na_5Pb_2 at its concealed melting point. Both powder and single-crystal (precession and Weissenberg) photographs were obtained for all three phases, those for (I) being necessarily taken above 190° C.; a single crystal of (II) on heating above 190° C. transformed into a twinned crystal of (I) with preservation of axial directions. The structures in Table 1 gave good agreement with powder spacings and qualitative single-crystal intensities.

Work leading toward the establishment of sodium-atom coordinates, with generalized line projections, is in progress; at present it can only be said that the sodium atoms presumably lie between lead atoms on the lines $0, 0, z$, $\frac{1}{3}, \frac{2}{3}, z$, and $\frac{2}{3}, \frac{1}{3}, z$ so as to give more or less uniform spacing. In (II) the total number of atoms of both kinds on the $0, 0, z$ line is eight per unit cell, while on the other two lines the number is nine. Horizontal atom shifts to fill apparent gaps may cause the superstructure. In (I) and (III) the total number of atoms on *any* line is respectively seven (or $6\frac{1}{2}$ for composition Na_9Pb_4) and twelve per unit cell. In (I) and (II) the lead atoms occur only in bonded pairs; in (III) four-fifths of the lead atoms occur in pairs and the remaining fifth as isolated single atoms (cf. Li_8Pb_3; Zalkin, Ramsay & Templeton). Structure (I) can be described as a superstructure on body-centered cubic. This is also perhaps true of the others, but their deviations from b.c.c. are more pronounced.

5·18. K. H. JACK & M. M. WACHTEL. *The structure of photoelectric caesium antimonide. Temperature factors in cubic crystals.*

An X-ray investigation (K. H. Jack & M. M. Wachtel,

Table 1

Phase	Ideal formula	Space group	a_0 (Å)	c_0 (Å)	Pb atom positions
I	Na_5Pb_2(?)	$R\bar{3}m$	5·54	23·15	6 (*c*): $0, 0, z$; ...; $z = 0{\cdot}07$
II	Na_9Pb_4	$P6_3/mmc$	5·47*	30·41	4 (*e*): $0, 0, z$; ...; $z = 0{\cdot}05$
					4 (*f*): $\frac{1}{3}, \frac{2}{3}, z$; ...; $z = 0{\cdot}30$
III	$Na_{13}Pb_5$	$P6_3/mmc$	5·51	40·39	2 (*b*): $0, 0, \frac{1}{4}$; $0, 0, \frac{3}{4}$
					4 (*f*): $\frac{1}{3}, \frac{2}{3}, z$; ...; $z = 0{\cdot}05$
					4 (*f*): $\frac{1}{3}, \frac{2}{3}, z$; ...; $z = 0{\cdot}13$

* There are for this phase weak superstructure reflections indicating a true cell with $a_0' = \sqrt{3}.a_0$, $c_0' = c_0$.

Nature, Lond. (1956), **178**, 1408; *Proc. Roy. Soc.* A (1957), in the Press) shows that the photo-electric surface material caesium antimonide is a 'normal valency' intermetallic compound with a small range of homogeneity probably from Cs_3Sb to $Cs_{3+x}Sb_{1-x}$, where x is of the order of 0·05. The atomic arrangement is pseudo body-centred cubic with a structure based upon the *B*32 sodium thallide type (NaTl). The cubic unit cell (a = 9·14–9·19 Å) contains sixteen atoms at special positions of space group $Fd3m$. Eight sites at (0, 0, 0; 0, $\frac{1}{2}$, $\frac{1}{2}$; $\frac{1}{2}$, 0, $\frac{1}{2}$; $\frac{1}{2}$, $\frac{1}{2}$, 0)+ 0, 0, 0; $\frac{1}{4}$, $\frac{1}{4}$, $\frac{1}{4}$ are occupied solely by Cs atoms and eight other sites at (0, 0, 0; 0, $\frac{1}{2}$, $\frac{1}{2}$; $\frac{1}{2}$, 0, $\frac{1}{2}$; $\frac{1}{2}$, $\frac{1}{2}$, 0)+$\frac{1}{2}$, $\frac{1}{2}$, $\frac{1}{2}$; $\frac{3}{4}$, $\frac{3}{4}$, $\frac{3}{4}$ are occupied randomly by 4 Cs and 4 Sb. The semi-conducting properties of the material are explained by a filled Brillouin zone containing two electrons per atom.

The observed diffraction effects are accounted for only if the amplitudes of thermal vibrations are very much greater for Cs atoms than for Sb atoms. The r.m.s. displacements of the atoms from their mean lattice positions (0·52 Å for Cs; 0·25 Å for Sb, at 291° K.) are approximately the same as the corresponding displacements in metallic caesium and metallic antimony. This large difference between the Debye temperature factors of the different atoms causes the appearance of a complete series of X-ray superlattice reflexions, with h, k and l all odd, which were at first erroneously thought to be due to specific shifts of some or all of the atoms from the special positions.

The need for the assignment of separate temperature factors to different atoms is emphasized by these results.

5·19. K. Schubert, W. Burkhardt, E. Günzel, J. Wegst & M. Wilkens. *Some crystal structures in alloys of gold with B-subgroup metals.*

These alloys are rather complicated as the Au atom has the tendency to exert special binding forces. A discussion is given of the crystal structures of $Cu_3Au(Zn)$ (that is a phase of the alloy system Cu–Au–Zn which goes over continuously into the phase Cu_3Au), CuAu(Zn), Au_4Zn, Au_3Zn and some variants, $AuZn_3$, $AuZn_7$, Au_3In and some variants in the system Au–Cd–In.

$Cu_3Au(Zn)$, CuAu(Zn) and Au_4Zn belong to a group of superstructure phases with 'out-of-step domains'. If $\delta_{x,y,z}$ is a peak function in the point x, y, z, and $L1_2$ is the cubic elementary cell of Cu_3Au with the edge a, and * is the folding symbol, then

$Cu_{50}Au_{25}Zn_{25}$ has the structure

$$L1_2*(\delta_{0,0,0}+\delta_{0,0,a})*(\delta_{0,0,0}+\delta_{\frac{1}{2}a,\frac{1}{2}a,2a});$$

$Cu_{55}Au_{20}Zn_{25}$ has the structure (first approximation)

$$L1_2*(\delta_{0,0,0}+\delta_{0,0,a})*(\delta_{0,0,0}+\delta_{\frac{1}{2}a,\frac{1}{2}a,2a})*(\delta_{0,0,0}+\delta_{0,a,0})*(\delta_{0,0,0}+\delta_{\frac{1}{2}a,2a,\frac{1}{2}a}).$$

CuAu(Zn) is similar to the structure of $CuAu_{II}$ found by Johansson & Linde (1936); and Au_4Zn has a structure similar to that of $Pd_{1+}Cu_3$ found by Watanabe *et al.* (1955). Au_3Zn has close packed structure derived from the above Cu_2AuZn structure by an inhomogenous distortion and a small homogenous strain in the [001] direction. $AuZn_3$ has a cubic structure with the icosahedra as coordination polyhedra. $AuZn_7$ has a complicated superstructure of the A3-type, and Au_3In, together with its variants, displays both a superstructure and regular stacking faults of the substructure in the [111] direction of the $A1$ structure. Au_3In is of the Cu_3Ti type; $Au_{78}Cd_{17}In_5$ $A\,B\,A\,C$ (DO_{24}-type); $Au_{72}Cd_{22}In_6$ $A\,B\,A\,B\,A\,C$; $Au_{75}Cd_{13}In_{12}$ $A\,B\,C\,B\,C\,A\,C\,A\,B$; $Au_{75}Cd_3In_{22}$ $A\,B\,A\,B\,A\,C\,A\,C$.

5·20. W. H. Zachariasen & F. Ellinger. *The crystal structure of α-plutonium.*

The room-temperature form of plutonium metal is monoclinic with

$$a = 6{\cdot}1835\pm0{\cdot}0005,\quad b = 4{\cdot}8244\pm0{\cdot}0005,$$
$$c = 10{\cdot}973\pm0{\cdot}001\text{ Å};$$
$$\gamma = 101{\cdot}80\pm0{\cdot}02°.$$

The unit cell contains 16 atoms, corresponding to a density of 19·82 g.cm.$^{-3}$. The space group is $P2_1/m$ with all atoms in reflection planes $\pm(x, \frac{1}{4}, z)$. The approximate parameter values are

Atom type	x	z	Atom type	x	z
I	0·332	0·152	V	0·013	0·617
II	0·767	0·169	VI	0·459	0·642
III	0·138	0·337	VII	0·335	0·924
IV	0·651	0·456	VIII	0·885	0·897

The coordination number is 14 with mean interatomic distance 3·20 Å, except for atoms I with twelve neighbors at a mean distance of 3·11 Å and atoms VIII with coordination number 16 and mean distance 3·31 Å. Each atom forms four short bonds with a mean bond length of 2·64 Å, except atoms VIII and I, which have respectively three and five close neighbors.

§ 6. Inorganic structures

6·1. S. Block, R. Mason, G. Burley & A. Perloff. *The crystal structure of triclinic magnesium pyroborate.*

Triclinic and monoclinic forms of $Mg_2B_2O_5$ have been reported. Utilizing a twinning operation and coordinate transformation of the parameters for the monoclinic form, Y. Takeuchi (*Acta Cryst.* (1952), **5**, 574) proposed a structure for the triclinic polymorph. A different structure has been reported by S. V. Berger (*Acta Chem. Scand.* (1950), **4**, 1054) for $Co_2B_2O_5$, which is isomorphous with triclinic $Mg_2B_2O_5$. Both structures are probable as neither was reported to contain abnormal bond lengths or chemical inconsistencies. This is an excellent example of two chemically acceptable structures which give good agreement with the observed structure factors. To differentiate between the two possibilities both structures were refined by Fourier techniques. The $Co_2B_2O_5$-type structure refined to a lower R value (12% compared with 20% for 104 ($hk0$) reflexions).

Three-dimensional data are being taken to confirm that $Mg_2B_2O_5$ is isostructural with $Co_2B_2O_5$ and also to allow accurate determination of bond lengths.

6·2. J. R. Clark & C. L. Christ. *The crystal structure of* $2CaO.3B_2O_3.9H_2O$.

As part of a program of study on calcium borates, the crystal structure of the synthetic compound

$$2CaO.3B_2O_3.9H_2O$$

has been determined. As reported previously (C. L. Christ, *Amer. Min.* (1953), **38**, 912), $2CaO.3B_2O_3.9H_2O$ is triclinic $P\bar{1}$, $a = 7{\cdot}05$, $b = 9{\cdot}45$, $c = 6{\cdot}41$ Å (all $\pm 0{\cdot}015$ Å), $\alpha = 101°21'$, $\beta = 101°19'$, $\gamma = 99°49'$ (all $\pm 05'$); $Z = 1[2CaO.3B_2O_3.9H_2O]$, density (calc.) = 2·002 g.cm.$^{-3}$, density (obs.) = 2·00 g.cm.$^{-3}$.

Intensity data were obtained with Mo$K\alpha$ radiation for the three principal zones to the value $(\sin\theta)/\lambda = 0{\cdot}9$ Å^{-1}. The visually evaluated intensity data were put on an absolute scale by the method of J. Karle & H. Hauptman (*Acta Cryst.* (1953), **6**, 473). Sharpened Patterson projections, in which the amplitudes were corrected for both atomic form factor and temperature motion, were calculated for the planes normal to the three principal crystallographic axes. From these, the position of the Ca was readily fixed. Vector shifts, based on this position, were evaluated by the minimum-function method of M. J. Buerger (*Acta Cryst.* (1951), **4**, 531), and the corresponding three approximate electron-density maps were obtained. The latter, considered together, revealed the structure of the compound.

In $2CaO.3B_2O_3.9H_2O$ is found the same polyion, $[B_3O_3(OH_5)]^{-2}$, that was previously found, for the first time, in meyerhofferite (C. L. Christ & J. R. Clark, *Acta Cryst.* (1956), **9**, 830). This polyion consists of two $BO_2(OH)_2$ tetrahedra and a $BO_2(OH)$ triangle linked to form a ring. Each Ca^{+2} is coordinated by six oxygens and two water molecules at an average distance of 2·5 Å. The average B–O distance in the triangle is $1{\cdot}3_6$ Å, and that in the tetrahedra $1{\cdot}4_7$ Å, in excellent agreement with our previous findings for meyerhofferite and for the infinite chains of colemanite (C. L. Christ *et al.*, *Acta Cryst.* (1954), **7**, 453). The chemical formula for the present crystal is therefore $CaB_3O_3(OH)_5.2H_2O$.

At the present stage of refinement the residual factors R and the temperature factors B are: $hk0$, $R = 0{\cdot}21$, $B = 1{\cdot}2$ Å^2; $h0l$, $R = 0{\cdot}19$, $B = 1{\cdot}0$ Å^2; $0kl$, $R = 0{\cdot}20$, $B = 1{\cdot}6$ Å^2. The atomic coordinates are:

Atom	x	y	z
Ca	0·161	0·369	0·154
O_1	0·187	0·751	0·975
O_2	0·237	0·278	0·802
O_3	0·322	0·000	0·675
O_4	0·334	0·836	0·351
O_5	0·148	0·417	0·535
O_6	0·046	0·822	0·504
O_7	0·365	0·596	0·170
O_8	0·057	0·619	0·214
O_9 (H_2O)	0·133	0·097	0·193
O_{10} (H_2O)	0·488	0·655	0·718
B_1	0·236	0·700	0·180
B_2	0·073	0·315	0·663
B_3	0·231	0·884	0·521

6·3. C. E. Nordman. *The structure of disordered* $NH_3B_3H_7$.

The room-temperature modification of ammonia–triborane is tetragonal, space group $I4mm$, with two formula units per cell. The structure consists of $NH_3B_3H_7$ molecules disordered with almost cylindrical symmetry about the fourfold axes. Axial and radial coordinates of the N and B atoms, determined by least-squares methods from 25 observed reflections, are consistent with a molecule composed of a boron triangle with a non-coplanar NH_3 group attached to one corner.

A phase transition occurs at or above −16° C.

6·4. [Withdrawn.]

6·5. W. N. Lipscomb, R. E. Dickerson, F. L. Hirshfeld & L. Trefonas. *Recent studies at low temperatures of* B_9H_{15}, B_6H_{10} *and* B_2F_4.

Three-dimensional data refined to $R = 0{\cdot}16$ indicate that the boron arrangement in B_9H_{15} is an icosahedral fragment obtained by removal of three adjacent borons not forming an equilateral triangle. The one BH_2 group linked by two bridge hydrogen atoms to the rest of the molecule is very similar to the corresponding part of the molecule is very similar to the corresponding part of the B_4H_{10} molecule. The three other bridge hydrogens in the other part of the molecule show a resemblance to those in B_5H_{11}. The isolated molecule has C_s symmetry, and is one of the two plausible models suggested when only the boron arrangement was known (R. E. Dickerson *et al.*, *J. Chem. Phys.* (1956), **25**, 606). Four molecules are present in a unit cell of symmetry $P2_1/n$ with parameters $a = 11{\cdot}80$, $b = 6{\cdot}94$, $c = 11{\cdot}25$ Å, $\beta = 109°9'$.

New X-ray data taken from a single crystal of B_6H_{10} are undergoing final refinement. The molecule has C_s symmetry (K. Eriks *et al.*, *J. Chem. Phys.* (1954), **22**, 754). A model with four bridge hydrogen atoms and no BH_2 groups has refined to a value of $R = 0{\cdot}117$, a lower value than was obtained for an alternative model (W. N. Lipscomb, *J. Chim. Phys.* (1956), p. 515) having three bridge hydrogens and one BH_2 group.

There are two molecules of B_2F_4 in a monoclinic unit cell of symmetry $P2_1/n$ and parameters $a = 5{\cdot}49$, $b = 6{\cdot}51$, $c = 4{\cdot}83$ Å, $\beta = 102\frac{1}{2}°$. The molecule is centrosymmetric, similar to B_2Cl_4, and final refinement is in progress.

6·6. R. L. Sass & J. Donohue. *The crystal structure of* $S_4N_4H_4$.

Crystals of $S_4N_4H_4$ are orthorhombic, space group D_{2h}^{16}–$Pnma$, with unit-cell dimensions $a = 8{\cdot}010 \pm 0{\cdot}010$, $b = 12{\cdot}20 \pm 0{\cdot}01$, $c = 6{\cdot}727 \pm 0{\cdot}009$ Å; $Z = 4$. Complete three-dimensional data were collected with equi-inclination Weissenberg techniques. A three-dimensional Patterson function, sharpened, and with the origin peak removed, was calculated. The sulfur atoms were located first, mainly by use of the Harker sections, and a complete trial structure was then found by an eightfold superposition, using the equivalent positions of one of these sulfur atoms. A refinement of the trial structure was carried out by (100) and (010) Fourier projections, followed by six cycles of three-dimensional least-squares treatment and three-dimensional Fourier analysis. There was no clear evidence of the positions of the hydrogen atoms in the electron-density maps. Since infra-red data had previously indicated that the molecule has N–H bonds and no S–H bonds, the positions of the hydrogen atoms were assumed. The molecules lie across mirror planes and contain two crystallographically non-equivalent sulfur atoms and three crystallographically non-equivalent N–H groups. The molecule is an eight-membered ring of alternating sulfur and nitrogen atoms and is similar in shape to the S_8 molecule. The molecular dimensions (averaged over chemically equivalent bonds) are: S–NH = 1·672± 0·012 Å, S–N–S = 122·2±0·5°, N–S–N = 108·4±0·5°. The dihedral angle is 99·4° compared to 99·3° found in S_8. The four sulfur atoms form a square having an edge of average length 2·927 Å. The four nitrogen atoms also

lie on a square having an edge of average length 2·715 Å. The planes of sulfur and nitrogen atoms are parallel to within 0·5° and are 0·627 Å apart. Since both the S–N distances and the S–N–S bond angles suggest trigonal, rather than tetrahedral, bonds about the nitrogen atoms, the groupings S–NH–S were assumed to be coplanar. The structure consists of chains of molecules held together by weak N–H...N hydrogen bonds of length 3·16 Å. Only one hydrogen atom per molecule is used in forming these hydrogen bonds. The chains are packed together sc that the other three hydrogen atoms are directed towards the centers of rings of sulfur atoms. There are no abnormally short van der Waals contacts.

6·7. N. G. VANNERBERG. *The structures of compounds of the type* $MO_2.2H_2O_2$ (M = Ca, Sr *or* Ba).

In connexion with investigations concerning the formation, structure and reactions of inorganic peroxides and superoxides the crystal structure of some compounds with the general formula $MO_2.2H_2O_2$ (M = Ca, Sr or Ba) has been studied. Compounds of the type mentioned above have earlier been prepared by E. C. Riesenfeld & N. Nottebohm (*Z. anorg. Chem.* (1914), **89**, 406) and by S. Z. Makarov & N. K. Grigar'eva (*Izvest. Akad. Nauk. SSSR Otdel, Khim. Nauk* (1954), pp. 385–91, 598–603), but, with the exeption of $BaO_2.2H_2O_2$, in rather impure form. We have developed methods of preparation giving pure, well crystallized substances. These have been investigated by X-ray methods. As the first result we have found that there are two series of isomorphous compounds that we will call α-$MO_2.2H_2O_2$ and β-$MO_2.2H_2O_2$. Among these, the structure of β-$SrO_2.2H_2O_2$ has been determined and that of α-$CaO_2.2H_2O_2$ and α-$SrO_2.2H_2O_2$ is at present under refinement.

In the system Sr^{2+}–O_2^{2-}–H_2O_2–H_2O we have until now confirmed the existence of the following phases:

$$SrO_2,\quad SrO_2.8H_2O,\quad SrO_2.H_2O_2,\quad \alpha\text{-}SrO_2.2H_2O_2,\quad \beta\text{-}SrO_2.2H_2O_2.$$

The last three have not previously been obtained in pure form. We have prepared them in the following way:

α-$SrO_2.2H_2O_2$: A solution of 0·5 g. $Sr(NO_3)_2$ in 20 ml. 30% H_2O_2 and a mixture of 0·5 ml. 25% NH_3 and 20 ml. 30% H_2O_2 were chilled to 0° C. and mixed cautiously together. The supersaturated solution was kept at 0° C. for 20 hr. Crystallisation of a compound took place. According to the analysis it has the formula $SrO_2.2H_2O_2$ and has crystallographic properties characteristic of what we will call the α phase.

β-$SrO_2.2H_2O_2$: A compound with the same composition as that mentioned above, but with different structure, was obtained when the concentration of strontium was twice as strong and that of ammonium four times as strong. Below it is referred to as the β phase.

$SrO_2.H_2O_2$: β-strontiumdiperhydrate is transformed into strontiummonoperhydrate, if it is kept about 3 hr. at a pressure of 30 mm. Hg and a temperature of +10° C. Under the same conditions the monoperhydrate slowly gives up another molecule of hydrogen peroxide and forms strontiumperoxide.

As mentioned above complete determination of β-$SrO_2.2H_2O_2$ has been performed. The result is the following:

Rotation, Weissenberg and Guinier photographs were taken with Cu$K\alpha$ radiation and gave the following data:

$$a = 7{\cdot}715\pm0{\cdot}004,\quad b = 8{\cdot}754\pm0{\cdot}005,\quad c = 6{\cdot}015\pm0{\cdot}003\ \text{Å},$$
$$\beta = 86°20'\pm2'.$$

Space group: No. 15 (C_{2h}^6); $Z = 4$.

The intensities were measured using the multiple-film technique. At this stage of refinement, structure amplitudes were corrected, using a temperature factor with $B = 1{\cdot}3$ Å^2.

The determination of the structure was here a straightforward one, as the heavy-atom method could be used. Projections of the Patterson function gave the following coordinates for the strontium atoms:

$$C_{2h}^6(e)\colon x = 0,\ y = 0{\cdot}179,\ z = \tfrac{1}{4}.$$

Using signs calculated with these parameter values, projections of the electron density on (001) and (110) were obtained. From these projections the positions of the 24 oxygen atoms were found and refined by the method of least squares. The result is given in Table 1.

Table 1. *Atomic positions for* β-$SrO_2.2H_2O_2$

	x	y	z
4 Sr in 4 (e)	0	0·179±0·001	¼
8 O_1 in 8 (f)	0·143±0·009	0·093±0·007	0·911±0·012
8 O_2 in 8 (f)	0·332±0·006	0·073±0·009	0·919±0·012
8 O_3 in 8 (f)	0·331±0·008	0·220±0·009	0·429±0·012

$$R_{(hk0)} = 0{\cdot}14 \quad \text{and} \quad R_{(hhl)} = 0{\cdot}19$$

The structure can be described as built up from strontium ions and ionic groups with the formula

$$[H.O{-}O.H.O{-}O.H.O{-}O.H]^{2-}.$$

The configuration of this group in β-$SrO_2.2H_2O_2$ is seen in Fig. 1(a). It is built up from three peroxide groups (O–O distances 1·47 and 1·55 Å) bonded together with

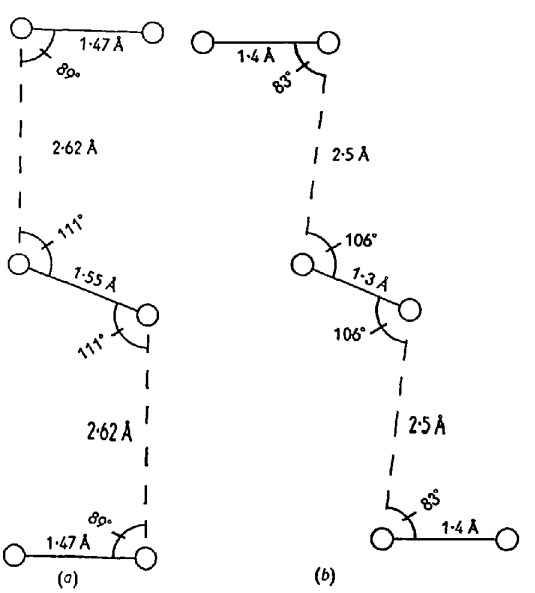

Fig. 1. The configuration of the $[HO_2HO_2HO_2H]^{2-}$ group (a) in β-$SrO_2.2H_2O_2$, (b) in α-$CaO_2.2H_2O_2$. Circles denote oxygen atoms.

hydrogen bonds (O–O distance 2·62 Å). The six oxygen atoms are distributed approximately in one plane. It

may be pointed out, that the shortest distance between two oxygen atoms belonging to different groups is 2·99 Å. The structure found seems to make the following formula for the compound reasonable:

$$Sr(O_2)_3H_4 \text{ or perhaps } Sr[HO_2HO_2HO_2H] .$$

The investigation of the structure of the isomorphous compounds α–$CaO_2.2H_2O_2$ and α–$SrO_2.2H_2O_2$ has not been quite terminated when this is written, but some words may be said about the main features of this structure type. Here, too, we have a lattice built up from strontium ions and ionic groups with the formula $[HO_2HO_2HO_2H]^{2-}$. The configurations of these, however, differs somewhat from those in the β-phase, as is shown in Fig. 1(*b*).

6·8. P. W. Hemily & J. A. Wunderlich. *Bonding systems in* NaOH *hydrates.*

Bonding systems of the mono- (J. A. Wunderlich, *Acta Cryst.* (1957), in the Press), tetra- (P. W. Hemily, *Acta Cryst.* (1957), **10**, 37) and hepta- (P. W. Hemily, *C. R. Acad. Sci., Paris*, (1953), **236**, 1579) hydrates have been determined. The crystallographic data are:

Hydrate	1 H_2O	4 H_2O	7 H_2O
a (Å)	6·21	15·45	7·34
b (Å)	11·72	4·05	16·41
c (Å)	6·05	9·43	6·90
β	—	116° 50′	92° 53′
Space group	*Pcab*	*C*2/*m*	$P2_1/c$

Sodium coordination increases with the degree of hydration, being tetrahedral in $NaOH.H_2O$, trigonal bi-pyramidal in $NaOH.4H_2O$ and octahedral in $NaOH.7H_2O$.

Oxygen coordination numbers vary between 3 and 6. Hydrogen bond systems are two-dimensional in the mono- and heptahydrates, three-dimensional in the tetrahydrate.

6·9. J. A. Wunderlich & P. W. Hemily. *Crystalline phases of the system* NaOH–H_2O.

Crystallographic data have been determined for nine hydrates of NaOH. The structures of the mono-, tetra- and the hepta-hydrates have been determined and are being refined in order to locate hydrogen atoms (see § 6, No. 8 for references).

The structure determination of $NaOH.3\frac{1}{2}H_2O$ is in progress (J. A. W.). Data of this phase are: a = 11·64, b = 12·38, c = 6·49 Å, β = 104° 7′, space group $P2_1/a$, asymmetric group $2NaOH.7H_2O$.

Possible existence of polymorphism (*h*0*l* zone) is indicated between the following three hydrates:

	$2\frac{1}{2}$ $H_2O(\alpha)$	$2\frac{1}{2}$ $H_2O(\beta)$	$3\frac{1}{10}$ H_2O
a (Å)	12·48	24·75	50·00
b (Å)	13·50	—	13·32
c (Å)	6·27	6·30	6·25
Space group	$P2_12_12$	—	*Pb*2*a*, *Pbma*
Asymmetric group	3 $NaOH.7\frac{1}{2}$ H_2O	—	10 $NaOH.31$ H_2O or 5 $NaOH.15\frac{1}{2}$ H_2O

The $2\frac{1}{2}H_2O(\beta)$ phase has been obtained only once. The (*h*0*l*) equator is the only X-ray data available of this phase.

Three-dimensional X-ray data have been obtained for a $2\frac{3}{4}H_2O$ hydrate, a = 23·55, b = 6·44, c = 22·19 Å, β = 114° 12′, space group *Aa* or *A*2/*a* with an asymmetric unit of $8NaOH.22H_2O$ or $4NaOH.11H_2O$.

The intensity distribution of $NaOH.5H_2O$ tends to suggest that it is a complex polymorph of a simpler phase. The data of this phase are: a = 15·78, b = 25·22, c = 12·90 Å, β = 102° 18′ with an asymmetric unit of $8NaOH.40H_2O$.

6·10. H. E. Petch. *An X-ray determination of the hydrogen positions in* $Ca(OH)_2$.

The structure of $Ca(OH)_2$ has been known for many years. However, some recent infra-red absorption results seemed to indicate that the unit cell was larger than that determined by X-ray analysis and that the hydrogen positions as deduced indirectly by Bernal & Megaw for this structure were incorrect. The accepted unit-cell dimensions and space group were confirmed by earlier X-ray work and the object of this investigation was to obtain, in a direct manner, the hydrogen positions using X-ray techniques.

The diffraction data were obtained with Mo $K\alpha$ radiation and an X-ray Geiger-counter diffractometer. The structure factors were placed on an absolute scale by comparison with the calculated values in the later stages of the analysis. The Hartree scattering factors, modified by thermal factors, were used in calculating the structure factors until systematic errors, which could be traced to the Hartree scattering factors for the calcium and oxygen ions, became apparent. In the final stages the Hartree scattering factors were therefore abandoned in favor of empirical curves which were obtained by calculating the changes in the Hartree curves necessary to give the best fit to the experimental data. Allowance was made for the very marked anisotropy in the thermal vibration of the calcium ions and for the slight anisotropy in the case of the oxygen ions.

In the final (F_o-F_c) synthesis, in which the contributions of the hydrogen atoms were not included, a single large peak was left on an undulating background in the projection of one half the unit cell on the $(2\bar{1}\bar{1}0)$ plane. The electron density at this peak was 0·9 e.Å^{-2} as compared to the calculated standard deviation in the electron density of 0·08 e.Å^{-2}. It is believed that this peak represents an electron associated with a hydrogen atom. The positions of the hydrogen atoms in $Ca(OH)_2$ as indicated by the maximum density of the associated electrons are:

$$\pm(\tfrac{1}{3}, \tfrac{2}{3}, 0{\cdot}395\pm0{\cdot}008).$$

6·11. R. L. Sass, R. Vidale & J. Donohue. *Interatomic distances and thermal anisotropy in sodium nitrate and calcite.*

All reflections accessible to Cu $K\alpha$ due to oxygen scattering only were collected for calcite and sodium nitrate. The single positional parameter and three anisotropic temperature factors were determined by least squares, and by a Fourier method which isolated the oxygen atoms from the other atoms. The shapes of the oxygen atoms in the electron-density plots were distinctly

reniform, corresponding to a librational motion of the anions about their $\bar{3}$-fold axes. The bond distances found are C–O = 1·294 Å and N–O = 1·218 Å, with estimated standard deviations of 0·004 Å in both. (These compare with the earlier determinations by Elliott, who found C–O = 1·31 Å and N–O = 1·21 Å from selected Laue data.) The C–O distance is within 0·01 Å of that predicted by the simple valence bond treatment for one-third double-bond character. The situation with regard to the N–O distance is not as satisfactory, because (*a*) the distance found in $NaNO_3$ is equal to that found in nitro compounds, and (*b*) the prediction of N–O distances by the valence-bond method is uncertain because the N=O distance is not known, nor can it be satisfactorily predicted with presently available data.

6·12. A. Durif. *Substitutions dans la structure de l'eulithine.*

Les groupements SiO_4 dans l'eulithine peuvent être remplacés par un certain nombre d'autres groupements tétraédriques avec conservation de la structure cubique.

La possibilité de ces substitutions montre une fois de plus que la stéréo-chimie des silicates ne peut être considérée comme un chapitre isolé.

6·13. K. H. Jack. *Trifluoride structures.*

Transition-element trifluorides are classified into three types which may be correlated with the position of the metal in the Periodic Table (see M. A. Hepworth *et al. Acta Cryst.* (1957), **10**, 63): (i) Typified by MoF_3, with a ReO_3-type cubic close-packing of fluorine atoms. (ii) The fluorine atoms are hexagonal close-packed, e.g. RhF_3, PdF_3 and IrF_3. (iii) The arrangement of fluorine atoms is intermediate between that of type (i) and that of type (ii), e.g. VF_3, FeF_3 and CoF_3.

Monoclinic manganese trifluoride (space group $C2/c$; $a = 8·904$, $b = 5·037$, $c = 13·448$ Å; $\beta = 92·74°$) is pseudo-rhombohedral and is classified as a type-(iii) structure. MnF_6 octhaedra are joined by sharing corners, and the lower symmetry, in comparison with other trifluorides, results from three different Mn–F bond lengths (2·09, 1·91 and 1·79 Å) within each octahedron. Reasons for the unsymmetrical bonding and for its unique occurrence in MnF_3 are offered in terms of ligand-field theory (M. A. Hepworth & K. H. Jack, *Acta Cryst.* (1957), in the Press).

The distorted ReO_3-type unimolecular rhombohedral structure reported for ScF_3 by Nowacki (*Z. Kristallogr.* (1939), **101**, 273) appears, on the above classification, to be anomalous. A re-determination of the structure now shows that it is an undistorted cubic ReO_3 type-(i) trifluoride ($a = 4·0096$ Å) like MoF_3 and TaF_3. Excellent agreement between the observed and calculated X-ray data is obtained by assigning different temperature factors to the scandium and fluorine atoms.

The structure reported for AlF_3 (J. A. A. Ketelaar, *Z. Kristallogr.* (1933), **85**, 119) seems also to be anomalous. It is more likely that AlF_3 is isostructural with the type-(iii) trifluorides and that the observed X-ray data may be accounted for on this basis if the temperature factors of the aluminium and fluorine atoms are different. The results of a re-examination of AlF_3 are discussed.

6·14. A. L. Loeb. *A binary algebra describing crystal lattices with closely-packed anions.*

The quantitative evaluation of interactions between lattice elements, be they electrical, magnetic, exchange or valence, requires a quantitative description of their relative locations and orientations. Three-dimensional models of a unit cell, and their two-dimensional projections, are used as visual aids, but do not themselves constitute an analytical description. The binary algebra presented here has been used to evaluate magnetic dipole interactions in antiferromagnetic crystals and provides a convenient means of supplying descriptions of periodic spatial distributions to automatic computers.

The crystals under consideration all have a close-packed anion lattice; in increasing order of complexity they are: simple rocksalt, antiferromagnetic rocksalt, sphalerite, and spinel. The lattice is divided into a number of component sublattices each of which is identified by a binary number, called the 'descriptor', whose digits are related to the parity of the Cartesian components of all lattice sites within the sublattice. For simple rocksalt, the descriptor consists of three binary digits, so that the lattice is divided into eight component sublattices, namely, four simple cubic anion and four simple cubic cation lattices. For antiferromagnetic cubic lattices another binary digit is needed to distinguish the two antiparallel dipole orientations. The positions of the sublattices relative to each other are derived from their descriptors.

This binary algebra has been used to calculate the magnetic interaction energy of all dipoles in an antiferromagnetic crystal, subject to exchange constraints. Orientations are found corresponding to a minimum interaction energy, and it is shown that these are in agreement with neutron diffraction data.

Sphalerite lattices consist of the same component lattices as do rocksalt lattices; the difference is the relative location of anion and cation lattices. Spinel lattices contain two of the eight component cation sublattices occurring in the rocksalt structure and four of the cation sublattices occurring in sphalerite. Formulas are given for the location of the cation neighbors nearest to any anion, as functions of the descriptor of the anion. It is shown that the spinel structure is a logical consequence of the valency of the cations.

6·15. E. F. Bertaut, P. Blum & A. Sagnieres. *Structure de* $Fe_2O_3.2CaO$.

Le ferrite bicalcique est un des principaux constituants du ciment de Portland. $Fe_2O_3.2CaO$ est orthorhombique: $a = 5·60$, $b = 14·78$, $c = 5·56$ Å. Le groupe d'espace est *Pcmn* (avec une forte pseudo-symétrie vers *Ibmm*). La structure qui n'a aucune ressemblance avec celle de $Fe_2O_3.CaO$, décrite antérieurement, a été résolue par la méthode statistique de détermination de signes relatifs. Les atomes de fer ont les coordinations 4 et 6. Ca se trouve dans un polyèdre à 8 sommets.

6·16. H. Kedesdy, G. Katz & S. B. Levin. *Structural relationship between ramsdellite and some synthetic manganese dioxides.*

Geiger-counter measurements of X-ray diffraction intensities and line-profile studies have revealed that a similarity exists between the diffraction powder patterns

of ramsdellite (Lake Valley, New Mexico) and synthetic ϱ- and γ-manganese dioxide*. The structure of ramsdellite, an orthorhombic modification of manganese dioxide, is built up of distorted oxygen octahedra arranged in double strings in the direction of the c axis, being linked together by sharing edges. These double strings are connected, with octahedra, to neighboring double strings by sharing corners. The diffraction patterns of ϱ- and γ-manganese dioxide, which deviate from the ramsdellite pattern, do so in line shift, line intensity and line broadening. The following orthorhombic lattice constants of the synthetic phase types were calculated from the line shifts and, for comparison, the lattice constants of ramsdellite are given:

	Ramsdellite	ϱ-MnO_2	γ-MnO_2
a (Å)	4·528	4·453	4·418
b (Å)	9·285	9·396	9·510
c (Å)	2·866	2·827	2·811

The deviations in the ramsdellite unit-cell dimensions range from 0·01 Å to 0·1 Å for the ϱ-phase (greatest deviation being along the a axis), and in the range of 0·06 Å to 0·2 Å for the γ-phase (greatest deviation being along the b axis). These dimensional variations in the ramsdellite unit cell are related to the shifts in the atomic parameters; therefore, the diffraction intensities found in the synthetic phase types, as well as the differences between types, can be accounted for by shifts in the atomic positions of the basic ramsdellite structure (space group D_{2h}^{16}) (A. M. Bystrom, *Acta Chem. Scand.* (1949), **3**, 163). The (111) and (040) reflections, the intensities of which proved to be the most sensitive to atomic-parameter changes, were selected for a systematic structure-factor calculation by varying the x and y atomic parameters of Mn, O_I and O_{II} in the ramsdellite structure. By comparing F_o with F_c, the approximate atomic parameters of the synthetic phase type structures were determined. It can be shown that in the case of the γ-manganese dioxide structure, the double strings of oxygen octahedra have been rotated around the c direction by about 27° with respect to their positions in the ramsdellite structure. The corresponding rotation in the ϱ-manganese dioxide structure is about 7°. Fom chemical analysis of the manganese dioxide phase types evidence is found that oxygen is partially replaced by hydroxyl groups. These deviations from an MnO_2 stoichiometry can account for the structural variations of the ramsdellite structure as observed in the synthetic ϱ- and γ-manganese dioxide structure. A similar relationship between the crystal structures of ramsdellite and the hydrous oxide of manganese, groutite, will be discussed.

6·17. A. Magnéli. *X-ray studies on some transition metal oxide systems (groups* IV–VII).

During recent years, comprehensive studies on metal oxides and related compounds have been carried out by research groups at the Universities of Stockholm and Uppsala (the letters *S* and *U* being used below in the section headings to indicate this) with financial support from the Swedish Natural Science Research Council.

* The ϱ-MnO_2 was prepared from sodium chlorate oxidation of manganous sulfate solution. γ-MnO_2 was prepared by electrolytic deposition from sulfuric acid solution of manganous sulfate on graphite anodes.

Reviews on a previous research program mainly covering oxides of molybdenum and wolfram and wolfram bronzes have been given (A. Magnéli, *Nova Acta Reg. Soc. Sci. Upsaliensis*, (1950), (4), **14**, No. 8; G. Hägg & A. Magnéli, *Rev. Pure Appl. Chem.* (1954), **4**, 235). Some general aspects on the crystal chemistry of molybdenum and wolfram have also been presented (A. Magnéli, *Acta Cryst.* (1953), **6**, 495).

Ti–O(*S*)

Preparations low in oxygen tempered at 800° C. show the hexagonal α-Ti pattern up to the composition $TiO_{0.5}$, which is in accordance with P. Ehrlich (*Z. anorg. Chem.* (1941), **247**, 53). The a axis goes through a maximum at $x = 0{\cdot}35$ while the simultaneous increase of the c axis is suddenly accelerated at the same composition. At $x = 0{\cdot}40$ the first trace of an extra line (003) shows up and at $x = 0{\cdot}50$ a few more extra lines indicating an ordered structure are visible.

By tempering preparations $TiO_{0.55-0.70}$ at 800° C. the so-called δ-phase reported by E. S. Bumps *et al.* is obtained. The actual composition of this phase has not so far been definitely established. The homogeneity range is narrow. The powder pattern may be accounted for by a hexagonal unit cell ($a = 5{\cdot}769$, $c = 4{\cdot}80$ Å). The structure is likely to be related to that of α-Ti.

The findings of P. Ehrlich (*Z. Electrochem.* (1939), **45**, 362) on the structure, range of homogeneity and occupancy of the atomic sites of TiO of defective sodium chloride structure have been confirmed for preparations obtained in the arc furnace. In samples tempered at 800° C., however, a new phase of invariable composition $TiO_{1.00}$ has been observed (U. Kuyienstierna & A. Magnéli, *Acta Chem. Scand.* (1956), **10**, 1195) (independently found by C. C. Wang & N. J. Grant (*J. Metals* (1956), p. 184)). The structure of this phase is probably of low symmetry, but the appearance of the powder pattern suggests a relationship with the sodium chloride type. The densities of $TiO_{1.00}$ samples obtained from the melt (4·95 g.cm.$^{-3}$) and by tempering at 800° C. (4·91 g.cm.$^{-3}$) suggest that the low-temperature form is of deformed NaCl type with ordered atomic vacancies.

For samples TiO_x (x somewhat higher than 1) heat-treated at 800° C., the low-temperature form of TiO appears together with the NaCl-type TiO, which, however, has a very narrow range of homogeneity at $x = 1{\cdot}18$.

With higher oxygen contents, the investigations have mainly been devoted to samples heat-treated at about 1100° C. Ti_2O_3 has been found to possess a very narrow range of homogeneity (less than $x = 1{\cdot}50 \pm 0{\cdot}01$).

The X-ray patterns of Ti_3O_5 are not in agreement with the data given by G. S. Zhdanov & A. A. Rusakov (*Trudy Inst. Krist. Akad. Nauk SSSR*, (1954), **9**, 165) (anosovite of pseudo-brookite type). The structure is monoclinic with $a = 9{\cdot}44$, $b = 3{\cdot}86$, $c = 9{\cdot}75$ Å, $\beta = 92°$ and four Ti_3O_5 per unit cell. Probable space groups: $C2/m$, Cm and $C2$.

Within the composition range $TiO_{1.75-1.93}$ no less than seven distinct phases have been observed (S. Andersson & A. Magnéli, *Naturwissenschaften*, (1956), **43**, 495). The experimentally derived compositions are in good agreement with a general formula Ti_nO_{2n-1}, with $n =$ 4, 5, 6, 7, 8, 9, and 10. The formula Ti_5O_9 has been confirmed by single-crystal studies (triclinic symmetry) and

density measurement. The powder patterns of these phases are of related appearance showing a stepwise approach, with increasing n, towards the rutile-type pattern. This suggests that these oxides constitute a 'homologous series' formed by regularly distributed atomic dislocations appearing in a basic structure of rutile type (cf. the homologous series (Mo, W)$_n$O$_{3n-1}$ based on the ReO_3-type structure).

Preparations of higher oxygen content ($TiO_{1.90-1.95}$) give powder photographs which suggest the existence of still higher members of the series Ti_nO_{2n-1}. Experimental difficulties have so far obstructed a detailed phase analysis of this composition range.

The TiO_2 (rutile) structure has a homogeneity range down to $TiO_{\sim 1.98}$.

V–O(*U*)

These studies are partially described by G. Andersson (*Acta Chem. Scand.* (1954), **8**, 1599; (1956), **10**, 623). The existence of the homologous series V_nO_{2n-1} (n = 4, 5, 6, 7 and 8) has been supported by the observation that V_5O_9 is isomorphous with Ti_5O_9. The powder photographs of the former could be indexed on the basis of the single crystal photographs of the latter (Andersson & Magnéli, *loc. cit.*).

Nb–O *and* Ta–O(*U*)

NbO_2 has a deformed rutile structure. The high-temperature form of Nb_2O_5 is monoclinic with cell dimensions a = 21·5, b = 3·83, c = 20·6 Å, β = 121·4°.

The existence of a high-temperature modification of Ta_2O_5 has been observed (S. Lagergren & A. Magnéli, *Acta Chem. Scand.* (1952), **6**, 444).

Mo–O(*U*) (L. Kihlborg & A. Magnéli, *Acta Chem. Scand.* (1955), **9**, 471)

Previous studies covering the phases formed by reducing MoO_3 with Mo or lower Mo oxides at temperatures about 700° C. have been extended to comprise the range 490–770° C. The following new phases have been observed:

ζ-Mo oxide of composition $MoO_{2.90}$, forming between 590 and 750° C. Bluish-black, irregular crystal aggregates.

θ-Mo oxide of approximate composition $MoO_{2.83}$, forming between 490 and 530° C. Dark brownish crystalline powder.

$\varkappa$-Mo oxide of approximate composition $MoO_{2.80}$ forming at 525° C. Blue-black crystalline needles. Probable spacegroup $P2_12_12$, with a = 21·6, b = 19·6, c = 3·94 Å.

η-Mo oxide of composition $MoO_{2.75}$, forming between 490 and 620° C. Brilliant red-violet needles or irregular plates.

Mo–O–H(*U*)

Several of the Mo oxide hydroxides first synthesized by O. Glemser *et al.* (*Z. anorg. Chem.* (1956), **285**, 173) have been prepared and X-rayed.

$Mo_4O_{10}(OH)_2$ is orthorhombic of probable spacegroup *Cmcm* with a = 3·886, b = 14·09, c = 3·734 Å.

$Mo_2O_4(OH)_2$ is monoclinic with a = 3·885, b = 14·63 Å, c = 3·795 Å, γ = 96·9° (the unconventional coordinate system chosen to stress the similarity with the unit cell of MoO_3).

The existence of genotypism between MoO_3 and these phases suggested by Glemser *et al.* is strongly suggested by the unit-cell data given above.

W–O(*S*)

Preliminary studies have shown that the phase relations within the composition range $WO_{2.90-2.95}$ are more complicated than reported previously.

Re–O(*S*) (A. Magnéli, *Acta Chem. Scand.* (1957), to be published)

Only the phases ReO_2 (dimorphic), ReO_3 and Re_2O_7 have been observed in this system. The structure of orthorhombic ReO_2 has been determined (A. Magnéli, *Acta Cryst.* (1956), **9**, 1038.

Attempts to prepare alkali rhenium bronzes analogous to the wolfram bronzes have been fruitless.

Metal–metal bonding in some dioxides (*S*)

The MoO_2-structure type may be described as a distorted rutile structure, with the metal atoms arranged pair-wise. The very close approach of the metal atoms indicates the presence of a metal–metal bond (L. Pauling, *Chem. Eng. News*, (1947), **25**, 2970), the bond distance decreasing with the number of valency electrons available per bond (A. Magnéli & G. Andersson, *Acta Chem. Scand.* (1955), **9**, 1378). The same qualitative relationship is valid for the short metal–metal distances in orthorhombic ReO_2 and in some mixed oxide phases of rutile type (TiO_2–VO_2, VO_2–MoO_2).

6·18. L. F. Dahl & R. E. Rundle. *Structures of the polynuclear metal carbonyls* $[Fe(CO)_4]_3$, $Mn_2(CO)_{10}$, *and* $Re_2(CO)_{10}$.

A structural investigation of the polynuclear metal carbonyls—$[Fe(CO)_4]_3$, $Mn_2(CO)_{10}$, and $Re_2(CO)_{10}$—was undertaken by means of single-crystal X-ray diffraction techniques.

Iron tetracarbonyl was found to possess monoclinic symmetry; the lattice constants are

$$a_0 = 8{\cdot}88,\ b_0 = 11{\cdot}33,\ c_0 = 8{\cdot}35\ \text{Å};\ \beta = 97°\ 9{\cdot}5'.$$

There are six $Fe(CO)_4$ species per unit cell. Systematic absences indicated the centrosymmetric space group $P2_1/n$, which would ordinarily require a trimeric molecule to possess a center of symmetry (i.e. two irons would be on centers of symmetry with the other four irons related in pairs by the center of symmetry), and would thereby make the iron atoms collinear. The iron atoms should then be located easily by Patterson projections, but this did not turn out to be the case.

The structural analysis has proceeded through a complete three-dimensional Patterson and three-dimensional 'sharpened' Patterson. The only model at all compatible with this analysis, and other evidence, involves a disordered structure in which the iron atoms are arranged at the corners of an equilateral triangle and are placed in each unit cell at random in one of two orientations approximately differing from one another by a rotation of 60° about the threefold axis. Iron–iron distances of approximately 2·75–2·85 Å were found. The configuration of the CO ligands still needs to be determined, since it has proven difficult to find the carbonyl positions in the disordered structure.

Three-dimensional Fourier sections computed on X-RAC at Pennsylvania State University appeared to verify the trigonal model, although additional three-dimensional work will be needed to confirm the proposed structure.

On the other hand, no linear arrangement of iron atoms, including the widely accepted D_{2d} structure, can explain the three-dimensional Pattersons. In fact, none of the structures thus far postulated appears to be correct.

An infra-red study of single crystals gave strong carbonyl bands at 1875 and 2040 cm.$^{-1}$ in the solid state, although in solution the band at 1875 cm.$^{-1}$ nearly disappeared, suggesting that there are no bridge carbonyls, at least in solution.

The manganese and rhenium carbonyls were found to be monoclinic and isomorphous. The lattice constants are as follows:

$Mn_2(CO)_{10}$: $a_0 = 14{\cdot}16$, $b_0 = 7{\cdot}11$, $c_0 = 14{\cdot}67$ Å; $\beta = 105°$;
$Re_2(CO)_{10}$: $a_0 = 14{\cdot}70$, $b_0 = 7{\cdot}15$, $c_0 = 14{\cdot}91$ Å; $\beta = 106°$.

The probable space group is $I2/a$ or Ia; there are four dimers per unit cell. A two-dimensional Fourier analysis of $Mn_2(CO)_{10}$ revealed that each manganese atom is octahedrally coordinated to five CO ligands and to another manganese atom by a direct metal–metal bond in such a way that the dimeric molecule possesses approximately D_{4d} symmetry (staggered CO's). A partial refinement of $Mn_2(CO)_{10}$ resulted in an R value of approximately 21% for the three principal zones.

These compounds are the first polynuclear carbonyls known to be held together by metal–metal bonds and, together with $(C_5H_5W)_2(CO)_6$ and $(C_5H_5Mo)_2(CO)_6$ (F. C. Wilson & D. P. Shoemaker, *Naturwissenschaften* (1956), **43**, 57) represent the first real evidence for a direct metal–metal bond between two transiton metals in which the metal–metal bond alone permits the existence of the dimer. The metal–metal bond is in accord with the diamagnetism of the compounds and the molecular weights in solution.

The long metal–metal distances found (i.e. 2·93 Å for $Mn_2(CO)_{10}$ and 3·02 Å for $Re_2(CO)_{10}$) for these compounds, as compared to the relatively short iron–iron distance of 2·46 Å for $Fe_2(CO)_9$, can be explained qualitatively by the large negative formal charge contribution of ligand electrons to each metal and by carbonyl–carbonyl repulsions. An infra-red vibrational analysis was found to be compatible with the D_{4d} structure.

6·19. F. C. Wilson & D. P. Shoemaker. *The structure of* bis-[*cyclopentadienyl molybdenum tricarbonyl*].

The compound *bis*-[cyclopentadienyl molybdenum tricarbonyl], $(C_5H_5Mo(CO)_3)_2$, and its tungsten homolog, were synthetized by Wilkinson *et al*. They are crystallographically isomorphous and crystallize with two molecules per unit cell in space group C_{2h}^5–$P2_1/c$. For the molybdenum compound, the crystal structure of which was fully determined and refined, $a_0 = 10{\cdot}38$, $b_0 = 8{\cdot}02$, $c_0 = 12{\cdot}03$ Å, $\beta = 125°\ 46{\cdot}5'$. Bonded to each molybdenum atom are one cyclopentadienyl ring in the manner of ferrocene, and three carbonyl groups (non-bridging). The two halves of the molecule are held together only by a Mo–Mo bond, of length 3·22 Å, making angles of 117° 38′ with lines from the molybdenum atoms to the centers of gravity of the cyclopentadienyl rings. Because of atomic contact repulsions, each half of the molecule is strained away from the pseudo-trigonal configuration that would be expected for it in the free state as an ion or radical; roughly, if the line from Mo to ring center is a cube [100] direction, the three Mo–carbonyl bonds and the Mo–Mo bond are in the body-diagonal directions $[\bar{1}11]$, $[\bar{1}\bar{1}1]$, $[\bar{1}1\bar{1}]$, and $[\bar{1}\bar{1}\bar{1}]$. The molecule as a whole has approximate symmetry C_{2h}–$2/m$, although in a site of symmetry C_i–$\bar{1}$. Average distances are: C–C (ring), 1·42 Å; Mo–C (ring), 2·35 Å; Mo–C (carbonyl), 1·96 Å; C–O (carbonyl), 1·16 Å. The molybdenum 18-shell apparently is precisely filled by six electrons from the molybdenum atom, five from the ring, two each from three carbonyl groups, and one from the other molybdenum atom. The structure was refined by six cycles of least squares (IBM 704, program by Sayre) with 1768 planes to a reliability factor (excluding unobservable reflections) of $R = 0{\cdot}103$.

6·20. Z. V. Zvonkova. *The development of crystal-chemical theory of the structure of complex compounds.*

Crystal-chemical research on the intermolecular interaction shows some interesting and significant features of the nature of the hydrogen bond. The new values obtained for intermolecular radii of the hydrogen atom in the structure $[ClTlC_6H_5]^+Cl^-$ ($r_H = 0{\cdot}74$ Å) and in the structure F_3B–NC_5H_5 ($r_H = 0{\cdot}80$ Å) are smaller than the generally accepted value $r_H = 1{\cdot}17-1{\cdot}20$ Å. The intermolecular distance H · · · F (1·93 Å) is shorter than the sum of the intermolecular radii of hydrogen and fluorine (2·52 Å). A strong hydrogen bond N–H · · · S has been found in the structure of captax. Strong hydrogen bonds are due to electrostatic attraction and can be obtained in two cases: (1) along the line of polar covalent σ-bond, and (2) for groups of double-bond character, for example S=C<, by the interaction of p_π-electron cloud of the sulphur atom and of the hydrogen atom of the $N^{-\delta_2}$–$H^{+\delta_1}$ bond.

Crystal-chemical analysis of chemical bond nature in the complex compounds is of greatest importance. Interatomic distances depend on the degree of s- and p-character of the atoms in the chemical bonds. Crystal-chemical analysis ($TlCl_3 \cdot 4H_2O$, $[ClTlC_6H_5]^+Cl^-$, TlI_3) indicates sp^2 and sp hybrid orbitals or lone-pair electrons s^2 of the thallium. Determination of the interatomic distances in the structure F_3B–NC_5H_5 made it possible to reveal the nature of the donor–acceptor boron–nitrogen bond. This co-ordinate link is assumed to be polar

$$\begin{matrix} F^{-\delta_2} & & \\ & \diagdown^{+\delta_1} & {}^{-\delta_3} \\ F^{-\delta_2} & \text{—} B \text{—} & N \leftarrow , \\ & \diagup & \\ F^{-\delta_2} & & \end{matrix}$$

with an overlap of a vacant orbital of the boron and a filled orbital of the nitrogen which contains an asymmetrical lone pair of electrons.

The crystal-chemical investigations show that in the complex compounds of metals (Hg, Tl, Pb) of incomplete s–p orbitals the degree of use of p-character of a metal atom in metal–halogen bonds increases in the succession Cl, Br, I. Therefore, in the p-$BrC_6H_4B(OH)_2$ structure the degree of use of p-character of the carbon atom increases in Br–C⟨ bond as compared to the Cl–C⟨

bond. In the complex compounds the degree of use of p-character of a metal atom in the metal–sulphur bond is greater than in the metal–bromine bond. In the $B_3S_3Br_3$ structure, therefore, valence angles are S–B–S $< 120°$ and B–S–B $> 120°$.

6·21. M. A. Paraj-Kojic, A. S. Antzishkina, L. M. Dickareva & E. K. Jukhnov.

The atomic crystal structure of complex acido-amine nickel compounds.

I. An X-ray structure investigation on six compounds was carried out: $Ni(C_5H_5N)_4X_2$, where X = Br, NCS; $Ni(NH_3)_4X_2$, where $X = NO_2$, NCS; and thiocyanate-amine compounds with the following general composition: $Ni(NCS)_2.NH_4NCS.3NH_3$ and

$$Ni(NCS)_2.2NH_4NCS.2NH_3.H_2O\ .$$

The purposes of the investigation were as follows: (1) to find the coordination number of the nickel atom and determine the position of the acid residuals X in compounds of the NiA_4X_2 type; (2) to determine the general charater of the structure of thiocyanate-amine compounds (ionic salts, double molecular compounds, complex compounds), which fall out at different solution concentrations; (3) to establish analogies and differences in interatomic distances from nickel to addendum in different compounds; (4) to find the configuration and orientation of thiocyanate groups, to determine the interatomic distances and the nature of N...C and C...S bonds.

The investigation of the above-mentioned compounds belongs, as a component part, to the systematic study of crystal chemistry of complex nickel compounds. It is of interest both in point of the theory of complex compounds in general and because it may well give an explanation for the peculiar properties of complex nickel compounds in particular.

II. Crystals $Ni(C_5H_5N)_4X_2$, where X = Cl, Br and NCS, are not isomorphous. The results of the investigations of tetragonal crystals $Ni(C_5H_5N)_4Cl_2$ were published earlier.

Crystals of $Ni(C_5H_5N)_4Br_2$ are orthorhombic; space group Pna; $a = 15·8$, $b = 9·3$, $c = 14·2\pm0·1$ kX.; $\sigma = 1·67$ g.cm.$^{-3}$; $N = 4$.

Crystals of $Ni(C_5H_5N)_4(NCS)_2$ are monoclinic; the space group $C2/c$ or Cc; $a = 12·3$, $b = 13·2$, $c = 16·2\pm0·1$ kX., $\beta = 120°$; $\sigma = 1·4$ g.cm.$^{-3}$; $N = 4$.

In both cases the structure investigation was carried out by means of Patterson projections, 'weighted' (generalized) Patterson projections of the first layer lines, with subsequent calculation of centrosymmetrical projections of electron density.

In both cases residuals Br and NCS are bound directly with nickel atoms and lie in transposition to each other.

Crystals $Ni(NH_3)_4X_2$, where $X = NO_2$ and NCS, are isomorphous; space group $C2/m$; $N = 2$.

In the first compound $a = 10·77$, $b = 6·85$, $c = 6·12\pm0·02$ kX. $\beta = 128°$; $\sigma = 1·72$ g.cm.$^{-3}$; in the second $a = 11·46$, $b = 8·18$, $c = 5·68\pm0·02$ kX., $\beta = 105°$; $\sigma = 1·55$ g.cm.$^{-3}$.

The structural type of crystals was determined from Patterson projections and electron-density projections. A more precise determination of interatomic distances was achieved with the help of 'weighted' electron-density projections of the first layer line; in the final stage, electron-density sections were used. In both compounds acid residuals NO_3 and NCS belong to the inner region of the complex. The molecular six-coordinated octahedral arrangement of the addenda seems to be typical of all nickel compounds of the NiA_4X_2 type, in contradistinction to the similar Pd and Pt compounds, whose structure is $[MA_4]X_2$.

III. The results of structure investigation of crystals $Ni(NCS)_2.3NH_3$ have already been published (M. A. Paraj-Kojic, *Proc. Inst. Crystallogr.* (1954), **10**, 117). The molecular complexes $Ni(NH_3)_3(NCS)_2$ have the shape of tetrahedral pyramids with Ni atoms in the centre of the base.

Trigonal crystals $Ni(NCS)_2.NH_4NCS.3NH_3$ possess considerable piezoelectricity; space group $P321$; $a = 10·2$ $c = 11·13\pm0·02$ kX.; $= 1·495$ g.cm.$^{-3}$; $N = 3$. The structure is determined with the help of Patterson-function projections and Harker sections at heights $\frac{1}{3}$ and 0 parallel to (001) and also by using electron-density projections along the second-order axis. The atoms are surrounded octahedrally by three molecules NH_3 and three groups NCS after the design a–a, b–b, a–b (edge isomer). Complex anions $[Ni(NH_3)_3(NCS)_3]$ are arranged according to cubic close packing, in the octahedral interstices of which ions NH_4^+, surrounded by six sulphur atoms, are to be found.

Crystals $Ni(NCS)_2.2NH_4NCS.2NH_3.H_2O$, which belong to the cubic system, also possess piezoelectricity; space group $I23$; $a = 13·41\pm0·02$ kX., $\sigma = 1·523$ g.cm.$^{-3}$; $N = 6$. Six octahedral complex ions *trans*-$[Ni(NH_3)_2(NCS)_4]^{2-}$ are arranged in all the corners of the eight cubes with edges $\frac{1}{2}a$, except the points 0, 0, 0 and $\frac{1}{2}$, $\frac{1}{2}$, $\frac{1}{2}$; these two are occupied by water molecules.

Eight cations NH_4^+ are in the centres of the same cubes and are surrounded octahedrally by sulphur atoms of the thiocyanate group. The remaining four ammonium groups, together with four polar water molecules, form two tetrahedra around two water molecules in the corners of the cubes 0, 0, 0 and $\frac{1}{2}$, $\frac{1}{2}$, $\frac{1}{2}$.

Thus, all the thiocyanate-amine nickel compounds that fall out of the solution are complex in structure type and must be described by the following formulae:

$$Ni(NH_3)_4(NCS)_2, Ni(NH_3)_3(NCS)_2, NH_4[Ni(NH_3)_3(NCS)_3],$$
$$(NH_4)_2[Ni(NH_3)_2(NCS)_4]H_2O\ .$$

IV. We succeeded in determining all interatomic nickel-addendum distances with sufficient precision only in centrosymmetrical structures. The distances are indicated in Table 1, showing that in $Ni(C_5H_5N)_4Cl_2$ and

Table 1

Compound	Bond	Distance
$Ni(C_5H_5N)_4Cl_2$	Ni–Cl	$2·39\pm0·01$ kX.
	Ni–N	$2·00\pm0·05$
$Ni(NH_3)_3(NCS)_2$	$Ni–N_{II}$	$2·04\pm0·04$
	$Ni–N_{I}$	$2·08\pm0·04$
	$Ni–(NH_3)_{II}$	$2·05\pm0·05$
	$Ni–(NH_3)_{I}$	$2·08\pm0·08$
$Ni(NH_3)_4(NCS)_2$	Ni–N	$2·07\pm0·03$
	$Ni–NH_3$	$2·15\pm0·02$
$Ni(NH_3)_4(NO_2)_2$	Ni–N	$2·15\pm0·03$
	$Ni–NH_3$	$2·07\pm0·03$

$Ni(NH_3)_3(NCS)_2$ all the nickel–addendum bonds are of covalent character.

The Ni–S distance in the second compound is the contact of different molecules, which completes the nickel coordination to six.

The Ni–Br and Ni–NCS distances in bromine- and thiocyanate-pyridine complexes, equal to 2·58 and 2·0 kX., also correspond to covalent bonds.

In spite of the isomorphism of $Ni(NH_3)_4(NCS)_2$ and $Ni(NH_3)_4(NO_2)_2$, the relation between interatomic metal-addendum distances is quite different. In the first case it is the distances to four neutral substituents that are increased; in the second, the distances to two acid residuals. Somewhat shortened distances between groups NO_2 and oxygen atoms of neighbouring molecules in $Ni(NH_3)_4(NO_2)_2$ lead us to suppose the existence of weak intermolecular hydrogen bonds. The abnormal colour of this compound may be accounted for by these structure peculiarities.

V. All the compounds containing NCS groups are isothiocyanates. In all cases linear groups NCS lie on one straight line with the Ni–N bond direction.

Group dimensions: in $Ni(NH_3)_3(NCS)_2$, $N_I–C_I = 1·15\pm0·05$, $C_I–S_I = 1·64\pm0·04$, $N_{II}–C_{II} = 1·12\pm0·05$, $C_{II}–S_{II} = 1·70\pm0·04$ kX.; in $Ni(NH_3)_4(NCS)_2$, N–C = $1·20\pm0·05$, C–S = $1·61\pm0·04$ kX.

In spite of the varying distances it is obvious that the N–C bond becomes shorter, and C–S longer, as compared to corresponding distances in methyl-isothiocyanate (N=C = 1·22, C=S = 1·56 kX.). There is no doubt that, at least in the first of these two compounds, the N...C bond must be characterized as triple, and the C...S bond as single.

6·22. E. C. Lingafelter, J. D. Breazeale & J. M. Stewart. *Salicylaldehyde and salicyldimine complexes of copper* (II) *and nickel* (II).

As a part of a program of study of the structure of nickel coordination compounds, we have determined by two-dimensional projections the crystal structure of four compounds: Cu (II) bis-salicylaldehyde, Cu (II) bis-salicylaldimine, Ni (II) bis-salicylaldehyde dihydrate, and Ni (II) bis-salicylaldimine.

Nickel (II) bis-salicylaldehyde dihydrate is monoclinic, space group $A2/m$, containing two (2) molecules in a cell of dimensions: $a_0 = 12·93\pm0·01$, $b_0 = 7·32\pm0·01$, $c_0 = 7·41\pm0·01$ Å, $\beta = 90°15'$. The molecule consists of a planar, *trans* Ni (II) bis-salicylaldehyde, with two water molecules completing the coordination octahedron. The octahedral coordination (C.N. = 6) is consistent with the observed paramagnetism of the compound. The Ni–O bond distances in the chelate are: phenol oxygen 2·01 Å, carbonyl oxygen 2·07 Å.

Copper (II) bis-salicylaldehyde is monoclinic, space group $P2_1/a$, containing two (2) molecules in a cell of dimensions: $a_0 = 12·41\pm0·01$, $b_0 = 6·25\pm0·02$, $c_0 = 8·77\pm0·01$ Å, $\beta = 117°40'$. The molecules are therefore planar and *trans*. The arrangement of the molecules is similar to that which has been reported for a number of other materials having large flat molecules, e.g. anthracene, Ni (II) bis-salicylaldoxime. This arrangement may be considered as consisting of two stacks of molecules, the molecular centers of one stack lying on the line $(0, y, 0)$ with $y = nb_0$, the others on the line $(\frac{1}{2}, y, 0)$ with $y = \frac{1}{2}+nb_0$. The molecular planes are tilted at a considerable angle from the normal to these lines. The Cu–O bond distances are: phenol oxygen 1·86 Å, carbonyl oxygen 1·94 Å.

Nickel (II) and copper (II) bis-salicylaldimine are isomorphous, which is consistent with the observed diamagnetism of the nickel compound. They are monoclinic, space group $P2_1/c$, containing two molecules in a cell of dimensions: $a_0 = 12·96\pm0·02$, $b_0 = 5·83\pm0·01$, $c_0 = 8·11\pm0·01$ Å, $\beta = 95°35'$. The molecules are therefore planar and *trans*. The arrangement of the molecules is of the same type as that of copper (II) bis-salicylaldehyde, but with a somewhat different tilt of the molecules. Thus here again, as in Ni (II) bis-salicylaldoxime, there are no Ni–Ni bonds as observed in Ni dimethylglyoxime. The M–O bond distance is 1·84 Å, the M–N bond distance is 1·87 Å.

The bond distance of the metal–phenol oxygen bond is seen to be essentially the same in the two square planar molecules, which are presumably essentially covalent, but appreciably larger in the octahedral nickel (II) bis-salicylaldehyde dihydrate, which is, by the magnetic criterion, essentially ionic.

6·23. M. R. Truter. *Co-ordination complexes involving ligands containing sulphur.*

The crystal structures of *bis*thioureazinc dichloride, $Zn[SC(NH_2)_2]_2Cl_2$, and *tetrakis*thioacetamidecuprous chloride, $Cu[SC(NH_2)CH_3]_4Cl$, have been determined by three-dimensional X-ray crystal structure analysis. Accurate determinations have also been carried out on thiourea and thioacetamide to obtain the dimensions of the uncoordinated organic molecules for comparison. Measurements of the infra-red absorption spectra of the four compounds have been made. The significance of the interatomic distances and angles found, and of the infra-red spectra will be discussed.

In *tetrakis*thioacetamidecuprous chloride there are discrete Cl^- ions and tetrahedral

$$\left[Cu\left(S=C\begin{matrix}NH_2\\CH_3\end{matrix}\right)_4\right]^+$$

ions. Copper and chlorine occupy special positions, symmetry $\bar{4}$, in the unit cell with $a = 12·449$, $c = 5·469$ Å and space group $I\bar{4}$. The final agreement index R is 0·108, and the bond lengths are Cu–S = $2·345\pm0·002$, $S–C_1 = 1·683\pm0·010$, $C_1–C_2 = 1·460\pm0·015$ and $C_1–N = 1·302\pm0·014$ Å; the thioacetamide groups are planar with $N–C_1–C_2 = 115·3°$, and $N–C_1–S = 122·0°$ and the Cu–S–C_1 angle is 110·4°.

Thioacetamide is monoclinic, $a = 11·062$, $b = 10·005$, $c = 7·17$ Å, $\beta = 99·5°$, with two molecules in the asymmetric unit. The molecules are planar and are both approximately parallel to (001). From two projections the bond lengths obtained are S–C = 1·67, C–C = 1·47 and C–N = 1·37 Å. Refinement of the structure is in progress.

The molecule of *bis*thioureazinc dichloride is covalent, the zinc being tetrahedrally bonded to two chlorine atoms and two sulphur atoms. The zinc and chlorine atoms lie in the mirror planes of the space group $Pnma$ ($a = 13·06$, $b = 12·72$, $c = 5·89$ Å). The thermal motions of the atoms are strongly anisotropic. Refinement of the thermal parameters is proceeding.

For thiourea the structure found in 1932 by two-

dimensional methods (R. W. G. Wyckoff & J. B. Corey, *Z. Kristallogr.* (1932), **81**, 380) has been confirmed. The space group is *Pnma* ($a = 7{\cdot}655$, $b = 8{\cdot}537$, $c = 5{\cdot}520$ Å). The C and S atoms lie in the mirror plane which bisects the N–C–N angle. Three-dimensional refinement has shown that the molecule is planar and that its thermal motion is markedly anisotropic. The thermal motions of the atoms have been analysed. The bond lengths are C–S = $1{\cdot}710\pm0{\cdot}01$ and C–N = $1{\cdot}332\pm0{\cdot}01$ Å; N–C–N = 115° and $R = 0{\cdot}112$.

6·24. E. S. Clark, D. H. Templeton & C. H. MacGillavry. *The crystal structure of gold* (III) *chloride.*

Gold chloride crystallizes in the monoclinic system with $a=6{\cdot}57$, $b=11{\cdot}04$, $c=6{\cdot}44$ Å, $\beta=113°\ 19'$, space group $P2_1/c$. The positions of the atoms were determined from three-dimensional Fourier summations. The accuracy of the atomic locations was improved through the use of a least-squares method of refinement, employing 1065 structure factors with calculations being performed on an I.B.M. 650 computer.

The unit cell contains two Au_2Cl_6 molecular units, which are planar with gold atoms located at the center of a square of chlorine atoms. The stacking of the discrete molecular units follows a general scheme exhibited by many planar organic molecules such as naphthalene.

6·25. G. B. Bokij & G. A. Kukina. *Crystal chemistry of complex divalent platinum compounds.*

I. During recent years at the Laboratory of Crystal Chemistry, Institute of General and Inorganic Chemistry named after N. S. Kurnakov, Academy of Sciences, USSR, an X-ray structure investigation was carried out on a number of complex compounds which belong to the chloramine series of quadrivalent and divalent platinum. A review of the crystal chemistry of platinum chloramine was made by G. B. Bokij in his works devoted to the final results of the research.

X-ray structure investigations confirmed the types of geometrical isomers, which were attributed to them owing to classic stereochemic methods. The formulation of the stereochemistry of inorganic compounds was the result of investigations on complex cobalt and platinum compounds.

It is in complex platinum compounds that I. I. Chernajev found '*trans*-directing influence' (1926).

II. In 1951 G. B. Bokij *et al.* made the first attempt to obtain the quantitative characteristics of *trans*-influence by employing the electronographic method in investigating the structure of potassium trichloroaminoplatinites $K[PtNH_3Cl_3]$. The distance obtained along NH_3–Pt–Cl_I(Pt–Cl_I = 2·32 kX.) proved to be somewhat smaller than the distance along Cl_{II}–Pt–Cl_{II}(Pt–Cl_{II} = 2·35 kX.), which we attributed to the result of the *trans*-influence existing in the molecule. Further, quadrivalent platinum compounds *cis*-$[Pt(NH_3)_2Cl_4]$ and the face isomer of $K_2[Pt(NO_2)_3Cl_3]$ were investigated. We failed, however, to obtain the quantitative characteristics of *trans*-influence; but we succeeded in proving that the nitro group in the quandrivalent platinum compounds possesses a weaker *trans*-influence than chloride and bromine. This was clearly shown by optical methods.

After establishing this fact we returned to the investigation on divalent platinum compounds of the series of chloroamine. We also made a study of compounds in which chlorine atoms were substituted by bromine and an addendum possessing the strongest *trans*-influence, namely the ethylene group.

An X-ray structure investigation on $K[PtNH_3Cl_3].H_2O$ and $K[PtNH_3Br_3].H_2O$ was carried out. The results of goniometric and optical investigations showed that the compounds are isomorphous and orthorhombic.

The dimensions of the unit cell were determined from oscillation photographs and X-ray goniometric diagrams. For $K[PtNH_3Cl_3].H_2O$, $a = 20{\cdot}88\pm0{\cdot}04$, $b = 8{\cdot}10\pm0{\cdot}02$, $c = 13{\cdot}55\pm0{\cdot}02$ kX.; $N = 12$; for $K[PtNH_3Br_3].H_2O$, $a = 21{\cdot}75\pm0{\cdot}04$; $b = 8{\cdot}37\pm0{\cdot}02$; $c = 14{\cdot}42\pm0{\cdot}02$ kX.; $N = 12$; space group D_{2h}^{14}–*Pbna*.

The coordinates of Pt, Br, K and NH_3 were found by the calculation of projections of interatomic functions on plane XY and XZ, and of electron-density projections on corresponding planes. (All of the data were obtained from the reciprocal-lattice photographs with Mo $K\alpha$ radiation.)

In contradistinction to the structure of the anhydrous salt, all the $K[PtNH_3Cl_3].H_2O$ complexes are inclined to Z at approximately 26°.

The threefold period (for $K[PtNH_3Cl_3]$, $a = 17{\cdot}6$, $b = 8{\cdot}84$, $c = 4{\cdot}19$ kX.; $N = 4$) is caused by the presence of water molecules, which displace potassium atoms from the inversion centre. This accounts for the increase of the period along X by approximately 3 kX. Potassium atoms are arranged in trigonal prisms and their coordination number is 6. The presence of water molecules in the outer region also influences the intermolecular interatomic distances.

III. At the beginning of 1954 we undertook an investigation on Zeise salts, $K[PtC_2H_4Cl_3].H_2O$ and $K[PtC_2H_4Br_3].H_2O$, to determine Pt–Cl and Pt–Br distances in case ethylene labilizes the chlorine and bromine, and also to find how carbon atoms are arranged in relation to the group $[PtCl_3]$ and $[PtBr_3]$.

The crystals belong to the monoclinic system, as was found by Jorgensen in 1900. Goniometric and optical investigations have shown that $K[PtC_2H_4Cl_3].H_2O$ and $K[PtC_2H_4Br_3].H_2O$ are isomorphous. The unit cells are determined by oscillation photographs.

For $K[PtC_2H_4Cl_3].H_2O$, $a = 10{\cdot}85\pm0{\cdot}02$; $b = 8{\cdot}53\pm0{\cdot}02$; $c = 4{\cdot}81\pm0{\cdot}01$ kX., $\beta = 97°$; $N = 2$; for $K[PtC_2H_4Br_3].H_2O$, $a = 11{\cdot}38\pm0{\cdot}02$; $b = 8{\cdot}78\pm0{\cdot}02$; $c = 5{\cdot}01\pm0{\cdot}01$ kX., $\beta = 97°$; $N = 2$; space group C_2^2–$P2_1$. The atomic coordinates are obtained from projections of interatomic functions on XY and XZ and from the projection of electron density on XZ. At the end of 1954 there was published an article by Wunderlich & Meller on the crystal structure of Zeise salts. The atomic coordinates in this article were definitely at odds with ours, but in 1955 the same authors published a paragraph with corrected coordinates, the latter being in agreement with our results.

To determine with greater precision the distance in case of an addendum with a strong *trans*-influence—the ethylene group—we investigated an isomorphous compound with bromine and obtained good results. The analysis of the electron-density projection on plane XZ made it possible to determine the carbon atomic coordinates and to find that the plane of the ethylene molecule itself is perpendicular to the plane of the group

$[PtBr_3]$, whereas carbon atoms are almost symmetrical to platinum atoms.

In this way coordinates of all the atoms were obtained and interatomic distances were calculated. Two of the bond lengths $Pt–Cl_{II}$ and $Pt–Br_{II}$ are normal (2·26 and 2·42 kX.); the third bond length $Pt–Cl_I$ and $Pt–Br_I$, which is in the *trans* position to the ethylene molecule, is 2·40 and 2·50 kX. respectively.

As the strong *trans*-influence of the ethylene molecule is well known, the increase of bond lengths $Pt–Cl_I$ and $Pt–Br_I$ seems quite natural.

Proceeding from crystal chemistry data it is possible to determine the position of hydrogen atoms. There are two variants of the arrangement of the flat group C_2H_4 in the molecule $[PtC_2H_4Cl_3]$. In the first variant this plane, when continued, passes through the line $Pt–Br_I$; in the second it is perpendicular to the line. The difference between the interatomic distances obtained for these two variant speaks definitely in favour of the second variant.

6·26. W. Nowacki & J. Silverman. *The crystal structure of zinc hydroxychloride* II.

Zinc hydroxychloride II was synthesized from zinc oxide and zinc chloride. In addition to a microcrystalline product which was employed as analysis substance, suitably dimensioned single crystals were obtained for single-crystal X-ray examination. Chemical analysis established that the composition is $Zn_5(OH)_8Cl_2.1H_2O$; the crystal water is lost and regained reversibly, this process being very slow.

Data obtained from single-crystal rotation, oscillation and Weissenberg photographs led to a complete crystal-structure determination of zinc hydroxychloride II. The space group is $R\bar{3}m$–D^5_{3d} and the lattice constants of the triply-primitive hexagonal cell H_R are: $a_H = 6·34 \pm 0·01$, $c_H = 23·64 \pm 0·02$ Å; this cell contains three formula weights. The atomic parameters have been determined from Fourier and Patterson projections.

The structure is of the layer type and may be systematically derived from the hypothetical *C*6 zinc hydroxide. Within one composite layer, 60% of the zinc atoms are octahedrally and the remaining 40% tetrahedrally coordinated. Coordination and interatomic distances indicate that the zinc octahedral bonds are predominantly ionic in nature and that the tetrahedral bonds possess appreciable covalent character. The structure is made up of these composite layers piled upon one another according to the rhombohedral repeat scheme. Certain shortened O–O and O–Cl distances between adjacent composite layers have been interpreted as O–H · · · O and O–H · · · Cl bonds; the formation of such bonds is believed to be favoured by the strongly polarizing action of the Zn ions.

The most important interatomic distances are: Zn–O (octahedral bonds) = 2·16 and 2·17 Å; Zn–O (tetrahedral bonds) = 2·02 Å; Zn–Cl (tetrahedral bond) = 2·33 Å; O–H · · · O (hydroxyl bond joining crystal water to OH groups) = 2·79 Å; OH · · · Cl (hydroxyl bonds joining Cl to OH groups) = 3·09 Å. The error in these distances is about ±0·05 Å.

The structure of zinc hydroxychloride II is compared to that of related compounds. It is suggested that the stability of $Zn_5(OH)_8Cl_2.1H_2O$, as opposed to $C6Zn(OH)_2$, is due to the much wider separation, in the former, of neighbouring OH groups from adjacent composite layers; this dilation of the structure is caused by the large chlorine atoms which are interposed between the *C*6-type layers.

In the course of the crystal-structure determination, the following matters of general interest have been investigated:

(1) Various methods of correcting for absorption were examined in detail and are critically discussed. The absorption integral has been evaluated for some special loci on the equatorial Weissenberg diagram of a crystal of rectangular cross-section. The displacement of atomic parameters due to absorption, in the special case of zinc hydroxychloride II, was quantitatively determined by comparison of Patterson and Fourier projections based on intensity data with and without absorption corrections; the effect was found to be *negligibly* small.

(2) Various statistical methods for the determination of the absolute intensity basis and natural temperature factor were applied to the intensity data from a *zone* of reflexions of zinc hydroxychloride II. It was found that the weighted-*general*-position intensity statistics (which employs no structural hypothesis other than a knowledge of crystal class) gives values of sufficient accuracy for the initial stages of the structure determination while the normal unweighted Wilson statistics does not yield satisfactory results. This is of considerable interest as only a zone of reflexions was employed and, in addition, all atoms of zinc hydroxychloride II occupy *special* space group positions.

6·27. S. Geller & M. A. Gilleo. *The crystal structure and ferrimagnetism of yttrium–iron garnet,* $Y_3Fe_2(FeO_4)_3$.

A refinement of the crystal structure of yttrium–iron garnet has been carried out by application of the least-squares method of calculation to single-crystal X-ray data. The oxygen parameters are $x = -0·027_4$, $y = 0·057_2$, $z = 0·149_2$; the tetrahedral Fe–O distance is 1·88 Å, the octahedral Fe–O distance is 2·00 Å and the Y–O distances are 2·37 and 2·43 Å. None of the oxygen polyhedra is regular, even though the symmetry would allow the tetrahedra and octahedra to be regular simultaneously.

Interatomic distances and angles which are important to the interaction between magnetic ions have been calculated. The strongest interactions occur between Fe^{3+} in 16(*a*) and 24(*d*) positions and between M^{3+} (24(*c*) positions) magnetic rare-earth ions substituted for yttrium, and Fe^{3+} ions in the 24(*d*) positions. Interactions between crystallographically equivalent ions are all small. The number of interactions per Fe^{3+} ion is $\frac{3}{5}$ that in a spinel ('ferrite') and, correspondingly, the Curie temperature observed is 0·64 that of magnetite.

No change of symmetry is observed up to 900° C.

6·28. E. Prince. *Neutron diffraction measurements on yttrium–iron and yttrium–aluminum garnets.*

The garnet structure compound with the composition $Y_3Fe_2(FeO_4)_3$, discovered by Bertaut & Forrat, and, independently, by Geller & Gilleo, is unique among known magnetic oxides in containing magnetic ions of only one valence. Because of the great theoretical im-

portance of this compound, a neutron diffraction study was undertaken to confirm the postulated magnetic structure and to help determine the crystal structure. At the beginning of the study there were no reliable neutron cross-section data available for yttrium. The yttrium scattering factor was therefore treated as a variable in trial-and-error refinement. A neutron diffraction powder pattern ($\lambda = 1{\cdot}00$ Å) had fully resolved peaks up to $h^2+k^2+l^2 = 32$, and peaks which could be broken down to the sum of several reflections out to $h^2+k^2+l^2 = 56$. Initial refinement was carried out with six reflections whose total intensities were more than 80% due to nuclear scattering. Further refinement by successive approximations was carried out with four additional reflections containing larger amounts of magnetic scattering. Final calculated intensities are based on oxygen parameters determined by Geller & Gilleo from single-crystal X-ray data.

Because there was still an uncertainty in the yttrium scattering factor, resulting from the presence of magnetic scattering, a further study was made on yttrium–aluminum garnet, $Y_3Al_2(AlO_4)_3$, in which, because this compound is not magnetic, only the three oxygen positional parameters and the yttrium scattering factor must be determined. The final oxygen parameters in $Y_3Al_2(AlO_4)_3$ are $x = -0{\cdot}029$, $y = 0{\cdot}053$, $z = 0{\cdot}151$. The yttrium scattering amplitude is $+0{\cdot}80\pm0{\cdot}01\times10^{-12}$ cm. The overall intensity discrepancy, $\Sigma|I_o-I_c| \div \Sigma I_o$ was 5·7%.

The magnetic contributions to the intensities are obtained by subtracting from the total intensities the nuclear intensities based on the ionic coordinates and the nuclear scattering factors. A model analogous to that of Néel for magnetic spinels accounts for the room-temperature magnetic intensities and moment. In this model, however, the magnetic moments assigned to the tetrahedrally and octahedrally coordinated iron ions are respectively 3·7 and 4·0 Bohr magnetons. These values differ from those found by Bertaut, Forrat, Herpin and Mériel.

The changes of the intensities of the magnetic reflections as the sample is cooled to liquid-nitrogen temperature indicate that the two sets of iron ions saturate at different rates.

6·29. D. H. Templeton. *Electrostatic calculation of structure for yttrium oxyfluoride.*

The substance YOF exists in two crystal structures, each of which is an ordered superlattice based on the CaF_2-type structure. The atomic coordinates were determined by W. H. Zachariasen (*Acta Cryst.* (1951), **4**, 231), but the diffraction data did not distinguish O and F. The nearest neighbor distances are 2·28 and 2·44 Å in the rhombohedral form and 2·30 and 2·47 Å in the tetragonal form. A calculation of the crystal energy, based on a simple model, shows decisively that the shorter distance corresponds to the oxygen neighbor in each structure.

In the present treatment the crystal energy is assumed to be given by the expression

$$U = \Sigma q_i q_j / r_{ij} + \Sigma B_{ij} / r_{ij}^n .$$

The first sum takes account of the Coulomb monopole interactions of all pairs of atoms and is computed by F. Bertaut's method (*J. Phys. Radium* (1952), **13**, 499) with careful attention to convergence (R. E. Jones & D. H. Templeton, *J. Chem. Phys.* (1956), **25**, 1062). The second sum is computed only for nearest neighbors. The constant B for Y–O (or Y–F) pairs is chosen so that U, calculated in the same way, is a minimum for Y_2O_3 (or YF_3) at the interatomic distances observed experimentally. Various values of the exponent n have been used, but one value is used consistently throughout a single calculation.

The rhombohedral structure is described as follows:

Space group: $R\bar{3}m$ (No. 166).

$a = 6{\cdot}697$ Å, $\alpha = 33{\cdot}20°$.

2 Y at $\pm(u, u, u)$, $u = 0{\cdot}242$ or $0{\cdot}258$.

2 F at $\pm(v, v, v)$, $v = 0{\cdot}122$ or $0{\cdot}130$.

2 O at $\pm(w, w, w)$, $w = 0{\cdot}370$ or $0{\cdot}378$.

The structures described by the two sets of parameters differ only in the interchange of O and F atoms. The crystal energy calculated for $u = 0{\cdot}242$ exceeds that for $u = 0{\cdot}258$ by about 100 kcal./mole. The minimum in U was sought as a function of a and u, with α held constant. The parameter v (or w) was determined so as always to equalize the two independent Y–F (or Y–O) nearest-neighbor distances. The value of u giving the minimum energy is 0·259 for n equal to either 8 or 9. The value of a giving the minimum energy agrees with the experimental value within 0·6% for $n = 8$ and 0·4% for $n = 9$.

Less complete calculations for the tetragonal structure indicate very similar results. It is hoped to extend the calculations to include anion–anion repulsion effects, but these effects are not expected to change the qualitative conclusions. All statements made concerning the structures of YOF are assumed to apply also to the compound LaOF, which is isostructural with both forms of YOF (Zachariasen, *loc. cit.*).

It is noteworthy that the Y–O distance is about what one estimates for coordination 5 or 6, which is intermediate between the number of oxygen neighbors and the number of anion neighbors. The Y–F distance, on the other hand, corresponds to hardly any repulsive potential and is considerably longer than the sum of ionic radii. A similar effect may be observed in other oxyhalides, for example the rare earth oxychlorides (D. H. Templeton & C. H. Dauben, *J. Amer. Chem. Soc.* (1953), **75**, 6069).

6·30. M. Hamelin. *Structure du composé* TiO_2–Al_2O_3.

Des cristaux orthorhombiques du composé TiO_2–Al_2O_3 ont été obtenus par fusion solaire et refroidissement lent, également après un chauffage de 6 heures à 1600° C.

La structure a été établie à partir des données des clichés de Weissenberg en utilisant la radiation du molybdène, par les méthodes modernes: projections et sections de Patterson, projections de densités électroniques. La structure a été précisée par les séries différences. Tous ces calculs ont été effectués par la voie optique du photosommateur harmonique de M. von Eller.

Nous avons à signaler que les coefficients de température se sont révélés différents selon les atomes considérés. L'aluminium possède un coefficient de température $B = 0{,}340$ Å^2 inférieur à celui des autres atomes. Pour

Table 1. *Lattice constants, hexagonal and rhombohedral of* Ti–Ti_2O_3 *solid solutions and of pure* Ti_2O_3 *(extrapolated and corrected for refraction) at* 25° C.

	Free Ti (%)	a (Å)	c (Å)	Vol. (Å^3)	c/a	$a_{rh.}$ (Å)	α (°)
Sample *C*	3·67	5·1402	13·6595	312·537	2·657	5·4349	56·442
Sample *B*	1·45	5·1486	13·6320	312·945	2·648	5·4299	56·601
Sample *A*	0·8	5·1482	13·6362	312·993	2·649	5·4310	56·586
Pure Ti_2O_3	0·0	5·1517	13·6244	313·151	2·645	5·4288	56·653
Measurements by:							
Lunde	—	—	—	—	—	5·42	56·53
Zachariasen	—	5·15	13·56	313·30	2·63	5·42*	56·83†
Ehrlich	—	5·141	13·61	313·35	2·65	5·421	—

* ±0·01. † ±0·08.

le titane $B = 1$ Å^2, pour les oxygènes l'un d'eux a une valeur inattendue $B = 1{,}1$ Å^2 alors que les autres oxygènes sont caractérisés par $B = 0{,}468$ Å^2.

6·31. M. E. Straumanis & T. Ejima. *Lattice parameters, thermal expansion coefficients, molecular weights and imperfections of* Ti_2O_3 *and of solid solutions with* Ti.

The oxide Ti_2O_3 is a compound within the binary system Ti–O (P. Ehrlich, *Z. Elektrochem.* (1939), **45**, 362; E. S. Bumps *et al.*, *Trans. Amer. Soc. Met.* (1953), **45**, 1008; T. H. Schofield & A. E. Bacon, *J. Inst. Met.* (1955), **84**, 47). The oxide was prepared by heating in vacuum at 1400° C. the constituents Ti and TiO_2 in amounts according to the reaction: $3\,TiO_2 + Ti = 2\,Ti_2O_3$.

The analysis of the dark substance obtained was made by the hydrogen-evolution method (M. E. Straumanis *et al.*, *Analyt. Chem.* (1956), **28**, 1883) by dissolving the oxide in HF. If free Ti still was present, the substance developed hydrogen; hence, calculated amounts of TiO_2 were added and the whole was heated again. This procedure was repeated until a preparation with a minimum amount of free Ti was obtained.

Of these samples three were chosen (which gave the sharpest diffraction patterns) to determine the lattice parameters of the unit cell, which can be regarded as hexagonal or rhombohedral (W. A. Zachariasen, *Skr. Akad. Oslo* (1928), No. 4, pp. 21, 165). The samples were designated *A*, *B* and *C* and their composition was as follows:

Sample *A*: Ti_2O_3 with 0·8% b. w. free Ti.
Sample *B*: Ti_2O_3 with 1·45% b. w. free Ti.
Sample *C*: Ti_2O_3 with 3·67% b. w. free Ti.

Sample *C* was just on the limit of the homogeneity of the Ti_2O_3 phase. Thus, the samples were solid solutions.

The intention of this work was to determine exactly the lattice parameters of these samples at different temperatures, so that the expansion coefficients could also be calculated, and then to find the lattice parameters for pure Ti_2O_3, extrapolating the parameters obtained for the three samples to a free Ti content equal to zero.

The lattice parameters of the samples were determined by the Debye–Scherrer method using the asymmetric modification and keeping the powder cameras in thermostats at constant temperatures while the exposures were made. Cobalt radiation was used, which produced the interferences 13.10 and 30.12 at the angles 77·55 and 82·26° respectively in the high back-reflection region. These are the only possible hexagonal indices for a rhombohedral unit cell because they satisfy the rhombohedral condition according to which the algebraic sum $-h+k+l$ is divisible by 3. Other indices than those above would lead to lattice constants quite different from those mentioned in the literature.

From the two Bragg angles the constants a and c of the hexagonal cell and then the constants $a_{rh.}$ and α of the rhombohedral cell were calculated. The parameter determinations were made at constant temperatures between 10·0 and 60·0° C. in 10° increments.

The results obtained for the samples are summarized in Table 1.

Table 1 shows the change of the constants with decreasing amount of free Ti in Ti_2O_3. It was assumed that the relationship is a linear one, so the extrapolated values for pure Ti_2O_3 could easily be obtained. They agree well with the values of previous investigators.

The expansion coefficients of the lattice constants (between 10 and 60° C.) are given in Table 2. Some of these have negative values.

In order to determine the soundness of the structure

Table 2. *Thermal expansion coefficients of the lattice constants of the solid solutions* Ti–Ti_2O_3 *between* 10 and 60° C.

(All values per unit per °C.)

	Sample *C*	Sample *A*
Linear exp. coeff. α_a	$-9{\cdot}08 \times 10^{-6}$	$1{\cdot}67 \times 10^{-7}$
Linear exp. coeff. α_c	$2{\cdot}74 \times 10^{-5}$	$2{\cdot}34 \times 10^{-5}$
Coeff. for c/a	$3{\cdot}70 \times 10^{-5}$	$2{\cdot}36 \times 10^{-5}$
Volume exp. coeff. β	$9{\cdot}20 \times 10^{-6}$	$2{\cdot}37 \times 10^{-5}$
Rhomb. lin. exp. coeff., $\alpha_{a,\,rh.}$	$1{\cdot}65 \times 10^{-5}$	$1{\cdot}65 \times 10^{-5}$
Exp. coeff. of the angle α	$-2{\cdot}76 \times 10^{-5}$	$-1{\cdot}76 \times 10^{-5}$

Table 3. *Macroscopic and X-ray densities* (d), *chemical and X-ray molecular weights* (M) *and the number of molecules per unit cell* (n) *of* Ti–Ti_2O_3 *solid solutions and of pure* Ti_2O_3 *(extrapolated).*

	Sample *C*	Sample *B*	Sample *A*	Ti_2O_3
Free Ti (% b.w.)	3·67	1·45	0·8	0·00
Macroscopic d at 25° C. (g.cm.$^{-3}$)	4·6134±0·0015	4·6060	4·5988±0·002	4·5969
d_X at 25° C. (g.cm.$^{-3}$)	4·5011	4·5462	4·5569	4·5735
Chemical M (from anal.)	141·24	142·84	143·20	143·79
M_X	144·77	144·72	144·52	144·45
M from atomic weight	—	—	—	143·80
n	6·150	6·079	6·055	6·030

of pure Ti_2O_3 and to find out where the metallic titanium was located which was dissolved in the samples, density determinations were made and were compared with the X-ray densities. The comparison showed that the experimental (macroscopic) densities (by weight) of the samples were higher than the respective X-ray densities. This indicates that the free titanium went into the interstitial space of Ti_2O_3 (A. Smakula *et al.*, *Phys. Rev.* (1955), **99**, 1747). The determination of the X-ray and chemical molecular weights (M. E. Straumanis, *Acta Cryst.* (1949), **2**, 83; *Phys. Rev.* (1953), **92**, 1155; *Amer. Min.* (1953), **38**, 662) of the solid solutions, of course, confirmed this conclusion. The data are given in Table 3.

Table 3 shows that M and M_X are approaching the standard molecular weight of Ti_2O_3 with increasing purity of the compound. However, the lattice of pure Ti_2O_3 seems to be not quite sound, as it still contains some interstitials. This is in agreement with the density measurements of Zachariasen (*loc. cit.*). Further, it follows clearly from Table 3 that metallic Ti, if dissolved in Ti_2O_3 in amounts within the solubility limits, goes into the interstitial space of the Ti_2O_3 lattice. Whether or not the whole amount of Ti dissolved in Ti_2O_3 goes into this space is also accessible to calculation (some of the Ti added might go also to regular positions).

6·32. A. S. Posner, A. Perloff & A. F. Diorio. *Refinement of the hydroxyapatite structure.*

Pure hydroxyapatite crystals were synthesized and studied with integrating Weissenberg techniques using nickel-filtered, Cu $K\alpha$ radiation. A least-squares refinement of the atomic coordinates and their individual isotropic temperature factors was performed on the IBM 704 electronic computer, using approximately 400 observed intensities.

6·33. F. Liebau. *On the crystal chemistry of silicates, germanates, phosphates, arsenates, vanadates, and alkali fluoberyllates of the general formula ABX_3.*

In a recent paper (F. Liebau, *Z. phys. Chem.* (1956), **206**, 73) among others it was shown that in the case of silicates of the formula $MeSiO_3$ (Me = cations of small or medium size) the type of structure depends essentially on the size of the cations. These investigations have been extended to corresponding silicates with large cations (Sr, Ba) as well as to germanates $MeGeO_3$, alkali-fluoberyllates $MeBeF_3$, -phosphates $MePO_3$, -arsenates $MeAsO_3$, -arsenatophosphates $Me(P, As)O_3$, and -vanadates $MeVO_3$.

The cell dimensions of a number of these compounds were determined by single-crystal and powder photographs. The results of these investigations are given in Table 1. The structures are arranged with increasing size of the cations, and increasing temperature respectively.

Some results still unpublished may be mentioned. There are two modifications of $BaSiO_3$ and of $BaGeO_3$. The low-temperature forms appear to have the same structure as pseudo-wollastonite while the high-temperature phases, together with $KBeF_3$ and NH_4BeF_3, form a group with a new structure type. $CaGeO_3$ has the β-wollastonite structure.

The existence of 7-periodic chains, i.e. chains with 7 SiO_4 tetrahedra per period, in pyroxmangite, and of 5-periodic chains in rhodonite seems to depend not only on the relative amounts of the cations present but also on the presence of transition elements (Mn, Fe) in these silicates.

The silicates and germanates of the alkali earth

Table 1

Structure type	$MeSiO_3$	$MeGeO_3$	$MeBeF_3$
1-periodic chain 2·93 Å	—	$CuGeO_3$	—
2-periodic chain ~ 5·25 Å	$MgSiO_3$, enstatite $CaMg(SiO_3)_2$, diopside $CaMn(SiO_3)_2$, johannsenite	$MgGeO_3$	$LiBeF_3$ $LiNa(BeF_3)_2$
7-periodic chain 17·4 Å	$(Ca, Mg)(Mn, Fe)_6(SiO_3)_7$, pyroxmangite	—	—
5-periodic chain 12·2 Å	$CaMn_4(SiO_3)_5$, rhodonite	—	—
3-periodic chain ~ 7·3 Å	$CaMn(SiO_3)_2$, bustamite $CaSiO_3(t)$, β-wollastonite	$CaGeO_3$	$NaBeF_3$
Pseudowollastonite structure	$CaSiO_3(h)$, pseudowollastonite $SrSiO_3$ $BaSiO_3(t)$	$SrGeO_3$ $BaGeO_3(t)$	—
$BaSiO_3(h)$ structure	$BaSiO_3(h)$	$BaGeO_3(h)$	$KBeF_3$ NH_4BeF_3

Structure type	$MePO_3$	$Me(P, As)O_3$	$MeAsO_3$
2-periodic chain ~ 5·2 Å	$LiPO_3(t)$ $LiPO_3(h)$?	$Li(As, P)O_3$ $Li(P, As)O_3$	$LiAsO_3$ $LiNa(AsO_3)_2$
5-periodic chain ~ 14 Å	—	—	$(Li, Na)AsO_3$
3-periodic chain ~ 7·4 Å	$NaPO_3$, Maddrells salt	$Na(P, As)O_3$	$(Li, Na)AsO_3$ $NaAsO_3$
Kurrol structure ~ 6·1 Å	$NaPO_3$, Kurrol's salt $AgPO_3$	—	—
2-periodic chain ~ 4,4 Å	$KPO_3(t)$ $KPO_3(h)$? $RbPO_3$ $CsPO_3$	$K(As, P)O_3$ $K(P, As)O_3$	$KAsO_3$ I $KAsO_3$ II $KAsO_3$ III

Structure type	$MeVO_3$
2-periodic chain ~ 5·8 Å	$NaVO_3$ KVO_3 NH_4VO_3

elements and the alkali fluoberyllates have the same sequence of structure types (pyroxene type—β-wollastonite type—pseudo-wollastonite type—$BaSiO_3(h)$-type) except for the absence of the pseudo-wollastonite type of the fluoberyllates.

For such series of compounds with the same sequence of structure types the name '*isomorphotropic series*' may be proposed.

The phosphates $MePO_3$, arsenates $MeAsO_3$, and arsenatophosphates $Me(P, As)O_3$ of the alkali elements also form three isomorphotropic series, but these are different from the three mentioned above. The phosphates, arsenates, and arsenatophosphates with small cations also have pyroxene and β-wollastonite structures. In the phosphate series there follows the 'Kurrol structure' of $(NaPO_3)_x$, a structure which has not yet been found in the other two series. In the case of compounds with large cations there are again structures built of 2-periodic chains.

All alkali vanadates examined up to now contain 2-periodic chains and show no relations to the other series of compounds mentioned.

6·34. P. B. Braun. *Comparison of a number of closely related structures in the system* $BaO–FeO–Fe_2O_3$.

In the system $BaO–FeO–Fe_2O_3$ a number of compounds has been found with structures related to that of the mineral magnetoplumbite. Some of these compounds are listed here, with formula, abbreviating letter, space group and cell dimensions.

M	$Ba...Fe^{III}_{12}O_{19}$	$P6_3/mmc$	23·2 Å	5·9 Å
W	$Ba–Fe^{II}_2Fe_{16}O_{27}$	$P6_3/mmc$	32·8	5·9
X	$Ba_2Fe^{II}_2Fe^{III}_{28}O_{46}$	$R\bar{3}m$	84·1	5·9
Y	$Ba_2Fe^{II}_2Fe^{III}_{12}O_{22}$	$R\bar{3}m$	43·6	5·9
Z	$Ba_3Fe^{II}_2Fe^{III}_{24}O_{41}$	$P6_3/mmc$	52·3	5·9

All of these structures can be thought to be built up from spinel blocks, either 4 or 6 oxygen layers thick, joined together by barium-containing close-packed layers. These latter layers are again of two different types.

In another possible description all these structures are built up from three structural units, containing 5, 6 and 2 layers respectively.

In the structure of Z, 'plates' of nine layers can be distinguished with a structure identical with 'plates' of nine layers out of M and 'plates' of ten layers out of Y.

In X similar identities are present in plates of 14 and 16 layers thickness, i.e. more than 30 Å.

6·35. P. T. Davies. *An X-ray study of lead dioxybromide.*

The compound $2PbO.PbBr_2$ is one which occurs in combustion-chamber deposits in gasoline engines. Crystals from a synthetic melt were orthorhombic, $a = 9·81$, $b = 12·25$, $c = 5·88$ Å, $Z = 4$.

The structure was studied by two-dimensional methods, a major step being the interpretation of the Patterson synthesis of the ($hk0$) reflexions, of symmetry Pgg. Individual lead–lead peaks were in general not resolved, but it was possible to locate one atom in the projection by consideration of Harker–Patterson peaks and single-weight peaks. The other two independent lead atoms were located by means of the minimum function (M. J. Buerger, *Acta Cryst.* (1951), **4**, 531). A Fourier synthesis, using phases determined by the lead atoms, revealed the bromine atoms.

Close agreement of intensities between alternate layer lines indicated the arrangement of the atoms in sheets at a spacing of one-half in the third coordinate z. Consideration of the intensities of ($hk1$) reflections enabled the appropriate combination of z values to be selected. The lead and bromine atoms are in 4(c) positions in space group D^{16}_{2h} $Pbnm$ as follows:

	Pb(I)	Pb(II)	Pb(III)	Br(IV)	Br(V)
x	0·082	0·380	0·216	0·176	0·089
y	0·422	0·209	0·060	0·311	0·131
z	0·250	0·250	0·750	0·750	0·250

6·36. A. Zalkin. *Crystal structure of* $Li_{22}Pb_5$.

$Li_{22}Pb_5$ represents the last of the series of Li–Pb intermetallic compounds investigated by X-ray diffraction by the author. The set of compounds studied so far have been Li_7Pb_2, Li_3Pb, Li_8Pb_3, and LiPb. In general these formulations are in agreement with the phase-diagram studies of G. Grube & H. Klaiber (*Z. Electrochem.* (1934), **40**, 745).

$Li_{22}Pb_5$ was prepared by Dr William Ramsey at this laboratory by fusing the two elements in the proper proportion *in vacuo*. Single-crystal and powder patterns were obtained with the use of Cu $K\alpha$ X-rays.

$Li_{22}Pb_5$ is face-centered cubic with $a = 20·08 \pm 0·02$ Å. There are 80 Pb atoms per unit cell. The measured density is $3·88 \pm 0·04$ g.cm.$^{-3}$; the calculated X-ray density is 3·86 g.cm.$^{-3}$.

The space group is $F23$. The Pb atoms are in the following positions:

24(f): $x, 0, 0$; $0, x, 0$; $0, 0, x$; $\bar{x}, 0, 0$; $0, \bar{x}, 0$; $0, 0, \bar{x}$; + face centering: $x_1 = 0·322$.

24(g): $x, \frac{1}{4}, \frac{1}{4}$; $\frac{1}{4}, x, \frac{1}{4}$; $\frac{1}{4}, \frac{1}{4}, x$; $\bar{x}, \frac{1}{4}, \frac{3}{4}$; $\frac{3}{4}, \bar{x}, \frac{1}{4}$; $\frac{1}{4}, \frac{3}{4}, \bar{x}$; + face centering: $x_2 = 0·072$.

16(e): x, x, x; $x, \bar{x}, \bar{x}$; $\bar{x}, x, \bar{x}$; $\bar{x}, \bar{x}, x$; + face centering: $x_3 = -0·086$.

16(e): x, x, x; $x, \bar{x}, \bar{x}$; $\bar{x}, x, \bar{x}$; $\bar{x}, \bar{x}, x$; + face centering: $x_4 = -0·336$.

The positions of the Li atoms cannot be determined with X-rays. From the geometry one can deduce approximate locations of the Li atoms. Packing considerations indicate that the cell can accommodate up to 352 Li atoms.

The atomic arrangement of the atoms in this alloy is closely related to that found for Li_7Pb_2, Li_3Pb, Li_8Pb_3, and LiPb (A. Zalkin & W. J. Ramsey, *J. Phys. Chem.* (1956), **60**, 234; A. Zalkin *et al.*, *J. Phys. Chem.* (1956), **60**, 1275; H. Nowotny, *Z. Metallk.* (1941), **33**, 388). The structures are basically the body-centered cubic lattice of elemental Li with the appropriate number of Li atoms replaced by Pb atoms. The Pb atoms enter in such a manner as to be uniformly distributed and separated from each other. There are of course small distortions from this idealized arrangement in some of the compounds, as is the case for $Li_{22}Pb_4$.

6·37. W. H. McCarroll, L. Katz & R. Ward. *Some ternary oxides of tetravalent molybdenum.*

Ternary oxides of Mo (IV) having the general formula $A_2Mo_3O_8$ have been prepared in which A is any one of the following: Mg, Mn, Fe, Co, Ni, Zn, or Cd. Single-crystal photographs of the Zn and Mg compounds showed hexagonal symmetry with probable space group one of $P6_3mc$, $P\bar{6}2c$, or $P6_3/mmc$. Unit-cell dimensions for the Zn compound are $a = 5{\cdot}78$, $c = 9{\cdot}92$ Å; for the Mg compound, $a = 5{\cdot}76$, $c = 9{\cdot}89$ Å. The powder photographs of the other compounds could be indexed on similar hexagonal cells; their appearance indicated closely similar structures.

A satisfactory fit of observed and calculated structure factors was obtained using the positions of $P6_3mc$ with (taking the Zn compound as the example) Mo in 6(*c*) $x = 0{\cdot}146$, $z = 0{\cdot}250$; Zn in 2(*b*), $z = -0{\cdot}063$; Zn in 2(*b*), $z = 0{\cdot}500$; O in 2(*a*), $z = 0{\cdot}385$; O in 2(*b*), $z = 0{\cdot}133$; O in 6(*c*), $x = 0{\cdot}490$, $z = 0{\cdot}363$; O in 6(*c*), $x = 0{\cdot}156$, $z = 0{\cdot}633$. $R = 0{\cdot}13$ for 90 observed reflections.

The structure may be described as a distorted double-hexagonal closest packing of oxygen in which oxygen layers are held together by alternate layers of Zn and Mo atoms. The molybdenum atoms are in octahedral coordination with oxygen. Half the zinc atoms are in tetrahedral coordination with oxygen while the other half are in octahedral coordination. The molybdenums form three-membered equilateral rings in which each molybdenum has two molybdenum neighbors at 2·53 Å. Bonding between molybdenum members of the rings accounts for the magnetic-data indication that these atoms have no unpaired electrons.

6·38. R. W. M. D'Eye. *The anomalous mixed crystal system* ThO_2/ThF_4 *and the structure of* $ThOF_2$.

We find that ThF_4 dissolves in ThO_2 forming solid solutions with a solid solubility limit at $ThO_{1{\cdot}75}F_{0{\cdot}50}$. By analogy with other mixed-crystal systems with the fluorite structure, it seems likely that the oxygen and fluorine atoms in these mixed crystals are statistically distributed over the normal anion sites of a fluorite lattice with the extra anions accommodated, statistically, in the interstitial positions ($\frac{1}{2}$, 0, 0) etc.

In the region from the solid solubility limit to mixtures of equimolar composition two phases occur, the limiting solid solution phase and thorium oxyfluoride. There is no evidence to suggest that $ThOF_2$ exists over a non-stoichiometric range.

According to Zachariasen, $ThOF_2$ has the LaF_3-type hexagonal structure. He suggests that the oxygen and fluorine atoms are randomly distributed over the normal anion sites of the LaF_3-type lattice. However, we find that diffraction photographs of $ThOF_2$ have many weak reflexions which cannot be indexed on the basis of the LaF_3-type hexagonal cell. Further, all reflexions having indices $hk1$ or $hk0$ are split. The line splitting is masked if the preparations are of small particle size and the extra reflexions will generally not be seen unless monochromatic radiation from a monochromator crystal is used. Our diffraction data are compatible with an orthorhombic unit cell with $a = 14{\cdot}07 \pm 0{\cdot}01$, $b = 4{\cdot}041 \pm 0{\cdot}005$, $c = 7{\cdot}25 \pm 0{\cdot}01$ kX. This orthorhombic cell is based on the hexagonal cell but has four times the cell volume. It is probable that the orthorhombic form of $ThOF_2$ represents an ordered state, with the oxygen and fluorine atoms in crystallographically different positions. The disordered state, when oxygen and fluorine atoms would be statistically distributed, would most probably have the LaF_3-hexagonal structure. Attempts to prepare disordered $ThOF_2$ have so far been unsuccessful.

Both UF_3 and $BaUF_6$ are reported to have the LaF_3-type hexagonal structure. We find no line splitting or extra reflexions on photographs of UF_3. However, photographs of $BaUF_6$ show extra lines. This might be caused by an ordering of the barium and uranium atoms.

6·39. W. Trzebiatowski, K. Lukaszewicz & St. Węglowski. *The crystal structure of barium tetratitanate and two zirconium arsenides.*

$BaO.4TiO_2$

The crystal structure of this compound has been determined on the basis of rotation and Weissenberg photographs by means of Patterson and Fourier series and the generalized-projection method of Cochran & Dyer. The orthorhombic unit cell ($a = 14{\cdot}53$, $b = 3{\cdot}75$, $c = 6{\cdot}30$ Å) contains two formula units. The space group is D_{2h}^{13}–$Pmmn$. The atomic positions are:

		x	z
Ba	2 (*b*)	—	0·709
Ti_I	4 (*f*)	0·035	0·807
Ti_{II}	4 (*f*)	0·126	0·250
O_I	4 (*f*)	0·510	0·140
O_{II}	4 (*f*)	0·592	0·733
O_{III}	4 (*f*)	0·154	0·958
O_{IV}	4 (*f*)	0·100	0·550
O_V	2 (*a*)	—	0·340

The atomic arrangement consists of chains of Ti–O octahedra similar to those occurring in barium dititanate, $BaO.2TiO_2$.

ZrAs

On the basis of powder diagrams the structure of this compound was identified as being isostructural with TiAs. The hexagonal unit cell ($a = 3{\cdot}80$, $c = 12{\cdot}87$ Å) contains four formula units. The space group is D_{6h}^4–$C6/mmc$. The atomic positions are:

Zr 4(*f*): $\frac{1}{3}, \frac{2}{3}, z$; $\frac{2}{3}, \frac{1}{3}, \bar{z}$; $\frac{2}{3}, \frac{1}{3}, \frac{1}{2}+z$; $\frac{1}{3}, \frac{2}{3}, \frac{1}{2}-z$.

As 2(*a*): 0, 0, 0; 0, 0, $\frac{1}{2}$.

2(*d*): $\frac{1}{3}, \frac{2}{3}, \frac{3}{4}$; $\frac{2}{3}, \frac{1}{3}, \frac{1}{4}$.

The parameter z, as determined by trial, is $0{\cdot}117 \pm 0{\cdot}002$. The interatomic distances are:

$$Zr\text{–}As_I(3) = 2{\cdot}66 \text{ Å}, \quad Zr\text{–}As_{II}(3) = 2{\cdot}79 \text{ Å}.$$

Comparing the analogous distances of TiAs, the augmentation corresponds strictly to the difference of the atomic radii of Zr and Ti, being 0·13 Å.

$ZrAs_2$

Single crystals of this compound were prepared by heating Zr filings with excess of As in closed, thick-walled silica tubes at 1250° C. for 24 hr. Rotation photographs and Preston diagrams showed that the unit cell is orthorhombic ($a = 6{\cdot}80$, $b = 9{\cdot}02$, $c = 3{\cdot}68$ Å) and

contains four formula units. The Patterson, Harker and Fourier syntheses resulted in the confirmation that $ZrAs_2$ is isostructural with $PbCl_2$ (*C*23) and indicated the following atomic positions:

	x	*y*	*z*
Zr	0·225	0·841	¼
As_I	0·122	0·541	¼
As_{II}	0·081	0·148	¼

6·40. P. HERPIN. *Structures de quelques trioxalates complexes.*

Les trioxalates complexes de formule $M(C^2O^4)^3K^3.nH^2O$, où *M* représente Al, Cr, Fe, Co, Rh ou Ir, sont répartis en deux groupes principaux: les premiers cristallisent dans le système monoclinique et l'on a pu déterminer leurs molécules d'eau de cristallisation et leur structure; les derniers sont tricliniques et peuvent se décomposer en leurs antipodes optiques. On a étudié la structure des sels actifs $Ir(C^2O^4)^3K^3$ et $Rh(C^2O^4)^3K^3$.

§ 7. Organic structures

7·1. A. I. KITAJGORODSKIJ. *Sur les cristaux mixtes de composants organiques.*

Mes idées générales relativement à la symétrie et à la densité de l'empaquetage des molécules dans le réseau cristallin permettent de formuler les règles de formation des cristaux mixtes organiques:

(1) Les solutions d'interclusion peuvent se former seulement quand les volumes des molécules se comportent comme 8–10:1.

(2) Les solutions de substitution existent toujours quand les configurations des molécules formant le mélange sont assez proches les unes des autres.

(3) Les cristaux mixtes peuvent en toutes proportions se former dans les conditions indiquées ci-dessus, mais seulement dans le cas où la symétrie de l'empaquetage des molécules (groupe spatial et nombre de molécules dans la maille) est la même chez les composants.

Les molécules qui possèdent un centre de symétrie le maintiennent dans le cristal. De là et de la troisième règle nous voyons que les molécules telles que celles de naphtaline ou d'anthracène ne peuvent pas constituer une série continue de solutions avec ces monodérivés.

La plupart des données concernant les series continues sont en désaccord avec la condition indiquée. Nous devons en conclure que ces données sont erronées.

Pour vérifier les règles indiquées nous avons étudié les systèmes dibenzyl–stilbène, phénanthrène–anthracène et anthracène–acridine. Les données des travaux publiés indiquent que ces composants forment une série continue de solutions. La trosième règle nous montre au contraire que les solutions continues sont impossibles. Dans les trois cas mentionnés nous avons obtenu des monocristaux parfaits de mélanges de chaque composition. Les diagrammes de diffraction établis avec goniomètre Weissenberg avaient montré la justesse de notre règle et l'erreur des expériences antérieures.

Les systèmes étudiés ont des diagrammes d'état avec eutectique et avec pereutectique.

La substitution des molécules est absolument irrégulière, sans différence avec ce qui se produit dans les cristaux métalliques. L'entrée d'une molécule d'une autre sorte dans le cristal est réglée exclusivement par la loi d'empaquetage compact.

Cela indique que la molécule étrangère choisit une position dans laquelle les distances intramoléculaires se différencient le moins possible des distances normales. Cela explique aussi le saut dans les formes des mailles des deux composants.

7·2. G. M. J. SCHMIDT. *The influence of topochemical factors on reactions in the solid state.*

This Laboratory is conducting an analysis of the effect of lattice geometry on the course of chemical reactions in the solid state, particularly of photochemical transformations of organic compounds. Three such reaction types are being studied: (1) the dimerization of the C=C–C=C system to substituted *cyclo*butanes; (2) the rearrangement of *o*-nitrobenzaldehyde to *o*-nitrosobenzoic acids; (3) the reversible photocoloration of the anils of salicylaldehyde.

(1) The dimerization of the α- and β-modifications of *trans*-cinnamic acid (I) to α-truxillic acid (II) and β-truxinic acid (III), respectively, is directly interpretable in terms of the packing arrangement of nearest-neighbour molecules in the crystal structures of the monomer. Further qualitative evidence from a series of β-substituted acrylic acids and vinyl ketones supports the hypothesis that such dimerizations are dependent on lattice geometry, chemically and stereochemically specific, subject to a maximum distance between potentially reactive centres and to inhibition by bulky groups which prevent movement in the crystal lattice even when other geometrical factors are favourable.

(2) Partial structure analyses of several heavy-atom substituted *o*-nitrobenzaldehydes (IV) were carried out in an attempt to correlate the rates of photochemical rearrangement with the distances between the aldehydic C–H bond and the oxygen of the nitro-group. In spite of variations in the size and position of the (inert) substituent and in crystallographic structure types, molecular shape was found to be constant, providing good evidence for a 'hydrogen-bond' type interaction C–H · · · O–N–O.

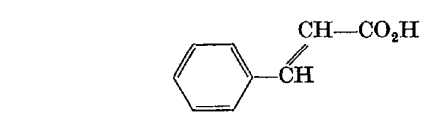

(I)

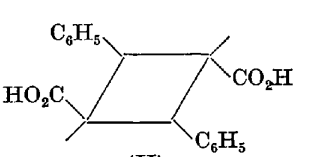

(II)

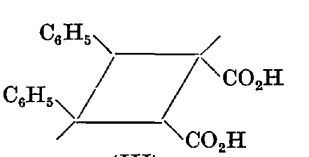

(III)

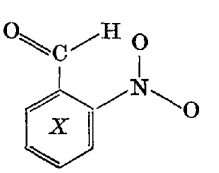

(IV)

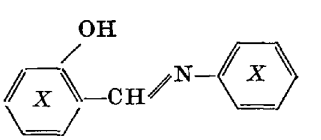

(V)

Further work in this series requires complete structure analyses and more accurate kinetic work.

(3) The problem of the phototropy of the solid anils of salicylaldehyde (V) is being studied by combined X-ray crystallographic and ultra-violet spectroscopic methods. The photocoloration process which, in the solid state, is confined to a few compounds of this series, has been shown to be common to all molecules of this type in the dissolved-rigid phase. In a survey of some 20 compounds a purely crystallographic criterion was found for the occurrence or non-occurrence of photocoloration, which at the present stage is believed to be connected with intramolecular versus intermolecular hydrogen bonding. Structural data will be presented to support this hypothesis. Spectroscopic evidence points to a (reversible) benzenoid–quinonoid transformation both in the dissolved and solid phases as being responsible for the coloration process.

7·3. R. Shiono, D. W. J. Cruickshank & E. G. Cox. *A refinement of the crystal structure of pentaerythritol.*

In view of the considerable improvement made in recent years in the method of accurate structure analysis, a refinement of the crystal structure of pentaerythritol was carried out. In the present work, 188 independent {*hkl*} reflexions were obtained from Weissenberg photographs with Cu $K\alpha$ radiation. The redetermined cell dimensions by the Straumanis method were $a = 6{\cdot}083 \pm 0{\cdot}002$, $c = 8{\cdot}726 \pm 0{\cdot}002$ Å.

The structure was refined by successive cycles of structure-factor calculations followed by observed and calculated differential synthesis. The computations were carried out on the Manchester University electronic computer with programmes modified by us for the space group $I\bar{4}$ from the one for $P2_1$. Two cycles each were calculated with the data by Llewellyn, Cox & Goodwin, and the new data respectively.

The estimated standard deviations of coordinates derived from the new data are

^{1}C: 0·010 Å x, y; 0·016 Å z.
O: 0·008 Å x, y; 0·013 Å z.

The bond length and angles calculated from the weighted mean coordinates with L. C. & G. data are as follows:

	L. C. & G.	Present refinement	E.s.d.
C–^{1}C	1·50 Å	1·548 Å	0·011 Å
^{1}C–O	1·46 Å	1·425 Å	0·014 Å
^{1}C–C–^{2}C	111½°	106° 43′	1° 1′
^{1}C–C–^{3}C	108½°	110° 52′	0° 31′
C–^{1}C–O	111½°	111° 8′	1° 7′

7·4. J. Ladell, T. R. R. McDonald & G. M. J. Schmidt. *The crystal and molecular structures of* α*-trans-cinnamic acid.*

In connection with the investigation of solid-state reactions, the crystal structure of α-*trans*-cinnamic acid was analysed from three-dimensional room-temperature and two-dimensional low-temperature data. The crystal structure will be discussed from the point of view of molecular packing and chemical reactivity. The accuracy achieved in the refinement of the low-temperature data enables us to describe certain molecular features, such as the location of the hydrogen in the carboxyl group.

7·5. J. L. Amorós & M. L. Canut. *Thermal vibrations in dicarboxylic acids.*

Diffuse scattering of succinic, adipic and pimelic acids has been studied to get information about motion of waves travelling along a chain-like structure. A complete recording of such diffuse scattering at room temperature was necessary and Lauegrams in a Unicam camera of 6 cm. diameter where taken by steps 3° apart in a range of 180° as the recording was taken with [010] as the vertical axis. The diffuse domains have two main features: (*a*) broad, round, definite domains, corresponding to a zone in the reciprocal space of about 30° having *a* as medium axis; (*b*) fine, long, extended domains (streaks) corresponding to directions in the reciprocal space normal to *c* chain direction.

Diffuse scattering was plotted in reciprocal space using Bernal & Martin charts. Many special features of the diffuse scattering domains were observed and will be described in two papers to appear in *Publicaciones del Departamento de Cristalografía*. Here we are concerned with the results:

(i) *Wave analysis of chain-like structures*

Experimental data are strictly consistent with the scheme that transverse waves are travelling both normal and parallel to the chain direction, and that longitudinal waves travel only normal to this direction, as deduced from Muller's experiments. The main feature of the diffuse scattering domains in reciprocal space is the presence of wide zones in reciprocal lattice (r.l.) planes normal to the chain direction in direct space. These zones are very thin but extend through many r.l. points, as Lonsdale postulated. The main phenomenon in chain-like structures is therefore the movement of chain versus chain, t.i. transversal waves travelling normal to the chain direction. A second feature is the vibration of the chain normal to the chain axis leading to the very important, elongated and kidney-shaped domain corresponding to (200), the plane that contains the chain in projection.

(ii) *Thermal motion and symmetry*

The (*a*) domains are consistent with space-group extintions but (*b*) domains are not. This gives a very nice image to interpret thermal vibration in a chain-like structure, as the (*b*) domains (streaks in Lonsdale's nomenclature) correspond to transversal waves travelling normal to the chain axis. The structure is centred in the static group, but in the dynamical one is not centred, and the streaks do not support space-group requirements.

Nevertheless, conditions structurally established by translation, as *P* or *I* cells, are well reflected in the dynamics of the crystal. In pimelic acid the recording of diffuse domains was always consistent with a *I* cell; succinic and adipic were consistent with a *P* cell. Therefore thermal vibration need not be consistent with the presence of a centre of symmetry in a structure but always must be with a translation lattice. This enhances the necessity of determining the dynamic space groups using diffuse-scattering studies.

Static group to which succinic and adipic belong is $P2_1/a$, having as subgroups $P2_1$, Pa, $\bar{1}$, 1. The dynamic group is $P2_1$. Pimelic acid belongs to $I2/a$, subgroups being $I2$, Ia, $I\bar{1}$, $I1$, differing only in the *P* or *I* condition. Diffuse scattering follows exactly the *P* condition in succinic and adipic acids, and the *I* condition in pimelic acid,

denoting that purely lattice conditions are observed by the dynamic motion in crystals.

7·6. R. F. Bryan & J. C. Speakman. *The crystal structures of some acid salts.*

Many monobasic carboxylic acids (HA) form crystalline acid salts (e.g. KHA_2); a number of them have now been studied by X-ray methods, and some recent results will be summarized. Nearly all these salts prove to embody in their structures a hydrogen bond that is crystallographically symmetrical: two oxygen atoms—about 2·5 Å apart—are related by a symmetry element, so that strong hydrogen bonding is implied, with the acidic hydrogen atom effectively at the mid-point. In most cases the intervening symmetry element is a *centre*; but in sodium hydrogen diacetate it is probably a *twofold axis*. (According to a personal communication from Dr Dunitz, a *plane* is similarly involved in the strong intramolecular bonding in the hydrogen maleate anion.)

Symmetrical hydrogen bonding is indirectly suggested when the two C–O lengths are observed to be equal in the centrosymmetric dimer of a carboxylic acid (e.g. in benzoic acid, which has been carefully studied by Dr Sim).

Effective crystallographic symmetry could arise in three ways: (1) the bond might be genuinely centric, with the proton occupying a single potential-energy minimum at the mid-point; (2) it might be statistically centric in space, because of disorder supervening upon a situation where the proton occupied a single minimum nearer to one oxygen atom than the other; (3) it might be statistically centric in time, because the proton oscillated (presumable by tunnelling) between two minima on either side of the mid-point.

On the basis of X-ray diffraction alone, it is difficult to distinguish between these explanations, and almost impossible between (2) and (3). But it is probable that one or other of these latter two applies in the dimers of carboxylic acids. That they might also cover the acid salts was suggested by the claim that the infra-red spectrum of potassium hydrogen bisphenyl-acetate was substantially a superposition of the spectra of the free acid and its neutral salt. However, more recent work (by Dr Hadzi) leads to an amended spectrum, for which this is no longer true, which implies a profound change in the OH group in the acid salt, and which by no means rules out explanation (1). The striking results of Dr Bacon's neutron-diffraction study of this compound appear to be even more definitely in favour of (1).

It had been tentatively suggested that an O...H...O bond would be centric only if the distance between the oxygen atoms were reduced to about 2·4 Å or less. Though they are short, the apparently symmetric hydrogen bonds considered here are not as short as this.

7·7. R. Shintani & I. Nitta. *The crystal structure of diacetylhydrazine.*

Diacetylhydrazine, $CH_3CONHNHCOCH_3$, was obtained from *n*-butyl alcohol solution as white plates, extended in the *b* and *c* directions. Crystallographic and physical data determined are: m.p. 123° C.; $Z = 4$; $a = 18{\cdot}30$, $b = 6{\cdot}52$, $c = 4{\cdot}80$ Å; $\varrho_c = 1{\cdot}35$ g.cm.$^{-3}$. From the systematic absence of spectra, (hkl) for $h+k$ odd, $(0kl)$ k or l odd, the space group was found to be D_{2h}^{18}–*Ccma*. Relative intensities of $(h0l)$, $(h1l)$ and $(h3l)$ reflexions were obtained by the integrated Weissenberg procedure and estimated by visual comparison with a calibrated scale. The multiple-film technique was used to correlate weak and strong reflexions, the maximum ratio being approximately 6000.

The signs of some structure factors were determined by the inequality method with Sakurai's chart. The refinement of the structure has been carried out by means of the two-dimensional and bounded-projection Fourier techniques.

The molecule has the centre of symmetry and is planar, hydrogen atoms being excluded. The N–N bond distance is 1·41 Å, a little shorter than those in other derivatives of hydrazine. The molecules form layers parallel to the *b* plane, within which they are connected by the NH...O hydrogen bonds extended to the *c* direction. The molecules in neighbouring layers are arranged in such a way that the C=O groups in antiparallel directions overlap with one another almost precisely in the *b* projection. From such structural features it will be concluded that the cohesive energy of the crystal lattice is thus predominantly contributed by hydrogen bonds within the molecular layer and by the $C = O$ dipole–dipole attraction between layers.

The crystal structures of a few hydrazine derivatives have been determined in our laboratory. Diformyl hydrazine, CHONHNHCHO, which has the centre of symmetry, is a planar, S-shaped molecule and its N–N distance, $1{\cdot}39_2$ Å, is the shortest among the derivatives. In the diacetylhydrazine hydrate, the molecule is not planar, presumably because of the hydrogen-bond formation between the molecule and waters of crystallization, while the N–N bond distance is 1·40 Å.

The structure of the anhydrous crystal is related to that of the hydrate in the following manner: the water molecules in the hydrate are replaced by the diacetylhydrazine molecules, which are now directed antiparallel to their surrounding molecules, the twisting in the configuration of the molecule around the N–N bond in the hydrated crystal being released to give the planar molecule in the anhydrous form.

7·8. E. L. Eichhorn. *The structure of* trans *4,4′-azopyridine-N-oxide.*

The substance is obtained through reduction and diazotization from 4-nitropyridine-N-oxide. It crystallizes in strongly dichroitic blood-red needles, elongated along *a*. A morphological examination shows the forms {100}, {010}, {001}, {011}, {021} and {10$\bar{1}$} to be well developed; the crystals have Laue symmetry C_{2h}. β was determined crystallometrically. The space group follows unequivocally from systematic absences: $P2_1/n$–C_{2h}^5. There are 2 molecules per unit cell of dimensions: $a = 4{\cdot}56$, $b = 12{\cdot}75 \pm 0{\cdot}02$, $c = 9{\cdot}75$ Å, $\beta = 114{\cdot}5 \pm 0{\cdot}1°$.

A set of three-dimensional intensities was obtained from equi-inclination Weissenberg photographs, taken at −10° C., to stabilize the geometrical isomer. 600 out of the possible 995 lattice points (Cu $K\alpha$ radiation) were observed. The (111) plane is by far the strongest in the set. However, (222) is less strong than (202), (101) being forbidden. $d_{111} = 3{\cdot}15$ Å and $d_{101} = 3{\cdot}27$ Å, both likely separations of a flat molecule. A scale model of the molecule was fitted into the (101) plane and adjusted for consistency with respect to the rest of the transform and

with respect to satisfactory packing (Bragg–Lipson procedure). The trial model proved to be correct in essence and was refined smoothly in four cycles of backshift-corrected differential syntheses for the (0*kl*) projection, and later by another five cycles of compensated differential syntheses upon the full three-dimensional set, including non-observed terms. In the final stage the percentage discrepancy was 15·2%, expressed as:

$$R_{21} = \sqrt{[\Sigma_H(F_o - F_c)^2 \div \Sigma_H F_o^2]} \cdot 100\% \ .$$

The value given includes all absent reflexions. An isotropic heat movement only was incorporated in the structure amplitudes. Even with this approximation the standard deviation of all atomic positions was less than 0·008 Å, utilizing Cruickshank's formula for computation.

The analytical expression for the molecular plane, found by averaging, is: $1{\cdot}009x + 0{\cdot}506y + 0{\cdot}877z = 0$. The molecule is found to be entirely flat, $d_M = 3{\cdot}31$ Å without unusual bond distances or angles. It is shown that despite oxidation of the pyridinic nitrogen the aromatic character of the ring is maintained, unlike the ring-structure in 4-nitropyridine-*N*-oxide, where the ring is quinonoidal.

7·9. T. L. Khocjanova & G. T. Struchkov. *The crystal structures of diphenylhalogenonium compounds.*

The present work constitutes a part of a more general investigation of halogenonium compounds which is now in progress. These compounds contain a halogen atom X = Cl, Br, I in a valence state $\rangle X^+ \longleftrightarrow \rangle X-$. The best known representatives of this series of compounds have the following general formulas: $\begin{matrix} R' \\ R \end{matrix}\rangle XY$, where R and R' are organic radicals, Y is an 'anion' (Cl^-, Br^-, I^-, $[BF_4]^-$ etc.). Some cases are known when an 'anion' and a 'cation' of halogenonium compound represent parts of the same molecule, as exemplified by phenyldimedonyliodon,

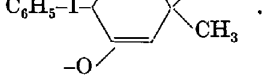

From the chemical point of view an investigation of such compounds is of interest for showing the nature of an X–Y bond (which in some cases is not purely ionic but has an intermediate character) and for establishing a valence configuration of a central halogen atom X.

The crystals of diphenyliodonium chloride and iodide are isomorphous:

	$(C_6H_5)_2ICl$	$(C_6H_5)_2II$
a (Å)	20·81±0·06	22·08±0·10
b (Å)	5·82±0·02	6·27±0·03
c (Å)	20·26±0·06	20·42±0·08
β	102° 34′±30′	101°±1°
n	8	8
Space group	*C*2/*c*	*C*2/*c*

The coordinates of heavy atoms have been determined by a two-dimensional Patterson function $P(x, 0, z)$ and by Harker section at $y = \frac{1}{2}$. The full structures of these compounds have been established by calculating a three-dimensional electron-density distribution.

Bond distances are: C–I = 2·08 Å, I–Cl = 3·08 Å, I–I = 3·29 Å. The bonds I–Cl and I–I are longer than covalent bonds and approach ionic bonds. The molecules of both compounds have T-shaped configuration: C–I–C = 98°, C–I–Cl = 87° and 174°. Benzene rings are turned about I–C bonds relative to the C–I–C plane in order to remove steric hindrances between them. The molecules in crystal are united in 'dimeric' pairs at symmetry centres ($\frac{1}{4}$, $\frac{1}{4}$, 0), approaching each other by their polar ends; the distances between these parts of the molecules (I · · · Cl = 3·20 Å, I · · · I = 3·34 Å) are remarkably shorter than the sums of the van der Waals radii. In iodide crystals intra- and intermolecular distances I · · · I are essentially equal so that this structure may be regarded as ionic. The packing of non-polar parts of the molecules (benzene rings) has the usual density (van der Waals radii are I 2·1 Å, C 1·8 Å, H 1·1 Å).

The crystals of fluoroborates of diphenyliodonium, diphenylbromonium and diphenylchloronium are not isomorphous:

	$[(C_6H_5)_2I][BF_4]$	$[(C_6H_5)_2Br][BF_4]$	$[(C_6H_5)_2Cl][BF_4]$
a (Å)	6·05±0·03	8·16±0·03	18·85±0·05
b (Å)	12·80±0·04	14·80±0·03	8·51±0·02
c (Å)	17·26±0·05	10·17±0·10	21·60±0·08
β	97° 15′±20′	96° 30′±30′	125° 20′±30′
n	4	4	8
Space group	$P2_1/c$	$P2_1/c$	$P2_1/c$

For determining the structure of diphenyliodonium fluoroborate two-dimensional Patterson functions calculated with reflections 0*kl*, also 1*kl* and 3*kl* (generalized projections) and three-dimensional electron-density distributions have been applied. The investigation of diphenylchloronium and diphenylbromonium fluoroborates is less detailed (two-dimensional Patterson functions, their minimizing, two-dimensional electron-density maps); it is intended to undertake further refinement by three-dimensional electron-density calculation. In these purely ionic structures cations have an angular configuration, the angle C–*X*–C exceeds 90° and benzene rings are turned out of the plane C–*X*–C to remove steric hindrance. The packing of these bulky cations and tetrahedral anions $[BF_4]^-$ is of interest.

The non-centrosymmetrical structure of a double compound $(C_6H_5)_2ICl.HgCl_2$ has been determined by three Patterson and electron-density projections. The crystals belong to space group $P2_12_12_1$ with four molecules in the unit cell ($a = 13{\cdot}50 \pm 0{\cdot}05$, $b = 5{\cdot}82 \pm 0{\cdot}03$, $c = 18{\cdot}60 \pm 0{\cdot}10$ Å). $HgCl_2$ molecules lose their individuality in crystal, forming a peculiar polyhedral chain with shared chlorine ions extended along a 2_1 axis parallel to [010]. Molecules $(C_6H_5)_2ICl$ have T-shaped configuration (similar to that found in the diphenyliodonium chloride crystals) and adjoin this polyhedral chain by their polar parts, approaching Hg atoms with their chlorines. Non-polar parts of these molecules pack themselves in the usual manner.

7·10 G. T. Struchkov & T. L. Khocjanova. *The X-ray investigation of crystals of some ferrocene derivatives.*

The investigation of substituted ferrocene derivatives has been undertaken to determine their molecular configuration in crystals, since from a theoretical point of

Table 1.

	$Fe(C_5H_4COC_6H_5)_2$	$Fe(C_5H_4COCH_3)_2$	$Fe(C_5H_4COC_2H_5)_2$	$Fe(C_5H_4COC_3H_7)_2$
a (Å)	11·69±0·02	14·89±0·07	13·50±0·04	11·91±0·11
b (Å)	25·36±0·05	13·03±0·06	5·80±0·04	14·20±0·12
c (Å)	6·27±0·01	5·90±0·03	16·30±0·12	9·74±0·05
β	90±1°	90±1°	89° 20′±40′	—
n	4	4	4	4
Space group	$P2_1/n$	$P2_1/a$	$P2_1/a$	Acm

view there are several possible configurations, corresponding to various rotational isomers. It is also necessary to establish what factors determine a choice of a configuration realized in crystal: a specific mutual influence of substituents or a tendency to minimize steric hindrances in a molecule and to acquiring maximum density of packing.

The crystals of the diketoferrocenes investigated are characterised by the data in Table 1.

The crystal structure of dibenzoylferrocene, $Fe(C_5H_4COC_6H_5)$, has been investigated in more detail. Tentative data on the signs of the structure amplitudes have been obtained by minimization of a three-dimensional Patterson function and by application of the statistical approach. Atomic coordinates have been determined by a three-dimensional electron-density distribution. Bond distances are: Fe–C = 2·05±0·02 Å; C–C = 1·41±0·03 Å (in the ferrocene nucleus), 1·39±0·03 Å (in the benzene rings) and 1·52±0·02 Å (between atoms of the cyclic rings and atoms of a ketogroup); C–O = 1·21±0·01 Å. The benzoyl groups are not located in planes of five-membered rings but are turned out of them by rotation about ordinary bonds C–C for minimizing steric hindrances in the molecule. In the crystal the molecule has an asymmetric configuration corresponding to the rotational 1,2′-isomer. The packing coefficient of this structure has the usual value 0·76.

Determination of the signs of structure amplitudes for diacetyl-, dipropyonyl- and dibutyrylferrocenes has appeared more difficult since the ferrous atom does not take part in a great number of reflexions because its coordinates have special values. This notwithstanding, comparison of unit cells of dibenzoyl-, diacetyl- and dipropyonylferrocenes reveals some similarity between them and has made it possible to propose an approximate molecular orientation for the two latter compounds. This approximate orientation has been made more precise by calculation of two-dimensional series which also indicate the 1,2′-configuration. A molecule of dibutyrylferrocene occupies in the crystal a special position with the symmetry 2; its orientation in the unit cell has been established by a two-dimensional approach.

The investigation of some other disubstituted ferrocene derivatives is in progress (di-*p*-bromophenylferrocene, dimethyl ester of ferrocene dicarboxylic acid and dialkylferrocenes).

7·11. A. I. Kitajgorodskij, T. L. Khodjanova & G. T. Stručkov. *The crystal structure of some tropylium salts.*

The X-ray investigation of tropylium salts $[C_7H_7]^+X^-$ ($X^- = Cl^-, I^-, [PtCl_6]^-$) and some others has been made. For determination of atomic coordinates three-dimensional Patterson series have been mainly used. In the cases of iodide and perclorate investigated in more detail statistical distribution (or rotation) of tropylium ions in crystal has been established since in a space group C_{3v}^5–$R3m$ these ions are in the onefold position with a symmetry $3m$. Some data about the structure of tropylium ion have been obtained. An investigation of salts with substituted tropylium ions is now in progress.

7·12. C. Stora. *Ébauche de la structure du triphenylmethane bromé,* $(C_6H_5)_2C_3$–Br.

La grande difficulté du tritane bromé réside dans la très grande hygroscopicité des cristaux (étude obligatoire sous tube de Lindemann) et leur instabilité aux rayons X. L'obtention des diagrammes ayant nécéssité deux cristaux assez gros (0,6–0,8 mm.) et de forme différente, les corrections d'absorption sur les intensités des taches dans l'espace à trois dimensions n'ont pu être éffectuées. Par suite; seule une ébauche de la structure a pu être atteinte.

Les cristaux sont rhomboédriques, de groupe spatial $C3$–C_{3i}^1. En axes hexagonaux, les paramètres de la maille sont, a = 13,85, c = 13,42 Å avec 6 molécules dans la maille.

La molécule est à symétrie ternaire, l'atome de brome se trouvant fixé sur le carbone central de la molécule (C_c) et les trois phényles faisant l'angle tétraédrique (109,5°) avec la liaison C_c–Br. Dans le cristal les molécules s'associent par paire, constituant un édifice bimoléculaire centrosymétrique, les deux molécules unies par leur brome étant tournées de 60° l'une par rapport à l'autre:

$$(C_6H_5)_3C_c\text{–}Br_1\ldots Br_2\text{–}C_c(C_6H_5)_3\ .$$

Les distances $Br_1\ldots Br_2$ et C_c–Br prennent les valeurs anormales de 3,33 Å et 1,99 Å, la première pouvant indiquer une association possible des brome.

Utilisant la méthode de l'atome lourd dans l'espace à trois dimensions, on a établi que les groupes phényles inclinés de 109,5° sur OZ avaient dans l'espace les positions suivantes:

(1) molécule centrés sur OZ: l'axe des carbone C_1–C_4 du premier groupe phényle, fait un angle de 47° avec l'axe OX et chaque phényle est incliné à gauche de 40° environ sur l'horizon;

(2) molécules centrées sur le premier axe ternaire direct: les phényles de la molécule qui est parallèle à celle de l'origine sont au contraire inclinés à droite de 40° sur le plan de l'horizon. Une telle disposition a pour effet d'entourer les atomes de brome placés sur les axes ternaires directs d'une couronne de six phényles tous inclinés dans le même sens.

7·13. H. Gillier. *Structure du violurate de rubidium.*

L'acide violurique aqueux donne en quantité stœchiométrique avec le carbonate de rubidium des cristaux de couleur bleu pur présentant la forme d'un prisme très aplati.

D'après les diagrammes de Weissenberg, le violurate de rubidium a le groupe spatial $P\bar{1}$. Les paramètres de la maille ont pour valeur:

$a = 4{,}80 \pm 0{,}02$, $b = 7{,}85 \pm 0{,}02$, $c = 9{,}61 \pm 0{,}03$ Å;
$\alpha = 103°10' \pm 30'$, $\beta = 90°45' \pm 30'$, $\gamma = 111° \pm 30'$.

Le nombre de deux molécules par maille exigé par le groupe spatial a été confirmé par une étude de densité.

Les intensités des taches enregistrées sur des films superposés ont été mesurées à l'aide d'un densitomètre Huet. Elles ont été corrigées du facteur de Lorentz-polarisation mais aucune correction d'absorption n'a été faite.

La structure proprement dite a été abordée par la méthode de l'atome lourd qui a permis de localiser avec efficacité la molécule. Les coordonnées atomiques ont été améliorées par les séries différences de Cochran.

Les calculs effectués à partir des coordonnées ont mené aux conclusions suivantes:

(1) L'ion rubidium est entouré de six atomes d'oxygène appartenant à cinq molécules différentes. Les valeurs des liaisons Rb^+–O, sont de 2,77, 2,79, 2,84, 2,98, 3,10, 3,11 Å. La précision calculée par la méthode statistique des ajustements linéaires, comme l'a proposé M. Rimsky, est de 0,04 Å.

(2) La partie organique de la molécule est plane; la distance de chacun des atomes au plan moyen calculé par la méthode des moindres carrés est comprise dans le domaine d'erreur (0,1 Å).

On ne peut pas dire que l'ion rubidium soit lié à une molécule plutôt qu'à une autre, mais si nous devions adopter pour le violurate de rubidium, sel bleu, une formule type, comme l'a fait Hantzsch, il vaudrait mieux prendre la formule proposée pour les sels rouges qui rend compte, dans une même molécule et pour le même atome de rubidium, d'une forte liaison (2,79 Å) avec un oxygène cétonique et d'une laiaison plus faible (3,10 Å) avec l'oxygène de la liaison oxime.

7·14. L. Brú. *Crystalline structure of a lead and thiourea inclusion compound.*

We have made a systematic study of the different crystalline compounds of thiourea and metal salts.

The compound $2(NO_3)_2Pb.11SC(NH_2)_2$ is tetragonal, space group D_{4h}^2, with $a = 10{\cdot}38$, $c = 24{\cdot}6$ Å.

The structural study was made, starting from rotating diagrams about a and c, and Weissenberg ($hk0$) and ($0kl$) photographs. The polarization Lorentz and absorption factors were applied to the intensities photometered with Mohl's microphotometer. Patterson $P(u, v)$ projection diagrams and $P(u, v, w_0)$ sections of the Patterson three-dimensional and Fourier's syntheses were obtained with the Eller's optical machine.

Main topics for possible discussion are:

(*a*) *Interpretation of the diffraction diagrams.*—These present a unique aspect, with diffuse zones indicating disorder, together with sharp spots corresponding to an ordered portion of the structure.

(*b*) *Establishment of a model of the structure.*—There is a perfectly ordered frame of thiourea, forming tubular cavities which accommodate lead nitrate molecules. The projection of this structure has been resolved to $R = 0{\cdot}15$ and is being more exactly adjusted.

(*c*) *The chemical formula.*—Being an inclusion compound, the ratio $SC(NH_2)_2/(NO_3)_2Pb$ must be fixed but not simple, it being impossible to give an exact and truthful chemical formula for this compound in a manner similar to the urea and thiourea adducts.

7·15. Y. Okaya, R. Pepinsky, Y. Takeuchi, H. Kuroya, A. Shimada, P. Gallitelli, N. Stemple & A. Beevers. *X-ray analyses of some complex-ion structures.*

The crystal structures or symmetries of a variety of complex ion compounds are presented.

Trivalent metal hexaurea complexes

The Fe and Cr hexaurea complexes form isomorphous anhydrous chlorides with cells as follows:

	Hexagonal setting ($Z = 6$)		Rhombohedral setting ($Z = 2$)	
	a (Å)	c (Å)	a (Å)	α (°)
$[Cr(urea)]_6Cl_3$	16·35	14·65	10·63	100·5
$[Fe(urea)]_6Cl_3$	16·50	14·90	10·75	100·0

The space group is $R\bar{3}c$. The Cr or Fe is at (0, 0, 0), etc., and Cl ions are at $(\frac{1}{3}, 0, \frac{1}{4})$, etc. The urea molecules lie in general positions, with oxygens coordinated to the Cr or Fe in an octahedral arrangement. The structures were readily deduced from Patterson and density projections along the trigonal axis.

The trihydrate of the chloride of the iron-hexaurea is rhombohedral, space group $R\bar{3}$. For the hexagonal setting, $a = 17{\cdot}83$, $c = 14{\cdot}10$ Å, $Z = 6$; for the rhombohedral setting, $a = 11{\cdot}30$ Å, $\alpha = 103{\cdot}9°$, $Z = 2$. The structure was determined from Patterson and density projections along the hexagonal a and c directions. Least-squares refinement (IBM 704) led to an R factor of 13% for the c-axis projection.

Sodium cobaltinitrite and sodium nitroprusside dihydrate

Sodium cobaltinitrite, $Na_3[Co(No_2)_6]$, is rhombohedral, space group $R\bar{3}m$. In the hexagonal setting, $a = 7{\cdot}83$, $c = 14{\cdot}28$ Å, $Z = 3$; in the rhombohedral setting, $a = 6{\cdot}56$ Å, $\alpha = 73{\cdot}2°$, and $Z = 1$. The Co atom lies at the origin and an Na ion is at the center of each face of the rhombohedral cell. The $[Co(NO_2)_6]$ octahedron is regular. The structure was solved by standard Patterson and density maps.

$Na_2[Co(CN)_5(NO)].2H_2O$ is orthorhombic, space group $Pnmn$, with $a = 11{\cdot}89$, $b = 15{\cdot}48$, $c = 6{\cdot}19$ Å, $Z = 4$, $\varrho_o = 1{\cdot}72$. The c-axis projection was solved by normal Patterson and density maps, and the a-axis projection was then solved to provide three-dimensional coordinates. The cobalt and the NO and one CN group lie in the mirror plane ($y = 0$). The octahedron of five CN and one NO groups around the cobalt is distorted; considering a plane parallel to (100) and through the center of the cobalt atom, the angles between bonds Co–(NO) and the two Co–(CN) on the same side of this plane are *greater* than the angles between the Co–(CN) bonds on the opposite side of the plane. Each Na ion is surrounded by a somewhat distorted octahedron comprised of two H_2O's and four N's from (CN)'s of two neighboring $[Co(CN)_5(NO)]$ groups. The nitro oxygen is not coordinated to anything outside of the complex ion.

Hexamminecobalt (III) *salts*

The following hexamminecobalt (III) salts have been examined; $[Co(NH_3)_6](SO_4)(ClO_4)$; $[Co(NH_3)_6](SO_4)Br$; $[Co(NH_3)_6](BF_4)_3$; $[Co(NH_3)_6](ClO_4)_3$; $[Co(NH_3)_6]_2(SO_4)_3 . 5H_2O$. All of these are interesting in that the structures are dependent mainly on the packing of the large hexamminecobaltic ions, and all of the crystals show solid-state transitions. Co $K\alpha$ radiation was used for the studies below.

$[Co(NH_3)_6](SO_4)(ClO_4)$ and $[Co(NH_3)_6](SO_4)Br$ are cubic and isomorphous, with space group $F\bar{4}3m$, $Z = 4$. For the perchlorate, $a = 10{\cdot}83$ Å, $\varrho_o = 1{\cdot}81$; for the bromide, $a = 10{\cdot}53$ Å, $\varrho_o = 1{\cdot}903$. Laue patterns of both crystals at room temperature show disorder. Co atoms are at the corners and face centers. There are three positions available for the central atoms of the anions (or for the Br ion), at $(\frac{1}{4}, \frac{1}{4}, \frac{1}{4})$, $(\frac{1}{2}, \frac{1}{2}, \frac{1}{2})$ and $(\frac{3}{4}, \frac{3}{4}, \frac{3}{4})$; but only two of these positions can be occupied.

$[Co(NH_3)_6](BF_4)_3$ is isomorphous with the preceding two crystals: space group $F\bar{4}3m$, with $a = 11{\cdot}21$ Å, $\varrho_o = 2{\cdot}000$, and $Z = 4$. Here all three of the available positions for the B atoms are occupied; but the F atoms are disordered—i.e., the BF_4 tetrahedra are not in fixed orientations, and it is possible that the boron itself may shift.

At room temperature, $[Co(NH_3)_6](ClO_4)_3$ is cubic, with space group $Im3m$, $a = 22{\cdot}85$ Å, $\varrho_o = 2{\cdot}053$, and $Z = 32$. This is a superstructure cell, with approximately 8 times the volume of the fluoborate cell. The smaller cell ($\frac{1}{8}$ of the true cell) is face-centered. Laue patterns at room temperature show thermal diffuse scattering. A λ-type transition occurs at 60° C. The phase of the perchlorate above 60° C. is the same as that of fluoborate at room temperature.

$[Co(NH_3)_6]_2(SO_4)_3 . 5H_2O$ is monoclinic at room temperature, with space group $C2/c$, $a = 21{\cdot}58$, $b = 12{\cdot}04$, $c = 21{\cdot}53$ Å, $\beta = 104°$, $\varrho_o = 1{\cdot}748$, and $Z = 8$. All atoms are in general positions. The positions of the two (non-equivalent) Co atoms have been determined from Patterson maps, and a full structure determination is in progress.

In addition to the solid-state phase transitions found in the above crystals, low-temperature transitions have been found in crystals of $[Co(NH_3)_6]I_3$ and $[Co(NH_3)_5(H_2O)](ClO_4)_3$. All of the transitions and the disorders are due to the excess space remaining for the anions between the large complex ions.

d,l-cis-*Dinitro*bis*ethylenediammine cobalt* (III) *nitrate*

Crystals of *d,l-cis*-$[Co(en)_2(NO_2)_2]NO_3$ are monoclinic, space group $P2_1/n$, with $a = 12{\cdot}68$, $b = 16{\cdot}18$, $c = 6{\cdot}41$ Å, $Z = 4$. The c-axis projection was analyzed by Patterson maps, usual iteration cycles, and least-squares refinement. This *cis* configuration of the nitrato groups is confirmed, and the chelating ethylenediammine groups are *gauche*. The crystals show a low-temperature transition.

Crystals of *trans*-$[Co(en)_2(NO_2)_2]NO_3$ are monoclinic, space group $P2_1/c$, with $a = 9{\cdot}0_9$, $b = 9{\cdot}6_7$, $c = 1{\cdot}34_0$ Å, $\beta = 106{\cdot}5°$, $Z = 4$. The cobalt atoms are in general positions, and these have been found from Patterson projections. The structure is presently under study. The crystals do not extinguish at room temperature between crossed nicols.

Structure and disorder of $K_3Co(CN)_6$ *and related salts*

Crystals of compounds of the type $K_3Me^{III}(CN)_6$ have been examined, with $Me^{III} = Cr^{III}$, Mn^{III}, Fe^{III} and Co^{III}. These are orthorhombic, space group $Pcnb$, with $Z = 4$. Cell constants are:

Me^{III}	a (Å)	b (Å)	c (Å)
Cr	10·62	13·58	8·62
Mn	10·62	13·59	8·52
Fe	10·43	13·45	8·40
Co	10·50	13·53	8·40
Ir*	10·55	13·73	8·36

* As reported by C. Gottfried & J. S. Nagelschmidt, (*Z. Kristallogr.* (1930), **73**, 357).

No definitive structures for the series have been published, and incorrect symmetries have been reported by some investigators.

X-ray patterns with Co $K\alpha$ radiation show that all (hkl) reflections with l even have integral indices; but for l odd the reflections are linked by diffuse streaks parallel to b^*, with integral h indices. In the case of some rapidly-grown crystals, no sharp reflections appear, and only streaks parallel to b^* are seen.

In addition to space-group extinctions, $(h,k,2n)$ is present only for $k+n$ even.

A c-axis Patterson projection aided in the location of all atoms. Positions were refined by electron density and structure-factor iterative calculations in two and three dimensions. Interatomic distances are:

Co–C_1 = 2·07 Å; C_1–N_1 = 1·16 Å;
Co–C_2 = 2·0* Å; C_2–N_2 = 1·1$_6$* Å;
about K_1 at 0, $\frac{1}{4}$, $\frac{1}{8}$: 2N at 2·57 Å and 4N at 2·77 Å;
about K_2 at $\frac{1}{4}$, 0, $\frac{1}{8}$: 2N at 3·02 Å, 2N at 2·87 Å, 2N at 3·14 Å.

* z coordinates are of lower accuracy.

R factors are 15% for $(hk0)$ and 16% for $(hk2)$ reflections.

The reflection anomalies for odd-l layer indicate one-dimensional disorder along b. This is due to the fact that layers perpendicular to b are occasionally displaced by $\frac{1}{2}c$. The disorder arises because the z coordinates of K ions on planes $x = \pm\frac{1}{4}$ permit random location of Co atoms at either $z = \frac{3}{8}$ or $\frac{7}{8}$ without configurational changes.

Similar disorder is found in the Cr, Fe, and Mn salts. The disorder probably accounts for the incorrect symmetries reported by V. Barkhatov & H. Zhdanov (*Acta Physiochim., U.S.S.R.* (1942), **16**, 43) and V. Barkhatov (*Acta Physiochim., U.S.S.R.* (1942), **16**, 123).

Cupric and nickelous glycinates

$[Cu(glycine)_2].H_2O$ is orthorhombic, space group $P2_12_12_1$, with $a = 14{\cdot}0_0$, $b = 10{\cdot}0_0$, $c = 5{\cdot}15$ Å, $Z = 4$. A c-axis projection is under analysis, Cu positions having been established from a Patterson map.

$[Ni(glycine)_2].2H_2O$ is monoclinic, space group $P2_1/c$, with $a = 6{\cdot}9_1$, $b = 6{\cdot}6_7$, $c = 9{\cdot}7_5$ Å, $\beta = 102°$, $Z = 2$. The molecule has a center of symmetry, and the *trans* configuration of the complex ion is therewith established.

The d,l-α and β forms of triglycine cobalt (III) are under examination.

Tetrahalogeno divalent-metal alkyl amines, etc.

A very interesting class of compounds are formed by

the co-crystallization of divalent metal halides and alkylamine halides. A representative member of the class is di-methylamine chlorozincate, $(CH_3NH_3)_2[ZnCl_4]$. The crystallography of a few of the large number of such compounds which have been prepared is given in Table 1.

These compounds were prepared because $(NH_4)_2ZnCl_4$ shows a low-temperature transition, as does $(NH_4)_2SO_4$, and it was suspected that substituted ammonium salts would likewise show transitions. This is certainly the case.

Representing the class by the formula $(RA)_2Me^{II}X_4$, crystals have been prepared and transitions examined with:

RA = CH_3NH_3, $CH_3CH_2NH_3$, $CH_2(OH)CH_2NH_3$, $CH_3(CH_2)_2NH_3$, $CH_3CH(OH)CH_2NH_3$, $CH_3(CH_2)_3NH_3$, $CH_3(CH_2)_4NH_3$, $CH_3(CH_2)_5NH_3$, $(CH_3)_2NH_2$, $(CH_3)(CH_3CH_2)NH_2$, $(CH_3)_2CHNH_3$, $(CH_3)_3NH$, $CH_3NH_2CH_2CH_2OH$, $CH_3CH_2NH_2CH_2CH_2OH$, $CH_3OCH_2CH_2NH_3$, etc.;

Me^{II} = Mg, Ca, Mn^{II}, Co^{II}, Ni^{II}, Fe^{II}, Cu^{II}, Zn, Sr, Cd, Sn^{II}, and Hg^{II};

X = Cl, Br, I.

The structures of $(CH_3CH_2NH_3)_2ZnCl_4$ and the corresponding Hg compound have been determined, and studies of the transitions are in progress. Various aryl amines are now being prepared.

d-tris *Ethylenediamine cobalt* (III).*halide*.d-*tartrate*.$5H_2O$

The structures of the salts d-$[Co(en)_3].X.d$-tartrate.$5H_2O$, where X = Cl or Br, have been examined as an illustration of the power of the $P_s(u)$ function and anomalous dispersion (R. Pepinsky & Y. Okaya, (*Proc. Nat. Acad. Sci., U.S.A.* (1956), **42**, 286)). The crystals are isomorphous, triclinic, space group $P1$, with one formula unit per cell, and cell constants:

	a (Å)	b (Å)	c (Å)	α (°)	β (°)	γ (°)	ϱ (g.cm.$^{-3}$)
B.chloride	8·34	8·44	8·08	95·5	97·5	103·0	$1{\cdot}573_2$
B.bromide	8·55	8·52	8·22	92·0	99·7	104·5	1·660

The symmetry is ideal for application of the new method. Use of Cu $K\alpha$ radiation permits viewing of the chloride structure, using $P_s(u)$, from the cobalt position; use of Co $K\alpha$, with $P_s(u)$, permits viewing from the bromide-ion position. The chloride structure is revealed directly with Cu $K\alpha$; and the bromide structure (which is of course readily deducible from the chloride) is under examination with Co $K\alpha$.

Table 1. *Crystallography of di-methylamine and diethylamine tetrahalogeno-divalent-metal salts at* 20° C.

	$(CH_3NH_3)_2.MnCl_4$	$(CH_3NH_3)_2.ZnCl_4$	$(CH_3NH_3)_2.CdCl_4$	$(CH_3NH_3)_2.CdI_4$	$(C_2H_5NH_3)_2.MnCl_4$	$(C_2H_5NH_3)_2.CdBr_4$	$(C_2H_5NH_3)_2.HgCl_4$
System	Tetragonal	Monoclinic	Tetragonal	Orthorhombic	Tetragonal	Tetragonal	Tetragonal
Space group	$P4_2/ncm$	$P2_1/c$	$P4_2/ncm$	$Pbca$	$P4_2/ncm$	$P4_2/ncm$	$P4_2/ncm$
a (Å)	7·29	7·63	7·42	11·00	7·28	7·95	7·87
b (Å)	—	12·65	—	12·20	—	—	—
c (Å)	19·40	10·75	19·18	21·06	22·10	20·80	20·60
β (°)	—	97°	—	—	—	—	—
ϱ (g.cm.$^{-3}$)	1·71	1·72	1·98	3·15	1·62	2·63	2·25
Z	4	4	4	4	4	4	4
Optics	Anomalous biaxial neg.; plane of optic axes (100)	Biaxial neg.; optic plane (010); on (010) $c:\gamma = 36°$	Anomalous biaxial neg.; optic plane (100)	Biaxial neg.; optic plane (001)	Anomalous, biaxial neg.; optic plane (100)	Uniaxial neg.	Uniaxial neg.
Twinning (plane)	Lamellar, (110)	Lamellar, (100)	Lamellar, (110)	(110)	Lamellar, (110)	Lamellar, (110)	Lamellar, (110)
Cleavage plane	(110)	(001); (100)	(110)	(110)	(110)	(110)	(110)

Table 2. *X-ray crystallography of some organic reineckates*

Organic base = B	Molecular weight of B	a (Å)	b (Å)	c (Å)	β	Space group	Z*	B/R†
Pyridine	70·10	*7·57×2*	*7·64*	*7·14×2*	102° 24′	$A2/a$	4	1
Choline‡	121·18	*6·35×2*	22·80	*6·75*	—	$Icma$	4	1
Tropine‡	141·21	11·92	*6·51×2*	*6·87*	—	$Pmcb$	2	1
L-Histidine	155·16	*6·37×2*	22·01	*6·59×2*	—	$P2_12_12_1$	4	½
Caffeine	194·19	*7·39×2*	25·30	*7·02*	—	$P2_12_12_1$	4	1 +$4H_2O$
Cystine	240·29	*6·48×2*	23·70	*6·75×2*	95°	$P2_1$	2	1
Strychnine	334·40	18·10	22·87	*6·81×2*	—	$P2_12_12_1$	8	1
α-Naphthylamine	143·18	12·47	23·96	*6·87×2*	—	$Pnma$	8	1
Benzidine	184·23	*6·91×3*	*7·52×2*	11·95	190·2°	$C2/c$	4	½

* Z = number of formula units per cell.
† B/R = ratio of organic to reineckate ions.
‡ Disordered structure.
Axial distances in italics may result from packing of reineckate ions. Other relationships can also be proposed.

Table 3. *X-ray crystallography of some organic ferrocyanides*

Organic base = *B*	Molecular weight of *B*	*a* (Å)	*b* (Å)	*c* (Å)	*β*	Space group	*Z**	*B*/*F*†+solvent
Pyridine	70·10	8·60	12·10	9·73	101° 51′	$P2_1/n$	2	$2+2H_2O$
Betaine	117·15	8·88	26·54	13·33	91° 48′	$P2_1/n$	4	$3+4H_2O$
Choline	121·18	8·76	13·15	10·26	—	*Pnnm* or *Pnn*2	2	$2+4H_2O$
Pinidine(I)	139·0	8·63×2	11·15	6·30	—	(Orthorh.)	‡	‡
Pinidine(II)	139·0	7·98	29·35	15·42	—	$P222_1$(?)	‡	‡
Pinidine(III)	139·0	8·27×2	—	6·16	—	(Hexagonal)	‡	‡
Nicotine	162·2	8·84	11·70	21·20	90°	$P2_1$	2	$4+H_2O$
Quinine	324·41	8·28×3	27·62	14·07	—	$P2_12_12_1$ or $P2_122_1$	‡	‡
Visnagan	388·0	8·09×3	13·47	9·78	—	*Pcnm* or *Pcn*	4	$1+2C_2H_5OH$
Antipyrine	188·22	12·23	12·35	20·60	—	$P2_12_12_1$	4	$2+\frac{1}{2}H_2O$
$K_4Fe(CN)_6.3H_2O$	—	9·34	8·44×2	9·34	90·0°	$C2/c$	4	$3H_2O$

* Number of formula units per cell.
† *B*/*F* = ratio of organic to ferrocyanide ions.
‡ Constitution not determined with certainty.

Crystallography of 'engineered' crystals

The principle of crystal designing or 'engineering', for the purposes of obtaining organic ions in crystals with symmetries amenable to X-ray analysis, and for establishment of absolute configurations, has been described elsewhere (cf. R. Pepinsky, *Phys. Rev.* (1955), **100**, 971; *Record Chem. Progr.* (1956), **17**, 145). The structures of pyridine reineckate, $(C_5H_5N)[Cr(NCS)_4(NH_3)_2]$, pyridine ferrocyanide, $(C_5H_5N)_2[Fe(CN)_6].2H_2O$, and choline reineckate, $[(CH_3)_3NCH_2CH_2OH][Cr(NCS)_4(NH_3)_2]$, have been determined. Table 2 gives the crystallography of nine organic reineckates, and Table 3 the crystallography of eleven organic ferrocyanides. A large number of additional organic reineckates, ferrocyanides, ferricyanides, cuprocyanides, cobalticyanides, nitroprussides, cobaltinitrites, fluosilicates, chlorostannates, ferri-*tris*-oxalates, cobalti-*tris*ethylenediamines, ferri-hexaureates, rhodanilates, etc., have been crystallized.

The structures so far determined confirm the prediction that the packing in these crystals is controlled chiefly by the large complex ions, and the organic ions fill in spaces between these. By proper matching of ionic sizes and shapes, charges, dipolar character, solubilities, etc., it is possible to exert a good deal of control over the arrangement of the organic ions within the crystal.

7·16. F. L. Carter & E. W. Hughes. *The crystal structures of the complexes cuprous chloride–2-butyne and cuprous chloride–*1, 6*-heptadiyne.*

The determination of the structures of these complexes, using three-dimensional data, is in progress with the former structure practically complete and a satisfactory trial for the latter. In the unit cell of the butyne complex (C_{2h}^4–$P2/n$) are two $(CuCl'C_4H_6)_4$ molecules in which four CuCl's form an eight-membered puckered ring of $\bar{4}$ symmetry. The complexed butynes lie approximately in the planes determined by a copper atom and it's two bonded chlorine atoms in such a manner that the copper atom is on the perpendicular bisector of the C–C triple bond. The complexed butyne molecules assume a *cis* configuration. This structure gives experimental confirmation of the Lucas and of the Dewar configuration of the Ag^+–olefine complexes.

The proposed structure for the cuprous chloride–1, 6-heptadiyne complex (C_{2h}^6–$C2/c$) is closely related to the butyne complex in the manner in which the copper atom is bound to the triple bond. However, the inorganic substitute forms a helical chain of alternating copper and chlorine atoms. These chains are tied together by the bifunctional organic substitute. Refinement has not proceeded sufficiently far for this structure to be regarded as certain.

7·17. J. Bregman, I. Fankuchen, J. L. Katz, M. Miksic, N. Norman & B. Post. *X-ray diffraction studies at low temperatures.*

The crystal structures of dimethyl fulvene, cyclooctatetraene, and *n*-methyl acetamide have been refined by Fourier and least-squares methods, using full three-dimensional data. Data were collected at −50° C.

The results of X-ray diffraction studies of low-temperature solid-phase transformations in dimethyl acetylene, tertiary butyl bromide and *n*-methyl acetamide will be presented. Dimethyl acetylene undergoes a phase transformation at −120° C.; on cooling through the transformation the crystal remains tetragonal but the *c* axis is doubled. *N*-Methyl acetamide undergoes a similar transformation at 10° C.; the crystal is orthorhombic above and below the transformation; the *a* axis doubles in length below the transformation temperature.

Details of both phase transformations will be discussed, as well as a related one which occurs in tertiary butyl bromide.

7·18. E. von Sydow, S. Abrahamsson & S. Aleby. *The crystal structure of some long-chain compounds.*

The normal hydrocarbons and the normal fatty acids have their chains arranged in one of two close packings, one orthorhombic and one triclinic. The methyl substituted fatty acids try to have their chains arranged in the triclinic manner, which is possible if the chains are tilted relative to the plane with the carboxyl groups to allow the substituted methyl groups to accommodate themselves in the space between the chain ends. The crystal structures of 9-DL-methyl-, and 16-DL-methyl-octadecanoic acids are in accordance with this concept, and it seems to be the case with most of the other acids in the series *X*-DL-methyl-octadecanoic acid. With this arrangement the carboxyl group will be forced into the chain packing which causes local distortions. When the substituent is close to the carboxyl group, as in 3-DL-

methyloctadecanoic acid, the molecules arrange themselves so that all methyl and carboxyl groups appear in the same regions leaving the chains undisturbed in the common triclinic packing.

When a methyl-substituted fatty acid is rapidly crystallized from melt a crystal form is obtained which has an almost constant long-spacing value irrespective of the position of the methyl group. The chains must so arrange themselves that the substituted methyl group can accommodate itself anywhere in the structure without severe distortion. This packing must therefore be less tight, which postulate is in accordance with the lower melting points of these polymorphs. The low-melting form of 14-DL-methyloctadecanoic acid is being investigated.

The crystal structure of (−)-2-methyl-2-ethyl-eicosanoic acid is roughly similar to the structure of 3-DL-methyloctadecanoic acid in that the substituents and carboxyl groups appear in the same regions in the crystal. The larger substitution causes, however, two severe discrepancies: the chains arrange themselves in a packing, never found before, and the hydrogen bonds do not bind the molecules by two and two, but in a chain system along the shortest axis, which is in accordance with the physical properties of the crystals. The space group is No. 18 ($P2_12_12$). The chains are packed orthorhombically, but, contrary to the common orthorhombic chain packing, with all chain planes parallel. If one knew nothing about long-chain structures this would certainly be the packing one would think of first as being the simplest and the most stable for any long-chain compound. This, however, is not the case, as has been pointed out. The hydrogen bonds form helices around $y = \pm\frac{1}{4}$, $z = 0$.

The methylesters of even-numbered fatty acids, and under certain conditions of odd-numbered fatty acids, crystallize in dimers, while higher esters crystallize in monomers. In order to investigate this phenomenon the structure of methylstearate is being investigated. The structure is in many respects like the structure of the *B*-form of stearic acid, but it is centred on its largest face, giving a cell with 8 molecules and having the long axis equal to 102·5 Å.

7·19. A. I. KITAJGORODSKIJ. *L'empaquetage de molécules longues.*

Un cristal formé de molécules longues est constitué à coup sûr de couches de molécules parallèles. Ce fait simplifie l'analyse de tous les modes de dispositions de molécules possibles et permet de poser le problème de déduction géométrique de toutes les structures cristallines possibles.

Le problème peut être résolu si nous prenons pour base les règles d'empaquetage compact des molécules. Une supposition supplémentaire simplifie le raisonnement: nous prenons que le mode de disposition le plus favorable pour deux molécules identiques (liées par translation simple) reste le même dans le cristal.

La recherche est restreinte au cas de molécules aliphatiques (paraffines normales). Premièrement il a été étudié l'empaquetage de molécules indéfiniment longues.

Nous trouvons cinq modes de dispositions: deux avec maille dimère obliquangle et trois avec maille dimère rectangle. En prenant pour rayon intramoléculaire de H 1,30 Å nous arrivons aux chiffres suivants:

Mailles obliquangles:

$a = 4{,}3$ Å	$b = 4{,}2$ Å	$\gamma = 117°$
$a = 4{,}3$	$b = 4{,}0$	$\gamma = 107$

Mailles rectangles:

$a = 5{,}0$ Å	$b = 7{,}2$ Å	axe $2_1 \parallel b$
$a = 4{,}3$	$b = 8{,}0$	axe $2_1 \parallel a$
$a = 4{,}2$	$b = 9{,}0$	axe $2_1 \parallel b$

Le plan de zigzag aliphatique fait un angle de 110° et 100° avec l'axe *b* des mailles obliquangle, et de 7°, 40° et 110° avec l'axe a des mailles rectangles.

La place qui correspond à une molécule est 16,2 Å² pour les couches obliquangles, et 17·5 Å², 18 Å² et 19 Å² pour les couches avec mailles orthogonales.

Pour comparaison avec les données expérimentales nous connaissons les dimensions de la maille de polyéthylène et de submailles de quelques substances aliphatiques.

Un mode de disposition théorique avec maille rectangle 4,2 Å × 9,0 Å ne se rencontre pas parmi les structures connues. Le premier mode de disposition rectangle s'effectue dans le polyéthylène. Nous trouvons les autres mailles dans les paraffines et les acides gras divers.

Ce pas fait, nous devons considérer l'influence de groupes terminaux. Le plan dans lequel se trouvent ces groupes peut être orthogonal ou oblique par rapport à l'axe de la molécule. Chacun des deux genres de couches doit être étudié séparément en rapport avec le mode de superposition.

Pour chaque genre de couche il y a deux modes de superposition en analogie avec l'empaquetage compact de sphères.

La superposition de couches avec maille obliquangle nous mène vers le cristal triclinique. La superposition de couches rectangles peut donner des cristaux avec maille orthogonale, monoclinique ou triclinique.

Par analyse géométrique nous avons déduit les modes possibles de dispositions des molécules et trouvé les dimensions des mailles et la symétrie des groupes spatiaux.

La différence entre les structures de cristaux de substances aliphatiques avec le nombre des atomes C pair et impair est l'effet de modes différents de superposition des couches.

Ce travail par méthode géométrique montre encore une fois la valeur de la théorie de l'empaquetage compact des molécules.

7·20. A. E. SMITH. *The structures of stable ordered phases in mixed paraffins and their relation to the structures of pure n-paraffins.*

The pure normal paraffins with an odd number of carbon atoms are orthorhombic space group *Pbcm* at room temperature. The pure even *n*-paraffins from n-C_{18}-C_{26} are triclinic while those above n-C_{26}, C_{28} to C_{36}, are monoclinic $P2_1/a$ (A. E. Smith, *J. Chem. Phys.* (1953), **21**, 229; A. Muller & K. Lonsdale, *Acta Cryst.* (1948), **1**, 129; H. M. M. Shearer & V. Vand, *Acta Cryst.* (1956), **9**, 379). The addition of a few per cent of neighboring homologs to the triclinic and monoclinic forms observed with the even-numbered *n*-paraffins converts them to an orthorhombic form. During the investigation of binary mixtures of *n*-paraffins the slow separation of ordered

stable phases of mixed *n*-paraffins was observed. Single crystals of the ordered phases of binary mixtures of *n*-paraffins differing by 1, 2, or 3 carbon atoms with composition ratios of 1:1, 2:1, 5:1, etc., were prepared and their structures determined by X-rays. Binary mixtures of components in the range C_{18}–C_{36} were examined.

More detailed single-crystal work was carried out with 1:1 and 2:1 mixtures of *n*-$C_{24}H_{50}$ and *n*-$C_{26}H_{54}$. For the 1:1 mixture the unit cell is orthorhombic, $a = 4{\cdot}96_3$, $b = 7{\cdot}48_6$, $c = 137{\cdot}2$ Å, space group *Pbnm*, $Z = 8$. For the 2:1 mixture $a = 4{\cdot}96_3$, $b = 7{\cdot}48_6$, $c = 202{\cdot}0$ Å, *Pbnm*, $Z = 12$. The detailed packing arrangements were determined by the method of Fourier transforms. The transforms for various reasonable packing arrangements consistent with the space-group data were derived and the z, x, y parameters evaluated from the (00l) (h00) and (0k0) reflections. The z parameters were quite accurately determined from the high-order (00l) reflections (l = 108–112 for the 1:1 mixture and l = 150–168 in the 2:1 mixture). Calculation of the intensities for a limited number of high- and low-order (10l) (20l) and (02l), (04l) reflections made it possible to eliminate most of the configurations. The calculated and observed intensites are in good agreement for both the 1:1 and 2:1 packing arrangements. The crystal compositions were determined by mass spectrometric analysis.

Single-crystal data for *n*-C_{23}+*n*-C_{25}, *n*-C_{24}+*n*-C_{27}, *n*-C_{28}+*n*-C_{30}, and *n*-C_{23}+*n*-C_{24} indicate the packing arrangement for the 1:1 and 2:1 composition ratios are essentially the same as those found for the *n*-C_{24}+*n*-C_{26} mixtures.

Single-crystal data have also been obtained for 5:1 and higher ratios for a number of binary mixtures but the detailed packing has not yet been definitely established.

7·21. T. Brotherton & G. A. Jeffrey. *The crystallography and structure of some* C_{19} *cyclopropane fatty acids.*

Five $C_{19}H_{36}O_2$ *cyclo*propane fatty acids are known from the work of K. Hofmann *et al.* (*J. Amer. Chem. Soc.* (1954), **76**, 1799); the *trans*-DL-9,10-methylene octadecanoic, *trans*-DL-11,12-methylene octadecanoic and *cis*-DL-11,12-methylene octadecanoic acids, which were prepared synthetically; the lactobacillic and dihydrosterculic acids, which were obtained from natural products.

The two synthetic *trans* acids have crystal lattices which are nearly identical for reasons which are apparent from the results of a crystal-structure analysis of the 9,10 compound.

The crystallographic data of these acids, in conjunction with chemical evidence, leads to the assignment of the *cis* D *or* L-11,12 methylene octadecanoic acid structure to lactobacillic acid and the *cis*-DL-9,10-methylene octadecanoic acid to dihydrosterculic acid.

7·22. J. Iball. *Three-dimensional refinement of the structures of some organic compounds.*

The structure of the compounds, chrysene, 20-methylcholanthrene and 9:10-dihydroanthracene have been determined by normal two-dimensional Fourier methods and then the atomic coordinates have been refined by three-dimensional methods. The methods of three-dimensional differential syntheses and of least squares have been used.

7·23. J. M. Robertson, M. G. Rossmann & J. Trotter. *The structure of some higher condensed-ring hydrocarbons.*

Pentacene, $C_{22}H_{14}$.

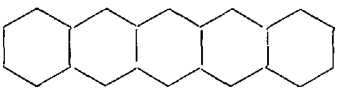

Triclinic, $a = 7{\cdot}90$, $b = 6{\cdot}06$, $c = 15{\cdot}95$ Å, $\alpha = 101{\cdot}3°$, $\beta = 111{\cdot}8°$, $\gamma = 94{\cdot}4°$. $U = 686$ Å^3, $D_m = 1{\cdot}333$, $Z = 2$, $D_X = 1{\cdot}345$. Space group, $P\bar{1}$–C_i.

Dibenzperylene, $C_{28}H_{16}$, m. p. 343° C.

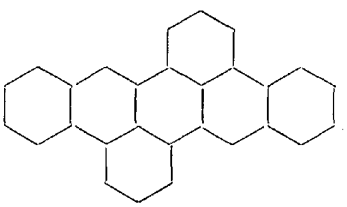

Monoclinic, $a = 16{\cdot}59$, $b = 5{\cdot}23$, $c = 20{\cdot}6$ Å, $\beta = 107{\cdot}8°$. $U = 1702$ Å^3, $D_m = 1{\cdot}348$, $Z = 4$, $D_X = 1{\cdot}375$. Space group, $A2/a$–C_{2h}^6.

Diperinaphthylene-anthracene, $C_{34}H_{18}$, m. p. 333–334° C.

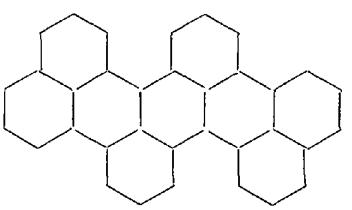

Monoclinic, $a = 11{\cdot}95$, $b = 7{\cdot}83$, $c = 11{\cdot}17$ Å, $\beta = 92{\cdot}3°$. $U = 1044$ Å^3, $D_m = 1{\cdot}359$, $Z = 2$, $D_X = 1{\cdot}355$. Space group, $P2_1$–C_2^2.

Dinaphthoperopyrene, $C_{38}H_{18}$, m. p. 338–339° C.

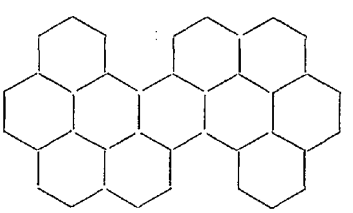

Monoclinic, $a = 30{\cdot}73$, $b = 3{\cdot}855$, $c = 19{\cdot}87$ Å, $\beta = 113{\cdot}0°$. $U = 2167$ Å^3, $D_m = 1{\cdot}446$, $Z = 4$, $D_X = 1{\cdot}447$. Space group, $C2$–C_2^3 but approximately $C2/c$–C_{2h}^6.

Circumanthracene (*decabenzoanthracene*), $C_{40}H_{16}$, m. p. > 480° C.

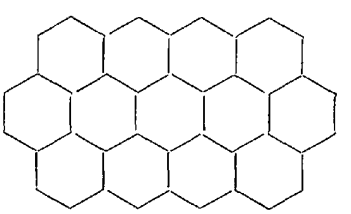

Monoclinic, $a = 23{\cdot}76$, $b = 4{\cdot}59$, $c = 9{\cdot}98$, $\beta = 99{\cdot}9°$. $U = 1075$ Å^3, $D_m = 1{\cdot}52$, $Z = 2$, $D_X = 1{\cdot}53$. Space group, $P2_1/a$–C_{2h}^5.

Although pentacene is triclinic, the arrangement of the two molecules in the unit cell is very similar to that in naphthalene and anthracene. Unsuitable crystals have prevented a sufficiently detailed analysis for the accurate determination of atomic coordinates and bond lengths, but the molecules are almost certainly planar and centrosymmetric.

For dibenzperylene a detailed analysis has been made, and a clearly resolved projection of the molecule obtained. To a first approximation the molecule is planar, but intensive refinements by means of generalized projections show that the atoms in the outermost rings are probably displaced by between 0·1 and 0·2 Å from the mean molecular plane. This is an example of minor overcrowding causing a small distortion.

In diperinaphthylene-anthracene and dinaphthoperopyrene there is severe intra-molecular overcrowding, causing extensive distortion. An accurate measurement of the molecular thickness in the latter compound is given by the length of the short b axis, which coincides with a twofold symmetry axis in the molecule. Good resolution of all the atoms can be obtained in this compound, and in both compounds the distortions can be studied by means of generalized projections.

With the completion of the ring system in circumanthracene the molecule becomes planar again. This crystal structure is strictly analogous to that of coronene and ovalene. At present the compound has not been obtained in a completely pure form and the extremely high observed temperature factor ($B = 10$ Å^2) is almost certainly due not to thermal movement but to stacking disorders caused by the occasional presence of a distorted molecule of the dinaphthoperopyrene type.

7·24. D. W. J. Cruickshank. *A detailed refinement of the crystal and molecular structure of naphthalene.*

A detailed refinement of Abrahams, Robertson & White's (1949) data for naphthalene has been carried out. The many calculations needed were performed on the Manchester University electronic computer. As for anthracene, the difference map indicates some channelling of the electrons along the lines of the bonds. The anisotropic vibrations of the carbon atoms can be interpreted in terms of anisotropic translational and rotational oscillations of the molecules. The magnitudes of the angular oscillations ($\sim 4°$) agree well with those inferred from Raman spectra. C–C bond lengths with e.s.d.'s of about 0·004 Å are obtained. Comparison of the latest bond lengths (including the rotational oscillation corrections) for naphthalene and anthracene shows better agreement with the theories. The simplest Pauling theory with an up-to-date bond-order/length curve predicts the bond lengths within about 0·01 Å.

7·25. J. Clastre & H. Rabaud. *Structure cristalline du 9-cyananthracène.*

Le 9-cyananthracène cristallise dans le système orthorhombique. Le groupe spacial est $P2_12_12_1$–D_2^4. Les dimensions de la maille sont:

$a = 17{,}15$, $b = 15{,}11$, $c = 3{,}93$ Å. Il y a 4 molécules par maille, et la densité calculée est de 1,33 g.cm.$^{-3}$.

La structure a été déterminée par l'analyse de la fonction de Patterson. Les molécules se présentent sous forme de chaines parallèles à la rangée [100]. Elles sont pratiquement parallèles au plan (001).

Les positions atomiques, les agitations thermiques et les distances interatomiques et intermoléculaires seront données dans le résumé définitif.

7·26. M. Rouault & Z. L. Waziutynska. *Structure de la molécule de fulvène par diffraction des électrons.*

Le fulvène (Fig. 1), isomère du benzène, a fait l'objet de nombreux travaux théoriques.

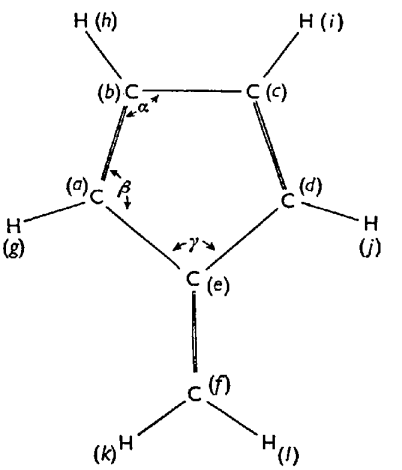

Fig. 1.

La seule tentative de détermination des distances interatomiques est théorique (J. F. F. Alonso, *C. R. Acad. Sci., Paris*, (1951), **233**, 56). G. Berthier (*J. Chim. phys.* (1953), **50**, 344) suppose *a priori* la structure définie par

$$ab = cd = ef = 1{,}35 \text{ Å}, \quad bc = ae = de = 1{,}46 \text{ Å};$$

les angles ne sont pas précisés et sont supposés voisins de 108°; le calcul du moment de dipôle fait à partir de ces distances par une méthode d'orbitales moléculaires avec champ *self-consistent*, donne une valeur 1,13 D en bon accord avec la valeur 1,2 D déduite du moment dipolaire des fulvènes substitués.

Expériences

Le fulvène a été préparé pour la première fois au laboratoire de Chimie de l'École Normale Supérieure à Paris (1954) et nous avons pu disposer d'un échantillon maintenu à la température de la glace carbonique pendant le transport de Paris à Montréal et jusqu'au moment des expériences. À 18° C. c'est un liquide jaune dont la tension de vapeur est 67 mm.

N'ayant pu obtenir qu'un nombre limite de photographies de diffraction d'électrons, 10 étaient utilisables, nous avons seulement calculé les courbes théoriques de répartition angulaire d'électrons diffractés par la vapeur de fulvène pour quelques modèles vraisemblables et les avons comparés aux courbes expérimentales (M. Rouault, *Ann. Phys., Paris*, (1940), **14**, 78) pour rechercher le meilleur modèle; la comparaison a porté sur la fonction $s^3I(s)$ ($s = 4\pi \sin \frac{1}{2}\theta/\lambda$).

La diffraction des électrons de 50 keV. par la vapeur de fulvène a été obtenue au moyen du diffracteur de l'Université de Montréal; la répartition angulaire des électrons diffractés a été obtenu en enregistrant la densité optique au moyen d'un microphotomètre Leeds and Northrup sur lequel les photos tournent autour de leur centre pendant l'enregistrement, puis repérant l'intensité correspondante sur une courbe sensitométrique de l'émulsion utilisée établie dans une expérience séparée; la valeur de $s = \sin \frac{1}{2}\theta/\lambda$ correspondant à chaque distance au centre des photographies a été trouvée sur des photographies de diffraction d'électrons de même énergie par le chlorure de thallium TlCl.

La répartition des électrons diffractés par un gaz pur, représentée par la formule

$$s^3I = \sum_i \sum_j \varphi_i\varphi_j \frac{\sin sl_{ij}}{sl_{ij}} + \sum_i s^{-1}Z_iS_i \qquad \left[\varphi_i = \frac{Z_i - F_i(s)}{s^{\frac{1}{2}}}\right]$$

peut se diviser en deux parties:

$$s^3I_{\text{mol.}} = \sum_{i\neq j}\sum \varphi_i\varphi_j \frac{\sin sl_{ij}}{sl_{ij}}, \quad s^3I_{\text{at.}} = \sum_i \varphi_i^2 + \sum_i s^{-1}Z_iS_i\,.$$

La première partie seule présente des oscillations dues à la structure de la molécule; la deuxieme partie est un 'fond continu' auquel s'ajoute la 'diffusion parasite' par les parois du diffracteur, le gaz restant, etc., que nous noterons $s^3I_{\text{par.}}$.

Pour trouver la courbe $s^3I_{\text{mol.}}$ nous avons tracé sur chacune des courbes s^3I déduite de l'étude d'une photographie, une 'courbe moyenne' autour de laquelle oscille la courbe expérimentale, et que nous supposons représenter $s^3I_{\text{at.}} + s^3I_{\text{par.}}$. Nous avons vérifié que les incertitudes sur le tracé de cette courbe n'affectent pas sensiblement la détermination des positions des maxima et minima de la courbe $s^3I_{\text{mol.}}$.

La Fig. 2 représente une courbe expérimentale ainsi obtenue, elle présente cinq maxima visibles numérotés de 2 à 6.

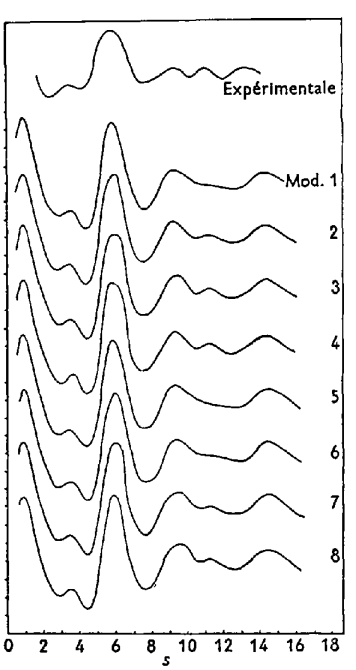

Fig. 2.

Les courbes théoriques ont été tracées pour quatre 'modèles de Berthier' et quatre 'modèles de Alonso' définis par

Modèles 1, 2, 3 et 4: $ab = cd = ef = 1{,}35$ Å, $bc = ae = de = 1{,}46$ Å;

Modèles 5, 6, 7, 8: $ab = cd = ef = 1{,}37$ Å, $bc = 1{,}42$ Å, $ae = de = 1{,}44$ Å; pour tous les modèles C–$H > 1{,}06$ Å.

L'angle α qui suffit à déterminer les angles du pentagone prend les valeurs 107° (1 et 5) 108° (2 et 6) 109° (3 et 7) 110° (4 et 8); les courbes théoriques $s^3I_{\text{mol.}}$ pour les huit modèles ci-dessus sont représentées Fig. 2.

Comparaison des courbes (Rouault, *loc. cit.*).

1°. L'existence du maximum M_5 exclut les modèles 1,5 et 6.

2°. Les φ_i variant lentement avec s dans la plus grande partie du domaine utile, s^3I est fonction des produits sl_{ij}.

3°. Pour deux modèles semblables géométriquement, les l_{ij} sont proportionnels, c'est à dire fonction de l'une des distances l (distance bc par exemple) que j'appellerai distance de base, s^3I est fonction du produit sl; par comparaison de la valeur expérimentale $s^{(i)}_{\text{exp.}}$ d'un maximum No. i avec la valeur de $s^{(i)}_{\text{th.}}$ sur la courbe correspondant à un certain modèle M, on peut en déduire une valeur de la distance $ls^{(i)}_{\text{exp.}} l_{\text{exp.}} = s^{(i)}_{\text{th.}} l_{\text{th.}}$; nous admettrons que le modèle M est en accord avec la diffraction si les valeurs de $l_{\text{exp.}}$ déduites ainsi des différents maxima et minima sont égales aux erreurs d'expérience près, ou encore si les valeurs de $s_{\text{exp.}}/s_{\text{th.}}$ sont concordantes.

4°. La valeur moyenne de $\sigma = s_{\text{exp.}}/s_{\text{th.}}$ correspondant à un modèle acceptable, fournit une valeur expérimentale de la distance de base $l_{\text{exp.}} = l_{\text{th.}}/\sigma$.

Résultats

La dispersion des valeurs de $s_{\text{exp.}}/s_{\text{th.}}$ est la plus petite pour les modèles 3 et 8 avec les valeurs $s_{\text{exp.}}/s_{\text{th.}} = 0{,}976$ $s_{\text{exp.}}/s_{\text{th.}} = 0{,}971$.

Les distances interatomiques et les angles de liaison qui en résultent sont:

Modèle 3: $ab = cd = ef = 1{,}382$ Å, $bc = ae = de = 1{,}496$ Å, $\alpha = 109°$, $\beta = 107°46'$, $\gamma = 106°28'$.

Modèle 8: $ab = cd = ef = 1{,}41$ Å, $bc = 1{,}46$ Å, $ae = de = 1{,}483$ Å, $\alpha = 110°$, $\beta = 105°4'$, $\gamma = 109°52'$.

Nos expériences ne nous permettent pas de distinguer entre ces deux modèles. La dispersion des valeurs de $s_{\text{exp.}}/s_{\text{th.}}$ varie peu de chacun de ces deux modèles aux modèles voisins considérés. Dans chaque série de modèles le meilleur modèle correspond à la valeur du rapport $s_{\text{exp.}}/s_{\text{th.}}$ la plus voisine de 1.

7·27. H. M. M. Shearer & J. M. Robertson. *The structure of azulene.*

The unit-cell dimensions of azulene have been re-investigated and found to be $a = 7{\cdot}884$, $b = 5{\cdot}988$, $c = 7{\cdot}840$ Å, $\beta = 101°\,33'$, with two molecules in the unit cell. An examination of the intensities of the $(h0l)$ reflexions by the distribution test of Howells, Phillips & Rogers and the calculation of the Wilson ratio indicate that the projection on the (010) is non-centred and the space group C_s^2–Pa, and not C_{2h}^5–$P2_1/a$ as previously

suggested. By trial-and-error methods a structure has been postulated for the (010) projection and refined by successive difference syntheses. By assuming a planar molecule, values of the y coordinates of the atoms have been deduced and refinement has been carried out in the [100] projection. In both these projections the ratio of observed reflexions to derived parameters is small, and further refinement has been obtained by difference generalized projection methods using the ($h2l$) reflexions. At this stage the molecule is essentially planar; the lengths of the bonds in the ring vary between 1·33 and 1·42 Å with the central bond 1·49 Å in length. Refinement is now about to proceed using the full three-dimensional data. It is hoped that from these results it will ultimately be possible to map out the electron distribution accurately in this ring system.

7·28. Y. Sasada & I. Nitta. *The crystal structure of* 1-*oxa-azulan*-2-*one.*

As a part of the fundamental studies of the so-called tropoid and azulenoid compounds, we have determined the crystal structure of 1-oxa-azulan-2-one, $C_9H_6O_2$,

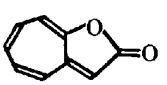

m. p. 72–73° C. This compound is yellow with fine needle-shaped crystals elongated along c; space group $P2_12_12_1$; $a = 21{\cdot}4$, $b = 8{\cdot}23$, $c = 3{\cdot}96$ Å; $Z = 4$. The intensity data were taken by the integrated Weissenberg procedure using the multiple-film technique, ranging 22000:1.

The crystal structure was determined by a systematic trial method, applied to the ($hk0$) reflexions, in which all possible sets of atomic coordinates explaining the intensities of lower-order reflexions are reduced by the requirements of the intensities of the next higher-order reflexions. This method has been proved very suitable for a case in which the intensity distribution shows some characteristic features and in which the approximate molecular shape is known. The atomic coordinates thus determined deviated from the final values by $\gtrsim 0{\cdot}01$. The ordinary two-dimensional Fourier and successive ($F_o - F_c$) syntheses were calculated and x and y coordinates of all atoms, including hydrogen, were determined with considerable accuracy. Since the period of the c axis is very short, approximate values of z coordinates estimated from the layer-line reflexions are enough to discuss the molecular dimensions and orientation.

The molecule is planar except the keto-oxygen, which deviates slightly from the mean molecular plane. The fluctuations among the interatomic distances in the seven-membered ring are rather larger than those in sodium tropolonate and tropolone hydrochloride.

The long axes of the molecules are oriented along the b axis. The crystal structure may be described as follows: The seven-membered carbon ring, which is supposed to be the electrically positive part of the molecule, has as first neighbours six five-membered rings, the negative parts, including the one with which the former is combined covalently, and the five-membered ring is surrounded by six seven-membered rings. Such characteristics of the molecular orientations are discussed in comparison with the structures of azulene (Y. Takeuchi & R. Pepinsky, *Science* (1956), **124**, 126; J. M. Robertson & H. M. M. Shearer, *Nature*, Lond. (1956), **172**, 885) and 2-aminoazulene, in connexion with their dipole moments, (the values of dipole moments being 5·64, 2·09 and 1·0 D for this compound, 2-amino-azulene and azulene respectively).

Low-temperature experiments are being attempted to reduce the thermal agitation.

7·29. W. K. Grant, A. Vos & J. C. Speakman. *The crystal structure of* 2:3-*dihydro*-2:3-*methylene*-1:4-*naphthaquinone.*

This substance (I), which is of some interest because a variety of stereochemical features are embodied in a

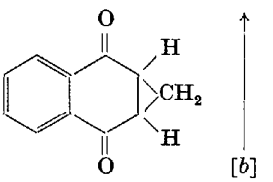

(I)

relatively small molecule, crystallizes in the monoclinic system, with two molecules in a unit-cell of dimensions $a = 6{\cdot}9_8$, $b = 10{\cdot}5_5$, $c = 5{\cdot}4_7$ Å, $\beta = 94°$. Absent spectra indicate the space group to be either $P2_1$ or $P2_1/m$; statistical tests decide unambiguously in favour of the latter. The molecule is therefore bisected by a plane of symmetry, perpendicular to [b], passing through the three atoms of the methylene group; and the crystal structure is a very simple one, which was readily solved by trial and error.

So far analysis has proceeded by projections. That along [c] is particularly favourable, all the atoms (except one methylenic hydrogen) being resolved. The lengths of the three C–C bonds parallel to [b] depend only on single co-ordinates, and they can be accurately established from this one projection; they differ significantly in accordance with the various types of carbo-cycles in which they are involved. The most striking feature of this projection is that the C=O bonds are not collinear, as they are in p-benzoquinone and in naphthaquinone. This deviation of the C=O bonds can be attributed to the distortion of the quasi-quinonoid ring caused by the *cis*-fusion to it of the cyclopropane ring. The arrangement of the four bonds round the three heavily strained carbon atoms is of interest.

Refinement of the other principal projections is in progress.

7·30. G. M. Brown, H. G. Norment, Jr. & H. A. Levy. *The crystal structure of* 2,6-*dimethyl*-γ-*pyrone.*

The present investigation was undertaken to obtain detailed information on the bond lengths and valence angles in the molecule of 2,6-dimethyl-γ-pyrone, in relation to the problem of the electronic structure and the unusual chemical behavior of the γ-pyrones.

Crystals of the pyrone are monoclinic, space group $P2_1/c$, with $a = 7{\cdot}672$, $b = 7{\cdot}212$, $c = 13{\cdot}92$ Å ($\pm 0{\cdot}2\%$), $\beta = 120°\ 59'$ ($\pm 5'$), $Z = 4$, as has been reported earlier (G. M. Brown & H. G. Norment, *Acta Cryst.* (1955),

8, 363). On transformation to the setting $P2_1/n$, the parameters given correspond to the axial ratios reported by Groth and to the approximate parameters reported by J. Toussaint (*Bull. Soc. Chim. Belg.*, (1956), **65**, 213). Intensities of a total of 1458 reflections, all those accessible within the copper sphere, were recorded by the multiple-film Weissenberg technique. Of these, 200 have zero value.

An apparently satisfactory preliminary structure was found by use of structure-factor graphs for the [010] and [100] projections. Refinement was carried out in the following stages: two [010] difference syntheses; three [100] half-cell projections; four three-dimensional Fourier syntheses, interspersed with two back-shift syntheses; two cycles of least-squares refinement of position parameters, individual anisotropic temperature-factor parameters, and scale factors for various groups of data; one [010] difference synthesis and one [100] half-cell difference synthesis, which allowed determination of approximate hydrogen parameters; one cycle of least-squares refinement of the heavy-atom parameters, after correcting the observed F's for the hydrogen contributions. The final value of the discrepancy factor R for all of the reflections is 0·104 (0·091 if the reflections with $F_o = 0$ are omitted). The standard deviation of an observation of unit weight is 0·924.

The final fractional x, y, z parameters of the heavy atoms are: O_1, 0·1780, 0·4688, 0·4254; C_2, 0·2557, 0·4441, 0·5374; C_3, 0·3707, 0·5732, 0·6132; C_4, 0·4227, 0·7447, 0·5792; C_5, 0·3332, 0·7641, 0·4589; C_6, 0·2187, 0·6298, 0·3888; C_7, 0·1198, 0·6306, 0·2638; C_8, 0·1994, 0·2594, 0·5616; O_9, 0·5367, 0·8636, 0·6472.

At the time of writing this abstract the bond lengths and valence angles have been calculated only from the penultimate set of heavy-atom parameters. The values are: $d(O_1–C_2) = 1·369$, $d(O_1–O_6) = 1·370$, $d(C_2–C_3) = 1·336$, $d(C_5–C_6) = 1·337$, $d(C_3–C_4) = 1·457$, $d(C_4–C_5) = 1·453$, $d(C_2–C_8) = 1·496$, $d(C_6–C_7) = 1·497$, $d(C_4–C_9) = 1·245$ Å; $O_1–C_2–C_3 = 122·18$, $O_1–C_6–C_5 = 122·29$, $C_2–C_3–C_4 = 120·92$, $C_6–C_5–C_4 = 120·89$, $C_3–C_4–C_5 = 114·50$, $C_2–O_1–C_6 = 119·16$, $O_1–C_2–C_8 = 111·54$, $C_3–C_2–C_8 = 126·28$, $O_1–C_6–C_7 = 110·98$, $C_5–C_6–C_7 = 126·73$, $C_3–C_4–C_9 = 122·89$, $C_5–C_4–C_9 = 122·59°$. The carbon–oxygen skeleton of the molecule is essentially plane. It may be concluded from the bond lengths that the most important resonance structure for the molecule is the normal covalent ketonic structure.

7·31. J. G. Sime & S. C. Abrahams. *The crystal structure of 4,4′-dichlorodiphenyl sulphone.*

4,4′-Dichlorodiphenyl sulphone crystallizes in the monoclinic system with lattice constants $a = 20·20 \pm 0·03$, $b = 5·01 \pm 0·02$, $c = 12·24 \pm 0·02$ Å, $\beta = 90·6 \pm 0·3°$. There are four molecules per unit cell, with space group $I2/a$. The crystal structure has been solved by use of the Patterson function, and the x, z atomic coordinates have been refined by double-Fourier-series syntheses; further refinement is being undertaken by three-dimensional methods. Present values of the bond lengths are: Cl–C = 1·75, C–S = 1·85, S–O = 1·4 Å; and of the bond angles: C–S–C = 98°, O–S–O = 121°. The dihedral angle between the two aromatic rings is 82°; these values are not final and are likely to alter as the refinement process is continued.

7·32. W. L. Kehl & G. A. Jeffrey. *The structure of 4-methyl 1-2 dithia-4-cyclopentene-3-thione.*

The compound 4-methyl 1-2 dithia-4-cyclopentene-3-thione is the member with $R_1 = CH_3$, $R_2 = H$, of a large class of compounds of the general type (I) (R. S. Spindt *et al.*, *J. Amer. Chem. Soc.* (1951), **73**, 3693) which have been obtained from reactions of olefins and sulfur, and are sometimes called trithiones (B. Böttcher & A. Lüttringhaus, *Liebigs Ann.* (1947), **557**, 89; F. Bauer, *Chemiker-ztg.* (1951), **75**, 623).

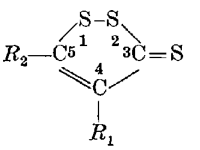

(I)

Orthorhombic orange needles, with a melting point of 40·5–41·5° C., were obtained from an ethyl ether–pentane mixture. The crystallographic data are:

$a = 12·35$, $b = 12·44$, $c = 4·11$ Å, $U = 631·44$ Å^3, $Z = 4$, $D_x = 1·559$, $D_m = 1·560$. Space group $P2_12_12_1$.

The structure was solved for the well-resolved c-axis projection by the Harker–Kasper inequalities method, and was refined first by difference syntheses on the ($hk0$) data, and then by both least squares and differential syntheses on the 680 (hkl) reflections. The two methods of refinement lead to discrepancies in the coordinates of the carbon atoms of the order of 0·05 Å. This is ascribed to the omission of weighting factors in the least-squares calculations.

The molecule lies approximately in a plane at 25° to the ab plane. From the observed bond lengths the five-membered ring has some aromatic character. The $C_5–S_1$ (1·67 Å) and the $C_3–S_2$ (1·74 Å) bonds are shorter than single bonds, while the $C_3–C_4$ bond (1·42 Å) and the $C_4=C_5$ bond (1·38 Å) are respectively shorter than a single bond and longer than a double bond. This π-bonding does not, however, appear to include the $S_1–S_2$ link, which has a normal single bond length (2·03 Å). The bonds external to the ring ($C_4–C_{R_1}$ (1·49 Å); $C_3=S$ (1·65 Å)) are close to normal in length.

7·33. H. von Eller. *Sur le polymorphisme de l'indigo.*

La comparaison est faite entre la forme cristalline stable de l'indigo et une seconde forme capable de se transformer dans la première.

Les deux mailles cristallines, de groupe spatial $P2_1/c$, sont très voisines. Les paramètres c sont égaux; les paramètres b diffèrent d'un dixième d'Ångström; de plus, la distance entre les plans réticulaires [100] est la même dans les deux cas.

On peut considérer la structure de la deuxième forme comme bâtie de la même façon que la première forme de l'indigo. Les molécules dont le centre de symétrie coïncide avec un des centres de symétrie de la maille, sont unies entre elles par des liaisons hydrogène de manière à constituer de véritables feuillets plans parallèles aux axes OY et OZ. La cohésion entre feuillets est uniquement assurée par les forces de van der Waals. Lorsque l'équilibre de la seconde forme est rompu, il se produit un glissement d'environ $\frac{1}{4}c$ des feuillets les uns sur les autres

jusqu'à une autre position d'équilibre, celle de la première forme.

7·34. R. Mason. *The crystal and molecular structures of the carcinogenic biscyclic dibenzacridines.*

C–C and C–N bond lengths in these isomeric molecules have been determined with an average standard deviation of 0·003 Å. Theoretical predictions of electron distribution in these molecules are examined in relation to their biological properties and to the observed electron-density distribution. Bond-order length curves based on these measurements suggest that the simple molecular-orbital approximation predicts bond lengths with an accuracy of 0·01 Å.

7·35. D. J. Sutor. *The crystal structures of caffeine and theophylline.*

The alkaloids, caffeine and theophylline, are nearly isomorphous:

Caffeine

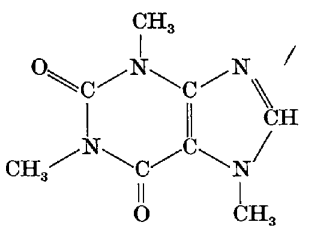

$+ 1\,H_2O$

$a = 14{\cdot}8$, $b = 16{\cdot}7$, $c = 3{\cdot}97$ Å, $\beta = 97°$; space group $P2_1/a$; 4 units of $C_8H_{10}N_4O_2.1H_2O$/unit cell.

Theophylline

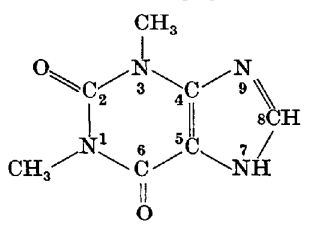

$+ 1\,H_2O$

$a = 13{\cdot}3$, $b = 15{\cdot}3$, $c = 4{\cdot}5$ Å, $\beta = 99\frac{1}{2}°$; space group $P2_1$, nearly $P2_1/a$; 4 units of $C_7H_8N_4O_2.1H_2O$/unit cell.

In theophylline, a few $h0l$ planes with $h = 2n+1$ are present, but are weak and so the departure from $P2_1/a$ cannot be very great. The space group has been taken as $P2_1/a$ and the deviation from it has not yet been determined.

The x and y coordinates were obtained by the isomorphous-replacement method, employing instead of the conventional 'heavy atom', the extra methyl group in the iminazole ring of caffeine. The $hk0$ projection has been refined by F_o-F_c syntheses to $R = 12\%$ and 7% for caffeine and theophylline respectively, the higher value for caffeine being due to the less accurate intensity data (the crystals effloresce readily, and then decompose). The z coordinates were obtained from packing considerations and are being refined by c-axis difference generalized projections. Positions for the hydrogen atoms have been found, as well as individual isotropic and anisotropic temperature factors.

The water molecules form a zigzag arrangement of hydrogen bonds in which each water molecule is linked to the two adjacent ones across the 'pseudo' centres of symmetry. Each water molecule participates in a third hydrogen bond with the nitrogen in the 9 position of the iminazole ring. In theophylline a further hydrogen bond exists between the oxygen of the carbon in the 6 position and the >NH in the 7 position of adjacent molecules.

7·36. M. B. Crute. *Crystal structure of nickel etioporphyrin II.*

Nickel etioporphyrin II, $C_{32}H_{36}N_4Ni$, designates the following structure:

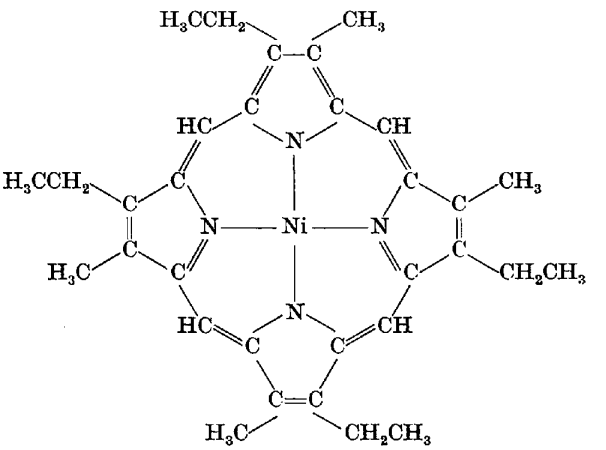

The crystals used in this study were prepared by Dr Winslow Caughey. They are tetragonal dipyramids, pseudo-octahedra, approximately 0·1 mm. on an edge. They are very soft, opaque, deep purple in color with high vitreous luster. The following X-ray patterns were obtained with Cu $K\alpha$ radiation; rotation about the c axis; precession photos containing reflections $hk0$, $hk1$, $h0l$, hhl; and equi-inclination Weissenberg photos of nine levels taken about the c axis. Intensities were measured on the Weissenberg films by visual comparison with a calibrated strip.

The cell is body-centered with $a = 14{\cdot}68$, $c = 12{\cdot}51$ Å, both $\pm 0{\cdot}3\%$. With four molecules per cell, the calculated density is 1·37 g.cm.$^{-3}$; the observed density is 1·54 g.cm.$^{-3}\pm 0{\cdot}15$. Systematic absences uniquely determine the space group as $I4_1/amd$. With the origin at a center of symmetry, the space group requires the Ni atoms, the centers of the molecules, to lie at position (a) or (b), depending on the choice of origin. They were placed in position (b) at heights $\frac{1}{8}$, $\frac{3}{8}$, $\frac{5}{8}$, and $\frac{7}{8}$. The space group also requires that four equivalent atoms (either N or methine-bridge C atoms) lie co-planar with the Ni atom in the horizontal plane. The four molecules are related by a 4_1-axis at $(\frac{1}{4}, \frac{1}{2}, z)$. The only unknown with respect to the orientation of the molecules is their orientation in the xy plane. The space group allows only two possible orientations in that plane (one differing from the other by a 45° rotation), and all four molecules must have one and the same orientation. The molecule lies on a site of symmetry $\bar{4}m2$, hence its horizontal projection is centrosymmetric. Since the only heavy atom is situated at the center of the molecule, the Patterson section at $z = 0$ shows an image of the molecule, thus confirming the

approximate planarity of the molecule except for the β-carbon atoms of the ethyl groups. The Patterson section shows that the Ni–N bonds are oriented parallel to a.

Structure factors were calculated using coordinates obtained from the Patterson section and omitting the β-carbon atoms, which do not appear in the section. Using the signs of these calculated structure factors, an electron-density section was made at $z = \frac{1}{8}$ to obtain x, y coordinates for all atoms except the β-carbon atoms. For the x, y coordinates of the latter, a difference projection of electron density was made on (001) using $(F_o - F_c)_{hk0}$. The Ni atoms and the methine-bridge C atoms are required to lie in a plane at $z = \frac{1}{8}$ but this is not true of the N atoms and the other C atoms. A line section parallel to c was made through each of the atoms in order to obtain its z coordinate. The N atom is at $z = 0{\cdot}125$ but the C atoms of the pyrrole ring are out of the plane by approximately 0·2 Å. Refinement of the structure is in progress.

7·37. D. C. Phillips & F. R. Ahmed. *The crystallography of acridine. Part* III. *The structure of acridine* II.

Acridine II, $C_{13}H_9N$, is monoclinic with $a = 16{\cdot}292$, $b = 18{\cdot}831$, $c = 6{\cdot}072$ Å, $\beta = 95°\,4'$, $Z = 8$, and space group $P2_1/a$. The asymmetric unit consists of two molecules with different environments, the effect of which on their structure has been an interesting feature of the investigation. For Cu $K\alpha$ radiation, there are 4225 possible reflections but only 2679 (63·4%) were observed. The intensities of 803 reflections were estimated once, 1263 twice (i.e. on separate photographs taken about different axes), and 613 three times. From these measurements $\sigma(F)$ varies approximately as $0{\cdot}09F$, but has a minimum value of about 0·6. The structure was established by trial-and-error methods involving Fourier projections, difference syntheses, and generalized projections along [001]. The atomic co-ordinates were refined by two cycles of three-dimensional observed differential syntheses. In the first cycle, the co-ordinates changed by an average of 0·033 Å and a maximum of 0·109 Å, while for the second cycle the average shift was 0·005 Å and the maximum 0·021 Å. The errors in the atomic co-ordinates due to finite summation were then estimated by the calculated differential synthesis method, and averaged 0·005 Å with a maximum of 0·015 Å. The isotropic temperature factor was first taken as 3·93 Å^2 for all the atoms of both molecules, but comparison of the observed and calculated peak heights indicated that the atoms further from the centre of each molecule have the higher temperature factors, as have all the atoms of that molecule which is less firmly bonded within the structure. As a result of the two cycles of refinement of the co-ordinates and the isotropic temperature factors, the discrepancy (including the correction due to finite summation but excluding the effect of the hydrogen atoms) was reduced from 0·25 to 0·16. The three-dimensional refinement was carried out on FERUT using new generalized crystallographic programmes applicable to all space groups. Further refinement of the structure by a difference Fourier synthesis is to be carried out before the Congress, and it is expected that details of the hydrogen atom positions together with the bond lengths and the planarity of the two molecules can be presented and compared with corresponding data for the single asymmetric molecule of acridine III.

7·38. W. Nowacki, H. Bürki, G. F. Bonsma & H. Jaggi. *Direkte Kristall- und Molekülstrukturbestimmung von 7α-Bromcholesterylbromid, des Alkaloids Erythralin-Hydrobromid und der Phthalsäure.*

(*a*) *7α-Bromcholesterylbromid, -chlorid und -methyläther*

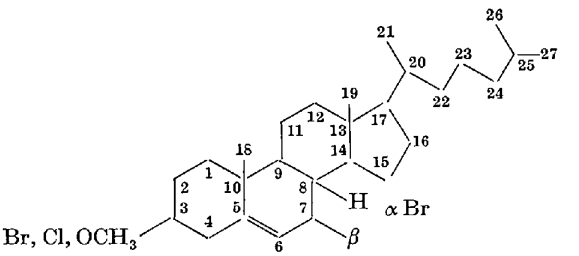

Für einen Substituenten (z. B. Br) am C_7 des Sterinmoleküls gibt es zwei Möglichkeiten α [oder β], *trans* [oder *cis*] zum H am C_8 (oder zur Methylgruppe C_{18} am C_{10}) orientiert. Die zwei C_7-Epimere sind stark links- (= I) bzw. schwächer rechtsdrehend (= II). Die Frage war, ob die linksdrehende Verbindung I die Konfiguration α oder β aufweist. Das Problem konnte röntgenkristallographisch durch Untersuchung von 7-Bromchlesterylbromid (= S_1); -chlorid (= S_2) und Methyläther (= S_3), die sich als isotyp erwiesen, gelöst werden. Die Gitterkonstante sind:

	a (Å)	b (Å)	c (Å)	β	Raumgruppe	Z
S_1	12,05	8,75	12,57	101° 19′	C_2^2–$P2_1$	2
S_2	11,95	8,78	12,54	101° 11′		
S_3	12,46	8,88	12,32	99° 10′		

Patterson-Projektionen ergaben die Lagen der vier Br-Atome. Durch Anwendung der Methode des schweren Atomes, des isomorphen Ersatzes (Vergleich von S_1 und S_2), der Kombination beider Methoden und der Patterson-Superpositionsmethode (rechnerisch und graphisch) konnten die Vorzeichen für eine Fourier-Projektion $\|b$ für S_1 und S_2 erhalten werden. Die Projektionen wiesen zum Teil eine beachtenswert gute Auflösung der meisten Atome auf und zeigten eindeutig, dass in den Verbindungen S_1 und S_2 (Typus I) das Br-Atom am C_7 sich in α-Stellung (d. h. *trans* zum H am C_8) befindet. — Die lange Achse des Moleküls liegt ungefähr in (010); die mittlere Ringebene ist um etwa 20° um die Richtung $[20\bar{1}]$ aus der Ebene (010) herausgedreht. Die Moleküle bilden daher Schichten $\|(010)$, welche durch die 2_1-Schraubenachsen übereinander gelagert sind. Die Kristall- und Molekülstruktur von S_1 und S_2 ist derjenigen von Cholesteryljodid (Form *B*) (Carlisle–Crowfoot) sehr ähnlich.

(*b*) *Erythralin*.HBr

Die Konstitution des Curare-Alkaloids Erythralin ($C_{18}H_{19}O_3N$) wurde während mehrerer Jahre von organischen Chemikern (Folkers, Prelog *et al.*) untersucht. Ursprünglich war eine lange Formel vorgeschlagen worden (I).

Im Jahre 1950 begannen wir mit einer Röntgenuntersuchung des Hydrobromides: $a = 13{,}36$, $b = 10{,}46$, $c = 11{,}67$ Å, Raumgruppe D_2^4–$P2_12_12_1$, $Z = 4$ Moleküle pro

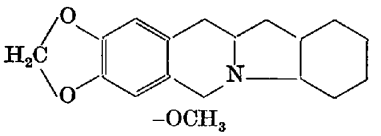

(I)

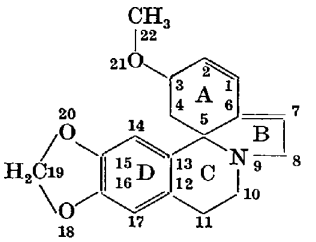

(II)

Zelle. Die Kristalle sind optisch negativ mit $n_\alpha = b$, $n_\beta = c$, $n_\gamma = a$ und weisen eine ausgezeichnete Spaltbarkeit ||(010) auf (W. Nowacki, *Angew. Chem.* (1950), **62**, 124). Es war schwierig, vier solche lange Moleküle mit ihrer Hauptebene ||(010) in der Zelle unterzubringen.

Patterson-Projektionen ||a, b und c ergaben die Lagen der vier Br-Atome, welche durch Fourier-Projektionen verbessert wurden. Hierauf wurde eine *drei*dimensionale Patterson-Superpositionssynthese (über die 4 Bromlagen superponiert) unter Subtraktion der (Br–Br)-Vektoren *berechnet*, welche 24 (nicht 22, wie es 18C+3O+1N entspräche) hohe Maxima lieferte. Sauerstoffe wurden in drei Maxima, welche einer neuen chemischen Formel von V. Prelog *et al.* (*Helv. Chim. Acta* (1949), **32**, 453; (1951), **34**, 1601, 1969) entsprach, eingesetzt und Kohlenstoffe in allen übrigen 21 Maxima. Hätte man überall C-Atome eingesetzt, wäre das Resultat schlussendlich sehr wahrscheinlich dasselbe geblieben. Unter dieser Voraussetzung wurden die Phasenwinkel bzw. A- und B-Werte ($F = A+iB$) für etwa 2100 Reflexe berechnet. Diese Phasenwinkel zusammen mit den beobachteten $|F|$-Werten ermöglichten eine dreidimensionale Fourier-Synthese, welche eindeutig die Konstitution (II) ergab, in Übereinstimmung mit den neuesten chemischen Resultaten (V. Prelog *et al.*, *Helv. Chim. Acta* (1956), **39**, 498). Darüber hinaus ergab sich mit Sicherheit die Stellung der Methoxygruppe am C_3 und die *cis*-Stellung dieser Gruppe zum tertiären Stickstoffes am C_5. Eine zweite Phasenberechnung und eine zweite dreidimensionale Fouriersynthese ergaben die genauen Bindungslängen und -winkel ($R = 14{,}3\%$ für alle *hkl*).

(c) *Phthalsäure*

Phthalsäure kristallisiert monoklin: $a = 5{,}04$, $b = 14{,}30$, $c = 9{\cdot}59$ Å, $\beta = 93°\,11'$, Raumgruppe C_{2h}^5–$C2/c$, $Z = 4$ Moleküle pro Zelle. Weissenberg-Aufnahmen mit Cu K-Strahlung ergaben etwa 800 Reflexe, deren Intensitäten auf unitäre Strukturamplituden U_{hkl} umgerechnet wurden. Durch Anwendung der Methode der Ungleichungen und der statistischen Verfahren von Cochran–Sayre–Zachariasen konnte von etwa 200 Reflexen das Vorzeichen ermittelt werden. Damit wurde eine erste dreidimensionale Fourier-Synthese ausgeführt, welche durch eine zweite verfeinert wurde. Die bis auf einen Sauerstoff der Carboxylgruppen ziemlich planaren Moleküle werden durch H-Bindungen der Länge 2,68 Å zu einer Art Zickzackkette im Raum zusammengehalten. Die Bindungslängen und -winkel stimmen recht gut mit den theoretischen und experimentellen Werten, wie sie für ähnliche Moleküle gefunden wurden, überein.

Von T. G. D. van Schalwijk (*Acta Cryst.* (1954), **7**, 775) liegt eine Untersuchung der Struktur der Phthalsäure vor (Verwendung von nur zweidimensionalen Daten; nur Angabe der O–H · · · O-Länge = 2,67±0,05 Å), die mit unserer in Einklang zu sein scheint.

Sämtliche Berechnungen für die drei Strukturbestimmungen wurden mit Hilfe von IBM-Lochkartenmaschinen (insbesondere Tabulator Typ 420, Rechenlocher 602 A und 604) ausgeführt.

7·39. K. Lonsdale. *Structures of simple organic compounds having curare-like properties.*

The crystal and molecular structures of the polymethylene bismethyl ammonium salts are being studied in connexion with the variation of the curare-like pharmacological action of these substances, which is markedly dependent on their chain length.

7·40. J. P. Glusker. *Some details of the X-ray analysis of a hexacarboxylic acid obtained from vitamin* B_{12}.

X-ray crystallographic studies on a cobalt-containing degradation product of vitamin B_{12} were part of extensive researches on the structure of the vitamin carried out by Mrs Hodgkin at Oxford. The work to be described was done in collaboration with Mrs D. M. Hodgkin, Dr K. N. Trueblood, Dr R. J. Prosen and Dr J. H. Robertson.

The degradation product, isolated by Cannon, Johnson & Todd at Cambridge, was crystallised from mixed solvents. A red rock-like mass was obtained from which one good plate-like crystal was broken; all measurements were done on this crystal. Chemical analyses indicated that the compound had an approximate formula $C_{47}H_{66}O_{16}N_6CoCl$. It was known to be a hexacarboxylic acid, it probably contained a cyanide group and it had a similar ultra-violet absorption curve to vitamin B_{12}, indicating that the chromophoric part of the molecule was unchanged by the chemical degradation.

The compound crystallised in the space group $P2_12_12_1$ with one molecule in the asymmetric unit. The cell dimensions were $a = 24{\cdot}58$, $b = 15{\cdot}52$, $c = 13{\cdot}32$ Å. Three-dimensional intensity data were collected from Weissenberg photographs using copper radiation. The cobalt atom parameters were found from Patterson projections, and a three-dimensional electron-density map, using phases of the cobalt atom, was calculated. This map showed, around the high peak of the cobalt atom, peaks corresponding to atoms in four five-membered rings. There were also three bridging atoms between the rings but the arrangement was not truly porphyrin-like as one bridge atom was missing, two of the rings being directly joined. This was in agreement with results obtained by Mrs Hodgkin and other workers from studies on the vitamin itself. The nature of the rest of the molecule could not be deduced from this first electron-density series as there were so many spurious peaks.

A study of this compound was continued to find its complete molecular structure. The compound has a lower molecular weight (about 1000) than the vitamin (about 1350) and yet contains the relatively heavy atoms cobalt and chlorine. Furthermore, the cobalt atom and the

planar group surrounding it lie in quite different orientations in the unit cells of the two compounds. The data for the hexacarboxylic acid are the more extensive, with reflections to the limit of $\sin\theta$ for copper radiation. At the time of these studies chemical evidence on the nature of the inner core was very slight and any attempts at further degradation of the acid resulted in complete disruption of the molecule.

At this stage phases of 26 atoms in this inner ring system (including cobalt and chlorine) were used for an electron-density calculation. This map showed, in all peaks above an arbitrary level, the nature of nearly all the side chains—methyl groups, propionic acid and acetic acid groups and a lactone or lactam ring. However, several more electron-density maps were calculated before the structure was completely solved as there were a few atoms which were very difficult to locate. Some details of the methods of analysis used in these studies and the results obtained will be discussed.

When all the atomic positions had been found, refinements were continued by least-squares methods as it was of great interest to determine the arrangement of double bonds in the inner ring system. The chemical formula was deduced from the stereochemistry of the model found, using the original analysis figures.

7·41. J. G. White. *Structure analysis of vitamin* B_{12} *in the air-dried crystals.*

The technique of structure determination in very complex molecules containing only a 'light' heavy atom is discussed in the light of the experience gained in the Princeton work on the air-dried crystals of vitamin B_{12}. The effectiveness of the cobalt atom in phase determination appears surprisingly high considering its formal scattering power as against that of about 110 lighter atoms. Nevertheless, in the three-dimensional electron-density distribution based on the phases of cobalt alone only about 60% of the 110 strongest peaks which appeared actually correspond to atoms and this figure is markedly dependent on distance from the cobalt atoms.

Some form of trial was therefore necessary, and efforts were made to increase the weight of the phase-determining nucleus by adding groups of lighter atoms which appeared most convincing. The earliest such calculations showed clearly that, as expected in the non-centrosymmetric case, the overweighting of atoms when only a fraction of the total crystal asymmetric unit was included in the phase calculations, was so great that little if any information would be gained by examination of the parts of the structure inserted. For a considerable time, therefore, the operations carried out were not refinements in the usual sense, where positional change is expected in the atoms inserted in the calculations, but were attempts to cause improvement in the electron density in regions in which atoms had not been placed. Two particular advantages were gained by using these methods. First, a completely asymmetric nucleus could be chosen for phase determination which would give an electron-density distribution free from false symmetry. Secondly, the calculation of electron densities of the same region using very different nuclei in the phase calculations could give partially independent comparisons which were of great value. A disadvantage was that since the lighter atoms could be, at best, rather imprecisely placed, their calculated contributions in high-order reflections were somewhat meaningless, and a smearing of the density in many places made it impossible to formulate a chemically bonded structure until higher accuracy was attained in the positions of the phase-determining atoms.

With the introduction of a sufficiently large proportion of the crystal asymmetric unit, however, changes did occur in the parts of the structure included in the phase calculations. Essentially correct atoms did show movements from the positions in which they had been placed, making possible refinement in the orthodox sense. Groups of atoms which had been incorrectly formulated would eventually always show features which required reconsideration of their structure, usually by the occurrence of strong peaks in positions chemically incompatible with the postulated system. Individual atoms, however, might appear convincingly strong even at late stages of the analysis although some notable instances were found of an included atom being so weak in the electron-density map that it was obviously incorrect. In cases where the electron density showed that something was wrong with the system postulated, but where the correct formulation was not obvious, the most effective method was found to be withdrawal of all the atoms in the doubtful region from the phase calculations and the calculation of the electron density with no direct bias in this part of the structure, but with phases presumably better, owing to improvements in other parts of the structure, than those of the Fourier series from which the part in question had first been postulated.

The principles discovered in the earlier parts of the work were applied most systematically in the final formulation of the side chains of the molecule. The ninth major refinement of the Princeton series showed clearly the bonded system of almost the entire molecule. The very few remaining atoms still in doubt were easily placed after the comparison with the parallel work in Oxford on the hexacarboxylic acid fragment of B_{12}, which occurred at this stage.

7·42. R. Pepinsky, J. W. Turley, Y. Okaya, T. Doyne, V. Vand, A. Shimada, F. M. Lovell & Y. Sogo. *X-ray analyses of some biochemically important compounds.*

X-ray analyses and some least-square refinements (IBM 704) are reported of: divalent metal salts of aspartic and glutamic acid; a pyridyl antihistamine; potassium actithiazate; cycloserine hydrochloride; a methyl deserpitate (rauwolfia) derivative; barium *d*-glycerophosphate; cibrome-α (a large-ring compound); and gelsemine hydroiodide.

Aspartate and glutamate salts*

Divalent metal salts of aspartic acid and glutamic acid have been examined because of their importance in the activation of enzyme systems. The salts of L-aspartic acid with divalent zinc, cobalt and nickel crystallize from water as trihydrates, and are isomorphous. The space group is $P2_12_12_1$, and the cell constants are:

* Analysis of aspartate salts was accomplished jointly with T. Watanabe.

	Zinc aspartate $.3H_2O$	Cobaltous aspartate $.3H_2O$	Nickelous aspartate $.3H_2O$
a (Å)	$9{\cdot}38_6$	9·39	9·40
b (Å)	$7{\cdot}92_0$	7·85	7·83
c (Å)	$11{\cdot}53_2$	11·37	11·35

The structure and hand were obtained directly for the cobaltous salt through use of Cu $K\alpha$ radiation and the $P_s(u)$ function (R. Pepinsky & Y. Okaya, *Proc. Nat. Acad. Sci., U.S.*, (1956), **42**, 286) using Taylor's formulation of Buerger's image-seeking function, computed directly on X-RAC. Coordinates so obtained were used to refine the zinc salt. Least-squares computations (IBM 704) led to an R-factor of 9% in three dimensions.

The structure of the zinc salt is very interesting. Three atoms are attached to the zinc, from a single molecule, forming three rings. One arises from the planar four-membered group formed by chelation of the amino nitrogen and an α-carboxyl oxygen. The chelating O–N distance here is 2·62 Å, the short distance being forced by the well known resonance in this portion of the α-amino acid structure. The second is from a five-membered group chelated at the amino nitrogen and the β-carboxyl oxygen. The separation between the chelating O and N atoms here is 3·03 Å, and thus the angle between the Zn–O and Zn–N bonds is 87° 30′. The third chelating group is attached at the α-carboxyl and β-carboxyl oxygens; and there are thus six atoms in the group. The distance between the chelated oxygens here is 2·93 Å. Since the two Zn–O distances are 2·19 and 2·16 Å, the angle between the two Zn–O bonds is 84° 40′. If this angle were 90°, the O–O separation would be 3·08 Å. The diminution of this O–O distance suggests that these two oxygens are weakly hydrogen-bonded. This point remains to be confirmed, and a three-dimensional F_o-F_c map is now being computed. The reduced separation of the chelating oxygens does suggest a tendency for cyclization of the aspartate ion through hydrogen bonding between the carboxyl end groups. This type of cyclization is not the same as that suggested by F. C. Steward & J. F. Thompson (*Nature, Lond.* (1952), **169**, 739) for asparagine, where a direct covalent bond between the amide nitrogen and α-carboxyl oxygen is proposed; it is closer to the proposal of Huggins, as quoted by Steward & Thompson.

The remaining octahedra coordination about zinc, in the zinc aspartate trihydrate structure, is achieved by two water molecules and the second β-carboxyl oxygen of a neighboring aspartate molecule.

It is of further interest to note that the extended structure of asparagine monohydrate, as reported by Y. Saito *et al.* (*Science* (1955), **121**, 435) does not refine, and must be presumed to be incorrect. No satisfactory alternative structure has as yet been found for this crystal, but weakly hydrogen-bonded cyclized configurations are being examined.

The structure of cobaltous glutamate trihydrate has also been solved. The space group is $P2_12_12_1$, with a = 10·66, b = 7·26, c = 11·48 Å, and Z = 4. The cobalt atoms are essentially at the same positions in the cell as in the aspartate salt, and the cells are similar in dimensions and symmetry. A Patterson projection on (010) revealed that the chelation is similar to that in the aspartate salt, but the ligands are rotated 180° about the cobalts in the cell, compared to their position in the aspartate. A further difference appears in the fact that the remaining three octahedral positions about the cobalt are now all occupied by water molecules. At present the R factor for the (010) projection is about 20%, and the structure is being refined by least squares.

Pyridyl antihistamines

By dehydration of 1-*p*-chlorophenyl-1-α-pyridyl-3-pyrrolodinopropan-1-ol, two substituted prop-1-enes were obtained (D. W. Adamson *et al.*, *J. Chem. Soc.* (1950), p. 1039; *Nature, Lond.* (1951), **168**, 204). Chemical evidence indicates that these two compounds, identified as α and β forms, are geometric isomers; in one case it is assumed that the methylpyrrolodino group is *cis* to the pyridyl with respect to the propene double bond, and in the other case the groups are *trans*. The α-form is a powerful antihistamine, and the β-form is relatively inactive. Chemical identification of the configurations is difficult.

Crystals of the hydrochlorides and hydrobromides of both the α-chlorophenyl and α-bromophenyl derivatives, and hydrobromides of the β-chlorophenyl derivatives, were supplied by Dr Adamson. The four α derivatives were found to be isomorphous, but with space groups either $P1$ or $P\bar{1}$, and eight molecules per cell. The two β derivatives were found to be more amenable to analysis. These are isomorphous, with space group $P2_1/n$, and cell constants

	a (Å)	b (Å)	c (Å)	β (°)
Cl-phenyl-.HBr	6·01	11·2	25·9	97·4
Br-phenyl-.HBr	6·05	11·2	26·3	97·0

Patterson projections on (100) permitted location of the heavy atoms. Density projections on this plane, using halogen positions for sign assignments, immediately revealed the general molecular positions and configurations, and in fact unequivocally established that the β forms were *cis*.

The projection of the β-chlorophenyl derivative [β-1-(4-chlorophenyl)-1-(2-pyridyl)-3-pyrrolidinoprop-1-ene hydrobromide] was refined by usual methods, and eventually by least squares (IBM 704). R factors of 13·8% with F_o = 0 not included, and 19·4% with F_o=0 included, were achieved. The *cis* configuration was confirmed. From chemical evidence it is thus clear that the configuration of the active α-form is *trans*.

Refinement of potassium salt of actithiazic acid

The potassium salt of the antibiotic actithiazic acid, 2-(5-carboxypentyl)-4-thiazolidone, has a monoclinic cell, space group $P2_1/n$, with a = 5·07, b = 8·35, c = 29·9 Å, β = 92° (R. Pepinsky & P. F. Eiland, *Acta Cryst.* (1954), **7**, 652). The structure was solved in the (100) projection by the heavy-atom method, and refined by model-fitting and F_o-F_c syntheses to an R-factor of 23·3%. Recent least-squares refinement (IBM 704) has reduced the R factor to 14·4%.

The five-membered ring is very nearly planar, and the six-membered side chain is fully extended. Adjacent atoms in this side chain have very different individual temperature factors. Packing around the large sulfur atom, and the presence of the ionic potassium, account for this feature.

Refinement of cycloserine hydrochloride

The hydrochloride of cycloserine, 4-amino-3-isoxazolidone, is orthorhombic, space group $P2_12_12_1$, $Z = 4$, with $a = 9{\cdot}72$, $b = 10{\cdot}34$, $c = 5{\cdot}73$ Å (J. W. Turley & R. Pepinsky, *Acta Cryst.* (1956), **9**, 948). Since the published report of this structure, three-dimensional refinement has been accomplished by the least-squares method (IBM 704), resulting in an R factor of 14·4%. The structure shows six short intermolecular distances: O–H · · · O, N–H · · · O, and N–H · · · Cl; but only four hydrogens are available for H-bond formation. F_o-F_c syntheses of (001) and (010) projections, on X-RAC, indicate two bifurcated hydrogen bonds. A three-dimensional F_o-F_c synthesis is presently in process to permit improvement in locations of hydrogens.

Methyl deserpitate

The rauwolfia derivates methyl-18-desoxy-18-bromodeserpitate hydrochloride and hydrobromide are isomorphous, space group $P2_1$, with constants

	a (Å)	b (Å)	c (Å)	β (°)
B.HCl	8·84	9·52	12·97	99·6
B.HBr	9·05	9·44	12·84	102

and $Z = 2$. Material was furnished by Dr H. B. MacPhillamy of the Ciba Research Laboratory. Interatomic vector maps revealed the position of the covalently-bound bromine and the halogen ion. Three-dimensional density syntheses, based on phases of the heavy-atom contributions, and a three-dimensional image-seeking minimum function, assisted in locating the molecule in the cell. A least-squares refinement (IBM 704) of the (010) projection led to an R-factor of 13%, and a subsequent density map showed the molecular configurations. A three-dimensional refinement is in progress.

Barium d-*phosphoglycerate*

Barium *d*-phosphoglycerate is monoclinic, space group $P2_1$, with $a = 10{\cdot}96$, $b = 7{\cdot}95$, $c = 5{\cdot}43$ Å, $\beta = 108°$, $Z = 2$. The crystals are needles elongated along b. An (010) interatomic vector projection revealed the barium position; and (010) density map using barium phases showed the phosphate P and O atoms. A model was sought which fitted the remainder of the approximate density projection, and refinement was accomplished in the usual way. The carbon chain is curled. The absolute configuration is now being sought by use of the $P_s(u)$ function on the (001) projection.

Cibrome-α

Cibrome-α is the trivial name for 1,17-dibromo-cycloheptadecane-9-one, a 17-membered ring structure which crystallizes in space group $P2_12_12_1$ with $a = 18{\cdot}25$, $b = 16{\cdot}45$, $c = 6{\cdot}26$ Å, $Z = 4$. Beautifully crystalline material was furnished by Dr M. Stoll of Firmenich et Cie, in Geneva, Switzerland. Projections and generalized projections of the interatomic vector function revealed the bromine positions. Considerable overlap occurs in the (001) projection in the neighborhood of the bromine positions. This projection has been calculated with bromine contributions removed, and the ring structure has been established. A full three-dimensional analysis is in progress.

Gelsemine hydroiodide

The structure of the alkaloid gelsemine, $C_{20}H_{22}N_2O_2$, from the plant *Gelsemium sempervirens*, has been examined as the hydroiodide. The chemical character of the molecule, except for the stoichiometric composition, was essentially unknown. The space group is $P2_12_12_1$, and cell dimensions are $a = 7{\cdot}80$, $b = 9{\cdot}18$, $c = 26{\cdot}9$ Å, with $Z = 4$. The iodine position was found, from interatomic vector projections, to be at $x = 0{\cdot}180$, $y = 0{\cdot}150$, $z = 0{\cdot}250$ (referred to the origin used in the *International Tables*). The heavy-atom method for sign determination in the centrosymmetric (010) and (100) projections is rendered difficult because the iodine contributes to only half of the reflections; and if only these are used in a density synthesis, false symmetry is introduced. One very strong term in the (010) projection, to which term iodines did not contribute, was assigned an arbitrary sign, and introduction of this term so reduced the false symmetry that normal iteration and F_o-F_c maps led to a reasonable structure, with an R-factor of approximately 20%. This is now being refined in three dimensions.

7·43. J. W. Turley, Y. Okaya, V. Vand & R. Pepinsky. *X-ray analyses of miscellaneous organic structures.*

X-ray analyses, refined by the IBM 704 least-squares program, are reported of the structures of lauric acid, triaminoguanidine hydrochloride, urea phosphate, and tri-glycine sulfate, selenate and fluoberyllate.

The *C* (or α) form of lauric acid, $C_{12}H_{24}O_2$, is monoclinic, with $a = 9{\cdot}524$, $b = 4{\cdot}965$, $c = 35{\cdot}39$ Å, $\beta = 129° 13'$. The space group is $P2_1/a$. The structure was solved from two-dimensional projections by V. Vand *et al.* (*Acta Cryst.* (1951), **4**, 324), the refinement being stopped when R reached 21% for the b-axis projection and 29% for the a-axis projection. The structure has now been further refined using the IBM 704 program and three-dimensional data. The R factor dropped from 38% to 22% in three dimensions, with hydrogens included. The hydrocarbon chain is noticeably bent.

Triaminoguanidine hydrochloride, $[C(NH{-}NH_2)_3]Cl$, has space group $P6_3/m$, $a = 7{\cdot}528$, $c = 6{\cdot}253$ Å, $Z = 2$. The central carbon atom is at $(0, 0, \frac{1}{4})$, etc., and the chlorine ion at $(\frac{1}{3}, \frac{2}{3}, \frac{1}{4})$, etc. The structure was solved using Patterson and full and bounded electron-density projections, and was refined by least-square methods. Introduction of individual and anisotropic temperature factors and hydrogen positions resulted in R factors of 8·5% and 12% for the c and a axial projections, respectively. The molecular dimensions and N–H · · · Cl bond system are discussed.

Urea phosphate, $OC(NH_2)_2.H_3PO_4$, crystallizes in space group *Pbca* with $a = 17{\cdot}66$, $b = 7{\cdot}48$, $c = 9{\cdot}06$ Å, $Z = 8$. The structure was solved by R. V. G. Sundera-Rao *et al.* (*Acta Cryst.* (1957) in the Press). A least-squares refinement, carried out on the IBM 704 machine, led to an R factor of 15·8% in three dimensions. The seven available hydrogens are distributed so as to allow nine close approaches in an intricate hydrogen bond network. Sheets of phosphate tetrahedra alternate with sheets of urea ions, and five of the nine hydrogen bonds occur between these layers: one O–H · · · O distance among these is 2·414 Å, and four N–H · · · O separations appear with lengths 2·936, 2·976, 2·983, and 2·159 Å. Of the remaining four hydrogen bonds, two O–H · · · O

separations of 2·603 and 2·659 Å occur in the phosphate sheet, and two N–H · · · O distances of 3·103 and 3·167 Å appear in the urea sheet. Hydrogen peaks are found in a three-dimensional difference synthesis.

The three isomorphous tri-glycine salts have been examined both above and below their ferroelectric Curie points (B. T. Matthias *et al. Phys. Rev.* (1956), **104**, 849; R. Pepinsky *et al., Bull. Amer. Phys. Soc.* (1957), in the Press). The space groups are $P2_1/m$ above the transition points, and $P2_1$ below. The crystallographic constants at 20° C. are:

	Sulfate	Selenate	Fluoberyllate
a (Å)	9·64	9·54	9·59
b (Å)	12·75	12·92	12·75
c (Å)	5·90	5·86	5·70
β (°)	111	110	112
ϱ (g.cm.$^{-3}$)	$1{\cdot}656_4$	$1{\cdot}845_2$	$1{\cdot}631_5$

Weissenberg X-ray patterns at 20 and 90° C. (above and below T_C) were obtained for both the sulfate and fluoberyllate salts. The patterns of the sulfate show very little change in intensities, but the fluoberyllate shows appreciable changes. Introduction of a very small amount of mercaptoacetic acid in place of glycine in the sulfate results in a curious twinning about the c axis. The pure selenate shows stacking disorder along a, immediately above T_C. The structure above the Curie point involves one glycine and the sulfate ion in the mirror plane, and two glycines mirrored across the plane. The structure is maintained by hydrogen bonds. Below the Curie point, the true mirror symmetry is destroyed, although the change is due chiefly to shifts in H positions. It is evident, from the symmetry above T_C, why optically-active amino acids cannot form a related structure.

7·44. L. Brú. *Crystalline structure of* 1-*phenyl*-2-*mercapto*-4-*arabo-tetrahydroxibutylimidazol.*

1 - Phenyl - 2 - mercapto - 4 - arabo - tetra - hydroxibutylimidazol is a substance of great pharmacological interest. Its chemical reactions show an ambiguity which leaves its structural form undetermined and therefore the study of the structure has been carried out by means of X-ray diffraction.

Two different types of crystals are obtained during the process of crystallization, the monoclinic and orthorhombic, both of which are being studied simultaneously.

Monoclinic modification

From rotating-crystal and Weissenberg diagrams about c (Cu $K\alpha$ and $K\beta$) we have found $a = 14{\cdot}78$, $b = 10{\cdot}39$, $c = 4{\cdot}72$ Å, $\beta = 93°\ 31'$; $Z = 2$; space group $P2_1$.

Intensities were estimated by visual comparison with a scale obtained by reflexion from the same crystal. Lorentz and polarization corrections were applied but not an absorption correction owing to the small size of the crystal and its low μ value.

We calculated the Patterson function of the ab projection with the help of the V. Eller's optical machine, having located without difficulty the sulphur atom to which coordinates $x = 0{\cdot}225$, $y = 0{\cdot}00$ were assigned.

Preliminary coordinates confirm the presence of a pyranic ring in the molecule. We are now refining the structure.

Orthorhombic modification

We find $a = 9{\cdot}55$, $b = 12{\cdot}32$, $c = 11{\cdot}45$ Å; $Z = 4$; space group $P2_12_12_1$.

We have established a satisfactory trial structure which proves the presence of the pyranic ring.

§ 8. Proteins and related compounds

8·1. R. E. Marsh. *A refinement of the crystal structure of glycine.*

The crystal structure of glycine (the common, or α, form), which was first determined by Albrecht & Corey in 1939, has been extensively refined on the basis of complete three-dimensional intensity data.

Accurate values for the unit-cell parameters were obtained from Straumanis-type single-crystal rotation photographs; they are, at room temperature: $a_0 = 5{\cdot}1020 \pm 0{\cdot}0005$, $b_0 = 11{\cdot}9709 \pm 0{\cdot}0010$, $c_0 = 5{\cdot}4575 \pm 0{\cdot}0009$ Å, $\beta = 111°\ 42{\cdot}3' \pm 0{\cdot}4'$ (the uncertainties are limits of error). Intensity data were obtained from visual estimates on Weissenberg photographs prepared from molybdenum radiation for the 0–7th layer lines about the a, c, and [101] axes. Nearly 2800 reflections were recorded, of which about 1875 were strong enough to be observed.

The refinement was carried out principally on the basis of three-dimensional difference maps. Individual anisotropic temperature factors were included for each of the five 'heavy' atoms, and hydrogen atom contributions were introduced. The last two stages of refinement were least-squares adjustments of the positional parameters alone. The final R factor was 0·063 for the observed reflections. The resulting parameters lead to the following bond distances and angles:

C_1–O_1	1·252 Å	C_2–C_1–O_1	117·4°
C_1–O_2	1·255	C_2–C_1–O_2	117·1
C_1–C_2	1·523	O_1–C_1–O_2	125·5
C_2–N	1·474	O_1–C_2–N	111·8

The limits of error are estimated to be about 0·005 Å and 0·3°.

The maximum electron densities associated with the hydrogen atoms were obtained from a difference map calculated at a late refinement stage; these positions lead to apparent C–H distances of 0·91 Å and apparent N–H distances ranging from 0·85 to 0·92 Å. All of the bond angles involving these hydrogen atoms are within 4° of tetrahedral.

The hydrogen-bond system is essentially that described by Albrecht & Corey, in which one of the hydrogen atoms on the nitrogen is apparently shared between two adjacent oxygen atoms.

8·2. J. Peterson, L. K. Steinrauf & L. H. Jensen. *The crystal structure of* L-*cystine hydrochloride.*

The unit cell parameters and space group of L-cystine hydrochloride have been determined from appropriate oscillation and Weissenberg photographs. The results follow: $a_0 = 18{\cdot}61$, $b_0 = 5{\cdot}25$, $c_0 = 7{\cdot}23$ Å, $\beta = 103{\cdot}6°$; space group: $C2$, probable.

The structure in projection on (010) has been solved by the method of superposition and refined by successive F_o and ΔF syntheses. R_{h0l} stands at 11·9%. Work is in progress on the projection along [001].

8·3. Y. C. Leung & R. E. Marsh. *The crystal structure of* L-*leucyl*-L-*prolyl-glycine.*

The crystal structure of the tripeptide leucyl-prolyl-glycine 'mono'-hydrate

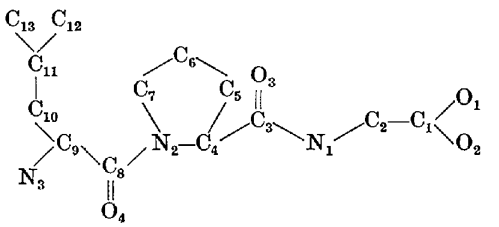

has been determined by Fourier and least-squares analysis of complete three-dimensional intensity data from copper radiation. The crystals are monoclinic; space group $P2_1$; $a_0 = 9{\cdot}44$, $b_0 = 6{\cdot}72$, $c_0 = 12{\cdot}10$ Å, $\beta = 100{\cdot}2°$. The approximate structure was deduced from a three-dimensional Patterson map and from packing considerations. The refinement included individual anisotropic temperature factors for each of the C, N, and O atoms; these were adjusted with the help of three-dimensional difference maps. The final set of positional parameters was obtained from a least-squares treatment of the 1697 observed reflections. The R factor for these reflections is 0·129.

A surprising feature of the structure, as shown on the difference maps, is the presence of only approximately 80% of a water molecule of crystallization per molecule of tripeptide. In addition, the atom C_6 in the pyrrolidine ring of the proline residue is disordered, being located with apparently equal probability about 0·4 Å to either side of the plane of the other four ring atoms.

The final interatomic distances and angles are:

C_1–C_2	1·512 Å	O_1–C_1–O_2	125·4°
C_3–C_4	1·519	O_1–C_1–C_2	118·2
C_4–C_5	1·497	O_2–C_1–C_2	116·4
C_5–C_6	1·514	C_1–C_2–N_1	114·5
C_6–C_7	1·504	C_2–N_1–C_3	122·2
C_8–C_9	1·499	N_1–C_3–O_3	123·2
C_9–C_{10}	1·542	N_1–C_3–C_4	115·3
C_{10}–C_{11}	1·515	O_3–C_3–C_4	121·4
C_{11}–C_{12}	1·510	C_3–C_4–C_5	113·3
C_{11}–C_{13}	1·511	C_3–C_4–N_2	111·2
		C_4–C_5–C_6	106·8
C_3–N_1	1·314	C_4–N_2–C_7	113·3
C_8–N_2	1·339	C_4–N_2–C_8	120·6
		C_5–C_6–C_7	105·6
C_2–N_1	1·454	C_6–C_7–N_2	103·4
C_7–N_2	1·458	C_7–N_2–C_8	126·1
C_4–N_2	1·452	N_2–C_4–C_5	103·7
C_9–N_3	1·492	N_2–C_8–O_4	122·4
		N_2–C_8–C_9	118·6
C_1–O_1	1·262	O_4–C_8–C_9	118·9
C_1–O_2	1·247	C_8–C_9–N_3	107·9
C_3–O_3	1·236	C_8–C_9–C_{10}	111·6
C_8–O_4	1·272	N_3–C_9–C_{10}	111·6
		C_9–C_{10}–C_{11}	117·9
		C_{10}–C_{11}–C_{12}	110·6
		C_{10}–C_{11}–C_{13}	109·4
		C_{12}–C_{11}–C_{13}	109·9

The calculated limits of error are about 0·03 Å and 2·0°. For distances and angles involving C_6, the values are averages of those obtained for the two 'half' atoms—one on either side of the proline ring.

With the exception of a twist required by the presence of the proline residue, the peptide chain is in a highly extended configuration. The molecule exists as the zwitterion, and the maximum number of hydrogen bonds are formed. The water molecule also forms hydrogen bonds, but its presence is not essential to the coherence of the structure.

8·4. R. L. Collin. *An X-ray diffraction study of long-range peptide chain folding in some soluble proteins.*

The X-ray scattering from dry, powdered bovine serum albumin, bovine hemoglobin and bovine insulin has been measured in the angular range of 1–15° 2θ by Geiger-counter techniques with Cu $K\alpha$ radiation and the data have been placed on an absolute scale by measurements at high angles with Mo $K\alpha$ radiation. The scattering in the small-angle region is independent of the exact values of the short distances within a molecule but is strongly dependent both on the large scale folding, or conformation, of the peptide chain and associated side groups and on the packing of neighboring molecules. These effects have been separated and attempts have been made to interpret the scattering in terms of simple models based on a helical folding of the peptide chain backbone. Both the peptide chain and side groups have been assumed to have cylindrical symmetry about the helix axis for the purposes of calculation, and the ordinary formulae for the scattering from cylindrical systems of infinite length have been extended to systems of finite length.

In a systematic investigation of regular, parallel-chain models consistent with known molecular weights, shapes, and sizes for bovine serum albumin and bovine hemoglobin, good quantitative agreement between calculated and experimental intensities could not be obtained.

A method has been devised to calculate the scattered intensity from models of inclined and bent cylinders and cylinders of unequal length. The model is divided up into small, identical, elements and the Debye formula is applied to the distances between elements. The scattering factor for an element is derived from regular models containing parallel cylinders of equal length. This method will give good results for models that do not deviate too much from the regular model that is used to derive the element scattering factor. This method has been programmed for machine calculation and various models for insulin and bovine serum albumin are being studied that are of somewhat greater complexity than parallel chains of equal length.

8·5. R. E. Burge. *The electron diffraction of high polymers.*

The problem of the orientation of high polymers for X-ray analysis does not appear in electron-diffraction work, and electron-diffraction results have been obtained from single crystals of three polymers—poly-L-proline, polyglycine I and polyglycine II. The results from poly-L-proline and polyglycine II are compared with the diffraction expected from current models of these structures, using Fourier transforms calculated with a digital computor (IBM 650) in the region from 0 to 0·8 Å^{-1}. Fourier transforms calculated using X-ray atomic scattering factors $f(\theta)$ are compared with those calculated using the atomic scattering factors for electrons $\varepsilon(\theta)$;

the importance of the scattering from hydrogen atoms in the latter case is discussed. For computational purposes both $f(\theta)$ and $\varepsilon(\theta)$ have been expressed as polynomials (in terms of powers of the radius of a given point from the origin of reciprocal space).

Comparison of the essentially two-dimensional diffraction from single crystals of a form of poly-L-proline which appears on evaporation of an aqueous solution with the calculated Fourier transforms has been used to fix the orientation of the chains with respect to the unit cell edge. In this type of poly-L-proline crystal adjacent chains point in opposite directions though the chain configuration is essentially that found in the dry powder by P. M. Cowan & S. McGavin (*Nature, Lond.* (1955), **176**, 501). As a result of this antiparallel arrangement of chains the space group and unit-cell dimensions are different from those found in the dry powder.

Poly-L-proline in solution has been found by A. Berger *et al.* (*Nature, Lond.* (1956), **178**, 1066) to exhibit a mutarotation, values of the specific optical rotation varying from about $+50°$ to about $-450°$, depending on the solvent. Some preliminary observations on the changes in chain configuration which occur during this mutarotation are reported.

8·6. G. N. Ramachandran. *Structure of collagen and feather keratin.*

The paper presents evidence from different sources that the structure of feather keratin, on the molecular level, is very similar to that of collagen. Accepting the triple-chain structure of collagen, an attempt is made to work out the details of the structure of feather keratin. It is found that the structure put forward earlier by Krimm & Schor is defective in that the calculated density is only about half the measured value. The structure proposed here has some similarity to that suggested by Pauling some years ago. It is in conformity with the infra-red and light-scattering evidence, in addition to being in reasonable agreement with the X-ray diffraction pattern.

8·7. R. Baro, M. Champagne, V. Luzzati & A. Nicolaieff. *La forme et les dimensions de la séralbumine de bœuf, déterminées au moyen de la diffusion des rayons X aux petits angles.*

On a étudié au moyen de la diffusion aux petits angles la variation de forme de la molécule de séralbumine à différents pH. On décrit la technique expérimentale et d'interprétation, qui présente plusieurs modifications des techniques couramment employées.

8·8. [Withdrawn.]

8·9. D. Harker, M. V. King, E. H. Pignataro, M. B. Adelman & T. C. Furnas, Jr. *The shape of the ribonuclease molecule as deduced from nine crystalline modifications.*

When ribonuclease crystals grow from a solution, the crystalline form obtained depends on the composition and pH of the solvent, and on the nature and concentration of added substances. Nine such forms have been prepared in this laboratory, as follows:

I, from 55% 2-methyl-2,4-pentanediol, pH 6·60, 5×10^{-3}M $NiCl_2$; orthorhombic, $P2_12_12_1$, $Z=4$, $a_0=44{\cdot}48$, $b_0=75{\cdot}74$, $c_0=37{\cdot}71$ Å.

II, from 50% tertiary butyl alcohol, pH = 5·0; monoclinic, $P2_1$, $Z=2$, $a_0=30{\cdot}28$, $b_0=38{\cdot}39$, $c_0=53{\cdot}16$ Å, $\beta=105{\cdot}83°$.

III, from 50% normal propyl alcohol, pH = 5·0; monoclinic, $P2_1$, $Z=4$, $a_0=42{\cdot}91$, $b_0=45{\cdot}38$, $c_0=77{\cdot}2$ Å, $\beta=114{\cdot}31°$.

IV, from 67% normal propyl alcohol, pH = 5; hexagonal, $P6_222$, $Z=24$, $a_0=88{\cdot}3$, $c_0=112{\cdot}6$ Å.

V, from 70% 1,3-propanediol, pH = 7; orthorhombic, $C222_1$, $Z=8$, $a_0=31{\cdot}60$, $b_0=61{\cdot}98$, $c_0=121{\cdot}8$ Å.

VI, from 50% tertiary butyl alcohol, pH = 5·2, iodophenol blue added; monoclinic, $C2$, $Z=4$, $a_0=70{\cdot}60$, $b_0=38{\cdot}99$, $c_0=51{\cdot}65$ Å, $\beta=103{\cdot}96°$.

VII, from 55% 2-methyl-2,4-pentanediol, pH = 7·05, 10^{-3}M $NiCl_2$; monoclinic, $P2_1$, $Z=2$, $a_0=46$, $b_0=28$, $c_0=46$ Å, $\beta=102°$.

VIII, from 55% 2-methyl-2,4-pentanediol, pH = 5·57, 10^{-3}M $CuCl_2$; monoclinic, $C2$, $Z=4$, $a_0=58{\cdot}65$, $b_0=53{\cdot}92$, $c_0=43{\cdot}40$ Å, $\beta=119{\cdot}65°$.

IX, from 55% methyl alcohol, pH = 5·0; orthorhombic, $P2_12_12_1$, $Z=4$, $a_0=42$, $b_0=53$, $c_0=46$ Å.

The unit cells and space groups of these crystals are all compatible with an asymmetric unit consisting of a roughly ellipsoidal molecule 30 Å × 30 Å × 38 Å. The different molecular packings depend on the surface charge distributions and on the chemical forces caused by complex formation with ions or small molecules.

The crystal form depends not only on the crystallization medium, but also on the history of the protein sample; this indicates sluggish transformations between slightly different structures of the protein molecule. Some of these transformations can be accelerated by adding suitable substances to the crystallization medium.

8·10. J. D. Bernal & C. H. Carlisle. *Some developments in the structure determination of crystalline monoclinic ribonuclease using the heavy-atom technique.*

The direct structure determination of crystalline (monoclinic) ribonuclease is now being attempted, using the heavy-atom isomorphous-replacement technique to determine the phases of the X-ray reflexions. So far crystals have been grown containing mercury parachlorbenzoate. This protein contains no free sulphydryl groups but there is good reason to believe that mercury atoms occupy specific sites in the crystal. There are two sites per molecule which can be completely filled by further diffusion of the mercury salt into the crystal. The substituted crystals are not truly isomorphous with the normal crystals, for the incorporation of the mercury derivative, as would be expected, has resulted in a displacement of the molecules. It is possible to diffuse the Hg derivatives into the unsubstituted crystal but this lowers its symmetry and the only safe procedure we have found in work of this kind is to grow crystals of the protein with the metal derivative.

The mercury atom positions have so far been located from Patterson difference maps and sharpened Patterson projections, and work is now in hand to check these positions from three-dimensional Patterson studies. It

has been possible to assign phases to some 60 *h0l* reflexions and from these sign determinations two electron-density maps, with and without the mercury atom respectively, have been calculated. The two maps, except for the mercury atom positions, are almost identical—there are minor peak shifts between them which could be attributed to a slight movement of the molecules in the substituted crystal. Naturally, the maps cannot be interpreted in terms of molecular structure but so far they show more detail than any hitherto published projection maps of a protein crystal. It is hoped to check their accuracy through the use of other metal derivatives and to extend it to three dimensions. If the effects of molecular movements can be allowed for, the experimental data already available should suffice for a complete structure determination.

8·11. R. E. FRANKLIN. *X-ray diffraction studies of tobacco mosaic virus.*

Tobacco mosaic virus (TMV) is a rod-shaped virus, of dimensions approximately 150 Å × 3,000 Å. It consists of protein together with approximately 6% by weight of ribonucleic acid (RNA). Highly detailed X-ray fibre diagrams can be obtained from well-orientated preparations of TMV gel.

From a quantitative study of the TMV diagrams alone, the general features of the helical arrangement of the sub-units of the virus protein can be deduced (Watson) and the external morphology of the particle can be determined in some detail.

To make further progress towards the solution of a structure of such complexity, however, it is necessary to use simultaneously a number of different methods of approach. In particular, the TMV diagrams must be compared with diagrams obtained from related substances. The related substances which we have used are: (1) Heavy-atom derivatives of the virus (isomorphous replacement); (2) the repolymerized RNA-free virus protein; and (3) other strains of the virus.

From (1) the signs of the J_0 component of the equatorial scattering were determined and hence, from a comparison with (2), the location of the RNA in the virus particle was established (40 Å from the particle axis). The exact parameters of the helical arrangement of the protein were also determined at this stage (Franklin & Holmes).

Heavy-atom derivatives are now being used to determine *phases* in other regions of the TMV diagram, with a view to obtaining particular *helical projections* of the structure. In this way it should be possible to determine the number and direction of the RNA chains in the particle and, at a later stage, to learn something of the configuration of the virus protein.

8·12. A. KLUG & J. T. FINCH. *X-ray studies on turnip yellow mosaic virus* (TYMV).

TYMV is a 'spherical' virus first isolated some years ago by Markham. Shortly afterwards Bernal & Carlisle obtained X-ray powder diagrams of crystals of TYMV and were able to show that the unit cell was cubic and of side 706 Å, the largest unit cell ever measured.

We have obtained precession photographs of single crystals of TYMV and found the space group to be $F4_13$. The suggestion by the earlier workers that the virus particles are packed in a diamond-type arrangement has been shown to be wrong, and to explain some of the absences it is necessary to postulate that there are 16 virus particles in the unit cell. This has been confirmed by ultra-violet absorption measurements on single crystals. The arrangement of the centres of the particles is thus body-centred cubic, but alternate particles along the cube edge are turned through 90°, leading to the large cell.

The cubic symmetry implies the existence of sub-units in the virus particle. Spikes of strong intensity in reciprocal space have been found and these can be interpreted as indicating that, to a strong extent, the individual virus particles have higher point group symmetry (532) than that required by the space group (23). This work parallels that of Caspar, Crick & Watson on tomato bushy stunt virus.

By means of powder photographs of the nucleic-acid-free protein particles, associated with the virus, we have been able to deduce the probable arrangement of the protein sub-units in the virus particle.

The theory of diffraction by the cubic point groups 23, 432 and 532 has been developed with a view to application to the 'spherical' viruses and objects of a similar kind.

8·13. A. G. MALMON. *Small-angle X-ray scattering studies of catalase.*

Information concerning the size, shape, and hydration of the catalase molecule in solution has been obtained from small-angle X-ray scattering. The scattering curve was determined over an intensity range extending to 6×10^{-4} of the central intensity. The radius of gyration of the molecule is $39{\cdot}8 \pm 0{\cdot}4$ Å. The shape appears to be that of a slightly elongated figure whose length is about twice the average cross-sectional diameter. The electron pair distribution is calculated from the scattering curve and indicates a maximum length of 146 ± 10 Å.

The scattering from catalase solutions for which the solvent density is varied is also described. The intensity is related to the difference between the protein density and the solvent density; thus the protein density may be estimated. The results for experiments using sucrose, glycerine, and sodium chloride to increase the solvent density show similar results. The average electron density of the catalase molecule in solution is 0·425 e.Å^{-3}, which may be compared with 0·441 e.Å^{-3} for the 'dry' molecule. The shape of the scattering curve out to 10^{-2} of the central intensity showed little change, indicating that the shape of the molecule itself was preserved under the conditions of high solvent density. The results are interpreted as indicating that there is considerable internal water of hydration which swells the molecule from its anhydrous configuration.

8·14. D. J. E. INGRAM. *The structural analysis of haemoglobin crystals by paramagnetic resonance.*

This paper describes the structural analysis of haemoglobin and its derivatives by paramagnetic resonance. The investigation of such large organic compounds affords a very good example of the advantages of this technique as compared with normal X-ray methods of crystallographic analysis. The data obtained by the latter are so complex that it is impossible as yet to deduce any details of the haemoglobin molecular structure with certainty.

In contrast, the paramagnetic resonance absorption has no obscuring spectra from the very large number of diamagnetic constituents, and the central iron atom and its immediate surroundings can thus be studied in detail. The large 'g value' variation of 2·0 to 6·0 which is obtained for the 'ionically bound' ferric derivatives affords a very sensitive method for measuring the haem plane orientations, and it has proved possible to determine these to within $\pm 1°$ for the haemoglobin molecule. Although no direct information is secured concerning the other parts of the molecule, further results on the probable packing of the other important groups can be obtained by comparing the precise orientation of the haem planes with the X-ray data. In this way the results of paramagnetic resonance and of X-ray crystallography can be combined to give information that neither would provide by itself.

8·15. W. W. Beeman, P. Geil, M. Shurman & A. G. Malmon. *The internal hydration of macromolecules.*

The diffuse small-angle X-ray scattering from dilute macromolecular solutions is measured as a function of the average electron density of the solvent. The latter is varied by the addition of small molecules, for instance sucrose. By extrapolating to zero scattered intensity the average electron density of the solvated molecule is determined. In general this is less than the electron density calculated from the dry partial specific volume and atomic composition of the macromolecule. The results can be brought into agreement only if the solvated molecule contains an appreciable internal hydration. This is found even for a small protein such as serum albumin.

§ 9. Fibrous structures

9·1. G. Honjo & M. Watanabe. *A study of cellulose fibre by a low-temperature specimen method of electron diffraction and electron microscopy.*

In general the atomic structure in cellulose fibres is damaged very rapidly by the irradiation of electron diffraction and electron microscopy. Thus Preston & Repley reported that electron diffraction pattern by Boersch-le Poole's method can be obtained from cellulose microfibrils in *Valonia* only by reducing very much the irradiating intensity. (Lowering of the accelerating voltage mentioned by them seems to be rather unfavourable, since it increases the interaction of electrons with matter.)

Cooling the specimen improved the situation and made it possible to obtain excellent diffraction patterns. This resulted from the facts that the temperature effects were reduced and the effective specimen area was confined electron-optically to a very small size (Boersch-le Poole's and Hillier's methods).

The diffraction patterns show reflexions up to the 10th layer line with fairly good resolution and contain as many as 200 non-equivalent reflexions ((hkl) and $(\bar{h}k\bar{l})$ reflexions have definitely unequal intensities). On layer lines other than the equatorial a number of reflexions appear with considerable intensity which can be indexed not by the well known Meyer–Misch unit cell but by a superlattice of it having a- and c-spacings twice as large. (It is certain that cooling of the specimen is not responsible for the occurrence of the superlattice structure.) This observation indicates the fact that the relative positions of cellubiose chains along the fibre axis in the structure of cellulose are different from those reported previously. Thus a renewed examination of the structure of cellulose fibre is necessary and the method mentioned here is very useful for it.

9·2. T. Petitpas & M. Oberlin, *Structure de la cellulose* II.

Dans un travail précédent (T. Petitpas & J. Méring, *C. R. Acad. Sci., Paris*, (1956), **243**, 47) la section méridienne de la distribution $P(r, y)$ des distances interatomiques (r, y, projections respectivement horizontales et verticales du vecteur distance ϱ) a été calculée par la transformation de Bessel de l'espace réciproque à symétrie cylindrique déterminé sur les fibres de 'Fortisan' (forme particulièrement bien orientée de cellulose II). La distribution $P(r, y)$ obtenue étant en desaccord avec celle que devrait donner le modèle de chaine de Mayer & Misch, un autre modèle a été proposé pour la cellulose II, plus conforme à $P(r, y)$ expérimentale. Ce modèle est assez proche de celui proposé par Hermans *et. al.* (*Kolloid Z.* (1943) **102**, 169) pour toutes les formes de la cellulose. Il se déduit de celui de Meyer & Misch par la rotation des anneaux autour des liaisons glucosidiques. Mais ce premier travail présente l'inconvénient de n'utiliser que les intensités des *réflexions discrètes*. Il en résulte des pics de distribution trop diffus ainsi qu'un pic à l'origine trop intense et trop large pour qu'il soit possible de mettre en évidence les distances de l'ordre de 1,5 Å correspondant aux liaisons. Ces difficultés apparraissent surtout avec un corps aussi mal cristallisé que la cellulose: en particulier l'opération habituelle de suppression du pic à l'origine devient dans ce cas trop imprécise. On connait les avantages de l'utilisation de la photométrie *continue* pour l'étude des distributions à grande distance (M. Oberlin & J. Méring, *C. R. Acad. Sci., Paris*, (1954), **238**, 1601); elle est plus avantageuse aussi pour les distributions à courte distance car elle fournit réellement une distribution moyenne des distances (au lieu du carré des convolutions de la 'structure moyenne' que fournit l'utilisation des réflexions discrètes). Elle présente aussi l'avantage de permettre la suppression complète du pic à l'origine et de réveler ainsi les pics correspondant aux liaisons.

La photométrie continue de toute la section méridienne du réseau réciproque présentant des difficultés matérielles, nous sommes limités à l'exploration de deux domaines restreints de l'espace réciproque cylindrique: domaine (a) centré sur le plan équatorial et limité par deux plans passant à mi-distance entre l'équateur et la première state; domaine (b) limité par le cylindre de rayon S_m centré sur l'axe de révolution de l'espace réciproque.

Le domaine (a) conduit à la distribution $P'(r)$ des projections sur le plan équatorial des distances entre les atomes espaçés de moins de 10,3 Å (période de la chaine) dans la direction de l'axe de fibre. La contribution des distances entre les atomes appartenant à deux chaines différentes ne se manifeste pas beaucoup dans le domaine de $r < 2$ Å: la partie centrale de $P'(r)$ est pratiquement indépendante de l'arrangement entre les chaines.

Le domaine (b) conduit à la distribution $P(y)$ qui représente la projection sur la direction de l'axe de fibre de la distribution spatiale $P(r, y)$ modulée par le facteur

$J_1(2\pi rS_m)/\pi rS_m$, où J_1 est la fonction de Bessel de premier ordre.

Pour une valeur convenable de S_m, la modulation atténue considérablement la contribution des distances interatomiques de r trop grand et réduit ainsi $P'(y)$ à la contribution prépondérante des distances interatomiques à l'intérieur d'une chaine.

Nous avons obtenu ce résultat en choisissant $S_m = 0{,}186$ Å^{-1}. Les deux distributions $P'(r)$ et $P'(y)$ ont été calculées sur les données photométriques obtenues sur le 'Fortisan' exposé dans le vide à la radiation Mo $K\alpha$ monochromatisée. Les intensités ont été corrigées pour la diffusion incohérente et normées. Les deux distributions expérimentales sont comparées aux distributions synthétiques construites d'après le modèle de Meyer & Misch (Modèle I) et le nouveau modèle (Modèle II). La distribution $P'(r)$ est d'autre part comparée à celle que fournit la cellulose I. Cette comparaison montre nettement le changement de la configuration interne de chaque chaine produite par la mercerisation. La comparaison entre les deux distributions expérimentales et les distributions synthétiques correspondantes conduit à admettre le modèle de chaine II pour la cellulose mercerisée. Le modèle de chaine de Meyer & Misch reste valable pour la cellulose I (naturelle).

§ 10. Order–disorder phenomena.

10·1. D. Evans. *Early aging effects in copper–1·76% beryllium single crystals.*

Matrix reflections from single crystals of Cu–1·76% Be having an initial perfection of 1–1·5 min. of arc were studied by means of the X-ray double-crystal diffractometer as a function of isothermal aging at 200° C. The same area was studied throughout and the half-width was found to increase up to 135 min. of arc (2° 15′) obtained after aging for 11 hr. Further aging up to 27½ hr. gave no additional increase in half-width or decrease in intensity beyond the value obtained after 11 hr. The single crystal was retained when solution heat-treated for 144 hr. at 820° C. and the half-width observed was 27 min. of arc. This value lay between those recorded for 6 and 7 hr. aging at 200° C., suggesting that part of the effects of low-temperature aging is reversible.

X-ray micrographs were recorded throughout and show interesting details of the matrix reflection during aging. They also reveal that the initial condition of the 'as quenched' specimens contains substructure.

10·2. P. A. Giguère. *Sur la capacité calorifique anomale de la glace.*

On compare la capacité calorifique de la glace avec celle du peroxide d'hydrogène solide et on montre que la première a des valeurs exceptionnellement grandes aux températures inférieures à 60° K. On calcule ensuite la capacité calorifique de ces deux solides en fonction de la température d'après le modèle d'Einstein et en se servant de données récentes sur les spectres de vibrations du cristal. De ces résultats il ressort que la capacité calorifique de la glace croît encore de façon exagérée en approchant du point de fusion. Ces deux anomalies doivent provenir de désordre dans la structure cristalline de la glace, tel que révélé par d'autres phénomènes.

10·3. J. Longuet-Escard & M. J. Méring. *Détermination directe, aux rayons X, des éléments statistiques, caractérisant l'empilement desordonné des particules d'hydroxyde de nickel.*

Le travail exposé est un exemple d'interprétation de la forme des pics de diffraction diffus, dans le cas où cette forme est conditionnée à la fois par les dimensions limitées des particules, et par les défauts de périodicité. La méthode de B. E. Warren & B. L. Averbach (*J. Appl. Phys.* (1950), **21**, 595) est inapplicable aux réflexions $00l$ de Ni(OH)^2 colloïdal, ces réflexions étant irrationnelles. Ce caractère irrationnel signifie qu'à côté des espacements élémentaires normaux ($d_{00l} = 4{,}6$ Å), il existe d'autres espacements (anormaux), présentant une *forte* différence avec les précédents. Heureusement, la substance peut être orientée par sédimentation, ce qui permet de déterminer avec précision la forme, la position et l'intensité de cinq réflexions $00l$ irrationnelles. On peut donc tenter de résoudre le problème par la voie directe en interprétant la transformée de Fourier $P(z)$ de la fonction d'interférence $G_{00l}(s)$ constituée par *l'ensemble* des cinq 'réflexions' irrationnelles normées ($G(s) \sim I(s)/|F^2(s)|$, $s = 2 \sin\theta/\lambda$).

Le travail peut se résumer ainsi:

(1) Les bandes *hkl*, transposées dans le réseau réciproque, conduisent à un ensemble de lignes *hk* identiques; le long ce chaque ligne, la fonction d'interférence G_{hk} est périodique de période égale à 1/4,6 Å^{-1}. La transformée de Fourier des G_{hk} conduit à la statistique des épaisseurs des paquets de couches ordonnées, chaque paquet constituant ce que nous appellerons particule primaire. Soit p_N cette statistique (N = nombre de couches élémentaires par particule primaire). Sa détermination ayant été décrite précédemment (J. Longuet-Escard & J. Méring, *J. Chim. Phys.* (1954), **51**, 440), dans le cas présent on peut la considérer comme une donnée du problème.

(2) La détermination expérimentale de G_{00l} est assez précise, mais comporte deux lacunes.

(*a*) Le 'fond' de G, dans les régions comprises entre deux 'réflexions' successives, échappe à la mesure par suite de la superposition des bandes *hk* (l'orientation de la substance est loin d'être parfaite). Ce fond ne contribue à la transformée $P(z)$ qu'au voisinage de l'origine, mais du fait de son omission la transformée $P(z)$ obtenue n'est pas réellement normée.

(*b*) Le maximum $G_{000}(s)$ échappe à l'expérience par suite de l'interférence entre les faisceaux diffusés par un grand nombre de particules. Le domaine interférant du centre de réseau réciproque est considérablement plus grand que celui qui intervient dans les autres réflexions. Il en résulte une diffusion aux petits angles pratiquement négligeable. C'est d'ailleurs à cette difficulté que répond la méthode de Warren & Averbach. Dans le cas présent, l'absence de G_{000} conduit à l'indétermination du zéro de la transformée $P(z)$.

(3) La transformée $P(z)$, calculée dans les conditions indiquées, présente une succession de maxima aux valeurs de z qui sont des multiples entiers de l'espacement normal 4,6 Å: ce sont des maxima normaux. A côté de ces maxima, on observe des maxima anormaux, mêlés aux maxima secondaires dus à l'interruption de $G_{00l}(s)$ à la valeur de $s = 1{,}2$. On vérifie d'ailleurs immédiatement que la forme des pics normaux est exactement celle qu'on calcule en tenant compte de cette limitation de s. Compte tenu de cette remarque, on peut calculer aisément tous les pics secondaires; leur soustraction de $P(z)$ expérimental laisse

subsister les pics anormaux réels. La même opération permet de fixer partout le zéro de la transformée, et de lever ainsi la difficulté (*b*) du paragraphe précédent. Le procédé utilisé joue un rôle analogue à celui de la série des différences, dans l'analyse des structures. Les pics anormaux représentent un espacement élémentaire de 12,8 Å, ce qui correspond approximativement à l'encombrement d'une double couche d'ions Cl^- emprisonnés entre deux particules primaires (l'hydroxyde étudié a adsorbé des ions Cl au cours de sa préparation) (O. Bagno & J. Longuet-Escard, *J. Chim. Phys.* (1954), **51**, 434).

(4) La loi de décroissance des pics normaux de $P(z)$ est plus lente que celle obtenue à partir des bandes *hkl*. Cela révèle l'existence d'un second type de défauts dans l'empilement: Les particules primairés peuvent aussi s'empiler sans emprisonnement d'ions, donc sans espacement anormal, mais avec un glissement arbitraire dans le plan des couches. La loi de décroissance des pics normaux permet d'estimer que les particules s'accolent par groupe de deux, et de calculer qu'environ la moitié des surfaces d'accolement emprisonne les ions.

(5) Sur la base de cette estimation et de la statistique de p_N du paragraphe (1), on peut recalculer la forme de $P(z)$, et cette distribution synthétique est en bon accord avec celle donnée par l'expérience. Cette comparaison permet de normer la transformée $P(z)$ expérimentale.

Le travail exposé est une contribution à l'étude de la cinétique de la croissance cristalline, qui fait intervenir le mécanisme de fusionnement entre les particules primaires. Ce mode de croissance est caractéristique du vieillissement des gels d'hydroxyde.

10·4. G. Fournet. *Prévisions de la température de Curie pour différents types de réseaux.*

A partir de la théorie des phénomènes coopératifs de Yvon modèle d'Ising nous avons pu déterminer l'équation (*C*) régissant la température de Curie. Cette équation, exacte et absolument générale, se présente sous forme d'un développement illimité dont la structure dépend du type de réseau cristallin étudié. Nous avons établi la règle de calcul de chaque terme.

Pour les réseaux suivants: carré plan, triangulaire plan, cubique simple, cubique centré, cubique faces centrées nous avons calculé les quatre premiers termes de l'équation (*C*). Une extrapolation effectuée sur les trois solutions correspondantes à l'emploi de deux termes, trois termes et quatre termes de (*C*) permet d'obtenir de très bonnes valeurs des températures de Curie. Ces valeurs sont les meilleures approximations déterminées pour les réseaux carré plan et triangulaire plan pour lesquels la solution exacte est connue; nous pensons qu'il en est de même pour les autres types de réseau pour lesquels les solutions exactes ne sont pas connues.

10·5. St. Hafner & F. Laves. *Lage und Intensität der Ultrarotspektren von Alkalifeldspäten und sauren Plagioklasen in Abhängigkeit der chemischen Zusammensetzung und der* Al/Si-*Ordnung/Unordnung.*

Die Ultrarotabsorption wurde von 7μ bis 25μ gemessen. Ausgehend von natürlichem Mikroklin und Albit (bzgl. Al/Si geordneter K- und Na-Feldspat) wurden durch kurzfristiges Erhitzen gepresster Pulvergemische 9 gleichmässig über den Konzentrationsbereich verteilte Mischkristallglieder der Mikroklin–Albit-Reihe hergestellt. Die Lage und Intensität der registrierten Spektren ändert sich kontinuierlich, aber nicht linear. Die Variation der Spektren wird verglichen mit der Variation der Gittergeometrie in dieser Mischkristallreihe. Die Spektren werden weiterhin verglichen mit denen von solchen Feldspäten, deren Al/Si-Verteilung durch langdauerndes Erhitzen ungeordnet gemacht wurde. Es wird diskutiert, wie die Ergebnisse dazu benutzt werden können, über die Zustände in der Natur vorkommender Feldspäte Aufschluss zu erhalten.

10·6. K. Dornberger-Schiff. *On symmetry in structures with stacking disorder (order–disorder structures) consisting of layers of one kind only.*

It has been shown previously (K. Dornberger-Schiff, *Acta Cryst.* (1956), **9**, 593), that in a number of structures with stacking disorder neighbouring layers have the same relative position throughout the structure and that in these cases the disorder arises from the fact that this relative position may be realized in more than one way. For such structures the name OD-structures (order–disorder structures) was proposed.

Symmetry operations* in such structures will, in general, bring only part of space into coincidence with either itself or another part of space. They will be called 'partial symmetry operations'. The complete set of partial symmetry operations of a structure forms a groupoid as defined by H. Brandt (*Math. Ann.* (1926), **96**, 360.†

Structures consisting of the same kind of layers with the same relative position of pairs of neighbouring layers and differing only in the precise way of stacking form a 'family of OD-structures'. Correspondingly, the groupoids describing their symmetry form a 'family of groupoids'.

To each family of groupoids there is a characteristic distribution of sharp points and diffuse rods in reciprocal space and of systematic absences which can be deduced from the partial symmetry operations present.

OD-structures may be characterized as complying with three conditions (or postulates). OD-structures consisting of layers of one kind belong to three categories. The method of obtaining a list of groupoid families is to be described elsewhere.

10·7. J. W. Gryder, G. Donnay & H. M. Ondik. *Disorder in the crystalline ultraphosphate* $Na_2P_4O_{11}$.

The compound reported by E. J. Griffith (*J. Amer. Chem. Soc.* (1956), **78**, 3867) as $Na_2H_2P_4O_{12}$ is found to consist of two crystalline forms. Single crystals were studied using rotation, Weissenberg and precession cameras with Cu $K\alpha$ (λ = 1·5418 Å) and Mo $K\alpha$ radiations. Form I, comprising about 10% by weight, consists of crystals of thick tabular habit and average dimensions 0·3 × 0·05 × 0·02 mm. They are monoclinic, elongated

* This term is used in its wider sense covering translations also (as the German term *Deckoperationen*).

† Brandt's groupoid is a generalization of the notion of the group. Not for each ordered pair of elements is a product defined; there are several 'unit elements'; to any given element there exists one particular 'left unit' and one particular 'right unit' which, in general, are not equal. To each element there exists an inverse element. Composition is possible, if the right unit of the left factor is identical with the left unit of the right factor. The composition of elements, as far as defined, is associative.

[010], with $a = 30{\cdot}01$, $b = 6{\cdot}77$, $c = 7{\cdot}09$ Å, all $\pm 0{\cdot}5\%$, $\beta = 92° 21' \pm 10'$, $V = 1439$ Å^3. A pronounced pseudo-repeat $a' = \frac{1}{2}a$ is evident. The space group is uniquely determined as $P2_1/a$. Only the forms {100} and {001} are observed, the larger faces being those of {100}. Cleavage is fibrous along b and for this reason good single crystals are difficult to obtain.

Form II, the bulk of the material, consists of thin-to-thick rectangular plates which grow up to 5 mm. in length. Only cleavage fragments can be removed from the matrix of the melt, and morphology, therefore, gives no clue concerning point-group symmetry. Cell dimensions are: $a = 18{\cdot}74$, $b = 14{\cdot}79$, $c = 7{\cdot}03$ Å, all $\pm 0{\cdot}3\%$, $\beta = 90° 0' \pm 5'$, $V = 1948$ Å^3. The space group is $B2/a$ or Ba, with pronounced pseudo-space-group $Bmam$, $Bma2$, or $B2am$. Three cleavages are observed: {100}, very easy and very good; {010}, easy and fairly good; {110}, fairly easy and good. They yield platy to fibrous fragments. Even optically the crystals are markedly pseudo-orthorhombic, with $\alpha = b$, $\beta = a$, $\gamma = c$ and $n_\alpha = 1{\cdot}485 \pm 0{\cdot}005$, $n_\beta = 1{\cdot}510 \pm 0{\cdot}005$, $n_\gamma = 1{\cdot}545 \pm 0{\cdot}001$ (determined by J. D. H. Donnay). Rotation patterns about the c axis show all odd layer lines as diffuse streaks whereas the even layer lines consist of sharp reflections. The intensity distribution within the streaky layer lines varies from crystal to crystal. Precession patterns show that all reflections with l odd are diffuse circular discs normal to the c^* axis.

The two forms are intimately intergrown so that the observed density ranges from 2·34 to 2·62 g.cm.$^{-3}$. Form II is the less dense of the two. Assuming 2·34 g.cm.$^{-3}$ for its density and 8 formula units per cell, we obtain the formula $Na_2P_4O_{11}$. In the structure that we consider most likely, rings of four phosphate tetrahedra are linked into chains parallel to c by the sharing of an oxygen between adjacent rings. Our hypothesis is supported by the following observations and reasoning. The four cleavage planes intersect in the c axis. The optical character is positive and the acute bisectrix is directed along c. The observed very slow rate of solution is explained if hydrolysis is a necessary first step in the dissolution of chains. The principal product of hydrolysis at pH ~ 7 is tetrametaphosphate, as is to be expected if hydrolysis occurs between rings. When the compound is treated with 6 f NaOH a viscous, plastic mass is formed. In basic solution ring phosphates hydrolyze much more rapidly than chain phosphates, so that, in our compound, the probability of breaking rings becomes comparable to that of breaking chains, and polyphosphate chains of varying lengths should form. They are known to form plastic aggregates. The ring dimensions determined by C. Romers *et al.* (*Acta Cryst.* (1951), **4**, 114) are such that eight rings can be accommodated in the cell, with the plane of the ring parallel to (100). The cell height, 7·03 Å, approximates the height of one ring. The diffuseness of the reflections with l odd can be accounted for by displacements of randomly chosen chains, parallel to the c axis through a distance of $\frac{1}{2}c$.

§ 11. Deformations and imperfections

11·1. A. J. C. Wilson. *A note on the line profiles associated with mistakes.*

Mistakes at random, as considered by A. J. C. Wilson (*Proc. Roy. Soc.* A (1942), **180**, 277; (1943), **181**, 360), and C. H. MacGillavry & B. Strijk (*Nature, Lond.* (1946), **157**, 135; *Physica*, (1946), **11**, 369; (1946), **12**, 129) lead to a Laplacian dependence of $J(t)$ on t, and so to a Cauchy line profile. Though the predictions of this model are in qualitative agreement with experiment, the detailed form of $J(t)$ is not confirmed. In particular, $J(t)$ is rounded and has zero slope at $t = 0$, instead of exhibiting a cusp, and the general shape of the curve is Gaussian (MacGillavry & Strijk, *loc. cit.*; I. G. Edmunds & R. M. Hinde, *Proc. Phys. Soc.* B (1952), **65**, 716; H. Steeple & I. G. Edmunds, *Acta Cryst.* (1956), **9**, 934). Rounding of the $J(t)$ curve would result from the accumulation of experimental errors, but the distortion from the Laplacian form towards the Gaussian seems too great to be attributed to experimental errors alone.

The model of mistakes at random is tacitly based on crystallization (or structure transformation) starting at one place and proceeding with occasional mistakes. If structure transformation begins in many places (nucleation) and the nuclei grow until they meet, the mistakes no longer occur at random, but their positions are correlated in a way that alters the form of $J(t)$ from the Laplacian. Models of this kind were investigated in some detail by L. Landau (*Phys. Z. d. Sow. Union*, (1937), **12**, 579) and E. Lifschitz (*Phys. Z. d. Sow. Union*, (1937), **12**, 623), but their work has not been properly taken into account in later developments.

11·2. V. I. Iveronova. *Distortion of crystal lattice in solid solution.*

The values of the mean square static displacement of atoms were calculated by means of the elastic model of solid solution. A comparison of the results of calculations with the experimentally measured values of $U^2_{st.}$ are given. The values of $U_{st.}$ determined experimentally agree in order of magnitude with the calculated values; however, the theoretically required proportionality in the difference of atomic radii is not observed. An analysis of the probable causes of this divergence is given. The most essential must be the comparison of the values of the mean square displacements with the short-range order, determined according to the intensity of the background of the X-ray pattern.

The dependence of the value of the mean square static displacements was studied in different alloys by different authors. For low concentrations all the curves show a linear dependence of α on concentration, which agrees with the calculations carried out on the ground of the elastic model. A saturation of the value of the mean square static displacements is observed at high concentrations; for Ni–Fe alloys the outline $\alpha = f(c)$ was obtained, which does not coincide with the theory. It was shown that in this case the values of $U^2_{st.}$ determined from X-ray patterns, with Mo and Cu radiation do not show mutual agreement. The picture observed is explained by the influence of primary extinction.

A curve of the dependence of the Debye temperature upon concentrations was deduced for Ni–Fe alloys. Using Cu_3Au and Ni_3Fe alloys, the dependence of the Debye temperature upon the long-range order was shown. The Debye temperature of the ordered solid solution was found to be lower than that of the disordered one.

11·3. С. Терминасов и В. Ф. Миндукшев. *Аннотация доклада. Рентгенографическое исследование искажений структуры металлов при статическом и динамическом сжатии в условиях комнатной и ниэкой температур* .

В работе описаны результаты рентгенографического исследования образцов дуралюминия и меди, подвергнутых статическому идинамическому сжатию при комнатной температуре и в жидком азоте.

Показано, что меньшая величина искажений кристаллической структуры исследуемыs металлов, имеющая место при динамическом сжатии по сравнению со статическим, об »ясняется влиянием »теплового отдыха«.

Деформирование металлов при низкой температуре вызывает значительное уменьшение влияния теплового отдыsа и при этом картина искажений решетки динамически деформированных металлов оказывается близкой к той, котораяимеет место при етатической деффрмации тех же металлов в условиях комнатной температуры.

При деформировании металлов в условиях низкой температуры происходит большее дробление кристаллических блоков и возникают большие кристаллитные искажения по сравнению с тем, что имеет место при деформации металлов в условиях нормальной температуры.

11·4. J. Umanskij, V. Yelutina, A. Kagan, L. Pivovarov. *X-ray investigation of changes in Micromosaics occurring during disintegration of supersaturated solid solutions.*

Disintegration of supersaturated solid solutions, as shown by means of X-rays, is followed by changes in mosaic structure, maximum hardness corresponding to minimum size of mosaic blocks.

A study of the disintegration of supersaturated solid solution of tungsten carbide in titatium carbide carried out by one of the authors showed that this process in its early stage is accompanied by an increase in the intensity of the (200) diffraction line of the solid solution. This increase could only be interpreted as caused by a decrease in the size of mosaic blocks of titanium carbide due to the influence of particles of precipitating phase. A similar increase of intensity was observed by other investigators after decrease of block dimensions caused by plastic deformation.

In the present investigation this assumption was studied on Ni–Be and Cu–Be alloys containing 2·28% and 2·40% Be respectively. Nickel content in the latter alloy was about 0·37%.

The intensity of the (111) diffraction line was measured. It was proved that the disintegration of solid solution after an isothermal annealing of quenched Ni–Be alloys at 630° C. and a similar annealing of quenched Cu–Be alloys at 250 and 320° C. is followed in its early stages by an increase in the intensity of this diffraction line. The corresponding curve for Ni–Be alloy has a sharp maximum after 10 min. annealing at 630° C., that for Cu–Be alloy has a sloping maximum after 10 hr. annealing at 320° C.

Calculations based on the equation $I'/I = th(nq)/nq$ (i.e. taking into account only primary extinction) gave the data in Table 1 for dimensions of mosaic blocks at various break-up stages.

Minimum dimensions of solid solution micromosaic correspond in both cases to maximum hardness. Coagulation of the precipitate leads to an increase in size of the blocks with corresponding decrease in hardness. According to the hypothesis suggested by one of the authors age-hardening is caused to a great extent by the decrease in the size of solid-solution blocks, whereas the decrease of hardness after over-aging is due to their coagulation.

Table 1. *Hardness and block dimensions of heat-treated alloys*

	Block dimensions			Vickers hardness		
	As quenched	Minimum	Over-aged	As quenched	Maximum	Over-aged
Ni–Be	1·2	0·3*	1	170	310*	260
Cu–Be	0·7	0·2†	0·5	100	380†	230

* 10 min. † 15 hr.

11·5. A. B. Wing, J. W. Davisson & P. L. Smith. *The correlation of optical and X-ray studies of imperfections in crystals.*

A study of the variations in the imperfections of a series of pure and doped alkali halide boules has involved the correlation of several X-ray, optical and etching techniques. Misorientation effects were largely isolated by comparing Wooster X-ray topographs with collimated-beam Honeycombe patterns, and X-ray reflecting-power variations were examined by comparing stepwise photographs through the Bragg reflecting region with both localized and overall Geiger-counter spectrometer measurements. The interpretation of results depended on the features detected optically in light topographs, by spot scanning for curvature, by oblique illumination of microscopic misorientations, and by metallograph records of etch-pit array, dislocation networks and fine cleavage steps. A special new etchant was found for the KCl specimens, which do not respond well to the usual etchants. Experimental and theoretical developments suggest that there is an additional factor in X-ray extinction which depends on alteration of the atomic X-ray scattering efficiencies at low angles through changes in the outer electron configurations of atoms lying in the dislocation network associated with the more mosaic crystals.

11·6. D. W. Pashley & J. W. Menter. *The observation of dislocations and their motion in the electron microscope.*

The paper describes the work of a group studying the changes which occur in the microstructure of a metal as it undergoes plastic deformation. The experimental work has been carried out mainly on the Siemens Elmiskop I. Three techniques for revealing the presence of dislocations have been employed: (1) diffraction contrast associated with the strain field, as previously used by Hirsch, Whelan & Horne; (2) direct lattice resolution, as developed by J. W. Menter (*Proc. Roy. Soc.* A (1956), **236**, 119); (3) indirect lattice resolution via moiré patterns.

Uniform and coherent single crystals of gold of 200 Å and upwards in thickness have been prepared by a special evaporation technique. Dislocations are made visible on the images of these specimens, as a result of the diffraction contrast. When the specimen is illuminated by the fine-focus condenser of the electron microscope, the localized heating causes the dislocations to move. This motion has been studied by: (*a*) visual observation of the fluorescent screen; (*b*) examination of sequences of still photographs; (*c*) cine photography. The specimens have

been studied also by selected-area electron diffraction and the formation of dark-field images. A description of the dislocation motions is given.

The gold films have been annealed in a controlled manner, and the formation of regular arrays and networks of dislocations has been studied. A furnace has been constructed to allow this annealing to be carried out whilst the specimen is under observation in the electron microscope.

A further apparatus has been built to allow the gold films to be put under tension whilst under observation in the electron microscope. This apparatus permits the observation of controlled plastic deformation, and the study of the resultant dislocation motions. Results are also given for the effect of the propagation of cracks through the films.

The investigation of the possibility of directly resolving the lattice planes in a metal has continued (see Menter). Although the resolution obtained for this purpose has now been reduced to below 6 Å, and includes the resolution of lattice planes in molybdenum oxide, this is still not sufficient. In the meantime, a number of dislocation features has been noted on the resolved lattices of some metal phthalocyanines. These are described.

It has been found possible to resolve the planes of a metal lattice by an indirect method. A composite film of two parallel oriented single-crystal metal films is prepared, and an electron microscope image of the moiré pattern is obtained. This moiré pattern may be regarded as representing the regions where the two lattices superpose on one another, and effectively represents a magnified image of the lattice planes in the two lattices. It is shown both by deduction and by means of a two-dimensional optical analogue that imperfections in the lattice of either metal will appear magnified in the moiré pattern. Thus numerous cases of edge dislocations have been photographed, so that the associated extra plane is clearly visible in the moiré pattern. Many other more complicated dislocation features are found also.

Thus this new technique allows the movement of dislocations to be studied via the observation of the movements which occur in the lattice planes themselves. Experiments are in progress to allow such movement to be observed when the specimen is heated, both by the electron beam and in a specimen furnace, as well as by controlled mechanical deformation.

11·7. E. W. Müller. *Field ion microscopy of metal surfaces.*

If a field emission microscope is operated with helium ions and if the tip is cooled by liquid hydrogen, a resolution sufficient to resolve completely the surface lattice of high-index net planes is obtained (E. W. Müller, *J. Appl. Phys.* (1956), **27**, 474; (1957), **28**, 1). On favorable locations of the crystal surface even adjacent atoms of about 2·7 Å distance can be seen separately (Fig. 1). The structure of the metal surface as obtained by annealing in high vacuum is not very perfect in as much as there are a large number of kinks along the lattice steps due to frozen-in thermal disorder. Only the low-index net planes are well developed, like 011 and 112 on W and Mo, and $10\bar{1}0$ and $11\bar{2}2$ on Re, while no high-index planes appear. Perfect crystal surfaces of approximately hemispherical shape of radius 1000 Å containing a large number of net planes with indices as high as 531 or

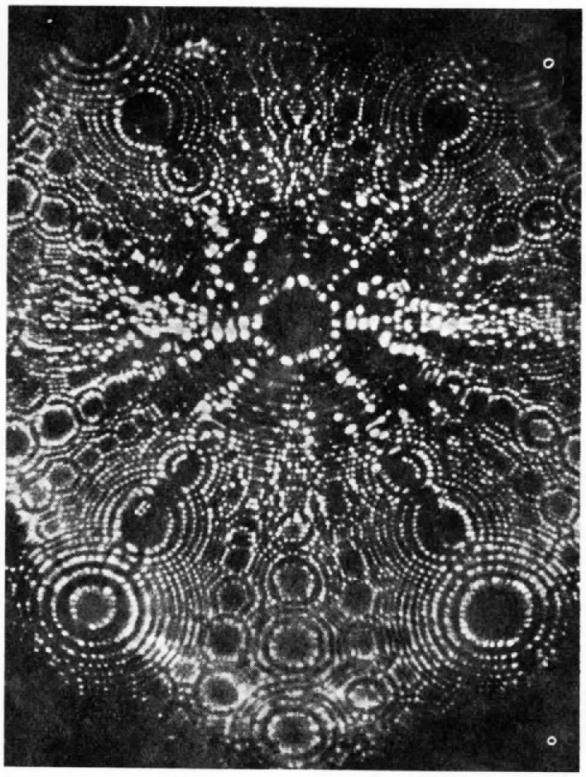

Fig. 1.

342 can be produced by field evaporation (E. W. Müller, *Phys. Rev.* (1956), **102**, 618). This is done on tungsten at or below room temperature with applied fields of about $520–550 \times 10^6$ V.cm.$^{-1}$, and on other refractory metals at slightly lower fields. As long as the low temperature and the high field are maintained, these surfaces remain in perfect condition of cleanliness; not even one foreign atom can be adsorbed during hours. Changes can be produced by bombarding with fast particles. The recovery of the damage to the lattice by annealing or by moving the disturbance out to the surface by the stress of a high field can be studied in atomic details.

Since a field strength of about 400×10^6 V.cm.$^{-1}$ is required to produce helium ions at the surface, the specimen is under a stress of 10^6 lb.in.$^{-2}$; therefore only metals of high strength can be observed. Of adsorbed matter, probably only chemisorbed oxygen is bonded strongly enough to stay at the surface, and is thus accessible for observation. The softer metals and less strongly bonded adsorption layers can be observed when the field ion microscope is operated with other gases, preferably hydrogen, which requires only half the field strength. However, even at liquid-hydrogen temperature the resolution is considerably less than with helium ions, practically about 4·5 Å, as can be seen by observing the same specimen with both kinds of ions.

11·8. P. B. Hirsch, R. W. Horne & M. J. Whelan. *Electron microscope observations of dislocations in metals.*

Dislocations can be revealed directly in thin metal foils by transmission electron microscopy. The arrangement and movement of dislocations have been studied

in a number of metals. Foils about 0·1 mm. thick are thinned by electropolishing or etching to a thickness of $\sim$ 1000 Å. The contrast at the dislocations is due to their strain field, which causes them generally to diffract more strongly than the surrounding crystal. In slightly deformed polycrystalline austenitic stainless steel the dislocations are found to be piled-up against grain boundaries. Many of the pile-ups are intersected by dislocations on other planes forming networks. The dislocations are pinned at the metal–oxide interface, and stresses $\mu/1000$ (μ = shear modulus) are necessary to move the dislocations. This and other results lead to an explanation of the reported high strength of thin metal foils. The stresses can be estimated from the curvature of the dislocation lines, and are large enough to drive the partial dislocations apart, leaving wide stacking faults. The stacking fault energy is estimated to be $\sim$ 15–20 ergs.cm.$^{-2}$. Dislocations are observed to cross-slip through twin boundaries, and these latter also appear to contain Frank–Read sources. Certain observations suggest that twins or thin lamellae of hexagonal phase are produced by a cone-source of partial dislocations. Dislocations are observed to nucleate near thin edges of the foil at comparatively low stresses. Some of these effects have been recorded on ciné film, which will be shown.

11·9. W. W. Webb, R. D. Dragsdorf & W. D. Forgeng. *Observations of dislocations in whiskers.*

It is commonly believed that the filamentary crystals of exceptional strength called 'whiskers' are devoid of dislocations, except possibly for one axial screw dislocation. Eshelby has shown that an axial screw dislocation should produce a lattice twist around the whisker axis that is measurable in sufficiently small whiskers. High-resolution X-ray methods have been developed sufficiently to detect a lattice twist one-twentieth that expected in typical whiskers. In some whiskers, no twist has been detected; in others quite large lattice twists are evident. Calculations suggest that two parallel screw dislocations of opposite Burger's vector would be sufficiently stable to provide lattice steps on the surface necessary for growth but that they would not necessarily produce a lattice twist. This two-dislocation model suggests also the possibility of dislocation-free whiskers since the two screw dislocations are capable of self-annihilation by combination. In some whiskers, X-ray diffraction evidence suggests that more complex dislocation configurations may be present. Electron stereomicroscopy, optical microscopy on polished cross sections, specular reflection from lateral surfaces, and various etching techniques have been used to observe the morphology of whiskers, particularly to search for evidence of lattice imperfections. For example, palladium whiskers, which appear perfectly uniform under the light microscope, were found to be irregularly twisted ribbons by electron stereomicroscopy.

11·10. R. D. Lowde & H. H. Atkinson. *Small-angle scattering of neutrons from deformed metals.*

Small-angle scattering from super-pure polycrystalline specimens of Cu and Al, respectively 0·6 and 5 cm. in thickness, has been measured using a Bi-filtered cold neutron beam of purity 99·9% and mean wavelength 8·7 Å. The differences between the cross-sections in millibarns steradian^{-1} atom^{-1} of deformed and recrystallized specimens for scattering into the angular range 2–12° were: Cu (90% cold-rolled) $2{\cdot}0\pm0{\cdot}8$; Cu (extended 60%) $1{\cdot}6\pm0{\cdot}8$; Al (extended 60%) $< 0{\cdot}05$. Less than 1% of the scattering of 1·54 Å X-rays observed by J. Blin is due to small voids or dislocations (*Phil. Mag.* (1957), **2**, 589). If attributed to the scattering from dislocations, our observed magnitudes are to be expected for a dislocation density of 10^{11} cm.$^{-2}$ in Cu and $\lesssim 10^{10}$ cm.$^{-2}$ in Al (to be published). With specimens fatigued (by push pull) to fracture in $\sim 5\times10^5$ cycles, the increase in scattering cross-section was $< 1{\cdot}0$ for Cu and $< 0{\cdot}05$ for Al. These results set an upper limit to the size and concentration of any small voids which may be supposed to exist in fatigued Cu and Al.

11·11. H. Wilman. *The lattice orientation at metal surfaces after unidirectional abrasion or scraping.*

In connexion with investigations of wear (with V. D. Scott, J. Goddard & H. J. Harker) we have used electron diffraction to study the surface structure caused by abrasion (on 0000 or 000 emery paper for 5 strokes 10 in. long, at 2–3 kg.cm.$^{-2}$ pressure and about 25 cm.sec.$^{-1}$) on polycrystalline metals having hexagonal (Be, Zn, Ti, Zr), face-centred cubic (Cu, Ag, Au, Pt) or body-centred cubic (Fe, Mo) structure.

On Be the immediate surface regions showed Be crystals orientated with the [001] axis lying in a plane which was normal to the metal surface and parallel to the abrasion direction, but the [001] axis was inclined away from the specimen normal towards the direction from which the abrasive particles came, by an angle varying from about 10° to 20° in different experiments. The main azimuthal orientation was with a {100} plane (containing the slip direction $\langle 100\rangle$) parallel to the abrasion direction, agreeing with Courtel's observations (1949) on Mg. The diffraction patterns showed, however, that an azimuthal spread of more than $\pm30°$ occurred round the [001] axis. This azimuthal spread appears to correspond to rotational slip on (0001), from the main orientation, due to the torsional effects of the heterogeneously applied stresses. Similar results were observed on various abraded faces of Be crystals, but with δ sometimes as high as 40° or more. In all cases etching soon revealed the extensive underlying rotationally-disoriented layer of the type shown by Evans, Layton & Wilman (1951), and Agarwala & Wilman (1954, 1955).

On the face-centred cubic metals the results were similar in nature to those from the Be, but here the main orientation was with a {110} plane normal to the surface and parallel to the abrasion direction, and in this plane the $\langle 1\bar{1}0\rangle$ direction was inclined backward by an angle δ varying from about 5° to 15° (20° in the case of Au). At first sight the diffraction patterns suggested an extensive azimuthal spread about this $\langle 1\bar{1}0\rangle$ axis, but closer inspection indicates rather azimuthal spreads round the respective $\langle 111\rangle$ axes of this main orientation, thus indicating rotational slip on the {111} planes. Finer abrasion of Au, using fine alumina, gave similar results but with δ reduced to 8–10°.

On the body-centred cubic Fe and Mo, a (111) plane was parallel to the abrasion direction and normal to the surface (as Courtel (1949) found for Fe), but a $\langle 1\bar{1}0\rangle$ direction was tilted back by an angle δ varying from about 8° to 10° in different experiments. The rotational

nature of the spread from this main orientation is being studied.

Uncertainty of interpretation of the results in relation to the form of the metal surface, due to the simultaneous effects of many abrasive particles, was avoided by studying also the surface structure of metals scraped with the atomically straight ⟨100⟩ edge of a silicon carbide crystal, which was found to yield results closely similar to those from abrasion.

11·12. S. Weissmann. *Study of the fine-structure of recrystallized, polycrystalline aluminum by X-ray microscopy and diffraction analysis.*

A method combining X-ray microscopy and diffraction analysis which was recently developed (S. Weissmann, *J. Appl. Phys.* (1956), **29**, 389, 1335) has been applied in an extended form to the study of the fine-structure of recrystallized, polycrystalline 99·998% aluminum. The extension refers to the first phase of the method, which deals with the X-ray microscopy aspect. The polycrystalline test specimen is irradiated by an unfiltered X-ray beam at low voltage and a Berg–Barrett X-ray micrograph of the specimen surface is obtained. Owing to the continuous radiation and large divergence of the primary beam, the images of a great number of reflecting crystallites are recorded. Although the X-ray micrograph obtained in this manner supplies a great deal of information concerning the surface texture and the topography of the grains, it is quite useless from the viewpoint of X-ray analysis, since the images cannot be traced outward and subjected to an analysis based on the double-crystal diffractometer principle, as previously described. Consequently, a monochromatizing crystal (calcite or germanium) is interposed in the path of the primary beam and the entire assembly of specimen, plate holder and cylindrical camera is rotated by an angle of 2θ around an axis coincident with that of the monochromatizing crystal; θ is the Bragg angle of the reflecting (hkl) planes of the monochromatizer. After the voltage has been stepped up the identical specimen area is now irradiated by an essentially parallel and monochromatized beam. The X-ray micrograph obtained in this manner registers fewer grain reflections and thus diminishes the topographical relationship of the reflecting crystallites, but, on the other hand, the resolution of fine-structure details is greatly increased and the outward tracing of the recorded images for the purpose of structural analysis is made possible. Furthermore, whereas with continuous radiation lattice curvature is revealed, the irradiation with the monochromatized beam pins down lattice regions of the same orientation. Thus, the alternate applications of continuous and crystal monochromatized radiation for the study of lattice inhomogeneities are mutually complementary.

A special superposition technique establishes uniquely the identity of the lattice regions during the successive irradiation processes. This technique consists of taking a duplicate X-ray micrograph at low voltage (e.g., below $9KV$ for Cu-radiation) and retaining rigidly the position of the photographic plate when the entire assembly is rotated by 2θ as described above. The images of the lattice regions, now reflecting the crystal monochromatized radiation at higher voltage ($35KV$ for Cu-radiation), are being superimposed on the images which were obtained with continuous radiation and the exposure is purposely extended so that the contribution of the monochromatized radiation to the image formation is clearly tagged. Subsequently, the plate is removed and on a second plate only the images are recorded which are obtained with crystal monochromatized radiation alone.

The analysis phase of the diffraction method, which consists of the outward tracing of the images and application of the double crystal diffractometer principle, remains unaltered. The resolution of the method is greatly enhanced through the use of the microfocus tube.

The application of this diffraction method to the study of recrystallized aluminum specimens annealed for 1 hr. at 400 and 600° C. respectively, and subsequently etched and electropolished, disclosed that the recrystallized grains are not strain-free but exhibit a concentration of fine lattice inhomogeneities near the grain boundaries and particularly near the triple or quadruple points. In some cases the deformation markings extend radially to the central portion of the grain, and in other cases run obliquely throughout the grain. From the X-ray micrographs and analysis of the reflections it can be deduced that the dislocation density in recrystallized polycrystalline aluminum is not randomly distributed throughout the grain but exhibits a preferred grouping near the grain boundaries suggestive of pile-ups.

Quantitative data of the disorientation of lattice regions and angular misalignment within these regions will be presented.

11·13. W. W. Beeman, R. Neynaber, W. Brammer, M. Webb & G. Sharp. *Small-angle X-ray scattering from cold-worked metals.*

Studies of the temperature dependence and polarization of the X-ray scattering at small angles from cold-worked Cu, Ni and Al will be described. There is very little evidence for cavity scattering except, perhaps, in diffusion couples. Most of the scattering can be explained as the result of two successive Bragg scatterings either from two subgrains of the same original grain or a double process within a single subgrain, the resulting forward beam, in this case, being physically broadened.

In annealed materials we have occasionally observed a sharp diffracted beam at angles too small to allow a single Bragg reflection. Such diffractions are the result of a double Bragg reflection from two grains accidentally so oriented as to permit the reflection. In cold working the number of independent reflecting domains is greatly increased and the continuous small-angle scattering is assumed to be the unresolved sum of a large number of double scattering processes.

11·14. J. J. Slade, Jr., L. F. Nanni, E. Sturm & R. Chang. *Distribution of imperfections in a germanium crystal of high purity.*

By the use of the X-ray double-crystal diffractometer studies of reflections from the (111) face of a high purity germanium crystal were made. The height of the irradiated area has been varied from 0·12 mm. to 1·5 mm. and the axis of rotation has been varied through the whole circle with respect to the $[1\bar{1}0]$ direction. The width of the reflection curve has been observed to vary from 23″ to 41″ depending on the opening of the slit system and orientation of the rotation axis. The phenomenon has been formulated as a stochastic process.

11·15. S. Caticha-Ellis & W. Cochran. *The X-ray diffraction 'spikes' of diamond.*

Raman & Nilakantan discovered that certain diamonds exhibited anomalous X-ray reflections. Expressed in terms of the reciprocal lattice, there are streaks or spikes of intensity through each reciprocal-lattice point parallel to each of the three cubic axes. The most recently published experimental work on the subject is that of J. Hoerni & W. A. Wooster (*Acta Cryst.* (1955), **8**, 187). Their suggestion that the spikes result from a defect which takes the form of a distortion of the electron distributions of certain atoms is at variance with the work of Lowde (unpublished), who found similar spikes in the diffraction pattern using neutrons. It has been suggested by F. C. Frank (*Proc. Roy. Soc. A* (1956), **237**, 168) that the defect consists of a segregation of silicon atoms into lamellae whose normals may be parallel to any of the cube axes. Replacement of a plane of carbon by a plane of silicon atoms increases the unit-cell dimension by about one-third in a direction perpendicular to the plane. As Frank points out, the dominant effect on the diffraction pattern is this change of spacing, and not the change of scattering factor, although this is not true near the origin of reciprocal space. Frank shows that this hypothesis will account fairly well for the general features of the spikes, but he does not discuss whether their absolute intensities can be explained by a reasonable proportion of impurity atoms. As a simple model of the defective diamond, we have assumed that there is a probability α for each plane to be displaced by $\zeta = \frac{1}{3}$ in the z direction. Neglecting terms involving α^2 (an approximation amply justified by our final value of α), one finds, using results given by Wilson, that for a crystal of $N_1N_2N_3$ unit cells, the intensity in reciprocal space is given by

$$I(\xi, \eta, \zeta) = \frac{\alpha N_3 \sin^2 \pi l\zeta}{(\pi\zeta)^2} \frac{\sin^2 \pi N_1 \xi}{\sin^2 \pi\xi} \frac{\sin^2 \pi N_2 \eta}{\sin^2 \pi\eta} F^2(hkl). \quad (1)$$

(ξ, η, ζ) are in the same units as (h, k, l), but are measured from a reciprocal-lattice point. This formula reproduces all the features of the one used by Frank. Suppose the reflecting sphere intersects the spike at a distance ζ from a reciprocal-lattice point. Expressing the counts J that would be recorded in unit time by a counter set to intercept this diffracted beam, as a fraction of the counts E that would be recorded by the counter set to record the Bragg reflexion when the crystal runs through the Bragg angle with angular velocity ω, one finds, taking $l = 1$,

$$\frac{J}{E\omega} \simeq \frac{3\alpha}{(2\pi\zeta)^2} \frac{a \sin 2\theta}{\lambda \cos \nu}, \quad (2)$$

where ν is the angle between the direction of the spike and that of the diffracted beam. This result gives a convenient method of estimating α.

An octahedral diamond exhibiting strong spikes was set with [110] vertical, and the intensity of the spikes in the zero layer was measured at various distances ζ from (111) using a Geiger counter. The integrated intensity of (111) was also measured. Since it was suspected that the latter was reduced by extinction, the integrated (200) reflexion from a small crystal of LiH was also recorded. A knowledge of $F(111)_{\text{diamond}}$, $F(200)_{\text{LiH}}$, the relative volumes of the two crystals and the absorption factor of the diamond (0·45 for $\lambda = 1{\cdot}54$ Å) led to the conclusion that the measured (111) integrated intensity was too low by a factor 4·4. Using the results with equation (2) gives $\alpha = 4{\cdot}6 \times 10^{-4}(\pm 20\%)$. Since faults in each of the three cube directions are equally likely, the fault density must be about $1{\cdot}4 \times 10^{-3}$. The concentration of silicon in a particular diamond exhibiting strong spikes did not exceed 10^{-5} (Lowde, private communication). It is most unlikely that the discrepancy of a factor of over 100 can be explained by our neglect of the possibly increased scattering factors of the atoms causing the displacement; in fact it seems unlikely that any impurity can be present in sufficient concentration to explain the spikes. Nevertheless, the experimental measurements made so far agree quite well with the idea that the spikes originate from a displacement $\zeta = \frac{1}{3}$. Equation (1) of course gives equal spike intensities for $l = 1$, 2 and 4 and zero for $l = 3$, whereas Hoerni & Wooster showed that the relative intensities were 100, 75, 5 and 30 for $l = 1$, 2, 3, and 4. This may be due to slight disorder at the defects simulating a temperature factor, as Frank suggests. Our measurements agree with Hoerni & Wooster's in that $I(\xi, \eta, \zeta)$ falls off more rapidly than ζ^{-2}. This is adequately explained by the variation of the trigonometric part of F^2. The variation of f^2 should cause the spike intensity to be lower for $l > 1$ than for $l < 1$. Our measurements show that in fact it is definitely slightly higher for $l > 1$. This can be explained by the variation of the factor $\sin^2 \pi l\zeta$ in (1), and favours $\zeta = \frac{1}{3}$ rather than $\frac{2}{3}$. Further accurate measurements are required, however, before this explanation can be accepted as the only possible one. There is as yet no convincing picture to put forward of a rearrangement of bonds between the atoms that would account for a displacement of one-third of a unit cell.

11·16. D. R. Hale. *Minor imperfections in synthetic quartz.*

Synthetic quartz, grown hydrothermally in a pressure vessel, shows the expected similarity to rock crystal. When grown on twin-free seed plates, it is free of Dauphiné twinning and substantially free of Brazilian twinning. It is 'electronic grade' and therefore can be used to make radio resonator plates—by far the largest technical use for rock crystal. Minor variations are found in its properties, and these are referred to defects in the lattice such as dislocations, and substituted impurity atoms.

Synthetic quartz shows higher transmission at 1849 Å because more free from iron. Various growing surfaces show selectivity with respect to accepting impurities from solution, an effect usually made visible in the grown crystal by different degrees of darkening with X-rays. Lattice constants are no more constant (in 4th or 5th place) for synthetic than for natural quartz, and seem regularly related to the conditions of growth. Two spiral dislocation patterns have been noted, and evidence for dislocation growth is increasing.

11·17. M. Lambert & A. Guinier. *Imperfections de structure du fluorure de lithium irradié aux neutrons.*

L'existence de plusieurs phénomènes de diffusion anormale des rayons-X par le FLi irradié aux neutrons a déjà été signalée. Nous avons fait l'étude quantitative par compteur G.–M. de la diffusion aux petits angles et des diffusions le long des axes ⟨100⟩ du réseau réciproque. Ces deux phénomènes correspondent à des imperfections de structure distinctes.

(1) On peut interpréter la diffusion centrale par des cavités (vides ou remplies de gaz) formées par la condensation de lacunes. Ces cavités croissent par chauffage après irradiation; le rayon de giration passe de 16 à 50 Å. Elles disparaissent quand la guérison est complète. La fraction maximale de volume qu'elles occupent dans un échantillon ayant reçu une dose de 5×10^{18} neutrons/cm.^{2} est de 10^{-4}.

(2) La diffusion localisée sur les axes ⟨100⟩ correspond à des désordres de plans {100}. Dans des zônes épaisses de quelques plans, d'un diamètre de l'ordre de 100 Å, l'équidistance des plans passe de la valeur normale 2,0 Å à 2,5 Å. Cette dilatation serait due au rassemblement d'atomes interstitiels sur ces plans {100}. L'hypothèse d'atomes neutres de lithium explique l'équidistance de 2,5 Å et s'accorde avec le fait que le FLi irradié émet du fluor.

11·18. W. L. Bond. *Dislocations in silicon.*

Photographs of single dislocations in silicon taken by polarized infra-red light are shown; also copper-decorated dislocations 2-*D* and 3-*D* photographs.

§ 12. Liquids, liquid crystals, amorphous material, glasses

12·1. B. N. Brockhouse. *Structural dynamics of water by neutron spectrometry.*

Measurement of energy distributions of initially monoenergetic scattered slow neutrons yields important information not otherwise easily accessible to experiment. For coherently scattering single crystals the measurements lead to the frequency/wave-number relations of the normal modes. For incoherently scattering solids the measurements lead to the frequency distribution of the normal modes. Equivalent interest attaches to measurements on liquids.

Water was chosen as the first subject for study because it is available as an isotopic pair which scatters coherently (D_2O) and incoherently (H_2O). In addition, the results were expected to be of importance in understanding neutron moderation in reactors.

Using neutrons of 1·12 Å, angular distributions have been obtained for both light and heavy water from 5° to 100°, in an energy-insensitive counter and in a $1/v$ counter. For light water the cross section decreases smoothly until at 100° it is only about one-third of its value near the forward direction. The decrease is consistent with expectations from the vibrational and hindered rotational motions of the hydrogens. For heavy water the cross-section shows a typical coherent liquid pattern.

Energy distributions have been obtained for light and heavy water at various angles of scattering (φ) for wavelengths (λ) in the range 1·1–1·6 Å, using initially monoenergetic neutrons, selected from the reactor spectrum by Bragg reflection, and a crystal spectrometer to measure the energy distributions of the scattered neutrons. The distributions obtained divide naturally into two components, a quasi-elastic component and a much broader inelastic component.

For light water the intensity of the 'elastic' component falls off with increasing angle of scattering in somewhat the same way as the Debye–Waller factor, $\exp(-Q_0^2u^2)$, where $Q_0 = (4\pi/\lambda)\sin\frac{1}{2}\varphi$, which controls the elastic incoherent scattering of a solid. By fitting the intensity of the elastic component to the above expression the parameter u is found to be about 0·4 Å at room temperature; it increases somewhat faster with temperature than would be the case for a classical solid for which $u^2 \propto T$. Since the scattering by light water is largely (95%) incoherent scattering by the protons, the parameter u applies to the motion of the protons. For comparison, it can be estimated from the work of S. W. Peterson & H. A. Levy (*Acta Cryst.* (1957), **10**, 70) on heavy ice that light ice at 295° K. would give $u = 0{\cdot}26$ Å. More detailed examination shows that the motion is more diffuse than that implied by a Debye–Waller factor. Under high resolution the 'elastic' component at room temperature shows a small energy broadening ($< 10^{-3}$ e.V. for $1{\cdot}88 < Q_0 < 2{\cdot}90$ Å^{-1}) which appears to increase with increasing angle of scattering or Q_0. At 100° C. the elastic component of the one distribution obtained (for $Q_0 = 1{\cdot}88$ Å^{-1}) showed a broadening of $\sim 1{\cdot}3 \times 10^{-3}$ e.V. half-width at half maximum, with energy losses more probable than energy gains.

The inelastic components for $1{\cdot}88 < Q_0 < 2{\cdot}90$ Å^{-1} can be fitted by spectra calculated for a monatomic gas of mass 18. At higher Q_0 no distinction between 'elastic' and inelastic components is possible. At $Q_0 \sim 8$ Å^{-1} the energy distribution is about that of a mass 18 gas but with some suggestion of larger energy transfers than occur for such a gas. In another experiment an energy distribution was obtained for $\lambda = 4{\cdot}5$ Å ($E_0 = 0{\cdot}004$ e.V.) and $\varphi = 90°$ using a difference technique with beryllium and lead filters to produce the monoenergetic neutrons and a time-of-flight apparatus to analyze the scattered neutrons. In this case much larger energy transfers were observed than those calculated for a mass 18 gas, including a very broad neutron group at ~0·06 e.V.

Energy distributions were obtained for heavy water with several different wavelengths and angles of scattering and, in particular, under high resolution at $Q_0 = 1{\cdot}88$ and 2·31 Å^{-1}. The intensity of the 'elastic' peak appears to correlate with the peaks in the diffraction pattern. At $Q_0 = 1{\cdot}88$ Å^{-1}, about the position of the main liquid diffraction peak, the width of the inelastic component is about half the width calculated for this Q_0 for a mass 20 gas. For $Q_0 = 2{\cdot}31$ Å^{-1}, about half-way off the main diffraction peak, the inelastic component is probably a little narrower than the appropriate mass 20 gas pattern.

A qualitative interpretation of these results is possible by comparison with effects in solids and gases. The existence of the 'elastic' component points to the existence of a structure which is only slowly changing in time. The energy broadening of the 'elastic' component measures the rate of variation change with time of this structure. The fall off with Q_0 of intensity of the 'elastic' peak in incoherently scattering H_2O gives the amplitude of the motion of a proton, the r.m.s. radius being $\sqrt{3}.u$. The energy broadening of the peak is related to self diffusion. The agreement of the inelastic component for small Q_0 with calculations for a mass 18 gas suggests that the motions of the molecule as a whole are gas-like, i.e. have little vibrational character. The narrowness of the inelastic component for D_2O at the diffraction peak suggests that the molecules tend to move together in groups.

The large energy transfers, particularly the broad neutron group observed at 0·06 e.V. in the filter time-of-flight experiment, are ascribed to highly damped hindered rota-

tions of the molecules, in agreement with conclusion from Raman-effect measurements (P. C. Cross *et al. J. Amer. Chem. Soc.* (1937), **59**, 1134). The broad Raman line at ~ 200 cm.$^{-1}$, which was ascribed to hindered translational motions, has not been indentified although the spectrum of the filter time-of-flight experiment has considerable intensity in the region of this energy transfer and could probably be fitted by a mass 18 spectrum plus broad components at roughly 200 cm.$^{-1}$ (0·025 e.V.) and 500 cm.$^{-1}$ energy transfer.

Some of the notions developed up to this point can be made more precise by use of the formalism of L. Van Hove (*Phys. Rev.* (1954), **95**, 249), according to which the partial differential cross section for incoherent scattering is the Fourier transform over space and time of a self-correlation function $G_s(r, t)$ which classically can be described as the probability that, given an atom at position 0 at time 0, the same atom is at position r at time t. Consider first a model of small diffusion jumps in which the radius of the proton self-correlation function gradually expands. For all except very small times then the self-correlation function can be taken as a Gaussian

$$G_s(r, t) \propto (u^2+\gamma t)^{-3/2} \exp\left[-r^2/4(u^2+\gamma t)\right].$$

The energy distribution turns out to have the form $\gamma Q_0^2/[(\gamma Q_0^2)^2+\omega^2]$, where $\hbar\omega$ is the energy transfer. The half-width at half maximum γQ_0^2 increases with Q_0, as observed, but its value is too large by a factor of 2 if γ is identified with the diffusion coefficient. On the other hand a model of large diffusion jumps can be considered in which an atom makes a diffusion jump to a distance so great that it is no longer of interest because of spatial interference, in our experiments distances $\gtrsim 2$ Å. $G_s(r, t)$ can be taken as $\exp(-r^2/4u^2)\exp(-\beta t)$. The energy distribution then has the form $(\omega^2+\beta^2)^{-1}$, which is independent of the angle of scattering. The present observations suggest that the widths increase with angle however, and the results therefore point to the probability that both large and small molecular motions are important in self-diffusion. The results also show that there are no important low frequency motions in water which do not involve motion of the molecule as a whole.

12·2. V. Luzzati & H. Mustacchi. *Structures des stases mésomorphes d'un système binaire savon–eau.*

Le diagramme de phase du système binaire savon–eau comporte divers domaines de propriétés physico-chimiques différentes. Au dessous d'une certaine température, le savon et l'eau se rencontrent sous l'état de gel ou de coagel suivant que l'équilibre atteint est métastable ou stable. Au dessus d'une certaine température (de l'ordre de 50–70° C. pour la plupart des savons communs) en augmentant la concentration en savon, les différentes phases rencontrées sont: la phase micellaire, une zône intermédiaire mal définie, la phase médiane, une nouvelle zône intermédiaire mal définie, la phase lisse et les formes cristallines. Pour l'étude de la structure des différentes phases d'un tel système, il nous fallait utiliser un savon représentatif, dont la chaîne ne serait ni trop courte ni trop longue, et dont les températures d'apparition des différentes phases ne seraient pas trop élevées. Nous avons ainsi fixé notre choix sur le palmitate de potassium (KC_{16}).

Partie appareillage

Pour obtenir les diagrammes de rayons X nous avons utilisé une chambre à focalisation avec monochromateur à lame de quartz courbée, sous vide, avec enrégistrement photographique, et un diffractomètre Philips à compteur de Geiger, auquel nous avons ajouté un monochromateur à lame de quartz courbée.

Partie expérimentale

Nous avons exploré systématiquement des mélanges palmitate K–eau, de composition variant de 15% à 90% en savon. Nous avons aussi fait varier pour chaque composition la température de 20 à 100° C.

Dans le domaine micellaire, nous obtenons un diagramme de rayons X à bandes floues.

Dans le domaine médian, nous obtenons un diagramme de rayons X à raies nettes dont les rapports des distances sont 1, $\sqrt{3}$, $\sqrt{4}$, $\sqrt{7}$. Tous les clichés du domaine médian sont du même type.

Dans la zône intermédiaire, les clichés sont variés et complexes (ils comprennent tantôt quatre raies, tantôt trois raies, tantôt deux raies): nous n'avons pas pu encore les interpréter.

Enfin dans le domaine lisse, nous obtenons un cliché à deux, trois ou quatres raies dont les rapports des distances sont 1, 2, 3, 4.

Nous avons étudié l'influence de la température dans les trois domaines médian, intermédiaire et lisse. Les résultats sont nets dans le médian et le lisse: on observe une diminution linéaire des espacements lorsque la température augmente. La pente des droites reste constante dans le domaine médian et varie légèrement dans le domaine du lisse. Ce phénomène de contraction par élévation de la température est typique d'un coefficient thermique d'origine entropique.

Interprétation des résultats

1. *Domaine médian.* — Les diagrammes de rayons X s'expliquent par un assemblage hexagonal compact de cylindres identiques indéfinis. En faisant une hypothèse raisonnable sur la densité des cylindres, il est possible de calculer pour chaque concentration le diamètre du cylindre et l'épaisseur d'eau comprise entre deux cylindres. On constate alors que le diamètre du cylindre est sensiblement constant dans tout le domaine et a pour valeur 38 Å. L'épaisseur d'eau varie de 22 Å pour 31% de PK à 11 Å pour 51% de PK. Dans chaque cylindre, les groupements polaires de la molécule de savon sont sur la surface extérieure et les chaînes paraffiniques à l'intérieur. Le signe du coefficient thermique et sa valeur indiquent que les chaînes à l'intérieur du cylindre ne sont pas complètement étirées mais sont plutôt désordonnées, tout en conservant une direction d'allongement préférentielle. Que les chaînes soient plus 'liquides' que 'cristallines' à l'intérieur des cylindres est confirmé par les diagrammes de rayons X.

2. *Domaine lisse.* — La série de raies des diagrammes de rayons X de ce domaine correspond à une structure en feuillet. En faisant la même hypothèse que précédemment sur la densité, on peut déterminer l'épaisseur du feuillet et l'épaisseur de la couche d'eau. On trouve que l'épaisseur du feuillet (et par conséquent celle de la couche d'eau) change considérablement avec la concentration. Elle passe de 26 Å (H_2O = 11 Å) pour une concentration de 68% en PK, à 34 Å (H_2O = 2,5 Å) pour 87%

de PK. Mais la somme de l'épaisseur de feuillet et de l'épaisseur de la couche d'eau varie relativement peu (moins de 2 Å pour l'intervalle de composition cité plus haut). Nous sommes conduits à admettre ici aussi, et pour les mêmes raisons que celles indiquées pour le domaine médian, que l'intérieur du feuillet est constitué par les chaînes paraffiniques partiellement liquides.

L'interprétation des résultats est un peu plus complexe dans ce domaine car on se trouve en présence de deux phénomènes contradictoires. Lorsque la concentration augmente, d'une part les feuillets tendent à se rapprocher, et d'autre part leur épaisseur tend à augmenter. Le paramètre d que l'on mesure sur les clichés pourra, suivant que l'un des phénomènes est plus important que l'autre, diminuer, rester constant ou même augmenter. C'est ce que l'on observe expérimentalement.

Pour le domaine micellaire et la zône intermédiaire entre le médian et le lisse, les recherches sont en cours.

12·3. J. KAKINOKI, T. INO, K. KATADA & T. HANAWA. *An electron-diffraction study on evaporated carbon films.*

In the studies on the carbon by X-ray diffraction, R. E. Franklin (*Acta Cryst.* (1950), **3**, 107) showed that 35% of the carbon was in so disordered a form that the X-ray scattering due to it was indistinguishable from the independent scattering. Since even in the highly disordered structure, however, some definite distances should remain, at least, between the first neighbors and between the second neighbors, the scattering due to 35% of the carbon is not indistinguishable from the atomic scattering but should show diffuse halos.

We examined, by electron diffraction, evaporated thin films of carbon usually used for the replica in the electron microscope. The thickness of the films is found to be about 100 Å by a multiple-beam interferometer.

We obtained eight or more diffuse halos the s values of which are shown in the third column of Table 1, where, for comparison, the s values of the rings of graphite

Table 1

Graphite			
hkl	s value	Carbon film	Polystyrene
(002)*	1·86 Å^{-1}	$s_1 = 1{\cdot}45$ Å^{-1}	$s_1 = 1{\cdot}38$ Å^{-1}
(100)*	2·95	$s_2 = 2{\cdot}95$	$s_2 = 3{\cdot}16$
(110)*	5·08	$s_3 = 5{\cdot}42$	$s_3 = 5{\cdot}54$
(200)*	5·90		
(210)*	7·80	$s_4 = 8{\cdot}45$	$s_4 = 8{\cdot}65$
(300)*	8·85		
(220)*	10·26	$s_5 = 10{\cdot}42$	$s_5 = 10{\cdot}32$
(310)*	10·65		
(400)	11·82		
(320)	12·87		
(410)	13·53	$s_6 = 13{\cdot}55$	$s_6 = 13{\cdot}36$
(500)	14·77		
(330)	15·35		
(420)	15·63		$s_7 = 15{\cdot}97$ (Shelf)
(510)	16·46	(Shelf)	
(600)	17·73		
(430)	17·97		
(520)	18·45	$s_8 = 18{\cdot}47$	$s_8 = 18{\cdot}32$

$s = (4\pi/\lambda) \sin \frac{1}{2}\theta$

crystal and their indices are listed. The diffuse rings corresponding to the indices starred are observed by Franklin. As seen from Table 1, the pattern obtained by electron diffraction is quite different from that due to graphite or from that observed by Franklin. The eight halos are rather similar to those obtained from thin films of polystyrene, which were studied by one of us and s values of which are listed in the fourth column of the table. From this similarity and the radial distribution function it may be conceived that the structure of the films is a three-dimensional network composed of usual diamond-like C–C distance and graphite-like shorter distance.

12·4. R. DIAMOND. *An analysis of the diffuse X-ray scattering from carbons by the method of least squares.*

The paper describes the development and application of a technique whereby size distributions (in weight percent) may be obtained for the graphite-like layers present in carbons. The method consists in the calculation of scattering functions characteristic of certain layer sizes (on the assumption of perfectly regular layers), followed by a least-squares fitting of a linear combination of these to each observed intensity curve. The layer size distribution is obtained as the product of a rectangular matrix (reciprocal to the calculated intensity functions) and a column matrix containing only observed intensities.

The working of the method will be briefly outlined, and examples of results obtained by this method in the course of a study of carbonized coals will be given.

It will also be shown that mean layer sizes may be obtained with random error $\sim 0{\cdot}3$ Å in the case of low-temperature cokes, and that mean C–C bond lengths may also be obtained with random error $\sim 0{\cdot}002$ Å.

Effects arising from imperfect layers, edge groups, foreign atoms, etc. may also be discussed so far as time allows.

12·5. M. D. DANFORD, P. A. AGRON, M. A. BREDIG & H. A. LEVY. *Structural analysis of molten salts.*

Using monochromatic X-radiation and the apparatus described elsewhere (§ 1(i), No. 4), reliable diffraction data up to a value of $s = 15$ have been obtained for several molten alkali halides ($s = (4\pi/\lambda) \sin \theta$).

Corrections for polarization and Compton scattering are applied to the data. Fourier inversions of the intensity patterns will be given. The radial distribution patterns indicate the interaction distances listed in Table 1. Measurement of the areas under the first two interaction peaks yields the average number of neighbors also shown in Table 1.

Table 1. *Molten alkali halides*

		Interaction distances (Å)		Number of neighbors	
Salt	Temp. (°C.)	*M–X*	*X–X*	*M–X*	*X–X*
CsI	635	3·85	—	4·5	—
CsBr	645	3·55	—	4·6	—
CsCl	650	3·50	4·90	4·9	7·1
NaI	665	3·15	4·80	4·0	8·9
LiI	495	2·85	4·45	5·0	11
LiCl	635	2·47	3·80	4·0	12

12·6. J. H. L. WATSON, A. VALLEJO-FREIRE, P. DE SOUZA SANTOS & J. PARSONS. *The fine structure of fibrous alumina.*

This paper summarizes the results of an investigation by X-ray diffraction and electron microscopy of the struc-

ture, composition and morphology of fibrous alumina; it is part of a larger project on the properties of colloidal aluminum hydroxides (J. H. L. Watson *et al.*, *Kolloid Z.* (1955), **140**, 102). 'Fibrous alumina' is the name given by Wislicenus (*Kolloid Z.* (1908), **2**, 11) to the voluminous, fibrous form of alumina which 'grows' on the surface of amalgamated aluminum in contact with moist air. Owing to its high specific surface after dehydration, it has been used extensively as an adsorbent in chromatography.

The material was studied by methods involving solubility in acids, birefringence, water content, aging in water, X-ray and electron diffraction and by electron microscopy. It was found to be composed chiefly of amorphous aluminum hydroxide with some adsorbed water and aluminum oxide. The birefringence of the fibers was discovered to be due to the existence of non-crystalline, 70–80 Å diameter fibrils, which were oriented fairly well parallel to the fiber length. Amorphous particles, arranged linearly and less than 50 Å in diameter, were found to be the ultimate building unit of these fibrils. The fibrils were often observed to lie in bundles about 200–300 Å across. The binding between fibrils was observed to be very weak and this was thought to account for the low density, extreme friability, and rapid disintegration of the fibrous alumina.

The electron-microscopic methods included those of ultra-thin sectioning and carbon mounting (J. H. L. Watson & M. W. Freeman, *J. Appl. Phys.* (1955), **26**, 1391) as well as the more usual procedures of specimen preparation. The results of this investigation of fibrous alumina are a good example of the power of carbon mounting for the study of ultramicroscopic, crystalline particulates by the electron microscope. Not only were the fine fibrils and fibril bundles more easily observed by carbon mounting but an inherent, fibrous, longitudinal structure was discovered in large sheets of the alumina which had been carbon mounted, etched, and shadow cast. Heavy rough areas about 0·3 microns across were found to alternate with relatively smooth fibers about 200 Å in diameter across the breadth of these sheets.

It has been shown that the formation of fibrous alumina is dependent upon the existence of a small amount of water and a small amalgamation in distinct locations over the aluminum surface. The mechanism of the formation is suggested to be similar to that of anodic films on aluminum.

§ 13. Phase transformation; martensitic transitions; ferroelectrics; λ-point transitions

13·1. D. F. Clifton & H. Eyring. *Kinetics of freezing.*

The velocity of growth (interface velocity) of a solid freezing out of a supercooled, single-component liquid is given in terms of absolute reaction rate theory by the equation (F. W. Cagle & H. Eyring, *J. Phys. Chem.* (1953), **57**, 942)

$$v = \bar{X}\lambda\frac{kT_e}{h}\left[\exp\left(-\frac{\Delta F_f^*}{RT_i}\right) - \exp\left(-\frac{\Delta F_b^*}{RT_i}\right)\right]. \qquad (1)$$

Here v is the interface volocity, $\bar{X}$ the transmission coefficient, λ the distance the interface is advanced by the addition to the solid of one layer of molecules, k is Boltzman's constant, h is Planck's constant, T_i the temperature at which the transformation is taking place, R the gas constant, and ΔF_f^* and ΔF_b^* the free energies of activation for the forward and backward transformations. The activation free energy in the backward direction is greater than in the forward direction by the free energy change on solidification, ΔF_s. It is thus possible to take the factor $\exp(-\Delta F_f^*/RT)$ outside the brackets. At T_e, the equilibrium temperature, ΔF_s is zero and $1=\exp(-\Delta F_s/RT_e)=\exp(-\Delta H/RT_e)\exp(\Delta S/R)$, where ΔH is the latent heat of fusion and ΔS the entropy of fusion. Using this expression as the divisor for the term in brackets the entropy term can be cancelled out. Then taking the first two terms of the series expansion of the exponential ΔH term puts the equation (1) in the form

$$v = \frac{\lambda k\Delta H}{hRT_e}(T_e-T_i)\,\bar{X}\exp\left(-\frac{\Delta F^*}{RT_i}\right). \qquad (2)$$

The temperature difference T_e-T_i is the source of the driving force for the reaction, liquid → solid.

The reaction releases the latent heat of fusion so the interface acts as a heat source with a strength per unit time and unit area of $q''=v\Delta H/V$, where V is the molar volume of the solid. In the steady state this heat must be removed at such a rate that T_i remains constant.

In many cases, depending on the degree of supercooling and other factors, the solid grows as thin needles. The growing tip of a needle-like crystal growing at a constant rate closely approximates a plane heat source of constant strength advancing at a steady rate along a cylinder. Heat loss can take place along the cylinder and also to the sides. The steady-state heat-flow equation for such a case is (M. Jakob, *Heat Transfer*, p. 343. New York: Wiley. 1929)

$$(T_i-T_0) = \frac{q''}{(k_1+k_s)}\left[\left(\frac{v}{\alpha_1+\alpha_s}\right)^2+m^2\right]^{-\frac{1}{2}}. \qquad (3)$$

Here T_0 is the temperature of the supercooled liquid, k_1 and k_s the thermal conductivity of the liquid and solid respectively, α_1 and α_s the thermal diffusivities, v the velocity of the heat source (the interface) and m^2 equals Nusselt's number divided by the square of the radius of the cylinder. Lacking the necessary information of the form of the growing solid, m^2 will be treated as a parameter.

Combining equations (2) and (3) and the expression for q'' gives

$$m^2 = \left[\frac{(k_1+k_s)V}{\Delta H}\left(\frac{T_e-T_0}{v} - \frac{hRT_e}{\lambda k\Delta H}\frac{1}{\bar{X}\exp(-\Delta F^*/RT_i)}\right)\right]^{-2} - \left(\frac{v}{\alpha_1+\alpha_s}\right)^2. \qquad (4)$$

The term T_e-T_0 equals $(T_e-T_i)+(T_i-T_0)$ since the reaction, liquid → solid, and the removal of the latent heat are the only processes requiring a share of the driving force supplied by the supercooling.

Using experimental values for linear freezing velocity as a function of the supercooling, m^2 is found as a function of $\bar{X}\exp(-\Delta F^*/RT)$.

A family of almost hyperbolic curves is obtained for each substance. The value of m^2 increases very rapidly with decreasing values of $\bar{X}\exp(-\Delta F^*/RT)$ below some critical value. Large values of m^2 necessitate very small radii for the growing needs of solid and so set a sharp lower limit to the value of $\bar{X}\exp(-\Delta F^*/RT)$. Consideration

of the probable mechanism of growth of the solid and comparison with other reactions rules out values of $\overline{X}\exp(-\Delta F^*/RT)$ near unity. Hence a fairly narrow range of probable values of $\overline{X}\exp(-\Delta F^*/RT$ is defined) for any one substance.

The value of $\overline{X}\exp(-\Delta F^*/RT)$ for yellow phosphorus is found to be some ten times that for water. The value for tin is slightly smaller than for water. In the case of phosphorus the activation energy for freezing is not as great as that for viscous flow unless the product of the transmission coefficient and m^2 has an improbably large value ten times the minimum that could give the observed interface velocity. The product $m^2\overline{X}\exp(-\Delta F^*/RT)$ increases with increasing supercooling for each substance investigated.

Numerical results obtained for several substances will be presented and discussed.

13·2. D. McLachlan, Jr. *The solid–liquid phase transformation.*

The model used for the study of the solid–liquid transformation is a linear array of atoms set in thermal vibration. The length of the array is controlled by forces applied at the ends. Force functions of various kinds are considered as acting between the nearest neighbors only. The model is further simplified by considering only three atoms at a time, the two outside ones being fixed while the central atom vibrates between them. The types of force functions that are considered are:

(*a*) The perfect gas function, which requires that the force of attraction is zero at all distances, r, except at $r = 0$, where the repulsion is infinite.

(*b*) The Abel gas function, which requires that the force of attraction is zero at all distances except at $r = a$, where the repulsion is infinite. The distance a is the accepted diameter of the atom considered as a hard sphere.

(*c*) The perfect solid-type force function, in which the force of attraction obeys the linear restoring force law, $F = -kr$. This type of force function assures that the central atom is attracted to the midpoint between the outside atoms by a linear force, $F = -2kx$, where x is the distance from the midpoint.

(*d*) The van der Waals-type force function requires an infinite repulsion at $r = a$ and an inverse sixth power law of attraction beyond a.

(*e*) The Goeppert-Mayer type function is a function having two discontinuities. At $r = a_0$, an infinite repulsive force compels the atom to behave as a hard sphere; and at $r = a_1$, an attractive force sets in. The resulting potential function forms a potential well bounded by an infinite wall at a_0 and a wall at a_1 having a height equal to the energy of dissociation.

(*f*) The Lennard-Jones function obeys the equation

$$F = -\frac{unm}{n-m}\left[\left(\frac{r_0}{r}\right)^{n+1} - \left(\frac{r_0}{r}\right)^{m+1}\right],$$

where n and m are numbers of the order of 6 and 13.

These six types of force functions are used to compute the potential energy, $\mathbf{E}_p$, of the central atom as a function of its displacement from the central position when the outside atoms are placed at various distances, 2V, apart. The two extreme cases are the perfect gas, where the potential energy is zero for all values of x less than V, and the perfect solid type, where the potential curve is a parabola

$$\mathbf{E}_p = K\mathbf{V}^2 + KX^2 .$$

This type of potential assures that the central atom vibrates as a harmonic oscillator whose frequency of vibration is $(\frac{1}{2}\pi)(2k/m)^{\frac{1}{2}}$ regardless of the amplitude of vibration or distance 2V between the outside atoms. The equilibrium points maintain a perfect lattice at all lengths.

Between these two extremes, the remaining functions show a mixed combination of both. The most interesting function is that of Lennard-Jones. This potential function behaves as a perfect solid at low values of 2V and behaves as a perfect gas as 2V approaches infinity because it approaches a parabola at low 2V and a flat bottomed potential well at large values of 2V. However, this function shows a very interesting characteristic at intermediate values of 2V. As 2V increases from small values near $2r_0$ to greater values, a central maximum or 'hump' develops at the midpoint and the central atom, in its vibrations, must pass over this hump in making its cyclic excursions, giving two points of equilibrium. This hump is associated with Max Born's instability of the lattice.

We have defined the solid, liquid, and gaseous states as follows:

1. The solid state is that state of matter in which the atoms spend almost all of their time vibrating about their points of equilibrium.
2. The liquid state is that state in which the atoms spend most of their time exchanging neighbors, i.e., going over the central hump from one point of stable equilibrium to the next.
3. The gaseous state is that state in which the atoms spend most of their time cruising between collisions.

Under the above definitions of the three states of matter, the six investigated functions exhibit the following characteristics:

(*a*) The perfect-gas-type function predicts a gaseous state at all temperatures and volumes.

(*b*) The Abel-gas-type function predicts a gaseous state at all temperatures and all volumes above $\mathbf{V}_0$.

(*c*) The perfect-solid-type function predicts a perfect solid at all volumes and temperatures.

(*d*) The van der Waals-type potential function predicts a liquid state and a gaseous state but no solid state. The reason for this is that a central hump is produced at the first increment of increase in volume beyond $\mathbf{V}_0$.

(*e*) The Goeppert-Mayer function predicts three states of matter but the upper and lower states both behave as gases.

(*f*) The Lennard-Jones type of function appears to be most fruitful and the greatest amount of effort is applied to it.

To facilitate computations on this simplified model three definitions are adopted:

(*a*) The period of vibration,

$$\tau = \oint dt = 4\left(\frac{m}{2}\right)^{\frac{1}{2}}\int_{x=0}^{x_{\max.}} \frac{dx}{(\mathbf{E}-\mathbf{E}_p)^{\frac{1}{2}}},$$

where **E** is the total energy of the atom and $\mathbf{E}_p$ is the potential energy.

(*b*) The degree of thermal agitation, which is the time average of the kinetic energy $\mathbf{E}_k$,

$$\mathbf{KT} = \frac{1}{\tau}\int_0^{t_{\max.}} \mathbf{E}_k dt = \frac{1}{\tau}\int_0^{t_{\max.}} (\mathbf{E}-\mathbf{E}_p)dt$$
$$= \frac{4}{\tau}\left(\frac{m}{2}\right)^{\frac{1}{2}}\int_0^{x_{\max.}} (\mathbf{E}-\mathbf{E})^{\frac{1}{2}}dx\,.$$

(*c*) The applied force,

$$\mathbf{P} = \frac{1}{\tau}\oint dp = \frac{2^{3/2}m^{\frac{1}{2}}}{\tau}[\mathbf{E}^{\frac{1}{2}}-\mathbf{E}_s^{\frac{1}{2}}]\,,$$

where p is momentum and $\mathbf{E}_s$ is either $\mathbf{E}_p$ at $r = r_0$ or $\mathbf{E}_p$ at $x = 0$ whichever is the greater.

These bold-faced functions **KT**, **V**, **E**, and **P**, applied to the single atom between two fixed atoms, must not be confused with the usual thermodynamic functions KT, V, E, and P although some of their properties are analogous.

The solution for **V** as a function of **KT** shows a range of values of **V** over which **KT** has ambiguous values. The lower value is designated $\mathbf{V}_M$, the length of the solid upon melting; and the upper value, $\mathbf{V}_L$, the length of the liquid upon freezing. The value of $\Delta\mathbf{V}$ on melting is almost the same as the change in length of the atomic array before melting due to thermal agitation. If this observation extended to three dimensions, one could compute the approximate mean coefficient of expansion between zero and the melting point

$$\bar{\sigma}(0 \to T_M) = \Delta V_M/T_M\,.$$

This equation is of the correct order of magnitude on the basis of recorded experimental data.

Another observation is that the ratios of the heats and lengths extended to three dimensions suggest the following:

$$\Delta H_M/\Delta H_S = \Delta V_M/V\,,$$

where ΔH_M is the heat of melting, ΔH_S the heat of sublimation, and ΔV_M the changes in volume during melting.

In order to compute the thermodynamic functions A, E, P, and S, a partition function must be computed considering each atom as the occupant of a cell in the usual way. However, owing to the ambiguity in **KT** over the range $\Delta\mathbf{V}$, a series of τ values are excluded from the computation. Consequently there is an interval of frequencies $\nu = 1/\tau$ missing between the solid and liquid states. Thus two partition functions, one for the solid and one for the liquid, can be written (as was proposed by Mott) with different limits on the frequencies of vibration.

13·3. C. J. McHargue, H. L. Yakel, Jr. & L. K. Jetter. *Allotropic modifications of metallic cerium.*

F. Trombe & G. Foëx (*Ann. Chim.* (1944), **19**, 416) reported metallic cerium to exist in three modifications. A f.c.c. phase was found to be stable above 473° K., while a c.p.h. phase was formed by slow cooling from 473° K. to room temperature. Finally they reported a low-temperature form of unknown structure present at 77° K. A. F. Schuch & J. H. Sturdivant (*J. Chem. Phys.* (1950), **18**, 145) showed that this low-temperature phase was also f.c.c., with a 16·5% smaller volume than the high temperature f.c.c. form, and that the two f.c.c. structures coexisted at 77° K. Since it has been suggested that the 'collapsed' low-temperature form is a result of an electronic transition in the high-temperature form, the situation should be unique among the known phase transitions of pure metals. The present paper reports details of these structures, studies of the kinetics of the transformations between them, and the effect of such variables as mechanical deformation on the transformations.

High-purity cerium received from the Institute for Atomic Studies, Ames, Iowa, was further purified by vacuum melting and degassing to remove volatile impurities. Spectrographic and gas analysis of the ingot indicated a purity of 99·9%. Polycrystalline sheets of this material were studied in a diffractometer-cryostat operable between 77° K. and 450° K.

Three crystallographic forms of cerium have been observed in the present investigation. At room temperature, a f.c.c. structure with $a_0 = 5{\cdot}15$ Å is stable in a previously uncooled sample. Just below the ice point, a transformation to a h.c.p. structure with $a_0 = 3{\cdot}68$ Å, $c_0 = 11{\cdot}92$ Å, and $c/a = 3{\cdot}239$ ($A\,B\,A\,C$ repeat) begins. At still lower temperatures, the remaining f.c.c. material begins to transform into the 'collapsed' f.c.c. form with $a_0 = 4{\cdot}85$ Å at 77° K. The hexagonal form itself does not transform on further cooling so that it is possible to have all three modifications present at 77° K.

Both f.c.c. → h.c.p. and f.c.c. → f.c.c. (collapsed) transformations appear to be 'martensitic' in nature. The amount of transformation product is a function of the ΔT below the temperature, T_s, which marks the start of transformation and is independent of time at temperature. The reverse transitions, which occur with marked hysteresis, are also apparently 'martensitic'.

The T_s temperature for the f.c.c. → h.c.p. transition was found to be 263°±5° K. The transformation proceeds rapidly as the temperature is lowered in the range 263–205° K. and then less rapidly on further cooling to 77° K. T_s for the reverse h.c.p. → f.c.c. transition is 363±5° K., and T_f, the temperature at which the transition is complete, is 405±5° K. The f.c.c. → f.c.c. (collapsed) transition starts at 123±5° K. in previously transformed samples heated 20–30° above 210° K. and cooled, and at 103°±5° K. in samples cooled from room temperature or higher. The reverse transition f.c.c. (collapsed) → f.c.c. begins at 170±5° K. and is completed at 200±5° K.

The effect of mechanical deformation on the transitions has been studied for deformation temperatures of 295, 195, and 77° K. Deformation at 295 and 195° K. greatly reduces the total amount of transformation of the normal f.c.c. phase. In annealed samples, approximately 95%* (by volume) of the f.c.c. form transforms to h.c.p. (85%) and f.c.c. (collapsed) (10%) on cooling to 77° K. whereas only 60% transformation occurs in worked specimens (50% f.c.c. (collapsed), 10% h.c.p.). The h.c.p. phase appears to be unstable under deformation. The f.c.c. → h.c.p. transition is also suppressed by working a previously annealed sample. As examples of this behavior, a specimen which contained 74% h.c.p., 16% f.c.c., and 10% f.c.c. (collapsed) at 77° K. before

* Volume percentages of various phases were estimated from comparison of relative integrated intensities and are probably accurate to ±7%.

working was found to contain 42% h.c.p., 9% f.c.c., and 49% f.c.c. (collapsed) after working at this temperature. Another specimen having 50% h.c.p. and 50% f.c.c. at 195° K., contained 28% and 72%, respectively, after working. Finally, a specimen containing both h.c.p. and f.c.c. at room-temperature (the hexagonal phase retained from a previous cooling) was found to have considerably less h.c.p. after working. Subsequent cooling from 295° K. to 77° K. did not cause any detectable amount of the hexagonal phase to form in this sample.

The amount of f.c.c. (collapsed) phase present in its range of stability is always greater in worked samples than in annealed samples. It is not known whether this is an effect of the deformation itself or rather an effect of having more of the normal f.c.c. phase available to transform (owing to the suppression of the f.c.c. → h.c.p. transformation).

13·4. Ju. A. Bagarackij & Yu. D. Tjapkin. *The mechanism of the structure transformations in the nickel-base age-hardening alloys.*

Binary, ternary and quaternary nickel-base alloys were investigated (see Table 1). In all the hardenable

Table 1

I. Hardenable alloys

	Composition (at. %)			Mean dimension of regions with superstructure (Ni_3Al type) (kX.)	Remarks
	Al	Ti	Cr		
A–1	14	—	—	60–120	(*a*)
A–2	17	—	—	100–200	(*b*)
(two alloys)					
T–1	—	12	—	50–100	—
T–2	—	14	—	200–400	—
T–3	—	15	—	?	(*c*)
TA–1	4	7	—	?	—
TA–2	6	6	—	40–80	—
XA	8	—	15	50–100	—
XT	—	8½	16½	< 50	—
XTA–1	2	3½	22	—	(*d*)
(Nimonick)					
XTA–2	5	5	15	40–80	—

II. Non-hardenable alloys (solid solutions)

A–0	7	—	—	—	(*e*)
T–0	—	9½	—	—	(*e*)

(*a*) 40–80 kX. after quenching from 1300° C.
(*b*) In the paper by Bagarackij & Tjapkin (*loc. cit.*) 200–400 kX. is given in error.
(*c*) Small addition of non-oriented η phase in quenched alloy.
(*d*) < 50 kX. after quenching from 1180° C.
(*e*) Only local order.

alloys, except *T*–1, *T*–2, *T*–3 and *XT*, the equilibrium precipitate (γ') possesses a close-packed ordered f.c.c. lattice with parameters little greater than those for nickel-base solid solutions. The alloys *T*–1, *T*–2, *T*–3 and *XT* have equilibrium precipitate (η) with composition Ni_3Ti and a hexagonal close packed four-layer lattice. Alterations of lattice parameter of solid solutions and precipitates, presence or absence of superlattice reflexions and character of X-ray reflexions on the oscillating diagrams obtained by soft (Cu $K\alpha$, Fe $K\alpha$) and hard (Mo $K\alpha$) radiations were studied. Non-hardenable alloys (solid solutions) *A*–0 and *T*–0 and some of hardenable alloys were also studied by X-ray diffuse scattering. Single crystals of alloys were cut from large ingots, which were first homogenized at 1200° C. for about 100 hr.

On the oscillating diagrams of all the hardenable alloys with equilibrium precipitates γ' and η (except the alloy *XTA*–1, quenched from 1250° C.) superlattice reflexions were found typical of the Ni_3Al lattice. They were diffuse at large angles θ; by their diffuseness one can estimate the dimensions of superlattice regions in the crystals (see Table 1). The superlattice parameter for alloys *A*–2 and *A*–1 (3·553 and 3·547 kX.) are more than those measured by non-superlattice reflexions (3·545 and 3·541 kX.); the former, within the accuracy of measurement, is equal to the lattice parameter of Ni_3Al (3·556 kX.). Analogous results were found for alloys with equilibrium precipitate η: the superlattice parameter for alloy *T*–2 was 3·577 kX. but the non-superlattice parameter was 3·570 kX. This all implies that submicroscopic regions in the crystals of supersaturated solid solution which possess the superstructure are enriched by Al and Ti nearly up to a composition $(Ni, Cr)_3(Ti, Al)$. Dependence of Al(Ti)-rich region dimensions upon the quenching temperature (see Table 1) suggests that inhomogeneity of location of solute atoms occurs also in single-phase (at high temperature) solid solutions. In the alloy *XTA*–1 quenched from 1250° C. we have found only local order by diffuse scattering; this was found also for equilibrium solid solutions *A*–0 and *T*–0.

After short aging at 500–700° C. (and sometimes after non-drastic quenching) satellite reflexions appear on the oscillating diagrams obtained with soft radiation for most of the alloys. This gives evidence about the dispersion of Al(Ti)-rich and Al(Ti)-poor regions in the crystals of alloys (modulated structure). In the alloy *XT* the picture is slightly different, but the oscillating diagrams obtained by hard radiation (Ju. A. Bagarackij & Yu. D. Tjapkin, *Rep. Acad. Sci. USSR*, (1956), **118**, 451) suggest that in both cases in the crystals there are regions of both types (rich and poor in Al and Ti atoms). In addition, in the quenched alloy *XT* there are regions with mean (initial) lattice parameter.

In the alloys with equilibrium precipitate γ' progressive aging causes growth of Ti- and Al-rich regions with superstructure. The maximum hardness is obtained when the dimensions of this regions are about 200–400 Å. In the crystals of alloys with equilibrium precipitate η (the *T* and *XT* alloys) after aging at 800–850° C. for some hours, submicroscopical regions with a h.c.p. structure appear; they arise from the Ti-rich regions. Simultaneously, the regions with mean lattice parameter (in alloy *XT*) are dissolved into Ti-rich and Ti-poor regions.

13·5. D. A. Evans & K. H. Jack. *The $\gamma \rightarrow \beta$ phase transformation in the* Mo–N *system.*

The currently accepted phase diagram for the Mo–N system (G. Hägg, *Z. Phys. Chem.* (1930), B, **7**, 339) must be modified. For example, a previously unknown nitride, now designated as ε, has a close-packed hexagonal metal-atom arrangement and a composition near $MoN_{0.38}$. A further discrepancy is the earlier description of β (*c.* $MoN_{0.4}$) as a high-temperature phase. It is now shown to be a low-temperature, ordered, tetragonal modification of the face-centred cubic γ-phase ($MoN_{0.38}$–$MoN_{0.43}$; $a = 4{\cdot}137$–$4{\cdot}157$ Å). γ is retained unchanged on quenching from above 700° C., but slower cooling gives a homo-

geneous β-phase, the tetragonality of which increases with decreasing nitrogen content. Repeated $\gamma \rightarrow \beta \rightarrow \gamma$ cycles are effected without loss of nitrogen, but a complete $\gamma \rightarrow \beta$ conversion is obtained only by continuous cooling and not by any isothermal treatment. A marked temperature hysteresis suggests also that the transformation is martensitic; M_s and M_f are near 650° C. and 530° C. respectively.

All β-phase X-ray photographs show weak reflexions which are not accounted for by the structure previously proposed by Hägg. Although the pseudo-cell is face-centred tetragonal ($a = 4{\cdot}200$, $c = 4{\cdot}005$ Å for β-$MoN_{0{\cdot}38}$), the true structural unit has $a' = a$, $c' = 2c$ and it contains 8 Mo atoms at sites (e) of space group $I4_1/amd$, with $z = 0{\cdot}258 \pm 0{\cdot}003$. Three N atoms randomly occupy four octahedral interstices at (a), while the remaining four interstices at (b) are always empty. The temperature factor for the metal atoms is anisotropic: $B_{[100]} = 1{\cdot}33$ Å^2, $B_{[001]} = 2{\cdot}66$ Å^2. This is probably due to random permanent shifts in the [001] direction of the Mo atoms from their mean lattice positions, and these in turn are a result of the incomplete interstitial-atom ordering.

The β-structure, which can be described equally well as distorted body-centred tetragonal with two Mo per pseudo-unit ($c/a = 1{\cdot}349$ at the lower nitrogen limit), shows striking analogies with iron–carbon and iron–nitrogen martensites (α'). Each is obtained by the lower-temperature transformation of a face-centred cubic phase; each structure shows partial ordering of its interstitial atoms; each has a body-centred tetragonal metal-atom arrangement, and in each there are abnormally large permanent but random displacements of these atoms in the [001] direction.

An objection to a martensitic-type mechanism for the $\gamma \rightarrow \beta$ change is that the latter involves an ordering of the interstitial atoms which is not diffusionless. The transformation probably occurs in two stages and is comparable with the change γ (austenite) $\rightarrow \alpha'$ (martensite) $\rightarrow \alpha''$ ($Fe_{16}N_2$) which occurs in the Fe–N system. It is suggested that a martensitic transition of the metal-atom lattice of γ is followed by a diffusion-controlled rearrangement of the nitrogen atoms to give the more ordered β-Mo–N phase.

In interstitial systems the metal atoms and the non-metal atoms may participate in structural transformations independently of each other.

13·6. H. L. Yakel, Jr., J. J. McBride & G. P. Smith, Jr. *A martensitic phase transformation in sodium nickelate* (III).

The room-temperature crystal structure of sodium nickelate (III), $NaNiO_2$, was described by H. B. Dyer *et al.* (*J. Amer. Chem. Soc.* (1954), **76**, 1499) as a monoclinic distortion of a rhombohedral $CsCl_2I$-type lattice. A transition to this $CsCl_2I$-type lattice was reported on heating the monoclinic form to 220±10° C. The parameters of the two phases are:

Monoclinic (low temperature)

$a = 5{\cdot}33$, $b = 2{\cdot}86$, $c = 5{\cdot}59$ Å, $\beta = 110°30'$

$Z = 2$ in C_{2h}^3–$C2/m$ with 2 Ni in (a); 2 Na in (d); 4 O in (i), $x = 0{\cdot}278$, $z = 0{\cdot}795$.

Rhombohedral (high temperature)

$a = 5{\cdot}52$ Å, $\alpha = 31°4'$.

$Z = 1$ in D_{3d}^5–$R\bar{3}m$ with 1 Ni in (a); 1 Na in (b); 2 O in (c), $x = 0{\cdot}27$.

The exact mechanism of the transition is uncertain since no homogeneous linear transformation can be found which will bring all the atoms of the two phases into coincidence with the positions calculated from the X-ray data. A mathematical operator which is equivalent to a simple shear plus adjustments of axial lengths will send sodium and nickel atoms from their positions in one structure to their positions in the other but will leave oxygen atoms slightly displaced.

Despite this uncertainty as to the detailed atomic movements which occur in the transition, microscopic and X-ray diffraction investigations have shown that it is a displacive transition with many so-called 'martensitic' characteristics. Microscopic studies were made with the aid of reflected polarized light. Examination of single crystals on an electrically heated, controlled-atmosphere hot stage across which a thermal gradient was impressed shows that the interface between the phases moves in rapid (of the order of 10 mm. sec.$^{-1}$ or greater) jumps across the crystal. In the cooling transition, successive twins of monoclinic $NaNiO_2$ are formed by this process. Natural growth lines on the original high-temperature rhombohedral crystal are retained in the low-temperature form but have a serrated appearance due to changes in direction as they cross band boundaries. The external morphology of the rhombohedral crystals (hexagonal platelets) is also retained except for irregularities at the intersection of bands with crystal surfaces.

The possible morphological orientations of the monoclinic bands in the transformed crystals appear to be few in number, but no information about their crystallographic orientations is available. No statement concerning the habit or growth planes is possible from the present investigation, but consideration of the monoclinic structure shows the {110} planes likely to be the twin planes.

Further evidence of the 'martensitic' character of this transition is supplied by the results of high-temperature X-ray diffraction studies of polycrystalline samples of $NaNiO_2$. These show that the transformation, both on heating and cooling, proceeds athermally with a considerable temperature region in which both phases are present. The degree of transformation at a temperature, T, within the two-phase region, depends on $\Delta T = T - M_s$ and on the rate of heating or cooling to that temperature. In general, slower rates of cooling from the high-temperature rhombohedral region favor the retention of the rhombohedral phase to lower temperatures and vice versa in the heating transition. A considerable (10–20° C.) hysteresis is observed between the heating and cooling transitions. The degree of hysteresis is a function of the rate of thermal cycling. The M_s temperature marking the beginning of the transformation also appears sensitive to the rate of thermal cycling, especially on heating. Representative values for slow heating are: $M_s = 193 \pm 4°$ C., $M_f = 250 \pm 10°$ C., $(\Delta C/\Delta T)_{max.}$ occurs at $T = 209 \pm 2°$ C. Values for slow cooling are: $M_s = 228 \pm 4°$ C., $M_f = 179 \pm 10°$ C., $(\Delta C/\Delta T)_{max.}$ occurs at $T = 197 \pm 2°$ C.

X-ray diffraction and microscopic data thus show the rhombohedral $\rightarrow$ monoclinic and the reverse monoclinic $\rightarrow$ rhombohedral transitions in $NaNiO_2$ to be displacive in

nature, to proceed only in the presence of thermal increments, and to be sensitive to heating or cooling rates. The occurrence of such 'martensitic' characteristics in transformations of stoichiometric inorganic compounds has been suspected previously (e.g. NaCN, $BaTiO_3$).

13·7. Y. Le Corre. *La boracite, un nouveau ferroélectrique?*

La boracite ($Mg_3B_7O_{13}Cl$) présente des domaines endessous de 265° C. Dans une zône de température très étroite autour de la transition, la répartition de ces domaines est sensible à l'action d'un champ électrique. Il est donc probable que la boracite est un nouveau cristal ferroélectrique, sans relation de structure avec les autres familles ferroélectriques actuellement connues.

13·8. R. Pepinsky, F. Jona, K. Vedam, Y. Okaya, M. S. Ahmed, P. Gallitelli, S. Hoshino, T. Mitsui, J. Johns, D. Eastman & F. Unterleitner. *Optical, dielectric, dilatometric, thermal and X-ray studies of crystal transitions.*

Optical observations have revealed reversible low-temperature transitions in a large number of complex ion salts, divalent metal fluoborates and perchlorates, monovalent and divalent metal and amine hexafluophosphates, urea and thiourea salts, basic beryllium acetate, various NH_4–Me^{II} double sulfates, various $Me^{II}(Me^{III})_2$ hexapropionates, $K_3Na(CrO_4)_2$, etc., a variety of ammonium and substituted ammonium alums; etc.; and reversible high-temperature transitions in a large series of normal-amine and iso-amine phosphates and arsenates, various complex ion salts, tetraethylamine and other amine fluoborates, divalent metal fluoborates, etc. Dielectric measurements indicate anomalies in various of these, in $(NH_4)_2S_2O_3$ and many other ammonium salts, and in various perovskites and pseudo-perovskites, including mixed crystals. Dielectric hysteresis observations are reported for various new ferroelectrics, as are dilatometric and differential thermal analyses.

X-ray diffraction studies are reported of the structures and transition mechanisms in various ferroelectrics and antiferroelectrics.

13·9. A. Bienenstock, H. Chessin & B. Post. *X-ray diffraction studies of thermal effects in crystals.*

Diffraction intensities of selected reflections of TiB_2 have been investigated over the temperature range −160° C. to +25° C., using a scintillation counter as detector. From these data Debye temperatures for the crystal have been computed as well as amplitudes of motion of the Ti and B atoms in the *a* and *c* directions separately.

A similar investigation has been carried out for calcite. Reflections of the type *hkl* with *l* odd (hexagonal indices) have been studied over the range of −160° C. to +200° C. Only the oxygen atoms contribute to these reflections. The amplitudes of thermal motion of the oxygen atoms in various directions, as well as the 'Debye' temperature for the crystal and for the oxygen atoms, have been computed.

The results of direct determination of temperature factors of various organic compounds will also be discussed.

13·10. K. Lonsdale. *Thermal vibrations and thermal expansions.*

13·11. V. G. Hill & R. Roy. *New data on the tridymite problem.*

In the SiO_2 system tridymite can be prepared easily by hydrothermal reaction, from starting materials in the quartz, cristobalite or 'X-ray-amorphous' form and with impurities in the p.p.m. range. At least two polymorphs can be distinguished at room temperature. The presently accepted version of the quartz–tridymite phase equilibrium relations appear to be confirmed.

Phase relations in the silica-rich end of the systems SiO_2–$LiAlSiO_4$ and SiO_2–$NaAlSiO_4$ show the enormous importance of the 'stuffing ion'. In the former system a new metastable polymorph, 'silica-*X*', quite similar to silica-*K*, is encountered, and the stability of quartz is enhanced with respect to tridymite as Li+Al is added. With Na+Al, tridymite structures are stabilized to temperatures as low as 650° C. *Low* quartz accepts very little of either Li+Al or Na+Al in solid solution.

13·12. A. J. Majumdar & R. Roy. *Experimental Phase-Rule studies involving transitions of various kinds.*

The question, whether or not all solid–solid transitions are changes of phase within the context of the Phase Rule has been approached by determining equilibrium diagrams for systems containing components with more than one polymorph. The problem of the applicability of the Clausius–Clapeyron and analogous expressions to solid–solid transitions has also been studied. *T*–*x* sections and *P*–*t* sections have been determined, using static quenching, high temperature X-ray differential thermal analyses from 1 to 3000 atmospheres, and ordinary hydrothermal equipment. Data on the systems AgI, CsCl, Na_2WO_4–Na_2MoO_4, and CsCl–RbCl will be presented to illustrate the conclusions.

13·13. H. P. Rooksby & M. H. Francombe. *Structure transitions in spinel-type compounds.*

The structure distortions shown by the simple monoxides of the transition elements on cooling through the antiferromagnetic Néel temperatures are now well established. The situation in spinel-type structures is more complex, although there are a number of instances of deformed spinels, particularly chromites. Attention has been drawn for example by C. Delorme (*C. R. Acad. Sci., Paris*, (1955), **241**, 1588) to the marked tetragonal deformation in $NiCr_2O_4$ at room temperature, the tetragonal structure cell having an axial ratio of 1·025.

An investigation of the system Fe_3O_4–$FeCr_2O_4$, in which all compositions are cubic at room temperature, has revealed some noteworthy structure changes at low temperatures. For the composition $FeCr_2O_4$, the structure cell at −180° C. has become tetragonal, with axial ratio below 0·97. With solid solutions having slightly lower concentration of chromium, orthorhombic symmetry is observed, but when the chromium is still further reduced a tetragonal cell with axial ratio greater than 1·0 is found. Careful examination over a range of temperatures of the development of the orthorhombic distortion shows that it results from the combination of two mutually perpendicular ⟨100⟩ distortions.

A progressive reduction in the room-temperature tet-

ragonal distortion of $CuCr_2O_4$ can be obtained by replacement of copper by zinc, and this distortion may therefore be largely explained in terms of atomic packing. In the iron chromites, however, other factors would appear to be more important in causing the observed lattice distortions, and antiferromagnetic interactions may well play the chief role.

13·14. D. S. Lieberman. *Determination of the inhomogeneous deformation in diffusionless phase changes.*

A simple graphical method is presented for determining from observations the inhomogeneous deformation which is part of the total transformation distortion in diffusionless phase changes. This pattern of inhomogeneity—plane and direction of slip and/or twinning in the parent and/or product phase—is of great importance since it is intimately related to the dislocation arrays which are taking part in the nucleation and growth and thus can provide information about the mechanism of such transformations. It is pointed out that since this pattern has not been observed except in very few systems, the several recent theories (B. A. Bilby & J. W. Christian, *Inst. Metals, Monograph and Report Series* (1955), No. 18, 121; J. W. Christian, *J. Inst. Metals* (1956), **84**, 386) which require a specification of this pattern to predict the salient crystallographic features of the transformation must *assume* a pattern of inhomogeneity in the many cases where this information is not known. Reference is made to recent work (M. S. Wechsler *et al.*, to be published) where considerable effort was spent examining several slip directions on an assumed slip plane and each set of predicted features was then compared with observations in order to determine which pattern of inhomogeneity corresponded to reality.

The method herein presented permits the determination of this pattern directly from observations. The essence of the scheme consists of working the problem previously done in reverse: given a particular set of observations of the lattice parameters of the initial and final structures, interface plane normal, orientation relationships, and magnitude and direction of shear, to determine uniquely that pattern of inhomogeneity which could produce that particular set of crystallographic features. It is demonstrated that if a single set which belongs to a single transformation process that results in a single plate or domain of the product phase is employed, the problem is simpler than if 'average', 'typical' or 'nearest rational' values (as usually reported in the literature) must be used. The technique involves a more elegant and considerably shorter version of the recent graphical formulation (T. A. Read, Third International Congress, International Union of Crystallography, Paris, 1954; D. S. Lieberman *et al.*, *J. Appl. Phys.* (1957), in the Press) of the Wechsler–Lieberman–Read theory of diffusionless phase changes (M. S. Wechsler *et al.*, *Trans. Amer. Inst. Min. (Metall.) Engrs.* (1953), **197**, 1503; D. S. Lieberman *et al.*, *J. Appl. Phys.* (1955), **26**, 473). Since this improved treatment has not yet been reported, it is first described briefly.

The W–L–R theory is based on the requirement that after partial transformation, the interface between the two phases be free of stress on a macroscopic scale. If this plane of zero average distortion is to exist, one of the principal distortions must be unity (i.e., one of the principal strains must vanish) and of the other two principal distortions, one must be greater than unity and the other less than unity (i.e., the other two principal strains must be of opposite sign). In general, the Bain distortion which brings about the *per se* change in crystal structure does not satisfy these requirements. Hence the total transformation must include an inhomogeneous distortion pattern in order to satisfy the above criteria and thus permit this plane (identified with the habit plane) to be one of zero average distortion. The plane will depend on the lattice parameters of the initial and final phases (and thus a reasonable Bain distortion) and on the assumed plane and direction of slip and/or twinning.

The operations of distortion, rotation, shear, etc. needed to solve the problem can be represented by matrices or by graphical constructions on a stereographic net. The loci of directions in the parent phase unchanged in length by the structure change (the Bain cone) and the loci of directions unchanged in length by the inhomogeneous shear (the shear plane and a plane $90° \pm \alpha$ from it, where α is the net angle of shear) are represented on the net. The intersection of these loci determine possible undistorted interface planes. The earlier version of the graphical method was based on the theorem* that if three non-collinear vectors in a plane are undistorted (unchanged in length) by a transformation, *all* vectors in that plane are undistorted, i.e., the plane is one of zero distortion. Thus the method consisted of finding a third undistorted vector on the possible interface planes mentioned above by a rather tedious interpolation or successive-approximation process.

A new version of the graphical method is delineated and illustrated. It depends upon a theorem which is a simple extension of that stated above: if two (non-collinear) vectors in a plane are undistorted (unchanged in length), and the angle between them unchanged, by a transformation, *all* vectors in that plane are undistorted (and all angles are unchanged), i.e., the plane is one of zero distortion. Since only angle measurements and rotations need be made, this method thus avoids the considerable supplementary calculations and constructions inherent in the earlier version, which required the calculation of length changes. Hence this method is much shorter and easier to use. In addition to the crystallographic features of the transformation mentioned above, the amount of shear associated with the inhomogeneous part of the transformation is also predicted by the graphical solution.

It is then shown how the plane, direction, and amount of slip and/or twinning can be determined from the observed crystallographic features of a transformation. In only two systems are accurate experimental data available on a single transformation process: the f.c.c. → b.c.t. austenite–martensite transformation in an Fe–Ni–C alloy (A. B. Greninger & A. R. Troiana, *Trans. Amer. Inst. Min. (Metall.) Engrs.* (1949), **185**, 591) and the b.c.c. → orthorhombic transformation in AuCd. The former case is treated in some detail. In performing the operations of the graphical method described above in reverse order, it is shown that the orientation relationships and the habit plane are the most useful of all the observations that can be made on a transformation process. The predicted pattern of inhomogeneity is found to be reasonable according to available experimental information. There is some discussion of how sensitive

* A proof of this theorem is given by Lieberman *et al.* (*J. Appl. Phys.* (1957), **28**, 532).

the result is to the accuracy of the various observed crystallographic features and how account must be taken of internal consistency and apparent over-determined conditions. Possible limitations as well as advantages of the method are presented and the need for more accurate observations of the features of diffusionless phase changes is emphasized.

13·15. G. S. Baker. *Isothermal diffusionless phase changes and quenching effects on transformations in* Au–Cd.

Electrical resistance measurements have been made on the cubic-to-orthorhombic (47·5% Cd) and cubic-to-tetragonal (49% Cd) diffusionless transformations which occur in β-phase of Au–Cd (L. C. Chang & T. A. Read, *Trans. Amer. Inst. Min. (Metall.) Engrs.* (1951), **191**, 47; D. S. Lieberman *et al.*, *J. Appl. Phys.* (1955), **26**, 473). Quenching from high temperatures has a remarkable effect on these transformations (M. S. Wechsler & T. A. Read, *J. Appl. Phys.* (1956), **27**, 194), changing the nature of the transformations themselves. In the quenched state the transformations, although normally athermal, can occur completely isothermally.

The 47·5% Cd alloy transforms from cubic to orthorhombic upon cooling at about 60° C., the reverse transformation occurring at approximately 80° C. The 49% Cd alloy transforms to tetragonal at approximately 30° C. upon cooling and changes back to cubic at approximately 35° C. upon heating. The transformations have been shown to be athermal (Chang & Read, *loc. cit.*; Lieberman *et al.*, *loc. cit.*; L. C. Chang, *J. Appl. Phys.* (1952), **23**, 725). Quenching from high temperatures results in an increased resistivity, due presumably to the presence of quenched-in defects (M. S. Wechsler, *Acta Metallurg.* (1957), to be published), and to profound changes in the transformation behavior. Quenching a 49% Cd specimen shifts the transformation temperature upon cooling to lower temperatures and increases the transition width. The transformation upon heating is shifted similarly to higher temperatures, thus increasing the hysteresis width.

The remarkable effects of quenching on 47·5% Cd crystals were studied in detail. Quenching from low temperatures causes the transformation upon cooling to shift slightly to lower temperatures. Upon quenching from higher temperatures there occurs a change from the normal cubic-to-orthorhombic transformation at about 60° C. to a transformation at approximately 25° C. to a different structure with a resistance characteristic of the tetragonal phase. The reverse transformation to cubic upon heating takes place at approximately 50° C. Thus upon quenching from a sufficiently high temperature, the behavior of a 47·5% Cd alloy changes to that characteristic of a 49% Cd alloy. The change takes place over a range in temperatures in which the specimen transforms into a partially orthorhombic and partially tetragonal structure.

In the quenched state, all transformations can take place isothermally. The rate of transformation decreases rapidly as the temperature approaches some temperature intermediate to the heating and cooling transformation temperatures. The transformation from tetragonal to cubic in the 49% Cd alloy has also been observed isothermally in an unquenched (slow cooled) specimen. The alloy is stabilized in the tetragonal structure by long holding in this state. Upon subsequent heating the alloy transforms isothermally at a temperature approximately 20° C. above its normal transformation temperature.

The kinetics of the isothermal annealing-out of the excess resistivity due to quenching was studied at several temperatures in the cubic phase for both alloys. Calculations based on these investigations indicate that the isothermal phase transformations described above were not simply related to the phenomenon of defect annealing.

§ 14. Crystal growth

14·1. I. N. Stranski. *Die Tracht reiner Kristalle und von Kristallen mit Adsorptionsfilmen.*

Struktur und Stabilitätsfragen bei kristallinen Oberflächen werden oft allein durch die Ermittlung der zuständigen Kristallgleichgewichtsform beantwortet, zumindest lassen sich die noch offenen Möglichkeiten übersichtlich ordnen.

Die Gleichgewichtsform war bisher nur für den Fall abgeleitet worden, dass der Kristall ausschliesslich von seinem eigenen verdünnten Dampf umgeben ist. Die hierfür bekannten zwei Methoden (die von den spezifischen Oberflächenenergien Gebrauch machende und die von der Abtrennungsarbeit einzelner Kristallbausteine ausgehende) führten praktisch zur selben Form.

Es konnte weiter gefolgert werden, dass nur die an der Gleichgewichtsform beteiligten Flächen über zweidimensionale (Netzebenen-) Keime wachsen, die übrigen Flächen über eindimensionale (Bausteinketten) bzw. dimensionslose Keime (direkte Einlagerung einzelner Bausteine). Die nicht zur Gleichgewichtsform gehörenden Flächen können vergröbern, indem sie von Subindividuen bedeckt erscheinen, die ihrerseits von Gleichgewichtsformflächen begrenzt sind.

Im folgenden wird nun auch der allgemeinere Fall behandelt, dass in der Kristallumgebung Fremdstoffe (zunächst in der Gasphase) vorhanden sind. Das ist ein in der Natur stets gegebener, beim Experiment kaum zu vermeidender und daher besonders wichtiger Fall. Hierzu werden Beispiele an Hand von einfachen Modellen und thermodynamischen Berechnungen erläutert.

Die verschiedenen Flächen eines Kristalls adsorbieren unter gleichen Bedingungen unterschiedlich. Daraus ergibt sich eine geänderte Gleichgewichtsform. In einfacheren Fällen findet nur eine Verschiebung des relativen Inhalts der für den reinen Fall geltenden Gleichgewichtsformflächen statt. In ausgeprägteren Fällen folgt eine völlig verschiedene Form. Die neu auftretenden Flächen wachsen alsdann über zweidimensionale Keimbildung, während diese Eigenschaft für die nicht mehr zur Gleichgewichtsform gehörenden Flächen ebenfalls vergröbern, indem die entstehenden Subindividuen ihrerseits von den neu gegebenen Gleichgewichtsformflächen begrenzt sind. Hierbei stellt sich beim Wachstum noch eine Komplikation ein, insofern mit dem Anlagern von Gitterbausteinen noch eine Umsetzung von adsorbierten Molekülen gekoppelt ist.

Die starke Bindung einer Molekel setzt eine bestimmte Bausteingruppierung an der Kristalloberfläche voraus. Da eine starke adsorption mit der Forderung nach einer möglichst grossen Dichte derartiger Gruppierungen verknüpft ist, folgt auch für die neu auftretenden Flächen eine verhältnismässig niedere Indizierung.

Liegt der Fall einer aktivierten Adsorption vor, so folgt für Flächen, die nicht zur resultierenden Gleichgewichtsform gehören, noch ein zusätzlicher Term der Aktivierungsenergie, der der Umgruppierung von Kristallbausteinen (Vergröberungseffekt) Rechnung trägt.

Für die Gleichgewichtsform eines Kristalls innerhalb seiner eigenen reinen Schmelze und auch innerhalb einer Lösung ergeben sich ähnliche Verhältnisse.

Die bis hierher berichteten Ergebnisse, die für einen Monokristall gelten, lassen sich im grossen und ganzen auf die Oberfläche eines polykristallinen Gebildes übertragen.

14·2. P. H. Egli, L. R. Johnson & W. Zimmerman. *The growth mechanism of ionic crystals.*

Many of the significant facts of crystal growth can be illustrated by a zonal diagram relating the degree of supercooling or supersaturation at which various solidification acts occur. The same general representation is useful for showing the rates of the various processes with different supercoolings or supersaturations. Other facts conveniently displayed include the effect of changing the equilibrium temperature of solution systems and the importance of operating variables such as temperature fluctuations.

One of the facts significant to the growth mechanism is a relation between the usable range of supersaturation for growing crystals free of flaws, and the total range of supersaturation that a system can support without spontaneous nucleation. The implications support the concept of growth by sizable rather well ordered subnuclei.

A second significant factor is a relation between the critical growth rate (beyond which flaws are initiated) and the macroscopic size of the growing face. The conclusion from this well established fact is that most crystal growth occurs with new layers forming at the corners and edges rather than by any defect or dislocation mechanism.

A more basic question concerns the difference in ease of growth between different faces on the same crystal and between different crystals. Evidence will be presented that this is controlled by the order and extent of association of solute in the liquid state.

14·3. W. Zimmerman & P. H. Egli. *Factors that control crystal growth from melt.*

Evidence will be presented that the classical growth mechanisms observed for solutions are also dominant factors in melt growth. Growth appears to occur normally by planes originating at the corners and edges, and is controlled by the association of the liquid state. Chemical additives exert the same powerful influence of improving purity and texture and increasing the critical growth rate. Additional factors important only in melt growth are the thermal properties of the solid and liquid, diffusion in both the solid and liquid, and heats of reaction.

Many of the significant factors in the growth process are revealed by examination of the solid/liquid interface. The source of a variety of imperfections is related to curvature of temperature isotherms.

Practical considerations of limitations in temperature control are shown to create a necessity for a large temperature gradient in the melt and small gradients, particularly in the radial direction in the solid. The importance of crystallographic factors and consideration of rate versus amount of temperature fluctuations will be discussed.

14·4. L. R. Johnson & P. H. Egli. *Factors that control growth of crystals from solution.*

The factors that control solution growth are discussed in terms of four important variables. The dominant variable in the system is the character of the solution, which includes choice of solvent, effect of pH and ionic form and treatments such as control of superheated nuclei. The second factor is the powerful effect of chemical purity, and particularly the use of deliberate additives to permit greatly increased crystal purity, perfection and more rapid growth rates. The third general area for consideration is the effect of operating variables, including temperature fluctuations, agitation, supersaturation by cooling, by evaporation and by salting out, and the effect of seed mounts, vibration and other mechanical effects. The fourth area is crystallographic factors, choice of seed, optimum growing plane and the effect of strain, misorientation and other defect structures.

These general factors can each be related to the origin of defects in terms of the growth mechanism, and equipment will be described which provides precise control of growth rate without exceeding the critical point, and minimizes other sources of flaws.

14·5. H. Wilman. *Factors affecting crystallization and crystal growth in oxide layers formed on metals thermally and anodically.*

Our recent results on the structure and growth of oxide layers on Be, by thermal or anodic oxidation, led to the conclusion that BeO crystallizes rapidly only above about 300° C., and hence that the crystalline nature of BeO formed anodically shows that the surface temperature of the growing anodic oxide exceeded 300° C.

Further work (with M. L. Levin) on the structure and growth of oxide layers formed thermally and anodically on various metals (Be, U, Sb, Al, Mo, W) is now described. It is concluded that the main factors determining whether the oxide grows in the amorphous or the crystalline state are first the crystallizing temperature of the oxide, and secondly the local current density reached at points on the anode surface. Evidently, with aqueous solutions having high electrical conductivity the current density tends to rise locally much above the average, so that high local temperatures can be attained. In non-aqueous solvents having low conductivity there is less possibility of the anions being attracted preferentially to particular small regions of the anode, thus much lower surface temperatures occur and, if the crystallizing temperature of the oxide is not too low, the oxide layer is built up in the amorphous state, to a limiting thickness at a given voltage.

14·6. J. S. Marshall & K. L. S. Gunn. *Growth of ice crystals from vapor.*

J. S. Marshall & M. P. Langleben (*J. Meteor.* (1954), **11**, 104) interpreted the experiments of U. Nakaya (*Snow Crystals, Natural and Artificial.* Cambridge: Harvard University Press. 1954) and his co-workers as evidence that snow-crystal habit is determined principally by the excess of ambient vapor density over that at equilibrium with the ice crystal at its own temperature. Changes in crystal type occur when this vapor-density excess is sufficient to

overcome the inhibitions, first to edge growth and secondly to corner growth, that must exist if the edges and corners have higher surface vapor densities than the flat faces of the crystal. The higher equilibrium vapor densities over the corners and edges of a shaped crystal should make the effective equilibrium vapor density for the particle taken as a whole somewhat greater than for flat ice.

A preliminary experiment to determine the effective equilibrium vapor density of a crystal was carried out in a small domestic freezer. Crystals were grown on a 2-cm. length of spider silk stretched across a wire yoke and were observed through a binocular microscope, one eyepiece of which was fitted with a micrometer cross-hair. Vapor was supplied by keeping the ceiling of the cold box wet. The ambient vapor density at values close to water equilibrium was measured to within 0·002 g.m.$^{-3}$ (0·1% relative humidity at −15° C.) by measuring the rate of change of diameter of a supercooled water droplet suspended in the working region.

Growth of plate, needle and column crystals was observed at temperatures from −6 to −20° C., for vapor-density excesses, relative to equilibrium over flat ice of greater than 0·1 g.m.$^{-3}$ but always less than water equilibrium. Marshall & Langleben had found that loci of constant vapor-density excess over (flat) ice equilibrium ($\varrho - \varrho_i$) gave as good boundaries between Nakaya's various crystal types as his own empirical ones. To fit the Marshall & Langleben boundaries to our rather limited data, their vapor-density-excess boundary values had to be reduced by some 0·044 g.m.$^{-3}$. The various boundary values are shown in the following table:

	$\varrho - \varrho_{ice}$ (g.m.$^{-3}$)	
	Marshall & Langleben	Values for our present experiment
Dendrites	0·194	0·150
Plates	0·182	0·138
Columns	0·161	0·117
Needles	0·110	0·066
No growth		

No growth was achieved at excess vapor densities lower than 0·066 g.m.$^{-3}$, suggesting that there is an effective equilibrium vapor density for shaped crystals 0·066 g.m.$^{-3}$ higher than for flat ice. The evidence is not conclusive and deserves further study. It is important because the rate of growth of the crystal is proportional to the excess of ambient over this effective density.

A study of growth rates under carefully controlled conditions is now under way, the growth rate being a factor of importance in the development of precipitation in natural clouds.

14·7. A. R. Lang. *Point-by-point X-ray diffraction studies of imperfections in melt-grown crystals.*

A method has been developed for rapidly obtaining information on the distribution of low-angle boundaries, and the intensity and angular range of X-ray reflections over the surface of a large single crystal. The crystal surface is scanned by an X-ray beam of narrow divergence, the crystal being mounted on an accurate linear traversing mechanism. Bragg-reflected X-rays are recorded by counter or by film. In the latter case, the horizontal magnification of the photographic image and the linear resolution of the crystal surface can be controlled by the appropriate choice of traversing direction. A set of traverses is made, covering a range of angles of incidence of the X-rays. At each traverse several square centimetres of crystal surface can be examined. The chief application of the technique is to the study of the development of the striation-type of low-angle boundaries in metal single crystals grown from the melt, and their relationship to impurity cell structures.

14·8. [Withdrawn.]

14·9. D. W. Pashley, E. Grunbaum & R. C. Newman. *The initial stages of growth of oriented copper nuclei on single-crystal surfaces of silver.*

The growth of extremely thin layers of copper has been examined by depositing the copper, from the vapour phase, on to single crystals of silver inside an electron-diffraction camera. The effect of varying the temperature of the substrates from 20° C. to 300° C. has been studied. The thickness of the deposits was measured accurately by using radioactive copper.

It was found that a diffraction pattern due to oriented copper crystallites appeared very rapidly and suddenly as the average thickness was increased beyond a certain critical value, which was about 0·8 Å for a substrate temperature of 20° C. This value did not depend upon the electron accelerating voltage over the range 10–60 kV. The critical thickness was reduced as the substrate temperature was raised, and was about 0·2 Å at a temperature of 300° C.

These results are discussed in relation to the sensitivity of electron diffraction as a means of detecting thin surface films. It is concluded that the sudden appearance of the diffraction pattern at the critical thickness is not controlled by the sensitivity of detection but by the mechanism of growth of the layer. The mechanism of growth is discussed, and its relation to the observed changes in the diffraction pattern is described.

14·10. G. D. Rieck. *Growth and preferred orientations of crystals in tungsten wires.*

Recrystallized wires of doped tungsten are found to contain large crystals with a [421] or [531] axis parallel to the wire axis, and smaller crystals which tend to have more of the original deformation texture [110]. Less dope gives more small crystals with [110] texture and less [531] oriented large crystals. Wires of pure tungsten contain many very small crystals which have a [110] texture after recrystallization.

The grains with a [531] axis in the wire direction are among the ones favourably oriented for a multiple glide along [111] and [100], and as a result of their more severe deformation they will polygonize easier during annealing. Their larger perfect areas then give them a better growing capacity compared with the rest of the grains. The dope is known to inhibite recrystallization and at higher temperatures favours exaggerated grain growth. During the latter process the fast growing [531] oriented grains are able to occupy an extended area of the wire. Less dope gives less inhibition of the [110] grains and more of these are able to grow out.

The nature of the fragmentation found in the large tungsten crystals is not quite in accordance with that to be expected from a grown polygonized nucleus. The difference can be explained if we assume (after Meyering) the dope to be stretched out as second phase in the direction of the wire axis so as to form 'tubes' with 'blocks' and 'leaks' at random places.

14·11. H. I. Matthews. *Crystal structure and growth of particles of smokes produced by arcs between metallic electrodes in gaseous atmospheres.*

Examination of these smokes by means of electron and X-ray diffraction and electron microscopy indicates the relationship between (*a*) the physical properties of the metals and their reactivity to the atmosphere, and (*b*) the structure and growth of the smoke particles. The results show particularly clearly the conditions leading to formation of spherical particles.

For electron microscopy and transmission diffraction specimen grids were coated with a film of carbon, formvar or collodion. For examination by reflexion diffraction the substrate was glass or stainless steel. In every case particles were collected at about 5 cm. from a d.c. arc passing approximately 2·2 A. For both transmission and reflexion electron diffraction the camera length and voltage were about 50 cm. and 60 kV. respectively. The X-ray powder patterns were obtained with Cu $K\alpha$ radiation and a 9 cm. camera.

In some cases useful information on the temperature of formation of the smoke was given by identification of the crystals collected: e.g., the presence of anatase in the Ti smoke, and of valentinite in that from Sb, indicated condensation at between 550 and 800° C., and above 570° C., respectively.

Examples of other points of interest arising from the diffraction results were an electron diffraction pattern showing the presence of yellow PbO only, whilst the X-ray powder pattern indicated that red PbO and Pb were also present; and a ZrO_2 pattern corresponding to a slight departure from the face-centred cubic to the tetragonal system, suggesting that the oxygen content was higher than that required for ZrO_2 composition.

Deposits were shown by electron microscopy to range from crystals of the order of 500 Å diameter, with well developed facets, to globules with no facets visible. In the first category were smokes from Cu, Zn, Cd, Sn, W, Fe, Co and Ni; and in the second those from Ag, Au, Pb, Al, Ti, Zr, Ta and Bi. Particles of both types were produced by Mo and Sb. The Ag and Au deposits consisted of the metal only, those of all the other metals (mentioned above) being oxides.

The essential requirement for the formation of globules is that free crystal nuclei shall be formed during transit by collisions of the atoms, ions or molecules; but that the rate of condensation shall be high in comparison with that of crystallization. The collisions are promoted by the diffusing effect of the gaseous atmosphere.

The relationship between the atmospheric pressure and the structure of the smoke was investigated by examination of deposits from volatilization of Ag and Au in air at reduced pressures, special attention being given to the transition from aggregates of spherical particles to the comparatively compact layers obtained at lower pressures.

14·12. L. W. Strock. *Anisotropic* ZnS *crystals with three-layer stacking.*

Double refracting crystals with three-layer stacking periodicity have been grown from the vapor phase, thus establishing the existence of trimorphism for ZnS single crystals. X-ray precession photographs reveal stacking sequences in both directions, so that the structure is twinned on a fine scale and is at least rhombohedral. From optical-anisotropy studies in progress the true symmetry appears lower, in spite of pseudo-cubic dimensions. These crystals also exhibit marked anisotropy in electroluminescent light emission, with maximum output for fields perpendicular to their *c* axis. The maximum index of refraction lies in the [*c*] direction, which is not always a prominent growth direction.

In addition to the optical and electroluminescent light emission anisotropy, these crystals are also characterized by frequent [11.0] elongation growth habit, with one perfect cleavage (perpendicular to this direction).

All of these properties are compatible with a structural model in which the bonds do not use hybridized sp^3 orbitals, but non-hybridized *s* and *p* orbitals. A survey of all possible combinations of these orbitals for several electronic configurations has shown that only the case of like sulfur orbitals being involved in bonds to any one zinc atom leads to structures compatible with the observed properties of the crystals; and in particular to the presence of a morphological structural unit of dimensions $3a_0$ and $\frac{1}{3}c_0$, with respect to the simple 3-layer X-ray unit cell previously deduced to account for the persistent development of prominent (10.3) and (10.6) crystal forms.

The optical birefringence of the crystals is sharply and finely banded perpendicular to the *c* axis with at least 15 different values ranging from 0·0023 to 0·028 for individual bands in a typical crystal. The band widths are in the range 1–10 microns. The percent of layers within any one birefringent band at which sequence reversals occur is concluded to determine the exact value of the birefringence, while their discontinuities are interpreted as a result of *half reversals* (one atom sort only) which produces a reversal in structure polarity. The crystal is thus composed of slices of opposite polarity (1–10μ thick) perpendicular to the *c* axis. Each slice contains a number (up to 100%) of *complete reversals* which are equivalent to *c*-axis rotation twins on a submicroscopic scale. The *half reversals* can arise during crystal growth by an atom selecting its alternate available 4-fold position, which generates a single boundary layer of the other atom sort in 6-fold coordination. Banded birefringence can thus be developed in parent three-layer stacking crystals of either isotropic (cubic) or rhombohedral (anisotropic) structure by development of *half- and complete reversals* during crystal growth. The ever-present fine surface striations are interpreted as fine scale changes in surface morphology caused by the *complete reversals*.

Anisotropy of electroluminescent-light emission was observed for both [11.0] elongation habit and [00.1] developed crystals, regardless of whether their photoluminescence is long decay green or shorter decay blue. Electric fields applied perpendicular to [*c*] produce an approximate order of magnitude more light emission than do fields parallel with [*c*] for equal crystal thickness.

14·13. L. M. Beljaev, V. A. Perlstein & V. P. Panova. *Investigation of activator distribution in alkali halide crystals by the radioactive isotope method.*

The distribution of activators is studied by the radioactive isotope method in the crystals potassium iodide, sodium iodide and cesium iodide. The process of non-uniform distribution of crystal activators in crystals grown by the Kyropoulos and Obreimov–Shubnikov methods is established.

14·14. D. R. Hale. *Growth of synthetic quartz crystals.*

The synthesis of quartz crystals has been successfully accomplished. These crystals, when grown under optimum conditions, are especially noteworthy because of regular shape, uniformity, chemical purity, high optical transmission, and excellent piezoelectric properties. The low solubility of quartz requires that the growing process take place in alkaline solution at elevated temperature and pressure, and with the provision of a supply of feed quartz. The crystallizing quartz will appear as microcrystals unless seeds are used, and the use of seeds permits large variations (illustrated) in shape and relative dimensions of crystals obtained.

Serious study of the problem in the U.S.A. was begun about ten years ago; reference to several papers since that time is made (English, French, U.S.). Study of growth conditions leads into fields of high-pressure equipment and phase-rule equilibria under elevated temperature and pressure. Recent work has involved changes in type of growing vessel, observation of growth rates as dependent on atomic plane exposed to the supersaturated solution, study of purity and crystal perfection as dependent on conditions of growth.

Technically this investigation is important because of the widespread interest in quartz radio resonators, quartz optical components (especially for spectrographs) and high purity silica for certain uses such as for the preparation of transistor-grade silicon.

14·15. I. S. Res, L. S. Rusakov & G. N. Stoikov. *The growth of piezoelectric crystals in USSR.*

In developing industrial and laboratory methods of growing piezoelectric single crystals in the USSR an attempt was made to secure the maximum output of perfect crystals of optimum dimensions. Therefore each crystal requires a specific technique.

Acceleration of growth was achieved by introducing dynamics into an initially static process; optimum habit was achieved by the use of seeds and additives, by annealing brittle crystals during growth, and by isothermal growth at elevated temperatures.

Rochelle salt (KNT), dipotassium tartrate (DKT) and ammonium dihydrogen phosphate (ADP) crystals are grown on an industrial scale, crystals of ADP in oriented single-crystal blocks; ethylene diamine tartrate (EDT), lithium sulphate monohydrate (LSH), guanidin aluminium sulphate hexahydrate (GASH) and sorbitolhexaacetate (SHA) are grown on a laboratory scale.

1. KNT is grown by the dynamic method in industrial 10 l.-capacity glass crystallizers, arranged in groups of 100–130 in thermostatic chambers. The seeds have the dimensions of $3 \times 1{\cdot}5 \times 6{\cdot}0$ mm. (x, y, z) and are mounted on stainless crystal holders, having the form of a tapered rod. During the growth period the temperature is reduced from 46 to 27° C. The crystals rotate at the rate of 26 rev.min.$^{-1}$. The duration of the growing cycle averages to 22–23 days. The crystal crop is 60 kg.m.$^{-2}$ of the floor area per month. Rate of growth on the x, y, and z axes amounts to 3·1–3·6, 4·3–4·8, and 3·3–4·4 mm.day^{-1}, respectively. The mean weight of the KNT crystal is about 4–5 kg. Additive to the solution: KOH+NaOH (1:1), 2·0 g.l.$^{-1}$.

2. DKT crystals are grown by the dynamic method in group crystallizers—180 l.-capacity stainless tanks, 32 crystals in each. Growth of single crystals starts from bar-shaped seeds of $100 \times 5 \times 5$ mm., with their length along the y axis, fixed in groups of eight on a flat crystal holder of polymethyl methacrylate. The common shaft is oscillated through an angle of 90–120°, 30 reversals per minute. During the growth period the temperature drops from 55 to 25° C. The duration of growth cycle averages 43–45 days. Additive to the solution: KOH, 9–10 g.l.$^{-1}$. Weight of 'half' crystals amounts to 0·6–0·7 kg. (weight of 'full' crystals is about 0·9–1·2 kg.); crystal crop 30 kg.m.$^{-2}$ floor area per month. Rates of growth on the x and z axes are $\leq 0{\cdot}3$ and $\leq 0{\cdot}7$ mm.day^{-1} respectively.

3. ADP crystals are grown by the dynamic method in group crystallizers—180 l.—capacity stainless tanks, 12 crystals in each. Growth is achieved from bar-shaped seeds of $100 \times 3 \times 3$ mm., oriented along [111]. The seeds are fixed on individual crystal holders, mounted on a common shaft. The shaft is oscillated through an angle of 90–120°, 30 reversals per minute. The temperature is reduced from 60 to $\approx$ 40° C. The duration of growth cycle is 27–29 days. The solution is prepared from c.p. ADP without any additives. The weight of ADP single-crystals (full form) amounts to 1·7–2·3 kg. Crystal crop is about 60 kg.m.$^{-2}$ floor area per month. Rate of growth on the z axis is 3·3–3·7 mm.day^{-1}; on the x and y axes it is negligible.

4. Growth of oriented ADP crystal blocks is carried out from solutions with pH $\approx$ 5·7. The rectangular seeds, cut in the y and z plane, are arranged to allow growth in the x direction only. The seeds are submerged in an array of crystallizers connected with saturating and filtering tanks. The temperature in the saturator is 8–10° C. higher than in the crystallizers of the battery. The convection-driven circulation secures perfect growth of crystalline blocks at the rate of 2–2·5 mm.day^{-1}.

5. EDT crystals are grown from flat seeds, oriented along the short diagonal of plane (010). The method used is isothermal, with a constant temperature difference between the saturator and crystallizer tanks of 42–39° C. The solution is continuously saturated with fresh salt and circulates through the closed system by means of a pump. The rate of growth on the y axis is 2·5–4 mm.day^{-1}. The presence of Fe$''$ ions causes tapering of the EDT crystals.

6. LSH crystals are grown isothermically from bar-shaped seeds, oriented on the z axis. Withdrawal of the condensate takes place at 102° C. in order to anneal the crystal during growth. In the process of growth the crystals are oscillated. The LSH solutions are acidified with 2–3 g.l.$^{-1}$ sulphuric acid. Acceleration of growth along the z axis is achieved by adding up to 10 g.l.$^{-1}$ sulphuric acid. The rate of growth is equal 1·3 mm.day^{-1}.

7. GASH is grown isothermically from water solu-

tions, saturated at 40–45° C. The seeds are pointed; supersaturation is regulated by controlled evaporation. The growth is static. The rate of growth is 1·5 mm.day^{-1}. A perfect GASH monocrystal, weighing 234 g., was grown in 28 days.

8. SHA is grown dynamically from solutions in 96% ethanol with the addition of 5 g.l.$^{-1}$ KOH. The seeds are bar-shaped and oriented parallel to the z axis. During growth the crystals are oscillated. The rate of growth on the y and z axes is about 2–3, and 0·4–0·6 mm.day^{-1} respectively. The temperature of saturation of the alcoholic SHA solution is about 60° C.

14·16. H. Wilman. *Some new electron-diffraction results on epitaxial crystal growth.*

A 'directed' disorientation about a definite lattice row is observed in Cu electrodeposits formed in parallel epitaxial orientation on smooth electropolished Ag (110) and (001) faces, but not in Ag electrodeposits on smooth Cu faces (D. N. Kumar & H. Wilman). It is concluded that the stresses arising from the misfit at the interface tend to cause deformation, leading to a directed disorientation of the overgrowth crystals, when these crystals are under tension, more easily than when they are under compression due to the epitaxial stresses. Epitaxial electrodeposits of Fe on electropolished Cu (111), (100) and (110) faces are also found (A. K. N. Reddy & H. Wilman) usually to show marked directed disorientation, in some cases tending consistently to be in a definite sense of rotation from the initial orientation.

Our recent experiments (with V. D. Scott) on thermal oxidation of Be single-crystal (0001) cleavage faces in air at about 300° C. show that the BeO is formed mainly in (0001) orientation with ⟨100⟩ BeO parallel to ⟨100⟩ Be, the misfit of the two lattices being 22%. Oxidation of other faces is also being investigated.

Oxidation of electropolished Pb (111), (100) and (110) faces (S. Pash) in air at 150–350° C., yielded red PbO orientated mainly with the axes of the face-centred tetragonal pseudo-cubic red PbO parallel to the cubic axes of the Pb substrate, in all possible permutations. In these PbO orientations the Pb atoms are thus in a similar arrangement in the oxide to that in the metal, but further apart owing to the interposed oxygen atoms.

Reduction, by atomic hydrogen, of Cu_2O which had been formed epitaxially on smooth Cu (111) faces is found (M. R. Piggott) to lead to epitaxially parallel-orientated Cu crystals when the reaction rate is slow enough, but to random Cu crystals at higher rates. The process of reduction is thus very similar to other types of reaction in respect of the conditions leading to epitaxy.

The thermal oxidation in air of pyrites natural faces of (111), (100), (213) and (650) types has been studied (G. B. Thomas & H. Wilman). As in the well known case of oxidation of zincblende, oxidation occurs above a well-defined temperature (here ~ 370° C.). In air no epitaxy of the oxide is observed, but only random α-Fe_2O_3 and γ-Fe_2O_3 on the FeS_2 (001) face; and on the (111) FeS_2 the α-Fe_2O_3 was random and the γ-Fe_2O_3 grew with (111) parallel to the surface but with no azimuthal preference. In air mixed with steam the γ-Fe_2O_3 was formed, and grew in an epitaxial orientation of particular interest. On FeS_2 (111), the γ-Fe_2O_3 grows with {111} parallel to the (111) surface, but with an azimuth difference of 20°. On (001) FeS_2 it grows with {111} parallel to, respectively, each of the {210} FeS_2 planes which meet at the surface in the cube edge along which are the S rows, and a $\langle 11\bar{2} \rangle$ row is parallel to this FeS_2 cube edge, a {153} plane being nearly parallel to (2° off) the FeS_2 surface. On (210) FeS_2, however, no γ-Fe_2O_3 was observed having {111} parallel to the surface, but only the other of the above relative orientations was shown. (111) γ-Fe_2O_3 growing parallel to (001) FeS_2 was observed in one case where the FeS_2 was heated slowly from room temperature instead of being put cold into the oven which was already at about 300° C. so that steam condensed on the surface.

14·17. V. A. Frank-Kameneckij. *Einige Eigentümlichkeiten der epitaxischen Verwachsungen der Silikatminerale.*

Hier werden Angaben der röntgen, der optischen und der goniometrischen Untersuchungen folgender gesetzmässiger Verwachsungen der Silikatminerale angeführt: Quarz-Feldspat, Quarz-Glimmer, Feldspat-Glimmer, Feldspat-Hematit (Sonnenstein), Glimmer-Tremolit, Glimmer-Apatit, Kaolinit-hydroglimmerige und montmorillonit-hydroglimmerige Verwachsungen der schiefrigen Silikate im Dispersionszustand u. a. m.

Das Studium der Oberfläche der Verwachsung und die Korrelation zwischen der Frequenz gesetzmässiger Verwachsung und dem Charakter der topochemischen Übereinstimmung gestatten primäre Verwachsungen von den sekundären zu unterscheiden und die Bedingungen der Entstehung der Verwachsungen zu präzisieren. Die epitaxische Natur der Verwachsungen wird am genauesten festgestellt auf Grund der Vergleichung der statistischen Angaben über die Verbreitung der Verwachsungen mit den strukturellen Angaben.

Allgemeine Gesetzmässigkeit der epitatischen Verwachsungen der Silikatminerale ist die Kongruenz im Verwachsungskeim der kieselsauerstofflichen und alumokiselsauerstofflichen Elemente der Tetraeder (allgemeine Sauerstoffschicht).

Bei der Verwachsung der Silikate mit den Phosphaten kongruieren die Tetraeder SiO_4 und PO_4.

Bei der Verwachsung der Silikate mit anderen Sauerstoffverbindungen (Feldspat–Hematit) verwirklicht sich die Kongruenz der Sauerstoffschichten.

Die Kationübereinstimmung und Kongruenz der Parameter des Gitters (Epitaxikriterium von Royez) haben an und für sich keine ausschlaggebende Bedeutung für die Entstehung der epitaxischen Verwachsungen der Silikate.

Es wird die Frage behandelt über die durch die epitaxischen Übereinstimmungen bedingten Vorgänge des Ersatzes und Zerfalls der festen Lösungen, welche unter den Silikaten stattfinden und sich gewöhnlich im festen Zustande verwirklichen.

14·18. K. R. Dixit. *Epitaxial growth of thin films.*

The author has already given a theory of the growth of deposits on amorphous substrates, upon which fibrous orientations are often observed. In the present paper an attempt is made to develop a general theory of the growth of thin films. The following cases are considered:

(1) The growth of evaporated metallic films on (*a*)

single metal crystals, (*b*) single crystals of alkali halides, (*c*) mica.

(2) The growth of electrodeposited metallic films on (*a*) amorphous metals, (*b*) single metal crystals.

(3) The growth from solution of ionic crystals on (*a*) amorphous metals, (*b*) metal single crystals, (*c*) other ionic crystals.

An evaporated metallic film is built up on a single-crystal surface, as a two-dimensional gas. The atoms in the film will be subjected to the same forces as considered previously, which give a particular orientation for a particular temperature of the substrate. The substrate is, however, no longer amorphous, and any subsequent growth will have to take account of the additional forces produced by the structure of the surface. In the first case, if the metals are evaporated on to their own single crystals, forces of the Frank type have to be considered. In other cases the relevant metallic or ionic forces must be considered. The observed crystal structure and the orientation will be the combined result of the forces of temperature orientation and the metallic or the ionic attractions.

In the second case of electrodeposition of metals we have to work within the framework of the Debye–Huckel–Onsagar theory of electrolytes. This theory will have to be slightly modified by the use of Frank's rules in the case of deposition on single metal crystals.

In the case of growth from solution of ionic crystals the motion in solution will be mainly governed by the laws of the theory of electrolytes. The rate of evaporation, which governs the rate of growth and the movement of the ions in the solution, will be the chief modifying factor.

The calculations made on this basis appear to agree reasonably well with the present observations.

14·19. A. V. Šubnikov. *Splitting of diphenylamine crystals followed by formation of spherulites.*

Diphenylamine spherulite formation with *Zweiblatt* is demonstrated by means of micro-film projection. The explanation of this fact is given on the basis of the Gibbs–Curie principle.

14·20. H. E. C. Powers. *Sucrose crystal studies.*

Crystallographically, sucrose is an interesting subject for study. There is a considerable amount of evidence indicating complex molecule formation in solutions of higher concentration. Solutions of high supersaturation may be preserved for long periods without spontaneous nucleation, the limiting example being spray-dried sucrose, which is variously termed amorphous or glass. Palmer *et al.* have shown by X-ray study that in spite of the extreme supersaturation, crystallization ensues only in the course of months. Nuclei-free solutions up to 1·4 supersaturation may be preserved for months without nuclei being formed but the author has confirmed and extended the Earl of Berkeley's findings (*Phil. Mag.* (1912), **24**, 254) that any sufficiently violent shock or disturbance will produce spontaneous nucleation, the more violent the shock the lower the degree of supersaturation thus triggered off. The author suggests that the well known diagram indicating metastable and labile zones should be interpreted only as a general indication of nucleation in a system subjected to mechanical shock of a definite intensity.

'Vegetative' nucleation, or nucleation in presence of pre-existing crystals, is also strongly influenced by mechanical shock or movement, and the author has explored both this and the previous nucleating conditions by counting the nuclei produced by mechanically compelling the rapid movement of (*a*) a large sucrose crystal and (*b*) a similarly shaped perspex model of the previous crystal.

The author has shown that sucrose crystals grow by layer growth, also that water may be included in the crystal, just as Bunn and others have shown with sodium chloride and other polar compounds. He has demonstrated the presence of this included water by comparison of vapour-pressure equilibria with the whole and with the crushed crystals. Micro-photographs have been taken indicating the actual 'growing over' of these inclusions by the surface layers. Microscopic examination of a large number of coloured sucrose crystals indicated the form of the syrup inclusions to vary greatly. Sometimes the inclusion exhibits a certain dendritic symmetry, sometimes it takes the form of drifts or lines of inclusions cutting right through the planes of symmetry, and sometimes relatively large local clouds and veils of approximately spherical droplets of the order of 1 micron in diameter. Large areas of the same crystal may be virtually colourless and the author's impression is that colour inclusion is almost entirely present in this form, and not as a molecular dispersion. The author has found that large sucrose crystals (mean aperture 1 in.) may contain included water to the extent of 0·4% down to 0·03%, whilst small crystals (mean aperture 0·03 in.) appear to contain about one-tenth of this proportion. Gas, presumably air, is also included to a varying degree, the whole being reflected in the clarity, and variation of specific gravity and melting point, etc.

The author has examined, under the microscope, sucrose crystals growing in syrups up to 1·3 supersaturation without being able to see any true dendritic growth at the corners or edges of the crystals. He pursued this search by examining crystals growing in various gelled syrups to protect fragile dentrites, and again obtained no evidence of dendritic growth, though this checking of local surface currents led to the local production of sub facets 101 etc., over the surface of the crystal, producing an effect the author has termed tesselated. The author feels that vegetative nucleation at lower supersaturations is not produced by the breaking-off of dendrites, but rather by the sheering-off of fragments of the growing surface not yet fully 'anchored' to the parent crystal. By analogy with the effect of air currents upon wave crests, he suggests the term 'spume' for these molecular aggregates, and points out that they will give rise to true crystals or will disperse in accordance with the degree of supersaturation of the mother liquor into which they are thrown.

The author feels that this conception harmonizes with the evidence of complex molecular groups in concentrated solution and with the spontaneous nucleation by shock wave. He visualizes the growing surfaces as being covered by a 'fluidized blanket' of molecules awaiting anchorage. One might consider this as an extension of the Burton, Calvera & Frank conception. The author has calculated that in normal pan boiling each crystal grows at the rate of some fifty molecular layers per second.

At higher supersaturation, where the conditions approach more nearly those of a melt, nucleation may be

dendritic in the absence of much sheering action. This might be considered reasonable, in view of the well known observation that in normal commercial pan boiling, if nucleation is effected at too high a supersaturation, then much conglomerate grain is produced. By contrast with this, in fondant production, even though nucleation is brought about at very high supersaturation, violent stirring of the syrup produces remarkably perfect grain, relatively free from conglomerates.

Illustrating the lower solubility of nuclei, the author has been able to record cine-micrographically a small crystal of about one micron length growing in the syrup well away from a very large crystal, drifting into the lower concentration gradient near the large crystal and there rapidly dissolving.

Internal cleavage faces of sucrose crystals (parallel to 100) submitted to the electron microscope have yielded one excellent example of mosaic, several suggestive of possible mosaic, and a number of layer structure. X-ray examination indicates scattering of the rays as would be produced by mosaic. The author's impression is that just as the liquor and gas inclusions are local, so mosaic may be local, and it would be interesting to find the conditions leading to maximum or minimum mosaic formation. A. Van Hook has recorded electron micrograph evidence of mosaic upon an etched surface of sucrose crystal (*Proc. Amer. Soc. Sugar Beet Tech.* (1950), **21**, 573).

Present evidence suggests that whereas much of the foreign matter within the crystal is associated with liquor inclusions, particularly colouring matter, yet some ionized salts appear to be adsorbed in the lattice and, if so, could logically lead to 'Frank' dislocations, though to date no spiral growths have been seen. Most layer fronts appear to resolve themselves into rectilinear steps, if examined under a sufficient magnification.

Etch figures are characteristic and frequently indicate the essentially layered structure of the sucrose crystal.

§ 15. Neutron diffraction

15·1. G. E. Bacon. *Molecular structure determination by neutron diffraction.*

The past few years have seen an increasing use of single-crystal neutron-diffraction techniques for producing molecular structure projections by conventional Fourier-synthesis processes. This has centred on the determination of hydrogen positions to supplement the existing structural data obtained with X-rays, with the particular aim of studying hydrogen bonds and C–H bonds. As examples of aromatic molecules to which these methods are particularly suited we have studied α-resorcinol, potassium hydrogen bisphenylacetate and 4:4 dichlorodiphenyl sulphone. In the first the C–H bond length is 1·08±0·04 Å and there are clear variations among the thermal vibrations of the hydrogen (and other) atoms in the molecule. In the phenylacetate the mean C–H length is 1·13 Å and there are markedly anisotropic vibrations for the hydrogen atoms which are remote from the centre of symmetry. Across the centre of symmetry itself a symmetrical hydrogen bond is not ruled out (in agreement with the infra-red results) and it is noteworthy that the seemingly isotropic hydrogen atom here is markedly diffuse, with a standard deviation of thermal displacement of 0·3 Å.

The study of 4:4 dichloro-diphenyl sulphone was commenced with the assistance of far fewer parameter data from X-ray work than has usually been the case. Concurrent with the neutron study the structure is being defined by X-rays at Glasgow. It is hoped that neutron measurements of the C–H bond lengths will be available for the Congress.

15·2. S. W. Peterson, H. A. Levy & V. Schomaker. *Neutron-diffraction study of N-acetyl glycine.*

Single-crystal neutron-diffraction data obtained for the [0*kl*] and [$\bar{h}$,*k*,2*h*] zones of *N*-acetyl glycine have been analyzed by Fourier and least-squares methods. The Fourier projections gave strong indications of a rotating methyl group, and accurately located all other atoms. The least-squares model subsequently used assigned the three methyl hydrogen atoms statistically to 12 equally spaced positions, and all other atoms were assigned independent position and asymmetric thermal parameters. The resulting heavy-atom positions and hydrogen bonding network is consistent with the earlier findings of G. B. Carpenter & J. Donohue (*J. Amer. Chem. Soc.* (1950), **72**, 2315).

15·3. H. A. Levy & S. W. Peterson. *Analysis of thermal and electron asymmetry of urea from combined neutron and X-ray diffraction data.*

Neutron-diffraction measurements of the *h*0*l*, *hk*0 and *hhl* reflections of urea have been analyzed by least-squares methods to give a complete set of position and thermal parameters. Comparison of these parameters with the values derived from X-ray measurements of P. Vaughan & J. Donohue (*Acta Cryst.* (1952), **5**, 530) and the results of the re-analysis of their data by H. J. Grenville-Wells (*Acta Cryst.* (1956), **9**, 709) indicated sizeable discrepancies between the neutron and X-ray results. Consequently a complete least-squares treatment of the V.–D. X-ray data has been carried out in order to test the adequacy of the earlier refinements. The atomic scattering factors of Berghuis *et al.* were used for C, N and O while James & Brindley values were used for H. The neutron-determined position and thermal parameters for H were assumed and were not varied in the refinement. The V.–D. data were weighted according to the formula $w(F^2) = [(0{\cdot}1F^2)^2+(0{\cdot}20)^2]^{-1}$ and the quantity $\Sigma w(F^2)(F_o^2-F_c^2)^2$ was minimized. General asymmetric temperature factors of the form $\exp(-\Sigma_i\Sigma_i\beta_{ij}h_ih_j)$ were assumed.

The least-squares treatment converged to a set of parameters differing in small details from the results of the earlier refinements but in essential agreement with them. The measure of agreement obtained between experimental and calculated structure factors is indicated by a value of $\{\Sigma_i w_i(F_o^2-F_c^2)^2/(m-n)\}^{\frac{1}{2}} = 1{\cdot}75$ and $\Sigma||F_o|-|F_c|| \div \Sigma|F_o|$ (including unobserved reflections at half the minimum observable value of F) of 4·3%. The major parameter shifts which occurred were in the direction to increase the discrepancy between the neutron and X-ray results and there were a number of discrepancies as large as 3–6 combined standard deviations of the measured parameters. The standard deviations of the parameters were obtained from the inverse matrices of the normal equations.

New X-ray spectrometer measurements on urea are

in progress which should determine whether the above results have been influenced by experimental error. Attempts to analyze the thermal parameter differences in terms of electron asymmetry are being made.

15·4. G. E. Bacon. *Neutron-diffraction study of copper–manganese alloys.*

A study of Mn–Cu alloys containing 70–95% Mn has shown the equivalence of the Néel temperature, at which antiferromagnetic alignment disappears, and the temperature of the diffusionless transformation from tetragonal to cubic structure, which was studied using X-rays by Z. S. Basinski & J. W. Christian (*J. Inst. Met.* (1951), **80**, 659). For a given alloy composition the actual temperature can be varied, by about 50° C. for a composition of 85% Mn, according to the initial heat treatment; but in all cases the equality is maintained. For homogenized quenched alloys the nuclear scattering intensities are in good agreement with those calculated on the assumption of a random distribution of Mn and Cu atoms. The magnetic intensities are in agreement with the model proposed by D. Meneghetti & S. S. Sidhu (*Phys. Rev.* (1957), **105**, 130) and lead to a magnetic moment of $2{\cdot}4\mu_B$ for γ-face-centred manganese.

When polycrystalline specimens are subjected to linear pressures of up to 40 kg.mm.$^{-2}$ it is found that the magnetic moments tend to line themselves along the pressure axis, giving a preferential alignment of c axes (c is less than a) along this axis. This conclusion is supported by X-ray diffraction and magnetic susceptibility measurements.

15·5. E. F. Bertaut, F. Forrat, A. Herpin & P. Mériel. *Structure des grenats ferrimagnétiques aux rayons-X et aux neutrons.*

Les combinaisons de formule générale $5Fe_2O_3.3A_2O_3$, où A est un ion trivalent de terre rare, ont la structure des grenats (groupe d'espace $Ia3d$) et sont ferrimagnétiques. En accord avec les prévisions de Néel, il y a deux sous-réseaux de fer, (en 16(a) et 24(d)) couplés ferrimagnétiquement et un sous-réseau de terre rare (en 24(c)) dont le moment magnétique est antiparallèle par rapport au moment résultant des ions Fe. La variation des paramètres de ces grenats en fonction du nombre atomique Z illustre bien la contraction des lanthanides.

15·6. W. L. Roth. *Antiferromagnetic domains in* NiO.

The antiferromagnetic arrangement of magnetic moments in NiO has been studied by powder and single-crystal neutron diffraction. The presence of antiferromagnetic domains in single crystals has been established from measurements of the distribution of intensity in the magnetic reciprocal lattice. Since a crystalline deformation results from magneto-anisotropy associated with the antiferromagnetic spin arrangement, structures observed by optical microscopy of single-crystal thin-sections may be correlated with the antiferromagnetic domains. Domains have presently been grown up to several millimetres in size, and the movement of domain walls by applying external stresses, heating through the antiferromagnetic Curie temperature, and applying magnetic fields has been observed and photographed. The relationship between antiferromagnetic domain boundaries, dislocation walls, magnetic stacking faults, and twin boundaries will be discussed.

15·7. W. C. Koehler, E. O. Wollan, M. K. Wilkinson & J. W. Cable. *Neutron-diffraction study of magnetic ordering in rare earth orthoferrites.*

The rare earth orthoferrites $AFeO_3$ in which A is La, Nd, Er, or Ho crystallize in the orthorhombic $GdFeO_3$ modification of the perovskite structure. In the ideal ABO_3 perovskite the A- and B-site cations form simple cubic lattices and each B-site cation is surrounded by an oxygen octahedron. Since these conditions are approximately realized in the rare earth orthoferrites, this system is particularly appropriate for a study of indirect magnetic interactions.

In each of the above-mentioned compounds a high-temperature ordering of the Fe^{+3} ions is observed, as evidenced by characteristic coherent magnetic reflections in the neutron-diffraction patterns. Transition temperatures, obtained by measuring the intensity of a strong reflection as a function of temperature are 750, 680, 630, and 660° K. for the La, Nd, Ho, and Er compounds respectively. The ordered configuration adopted by the Fe^{+3} ions is one in which each spin is surrounded by six antiparallel nearest neighbors. There are indications that in $HoFeO_3$ this antiferromagnetic configuration may not be completely ideal.

Near 77° K. the coherent intensities due to the ordered iron-ion spin system are temperature-saturated, and these are superimposed upon a paramagnetic diffuse scattering background due to randomly oriented rare earth ion moments.

In the liquid-helium region additional coherent reflections are observed for $ErFeO_3$ and $HoFeO_3$, and these are accompanied by a diminution in the background scattering indicating the onset of ordering of the rare earth ions. These additional reflections are essentially temperature saturated at 1·25° K. and transition temperatures of about 4·0 and 5·0° K. for $ErFeO_3$ and $HoFeO_3$ are indicated.

The configuration adopted by the rare earth ions appears to be one in which chains of like spin are surrounded by four chains of like spin oppositely directed. In $ErFeO_3$ the moment direction has a large component parallel to the direction of like spins, in $HoFeO_3$ a large component perpendicular to it. In both cases there is evidence that the alignment is not ideal.

15·8. W. C. Koehler & H. A. Gersch. *Types of magnetically ordered configurations on simple lattices.*

In crystals which contain magnetically active ions various ordered arrangements of the moments may exist, depending upon the details of the interactions among the spins and upon the space lattice appropriate for the crystal. Ordered configurations corresponding to energy minima under simplifying assumptions concerning the interactions (isotropic with specified interactions between nearest and next nearest neighbors) have been predicted for a number of simple lattices (P. W. Anderson, *Phys. Rev.* (1950), **79**, 705; J. M. Luttinger, *Phys. Rev.* (1951), **81**, 1015; J. S. Smart, *Phys. Rev.* (1952), **86**, 968; (1953), **90**, 55; J. H. Van Vleck, *J. Phys. Radium* (1951), **12**, 262), and have been found experimentally by neutron-diffraction experiments. These latter investigations have also uncovered other types of ordered configurations.

At the present time neutron magnetic scattering data are analyzed to a great extent by trial-and-error methods. It is therefore of some interest to investigate the diffraction effects to be expected from ordered configurations on a number of simple lattices. To this end a consistent scheme for enumerating the structure types possible for a given lattice without regard to energy considerations has been developed. Of course, once a configuration is known, its energy, in the same approximation as that of the above references, may readily be computed.

Our model assumes scalar spins so that at each lattice point there is either a spin up (+) or a spin down (−), and we seek configurations in which the distribution of like and unlike spins around a given one is the same for all spins. Within our approximation the Hamiltonian for the spin system is a quadratic form in the spin variables, each of which can take on only discrete values which for simplicity may be taken as (±1). Without this restriction to discrete values the Hamiltonian is analogous to the potential energy of a crystalline solid expanded about its energy minimum. If we now imagine the spin variables to be continuous, they can be represented in terms of normal coordinates. Each normal mode describes a spin configuration with definite phase relations between neighboring spins and the spin states we seek correspond to those normal modes for which neighboring spins are in phase (spins parallel) or 180° out of phase (spins antiparallel). If cyclic boundary conditions are imposed the requirement of equivalence of spins at different lattice sites is satisfied.

Following the procedure outlined above, the spin at a lattice site $\mathbf{R}_L = l_1\mathbf{a}_1+l_2\mathbf{a}_2+l_3\mathbf{a}_3$ is given by

$$S_{l_1l_2l_3} = \cos(\mathbf{k}.\mathbf{R}_L)+\sin(\mathbf{k}.\mathbf{R}_L), \qquad (1)$$

where $\mathbf{k} = \omega_1\mathbf{b}_1+\omega_2\mathbf{b}_2+\omega_3\mathbf{b}_3$ and the ω_i are restricted to the values $0, \pm\frac{1}{2}\pi, \pi$, $i = 1, 2, 3$. To each choice of the ω_i there exists a spin configuration which may be written down in accordance with the above equation. Alternatively one may observe that the propagation vector $\mathbf{k}$ is normal to planes of like spin. The manner in which these planes alternate in sign is determined from the 'wave length' $\lambda = 2\pi/|k|$. For a simple cubic point lattice, for example, the configurations $\frac{1}{2}\pi, \frac{1}{2}\pi, \frac{1}{2}\pi$ and π, π, π both describe (111) planes of parallel spins. For $(\omega_1\omega_2\omega_3) = (\frac{1}{2}\pi, \frac{1}{2}\pi, \frac{1}{2}\pi)$ the planes occur in the order $+ + - - + + - -$; for $(\omega_1\omega_2\omega_3) = (\pi, \pi, \pi)$ they occur in the order $+ - + - + -$.

Examples of the classification scheme for simple lattices and correlations with experiment are given. A consistent system of nomenclature for ordered spin systems, which is descriptive of the configuration, is proposed.

§ 16. Symmetry, morphology, twinning

16·1. W. Kleber. *Zur Genese der Hyper- und Hypomorphie.*

Ohne Zweifel ist es wachstumskinetisch von besonderer Bedeutung, wenn die morphologische (exogene) Symmetrie eines Kristallindividuums nicht mit seiner strukturellen (endogenen) Symmetrie übereinstimmt. Es ist klar, dass solche Fälle nur dann ernsthaft nachweisbar sind, wenn die Strukturs symmetrie etwa durch systematische Auslöschungen (z. B. Gleitspiegelebenen) belegt werden kann. Wie D. H. Templeton (*Acta Cryst.* (1956), **9**, 199) allgemein gezeigt hat, ist dieser Nachweis nicht immer eindeutig. Gelegentlich führen kritische strukturanalytische Diskussionen auch unabhängig von systematischen Auslöschungen zu Ergebnissen, die zur Morphologie in Widerspruch stehen.

Wir können zwei Fälle von Symmetriediskrepanzen unterscheiden: 1. Die morphologische Symmetrie ist gegenüber der Strukturs symmetrie erhöht ('Hypermorphie'); 2. Die morphologische Symmetrie erscheint gegenüber der Strukturs symmetrie erniedrigt ('Hypomorphie'). Als Beispiele für Hypermorphie können folgende Kristallarten angesehen werden: Beim Aluminiummetaphosphat, $Al(PO_3)_3$, sind unter besonderen Kristallisationsbedingungen 'Oktaeder' beobachtet worden. B. Gossner & H. Mussgnug (*Zbl. Min. Geol. Paläont.* (1930), S. 321) geben für Barytocalcit, $CaBa[CO_3]_2$ im Gegensatz zu der monoklinprismatischen Formenentwicklung $(2/m)$ auf Grund strukturanalytischer Betrachtungen die Raumgruppe $P2_1$ an. Bei Childrenit bzw. Eosphorit, $(Fe, Mn)Al[(OH)_2|PO_4].H_2O$, könnte eine Hypermorphie von *Bba*2 nach $2/m2/m2/m$ vorliegen. Nach den Angaben von J. C. Monier & R. Kern (*Bull. Soc. franç. Minér.* (1956), **79**, 500) zeigen Kristalle der kubischen Modifikation von SiC (Raumgruppe $F\bar{4}3m$) die Kombination von 'Oktaeder' und Würfel.

Beispiele für Hypomorphie sind von W. Kleber (*Wiss. Z. Humboldt-Univ., Berlin*, (1956), **5**, 1) angegeben und kritisch diskutiert worden: α-Schwefel ($Fddd \rightarrow 222$), Cuprit ($Pn3m \rightarrow 432$), Phosgenit ($P4/mbm \rightarrow 422$), Salmiak ($Pm3m \rightarrow 422$) und $Pb[NO_3]_2$, $Ba[NO_3]_2$, $Sr[NO_3]_2$ ($Pa3 \rightarrow 23$). Die angeführten Fälle zeigen eine spezielle Art der Hypomorphie, die durch den Fortfall der Spiegelebenen bzw. des Inversionszentrums bei der morphologischen Symmetrie gekennzeichnet ist ('Enantio-Hypomorphie'). Andere Typen von Hypomorphie repräsentieren möglicherweise Lepidokrokit ($Amam \rightarrow mm2$), Eis(I) ($Cbmc \rightarrow 3m$) und Diamant ($Fd3m \rightarrow \bar{4}3m$).

Für eine bestimmte Gruppe hypermorpher Fälle ist eine wachstumskinetische Deutung auf der Grundlage der Theorie von Kossel & Stranski durchaus gegeben. Es handelt sich um die Situation, dass die Struktur kein Inversionszentrum besitzt ('polare Hemiedrie'), die Kristallformen jedoch zentrosymmetrisch erscheinen. Nach J. C. Monier & R. Kern (*Bull. Soc. franç. Minér.* (1955), **78**, 585) gilt für die Wahrscheinlichkeit p bzw. $\bar{p}$ für die Anlagerung eines Bausteines an eine polare Fläche bzw. an deren Gegenfläche einer Kristallart mit zwei Komponenten folgender Ausdruck:

$$p/\bar{p} = \exp\{-(\alpha-\bar{\alpha})[\mathrm{grad}\,\varphi]^2/2kT\}.$$

Hierin sind α bzw. $\bar{\alpha}$ die Polarisierbarkeiten der beiden am Aufbau des Gitters beteiligten Atome, φ das Potential an der Oberfläche des Gitters, k die Boltzmann-Konstante, T die absolute Temperatur. Man erkennt, dass Unterschiede in den Anlagerungswahrscheinlichkeiten nur dann merkbar auftreten, wenn die Differenz der Polarisierbarkeiten der beiden Bausteine nicht zu gering ist. Demnach wird eine polare Flächenentwicklung nur dann auftreten können, wenn die Polarisationseigenschaften der Gitterbausteine hinreichende Unterschiede aufweisen. Dies ist z. B. bei Zinkblende und NH_4F, nicht aber etwa beim SiC der Fall. Möglicherweise liegt der gleiche Effekt auch beim $Al(PO_3)_3$ und beim $CaBa(CO_3)_2$ vor.

Grundsätzlich könnte eine exogene Symmetrieerhöhung auch durch flächenspezifische Adsorption erreicht werden. Dabei müsste die nur schwer erfüllbare Bedingung eingehalten werden, dass die Verschiebungsgeschwindigkeiten nicht-äquivalenter Flächen durch Adsorption so variiert werden, dass eine scheinbar einheitliche und höher symmetrische Form resultiert.

Wesentlich intensiver ist bisher die Erscheinung der Hypomorphie vom wachstumskinetischen Standpunkt aus diskutiert worden. In erster Linie gilt dies für den Fall der 'Enantio-Hypomorphie'. Es ist möglich, die Beobachtungen einwandfrei zu deuten, wenn eine flächenspezifische Adsorption asymmetrischer Komplexe vorausgesetzt wird. Dabei ist notwendige Bedingung eine *zwei*dimensionale Strukturaffinität zwischen adsorbierender Netzebene und Adsorptiv. Spiegelbildlich-äquivalente Kristallflächen, die durch eine und nur eine Spiegelebene in einander überführt werden können, zeigen notwendig eine $D-L$-Relation. Findet auf solchen Flächen eine flächenspezifische Adsorption von Gastelementen mit enantiomorphem Charakter statt, so kann diese Anlagerung auf der D- und der L-Fläche verschieden erfolgen. Die Erscheinungen sind analog jenen, die beim Ätzen von Einkristallen mit optisch aktiven Säuren beobachtet worden sind.

Die symmetrische Beziehung des Adsorptionsmechanismus kann aus folgender schematischer Beziehung ohne weiteres abgeleitet werden:

$$d+D,\ L \rightarrow dD+dL$$
$$l+D,\ L \rightarrow lD+lL\,.$$

Hierin bedeuten D und L zwei spiegelbildlich äquivalente Flächen, d und l die beiden Komplexantipoden. Die Symmetriekonsequenzen ergeben sich aus folgender Tabelle:

Nicht-enantiomorphe Kristallklassen	Zugeordnete enantiomorphe Kristallklassen
$\bar{1}$, m	1
$2/m$, mm, $\bar{4}$	2
mmm, $\bar{4}2m$	222
$4/m$, $4mm$	4
$4/mmm$	42
$\bar{3}$, $3m$, $\bar{6}$	3
$\bar{3}m$, $\bar{6}m2$	32
$6/m$, $6mm$	6
$6/mmm$	62
$m3$, $\bar{4}3m$	23
$m3m$	432

Die neuerdings von I. N. Stranski entwickelte Adsorptionstheorie (*Bull. Soc. franç. Minér.* (1956), **79**, 360; O. Knacke & I. N. Stranski, *Z. Elektrochem.* (1956), **60**, 816) gestattet eine quantitative Betrachtung des adsorptiven Einflusses bei der Bildung von Gleichgewichtsformen. Danach ergibt sich für die Erniedrigung der spezifischen freien Oberflächenenergie $\Delta\sigma$ folgende Gleichung:

$$\Delta\sigma = kT.\varkappa_0.\ln\,(1-\varkappa/\varkappa_0) \leqq 0\,.$$

Hierin sind $\varkappa$ die Belegung und $\varkappa_0$ die maximal mögliche Belegung der Kristallflächen mit adsorbierten Molekeln. Unter Verwendung der Langmuir'schen Adsorptionsisotherme erhält man:

$$\varkappa/\varkappa_0 = n/\{\varkappa_0.A.\exp\,(-\lambda/kT)+n\}\,,$$

worin n die Konzentration des Adsorbenden und A eine noch von der Temperatur abhängige Grösse darstellen. λ bedeutet die Adsorptionswärme. Bei der Adsorption an spiegelbildlich-äquivalenten Flächen bleibt $\varkappa_0$ unverändert. Und nur wenn asymmetrische Komplexe adsorbiert werden, kann λ für die beiden Fälle verschieden sein. Da auch σ im Falle des absolut reinen Kristalls für die spiegelbildlich-äquivalenten Flächen gleich ist, wird die spezifische freie Oberflächenenergie bei Adsorption nur durch $\Delta\sigma$ bestimmt. D. h. jene Fläche tritt bevorzugt auf, für die $|\Delta\sigma|$ und damit λ grösser ist.

Eine zweite — allgemeinere — Möglichkeit zur Deutung hypomorpher Kristallgestalten scheint mir in der Deformation der Oberflächen-Grenzschichten gegeben zu sein. In einer Untersuchung von K. Molière, W. Rathje & I. N. Stranski (*Disc. Faraday Soc.* (1949), No. 5, S. 21) wird gezeigt, dass solche Deformationen, insbesondere die durch die Polarisation bedingte Kontraktion, zu Verminderungen der Flächensymmetrie führen können. Sind die Deformationen an ursprünglich äquivalenten Flächen verschieden, so können die Anlagerungswahrscheinlichkeiten so modifiziert werden, dass schliesslich Unterschiede in den Verschiebungsgeschwindigkeiten auftreten.

16·2. I. I. Šafranovskij. *Évolution de la science sur les formes des cristaux.*

Les succès dans le domaine de la cristallomorphologie moderne ont appelé la nécessité de développer et de préciser les notions des formes des cristaux.

L'article donne un aperçu des travaux d'auteurs soviétiques concernant le problème en question.

L'apparition de la série de travaux mentionnés a été due aux recherches de A. V. Choubnikov qui a tracé de probables stries sur les faces de cubes à symétrie diverse ('La cristallographie distingue 5 cubes tandis que la géometrie n'opère qu'avec un seul', A. V. Choubnikov, 1923, 1935).

Les constatations de Choubnikov ont été suivies de 146 variétés cristallographiques des formes simples ('Deux formes simples égales sont différentes du point de vue physique si elles se distinguent par les éléments de symetrie ou bien par la disposition de ces derniers par rapport aux faces', G. B. Bokii, 1940). Une manifestation réelle de pareilles variétés est démontrée d'une manière évidente par le caractère de la sculpture des faces.

Plus tard ont été deduites 1403 variétés structurelles de formes simples des cristaux ('Deux variétés cristallographiques d'une forme simple si elles puissent être considerées comme des variétés structurelles, se distinguent par les éléments de symetrie de leur groupe spatial, ou bien par la disposition de ces éléments par rapport aux faces', I. I. Šafranovskij, 1948). Une manifestation réelle des variétés structurelles peut être démontrée dans le développement des faces de cristaux (d'après le principe de J. D. H. Donnay & D. Harker, 1937).

La littérature moderne, traitant la forme externe des cristaux comme fonction de leur structure, accentue le rôle important des rangées ou des arêtes (W. Kleber, 1954; P. Hartman & W. Perdok, 1955). C'est à cette cause qu'il est utile de déduire de simples formes à arêtes de la même manière que les formes à faces ('Une simple forme à arêtes est un assemblage d'arêtes égales du cristal, déduites d'une arête donnée à l'aide des éléments de symétrie', V. I. Mikheev & I. I. Šafranovskij, 1954, 1955). Parmi les formes à arêtes on distingue des

faisceaux à deux ou à trois dimensions, des 'cadres' et des carcasses. A présent, la déduction des formes à arêtes a été achevée pour les systèmes à basse symétrie (18 formes-carcasses). La connaissance des formes à arêtes permet de classer des formations à squelette, des formes de dissolution, des excroissances épitaxiques. Par analogie avec les formes à faces et celles à arêtes, il est aussi logique de distinguer des formes à sommets. (Une simple forme à sommets est l'assemblage de sommets déduits l'un de l'autre à l'aide des éléments de symétrie.) Leur nombre est 47 (à plan – 9). On classe parmi les formes à sommets les squelettes et certaines excroissances épitaxiques.

Il y a encore quelques nouvelles idées sur la symétrie dont il faudrait se servir dans la science sur les formes des cristaux. Ainsi, les notions, développées par A. V. Choubnikov sur les figures antisymétriques peuvent être utilisées avec succès lors de l'étude des surfaces induites pour les cristaux soudés (A. V. Choubnikov, 1951; V. A. Mokiévskii & I. I. Šafranovskij, 1957).

L'homologie des cristaux qui est la branche de la science creé par V. I. Mikheev, tient une place à part. L'idée centrale de cette branche de la science est le fusionnement des faces qui sont différentes, mais en même temps apparentées d'après leur structure.

De tels assemblages des faces produisent 'des formes simples homologues' (V. I. Mikheev, 1950).

Les formes altérées de cristaux réels donnent de précieuses indications sur les conditions de leur formation. La symétrie du milieu pose son empreinte sur la développement externe des faces ainsi que sur les détails interieurs des cristaux (zones et pyramides de croissance). Les cas les plus répandus des milieu cristallogènes naturels peuvent être caractérisés par un nombre réduit d'espèces (et de groupes) de symétrie.

Les deviations de polyèdres cristallins réels des formes idéales donnent une idée de la symétrie du milieu crystallogène (G. G. Lemmlein, 1945; D. P. Grigoriév, 1947; I. I. Šafranovskij, 1954).

'Pseudomonoèdres', 'pseudodièdres' et 'pseudopyramides' qu'on trouve le plus souvent sur les polyèdres cristallins naturels peuvent servir d'indicateurs surs de la symétrie du milieu qui les a produits.

16·3. N. V. Belov, N. N. Neronova & T. S. Smirnova. *The* 1651 *Shubnikov groups.*

The derivation of these groups is easily performed if we start from two-coloured translation groups; 36 such groups exist, of which 22 are two-coloured and 14 are ordinary Bravais lattices.

An obvious theorem states that with a two-coloured lattice every (two)-coloured element of symmetry either coincides with a non-coloured element of the same kind (plane, axis, centre) or alternates with it. In the notation of such Shubnikov groups it is sufficient to place behind the symbol of the coloured lattice only non-coloured elements of symmetry, i.e. one of the Fedorov groups.

With the non-coloured lattice, i.e. when we have the ordinary Bravais lattice, we have in the notation coloured elements. Introduction of them is governed by two simple theorems. According to the first one, odd element of symmetry (threefold axes) can be only uncoloured or grey, i.e. Shubnikov groups with these elements of symmetry do not exist. According to the second, if we have a finite or infinite two-coloured (black–white) pattern and then restitute the black half of components for the white ones, we obtain one of the ordinary (one-coloured) Fedorov groups. This means that when the lattice is an ordinary Bravais lattice all two-coloured groups can be derived by systematically substituting symbols of one, two or three independent elements in the appropriate Fedorov group by the two-coloured symbols.

We give (*Kristallografiya*, (1957), vol. 2) the complete list of the 1651 Shubnikov groups, which includes also the 230 Fedorov groups and an equal number of grey groups. Two-coloured elements are denoted by an apostrophe. Grey groups are denoted by an additional 1′. This symbol does not appear in cubic groups, where we consider it appropriate to displace this apostrophe to the symbol of the (odd) axis 3.

The derivation of Shubnikov groups was accomplished first by A. M. Zamorzaev (1953). In 1954 the authors derived them by the more crystallographic method, which had been used in a short textbook of Fedorov groups by N. V. Belov. In the last two papers one can find all the theorems which are of use in this derivation.

16·4. I. S. Žoludev. *The symmetry of homogeneous isotropic media in tensor and vector fields.*

Seventeen point groups of symmetry of homogeneous isotropic medias are obtained for the case when they are in the fields described by polar and axial tensors of the second order.

16·5. G. A. Wolff & J. D. Broder. *Microcleavage, bonding character and surface structure of materials with tetrahedral coordination.*

1. *Sphalerite-structure materials*

(*a*) *'Microcleavage' and bonding character.*—The impact of hard, sharp particles upon single-crystal spheres results in 'mechanical etch pits'; the same type of pits can be produced when single crystals are fractured or broken. The 'microcleavage' planes comprising these pits were investigated and photographically recorded by the light-figure method and it was found that this technique is superior to the conventional 'macrocleavage' technique for determining the ionic character of the bonding in materials of the sphalerite structure (G. A. Wolff, Spring Meeting, Electrochemical Society, 1954, enlarged abstracts).

The light-figure method was chosen, therefore, to study the microcleavage of AlSb, GaP, GaAs, GaSb, InP, InAs, InSb, ZnS, ZnSe, ZnTe, CdTe, HgSe, HgTe, and CuI. As a general rule, the ionic character of the bonding in sphalerite-structure materials has been found to increase as the molecular weight and valency of the constituents decrease. Two types of microcleavage were observed: (1) (011) cleavage, due to ionic bonding; (2) (111) cleavage and cleavage between (111) and (110), within the [1$\bar{1}$0] zone, due to covalent bonding.

(*b*) *Microcleavage and surface structure.*—A third type of cleavage was discovered in HgTe and HgSe, revealing that, in addition to the distinct (011) cleavage, which is due to ionic bonding, there is microcleavage in (001) and all the other planes of the [100] zone. This microcleavage is identical to that found in NaCl, with the exception of the relative amount of cleavage in the different planes. All three types of cleavage were seen in CdTe. A more detailed study of the third type of cleavage suggests that

the surface of crystals having this type is deformed, so that the atoms of the first, and possibly to a minor extent of the second surface layer, shift to new equilibrium positions; this would be true especially for the (001) plane. The fourfold tetrahedral arrangement changes to a more rectangular and octahedral NaCl (PbS) arrangement with sixfold coordination, that is, the sp^3 hybrid bonding degenerates partially to p bonding. This hypothesis is supported by the fact that such behavior is observed solely in crystals which have cations of little polarizing power and high polarizability (Cd and Hg), which can form compounds of a NaCl or NaCl-like structure with p bonding (CdO and HgS (cinnabar)). In view of this, it is interesting to note that there is $(11\bar{2}0)$ microcleavage in both hexagonal CdS and CdSe, in addition to (0001) and $(10\bar{1}0)$ cleavage, but no $(11\bar{2}0)$ cleavage in hexagonal ZnO and ZnS (wurtzite structure). This can be interpreted as in the case of the sphalerite structure. In chalcopyrite, $CuFeS_2$, which has a similar structure, there is still another type of cleavage found, arising from the differences in Cu–S and Fe–S bond strengths.

2. *Fluorite structure*

A similar difference in the cleavage, as found in the sphalerite structure, is seen in crystals of the fluorite structure. CaF_2 and Mg_2Sn show a Type 2 microcleavage pattern which is also found in sphalerite-structure crystals, while $AuGa_2$ and $AuIn_2$ show it together with a Type 3 pattern, as in CdTe. This, too, can be explained by surface deformation.

3. *Diamond structure*

In diamond, there is good (111) cleavage and microcleavage between (111) and (110) along the $[1\bar{1}0]$ zone, which corresponds to ideal covalent bonding and to a non-deformed surface such as is present in the molecular diamond structure of As_4O_6 and Sb_4O_6, both of which have the same cleavage pattern. Si and Ge each display a different cleavage, however: good (111) cleavage, a residual microcleavage in and near (110), and microcleavage between (111) and (001) in the $[1\bar{1}0]$ zone.

An examination of the circumstances leads to this explanation for the cause of this difference. In the diamond structure, the surface layer of the planes between (111) and (001) in the zone $[1\bar{1}0]$ are alone deformable. Therefore, the specific surface energy of these planes only can be lowered, as in the case of Si and Ge, but leaves the surface energy of the planes between (111) and (110) unchanged. While in the ideal diamond structure there are two maxima of the specific surface energy in (001) and (110) in the $[1\bar{1}0]$ zone, the higher being in (001), the reverse is true in Si and Ge. This is substantiated by the fact that, in the equilibrium forms of Si and Ge—(111), (001), (113), (011), (013) (G. A. Wolff, *Amer. Min.* (1956), **41**, 60)—a preference exists, with respect to (113), which is deformable, while on the other hand in the equilibrium form of diamond—(111), (001), (011)—the (113) plane does not appear. Furthermore, the white-tin modification, which represents a deformed diamond structure, indicates a tendency toward the formation of an octahedral coordination (4+2), as is similarly indicated in the sequence As, Sb, and Bi. The atoms in the surface are expected, therefore, to change position in the same manner as in HgTe and HgSe. The deformation on the surface of the materials investigated is expected to induce a higher electrical conductivity and electron-hole recombination than appears in the bulk of the material. The close relation between this phenomenon and the fast surface states in semiconductor theory is obvious.

4. *Materials with structural lattice vacancies; cleavage probability*

Structures such as Ga_2Te_3, In_2Te_3, $HgIn_2Te_4$, Cu_3AsS_3, Cu_3SbS_3, $NiIn_2$ seldom, if ever, show distinct cleavage, an explanation for which is that upon fracture the vacancies migrate rapidly, thus minimizing surface energy differences in the crystal planes. It would seem that the probability of brittle materials cleaving decreases exponentially with the specific surface energy. Therefore, the cleavage along planes of high surface energy is negligible and cleavage patterns, as obtained by the light-figure method, show up clearly in the low-surface-energy planes.

16·6. J. A. Kohn. *A boundary-structure theory for twinning in diamond-type crystals.*

Back-reflection X-ray studies of a multiply-twinned silicon crystal have revealed, in addition to normal twin boundaries, (1) lateral twin boundaries, i.e. twin plane (111) and boundary plane are not coincident; (2) second-order twin joins, i.e. boundaries between individuals related by two non-parallel stages of twinning; and (3) probable third-order twin joins. By constructing a superlattice made up only of positions common to both individuals of an 'interpenetrated' twin pair, it is shown that *all* the observed boundaries are confined to directions of higher coincidence site density. Further, the trans-boundary structure of *all* the observed boundaries can be rebuilt, or 'restored' to a degree approaching normalcy providing the discontinuity oscillates, or zigzags between two (or three) simple crystallographic directions in each case. Examination of (110)-projected coincidence nets for possible boundaries, with the requirements of (1) higher coincidence site density and (2) a considerable degree of trans-boundary structural 'restoration', revealed seven potential $(h\bar{h}l)$ boundaries for first- and second-order twinning. Indexed with respect to the axes of both individuals, these are:

First-order	Second-order
{110}–{114}	{221}–{221}
{111}–{115}	{114}–{114}
{112}–{112}	{111}–{115}
{001}–{221}	

By using zigzag discontinuities as 'restoration' mechanisms, the trans-boundary deviations from normal bonding are minimized, and excluding the normal first-order case {111}–{111}, preferred growth along these directions is to be expected. Six of the seven proposed boundaries have been observed experimentally in the same silicon specimen; only second-order {111}–{115} was not found. *No other* first-order lateral twin boundaries or second-order twin joins were observed.

Instances of probable third-order twinning were noted. The additional twin lamellae at these positions reflect the tendency of the crystal to avoid a non-restorable second-order twin join in favor of a partially restorable third-order boundary.

Boundary orientation can have a pronounced effect on grain boundary energy. The seven structurally restorable discontinuities represent low-energy cusps in the curve relating energy and boundary direction, for constant misfit angles. Experimentation has previously shown that such boundaries are intermediate in energy between those in which twin plane and composition plane are coincident (normal case) and those involving a common, non-twin-related grain boundary. Lateral twin boundaries and second-order twin joins in semiconductor materials are expected to affect structure-sensitive electrical properties, e.g., minority carrier lifetime and carrier mobility. Such boundaries, owing to their association with low-energy cusps, have a practical bearing upon semiconductor devices whose functioning depends upon high-energy grain boundaries.

16·7. A. PABST. *Some relations of the gnomonic projection and the reciprocal lattice.*

It can be shown that the gnomonic projection of a crystal is equivalent to a collapsed reciprocal lattice or to a projection of the reciprocal lattice on to the first plane from the origin by means of lines from each reciprocal-lattice point to the origin. This concept can be used in the proof that the array of reciprocal-lattice points constitutes a lattice. It is also useful in dealing with various crystallographic problems, for instance that of twin gliding. With the translation **s** of twin gliding in the direct lattice there is associated a translation **s*** in the reciprocal lattice. **s*** is normal to **s**. Thus, if a plane normal to **s** is chosen for projection, all reorientations of planes due to twin gliding, and these in general entail change of indices, can be shown by translations in a common direction that lie in the gnomonic plane.

16·8. Y. LE CORRE. *Pouvoir rotatoire et symétrie dans le temps.*

Dans les cristaux où la densité de courant des électrons n'est pas nulle en moyenne dans le temps, il faut tenir compte de la symétrie dans le temps (opérateur R.). Aux 32 classes de symétries classiques s'ajouttent les 58 groupes polaires mixtes de Shubnikof. La symétrie dans le temps transforme un tenseur en son complexe conjugué. Appliquée au pouvoir rotatoire, cette remarque conduit, entre autre, aux résultats suivants:

(1) L'holoédrie triclinique ponctuelle (C_i) se subdivise en deux classes (C) et (RC); la première est inactive, mais la seconde peut l'être.

(2) Les 5 classes cubiques ponctuelles (T, T_h, T, O et O_h) peuvent présenter le pouvoir rotatoire mais elles se subdivisent en 11 classes dont 6 seulement peuvent être actives.

§ 17. Teaching of crystallography

17·1. H. LIPSON & C. A. TAYLOR. *The Fourier transform as a basic concept in the teaching of X-ray diffraction.*

We claim that the use of Fourier transforms can lead to simpler approaches to the understanding of X-ray diffraction.

The chronological development of a subject rarely proceeds along the most logical lines and teaching follows, at first, the chronological sequence. It is felt that the time is now ripe for a revision of teaching methods to bring them into line with the logical treatment.

The major steps in the development of X-ray diffraction studies—Laue's equation, Bragg's Law, Bernal's use of the reciprocal lattice, without which the present stage of development would never have been reached—tend to foster the idea in the minds of students that the X-ray reflexions are independent entities; the Fourier-transform concept emphasizes their essential relationships.

The new approach is being used in teaching in this department. The treatment begins with a consideration of scattering by a general electron distribution and leads, via a consideration of scattering by a single atom, by a group of atoms and by the unit cell contents, to that by a complete crystal and emphasizes that, in using crystals, we lose a great deal of information in gaining the necessary intensity to make photographic records possible. Concepts such as the reciprocal lattice and Fourier synthesis emerge naturally as the development proceeds; the connections with optical diffraction are clear from the beginning; the qualitative basis of modern developments such as intensity statistics, direct methods, etc., are easy to demonstrate.

The most important result is that the subject is seen as a coherent whole rather than a collection of techniques largely borrowed from other branches of mathematics and physics. There is nothing really new in this presentation; Fourier transforms have been used, by those who are mathematically minded, in diffraction problems for many years. We contend that their use can be equally valuable and attractive to non-mathematicians and that the subject has far too long been surrounded by a mathematical air of mystery—largely because the standard works on Fourier-transform theory are all written in advanced mathematical language without physical illustration.

The use of optical transforms in illustration—which still further 'softens the blow' to the non-mathematicians—is described in a separate contribution.

17·2. H. LIPSON. *Optical methods of teaching the principles of structure determination.*

The diffraction of X-rays and the diffraction of light are exactly analogous, and thus one can use the latter—which we can *see*—to illustrate and drive home the principles of the former. All one needs is a spectrometer of large size, built extremely rigidly. Then one can see and measure diffraction patterns from objects whose dimensions are of the order of several centimetres. Since the instrument is not used for measuring spectra, it has been decided to call it an Optical Diffractometer.

With such an instrument, one can illustrate in two dimensions the following principles:

1. The scattering factor is analogous to the variation of scattering within the diffraction pattern of a hole. (Since the hole has sharp edges, its diffraction pattern has rings around it, whereas the scattering factor falls off asymptotically to zero.)
2. The juxtaposition of atoms on a regular lattice produces fringes which divide the simple diffraction pattern into separate spots—the reciprocal-lattice spots. Thus the reciprocal lattice is seen to be the diffraction pattern of the crystal lattice. This, perhaps,

is the most potent idea that the instrument puts over —that the reciprocal lattice has a physical meaning and is not merely the mathematical abstraction that most of the text books say it is.

3. By making a mask of a lattice with a *group* of holes as the repeating unit, one can reproduce the variation of intensity from one reciprocal-lattice point to another—in other words, the structure amplitude.
4. Following this, one can see how the structure amplitude is related to the amplitude of the underlying diffraction pattern of the single unit. This experiment has brought to the realization of Dr Taylor and myself the importance of the Fourier-transform concept, on which I am giving another paper in this session.
5. One can study lattices with imperfections.
6. One can study the development of superlattice reflexions from an ordered alloy. We have made a long grating in which the degree of order changes along the length, and as this traverses the diffractometer the superlattice reflexions can be seen to build up out of the diffuse background.

There are so many other illustrations which could be thought of and which will doubtless be thought of by others who use these methods, that one cannot enumerate them all. We have found from experience that even casual visitors have been able, in a couple of hours, to pick up the basic facts of X-ray diffraction and to appreciate, for example, the meaning of reciprocal space. To physicists particularly the realization of the relationship between X-ray diffraction and light diffraction is very helpful, and, in my department, is helping to produce some new fundamental ideas on crystal-structure determination.

17·3. A. PABST. *The use of 'band groups' in crystallography.*

Attention is called to the 'band groups', mentioned by G. Polya (*Z. Kristallogr.* (1924), **60**, 278) and described by A. Speiser (*Die Theorie der Gruppen von endlicher Ordnung*, 4th ed., pp. 81–3. Basel. 1956) under the heading 'Streifenornamente'. They have been referred to by various other writers but have been generally neglected by crystallographers. These are the groups of symmetry operations governing repeating plane patterns in which translation is restricted to one direction. The symmetry of any repeating design on a belt, border or frieze must conform to one of these groups. There are seven such groups and their derivation is an easy student exercise the answer to which cannot be found in textbooks or tables. Chains are conspicuous features of some crystal structures. Their projections or longitudinal sections are often shown in illustrations. These necessarily belong to one of the band groups. Among silicates the pyroxene, $(Si_2O_6)_n^{-4n}$, amphibole, $(Si_4O_{11})_n^{-6n}$, and the wollastonite, $(Si_3O_9)_n^{-6n}$, chains, as ordinarily pictured, each belong to a different band group. It appears that no names or symbols have been proposed for these groups and none is offered.

17·4. R. HOCART. *Développement historique de l'étude des zéolites.*

Les grandes étapes de l'étude des zéolites, avec Friedel, Taylor, Wyart, Hey, etc., sont instructives pour les étudiants 'post-graduates' qui commencent des recherches expérimentales. Méthodes et techniques, les unes rigoureuses dès le début dans le raisonnement, les autres perfectionnées peu a peu, aboutissent à des résultats cristallographiques que les physiciens utilisent en vue de préciser les lois de la sorption et de la diffusion dans les structures cristallines.

17·5. R. KIRIYAMA. *Growing single crystals—a students' exercise.*

We have found that the following method is satisfactory for preparing single crystals of suitable size for dielectric measurements or nuclear magnetic resonance absorption experiments. It can be used as a students' exercise in growing single crystals from solutions. Prepare a solution at a relatively higher temperature than its saturation point and stir it vigorously for a few minutes. After it is cooled down just above the saturation temperature, place a seed crystal in the solution and keep the temperature constant for several hours. The seed crystal will first dissolve slightly, and thereafter will maintain the same shape. Then cool down the solution, or let it vaporize slowly according to the nature of the substance.

As a students' exercise, we recommend sodium chlorate and bromate. They have wide ranges of supersaturation, and the former gives cubes while the latter gives tetrahedra.

The reason that vigorous stirring at an elevated temperature seems necessary to us is that any trace of a nucleus which might exist in a slightly undersaturated solution freshly prepared will be entirely divided into its constituents by this means.

17·6. E. FLINT & N. N. ŠEFTAL. *About the teaching of crystallography in U.S.S.R.*

Crystallography in U.S.S.R. is taught in many schools and institutes. Some of them (Universities of Moscow, Leningrad, Gorky, Mining Institute of Leningrad) have special chairs of crystallography.

A very detailed teaching of crystallography is carried out in schools, which prepare specialists in crystallography, crystal chemistry and X-ray analysis.

In other institutes, where crystallography is indispensable for the subsequent teaching of mineralogy, petrography and metallography, it is a secondary subject. To such type belong geologic prospecting and mining institutes and technical schools.

In the institutes of the first type are taught many special courses, for instance: crystal physics, crystal chemistry, optical crystallography, X-ray analysis, electronography, goniometry, growth of crystals, crystal thermodynamics. In such schools the teaching of crystallographic sciences occupies a substantial quantity of teaching hours, up to 680.

Besides lectures, the courses consist largely of practicums. During one of these practicums, a complete derivation of the 230 space groups is given by Prof. N. W. Belov.

The lectures are accompanied by numerous demonstrations, for which the institutes possess an adequate quantity of apparatus. For laboratory work in crystallography the chairs have large collections of models of crystal forms and crystal structures. Many new models

have been constructed in connection with the building of a new edifice for the University of Moscow. In other schools, where crystallography plays a secondary part, the number of lectures and practical work hours is rather limited; it does not exceed 65.

§ 18. Miscellaneous

§ 19. Crystallographic data

19·1. E. R. Pike, J. W. Hughes & A. J. C. Wilson. *Counter diffractometer: the measurement of line positions and intensities for the* A.S.T.M. Powder Data File.

The centres of gravity and integrated intensities of diffraction lines have greater theoretical significance than peak positions and intensities. They are also more easily corrected for instrumental aberrations. Integrated intensities are independent of crystallite size and distortion. If necessary, corrections may be applied for the transparency error to compare powder-camera and diffractometer intensity data. There is reason to suppose that results obtained by visual inspection of films correspond more nearly to positions of centres of gravity and integrated intensities than to peak positions and intensities. Accurate lattice parameters may be determined by extrapolation from positions of centres of gravity in the back-reflexion region.

There are, however, fundamental difficulties in measuring these quantities due to the Cauchy or 'witch' profile of an ideal diffraction line, and the need to determine the background level. An accurate determination of the centre of gravity of a Cauchy profile may involve successive approximations to reach the state in which the integration is carried out over limits which are symmetrical about the centre of gravity.

The advantages of using the positions of centres of gravity and integrated intensities for tabulation in standard data are discussed, and the precautions which are necessary to obtain significant results are derived.

An equipment for the production of standard patterns (J. W. Hughes & E. R. Pike, *J. Sci. Instrum.* (1956), **33**, 204) is described briefly and a method of computing the centres of gravity and integrated intensities with a desk adding machine is demonstrated.

19·2. V. Vand. *Advantages of using reciprocal spacings for powder diffraction data.*

The A.S.T.M. *Index* uses direct spacings and relative intensities of powder lines for identification purposes by means of sorting for the presence or absence of lines. Owing to the experimental errors, certain latitude, or sorting band-pass width, is used, either consciously or not. When search is done by hand, the efficiency of sorting is not important.

However, when it is intended to process automatically thousands of patterns by machine sorting or search methods, either by the use of IBM card sorters or IBM 704–709 tape facilities, efficiency of sorting becomes important. The yield may rapidly deteriorate with increasing band-pass width, especially when many sorting passes in series are required. If the error and the band-pass width varies as the function of the sorting parameters, allowance must be made for it. The simplest way is to transform the parameters into a new system having constant error over the useful range.

Analysis of the A.S.T.M. *Index* data shows that this can be achieved by using reciprocal spacings instead of direct spacings.

Various designs of IBM Cards to carry the information have been considered.

19·3. P. M. de Wolff. *Determination of unit cells from powder diffraction patterns.*

In the general indexing method of Ito, determination of the Bravais type of a provisional lattice need not be carried out by Delaunay's procedure. Ito's method is essentially a way of finding a zone relation among observed values of $\sin^2\theta$, and the symmetry (if any) of the zone thus found can at once be detected by looking for equal $\sin^2\theta$ values in an array of these values.

Similarly, the Bravais type of the lattice is immediately apparent from inspection of all $\sin^2\theta$ values arranged layer-wise. This leads to important simplifications. For triclinic lattices, a three-dimensional analogue of Ito's equation is useful in establishing the mutual orientation of three zones.

Using the technique, the determination of unit cells from high-quality patterns of high-quality powders, and the subsequent indexing of these patterns, becomes very nearly a routine—even for large unit cells (e.g., steroids), and independent of the degree of symmetry.

19·4. F. W. Matthews. *A new index to powder diffraction data.*

The X-ray diffraction data file most commonly used is at present in card form. This is a 'hold over' from the time when the cards formed the index. Now that a more useful index in book form is available, the publication of the data in book form should be considered.

At the same time the use of $1/d$ or $1/d^2$ as an alternative to the use of d should be evaluated.

Using library methods of coordinating indexing, a new type of index will be described.

Symposium 1: Physical techniques

*S*1·1. C. J. Gorter. *Magnetic resonance in crystalline solids.*

*S*1·2. G. E. Pake. *Magnetic dipole interactions in crystals.*

Useful crystallographic information is obtained from the radio-frequency absorption spectra of those atomic nuclei within a crystalline solid which have magnetic dipole moments. Although the frequency of the Larmor precession for a given nucleus is primarily fixed by the externally applied magnetic field, the effective local magnetic field associated with the magnetic interactions between the nuclear dipoles of a rigid lattice determines the width of the resonance and, in favorable cases, may provide a resolvable splitting of the resonance into component lines.

If nuclear moments occur in clusters of two, three, or possibly four, the resonance may have a resolvable splitting. Theoretical analysis gives this splitting as a function of the direction and length of the internuclear

vectors. When the nuclei occur in larger groups, a calculation by Van Vleck provides a rigorous theoretical expression for the mean square width of the resonance line in terms of crystal parameters. Comparison of theory with experiment often decides in favor of one of the crystallographically permissible structures.

The nuclear magnetic resonance is neither a substitute nor a competitor for X-ray and other techniques in crystallographic studies. However, it may be a powerful supplementary tool, particularly because nuclei with large nuclear moments include, for example, $_1H^1$, $_3Li^7$, and $_9F^{19}$, all of which belong to relatively light atoms which are correspondingly weaker X-ray scattering centers than the heavier atoms with which they may be crystallographically associated.

*S*1·3. E. R. Andrew. *Nuclear magnetic resonance study of molecular motion in crystals.*

The rapid movement of nuclei in a crystal lattice modifies, and in general reduces, the static magnetic dipolar interaction between the nuclei. This causes the width of the nuclear magnetic resonance spectrum to be narrower than it would be if the crystal structure were rigid. Nuclear motion in crystals can therefore be revealed by a study of their nuclear magnetic resonance spectrum. Specimens may be either in monocrystalline or polycrystalline form. The study usually extends over a wide range of temperature, since the rate of nuclear motion generally increases markedly with rising temperature.

A quantitative examination of the spectra usually discloses the nature of the nuclear motion. The nuclei may move by virtue of rotation, either free or hindered, of molecules, molecular ions or molecular groups containing the nuclei; they may move by virtue of vibration or rotational oscillation of molecules, ions or groups; they may move by individual translation or tunnelling between fixed sites; they may move by virtue of ionic or molecular diffusion. Examples will be given of different kinds of motion in ionic and molecular crystals, in polymers and in metals.

The nuclear motion causes the nuclear magnetic dipolar interaction to vary with time and thus provides an important mechanism for spin-lattice relaxation. A study of the relaxation time over a wide temperature range frequently yields the variation of the rate of the motion with temperature. In suitable cases an activation energy can be determined.

*S*1·4. S. Marič̆ić & J. A. S. Smith. *Nuclear magnetic resonance studies of some inorganic hydrates.*

Problems concerning the configuration of hydrogen atoms in inorganic hydrates can often be solved by nuclear magnetic resonance studies. Two recent examples are the monohydrate and dihydrate of molybdenum trioxide, MoO_3. Three formulae have been proposed for the dihydrate: $MoO_3.2H_2O$, $(H_3O)MoO_3OH$ and $(H_4O)MoO_4$. A study of the infra-red spectra and the proton magnetic resonance absorption lines shows that the formulae $MoO_3.2H_2O$ and $MoO_3.H_2O$ agree best with the experimental results, although a small percentage of the hydrogen in both compounds gives rise to a narrow magnetic resonance line, even at 77° K. The shapes and second moments of the resonance lines of both hydrates predict an inter-proton distance of $1{\cdot}58\pm0{\cdot}03$ Å in the water molecules. Similar values have been found recently in a number of hydrates. The application of these methods to the study of the structure of other inorganic compounds is also discussed.

*S*1·5. R. D. Spence & J. H. Muller. *Nuclear magnetic resonance studies of hydrogen in crystals.*

The dipole–dipole interaction provides a method of examining the relative positions of hydrogens in crystals. Although the method does not give an absolute determination of hydrogen positions it yields data which can supplement other crystallographic information. In this paper we consider experimental results on crystals in which the hydrogen is (1) in waters of hydration, or (2) on benzene rings, or (3) in OH groups.

As an example of results obtained from studies of waters of hydration we consider the ferroelectric guanidine aluminum sulfate hexahydrate. Here the situation is complicated by the fact that both the waters of hydration and the guanidine group give proton signals. Intensity considerations allow one to separate these, and the analysis of the data leads to results about the positions of the aluminums around which the waters of hydration are coordinated and about the motion of the guanidine group. An example of a more complicated hydrated system is furnished by $CuSiO_3.H_2O$ (dioptase). Here there is an additional paramagnetic splitting of the hydrogen lines. This is strongly temperature-dependent and is useful in studying the paramagnetic properties of the crystal.

The hydrogen pairs on the sides of benzene rings of *para*-substituted compounds often yield information about organic crystals. In this connection we report some studies of the α–β transformation in *p*-dichlorobenzene and of liquid crystals. As an example of the information obtained from OH groups we report some results on the mineral euclase.

*S*1·6. J. A. Ibers & D. P. Stevenson. *The calculation of internuclear distances from the second moments of nuclear magnetic resonance absorption spectra: the* N–H *distances in* NH_4Cl, NH_4F *and* $N_2H_6F_2$.

It is noted that the N–H distances in NH_4Cl, NH_4F, and $N_2H_6F_2$, as determined by previous workers from the second moments of the nuclear magnetic resonance absorption spectra, are inconsistent. It is shown that these inconsistencies arose principally from inadequate consideration of the effects on the calculated second moments of the zero-point-energy motions of the atoms; a more consistent set of N–H distances is derived from the experimental second moments of previous workers. The difficulties of the conversion of $\overline{r^{-3}}$, the function of r which can be obtained from the second moment, to r_e, the value of r corresponding to the minimum on an assumed potential curve, are considered both for the Morse potential and for the harmonic oscillator. The most meaningful way in which to compare values of $\overline{r^{-3}}$, determined from second moments, with values of $\overline{r^n}$, determined from other physical methods (e.g., $n = -2$ for spectroscopic methods) is considered. Finally, an assessment is made of the accuracy obtainable in the determination of internuclear distances by the second-moment method.

S1·7. D. J. E. Ingram. *Crystal symmetry of oxyion complexes as determined by paramagnetic resonance.*

There are three parameters that can be employed to make a direct determination of crystal-structure symmetry by paramagnetic resonance, namely: angular variation of (i) g value, (ii) electronic splitting, (iii) hyperfine splitting.

If g value varies markedly in magnitude it can provide a very sensitive probe for crystal-structure analysis, but often its value remains close to 2·0, in which case variation of the electronic or hyperfine splitting can often be used instead. Such cases are provided by a study of the tetrahedral oxyions of the first transition group. In the $(3d)^1$ configuration, such as potassium manganate, there is no electronic splitting but a very anisotropic hyperfine structure, and this can be used as a sensitive probe for determining the symmetry of the oxyion group. In the $(3d)^2$ configuration, however, such as potassium hypomanganate, or ferrate, the hyperfine splitting remains nearly isotropic while the electronic splitting between the triplet levels varies markedly. This can then be used as an alternative method of measuring the group symmetry. The results obtained for the different crystallographic planes of such compounds are briefly summarized in this paper and the determination of crystal symmetry from them is then outlined.

S1·8. R. E. Rundle. *Nuclear magnetic resonance in the determination of magnetic electron wave functions.*

Paramagnetic resonance studies have been used to infer magnetic electron distributions. A very sensitive and easily interpretable method for determining such distributions can also be developed from nuclear magnetic resonance. The method depends upon the use of a nuclear magnetic dipole, through nuclear resonance, as a probe of the magnetic field at specified locations within the crystal. This requires that the crystal structure of the material investigated be known.

Application of the method to $CuCl_2.2H_2O$ is illustrated using the proton magnetic resonance data of N. J. Poulis & G. E. G. Hardeman (*J. Chim. Phys.* (1953), **50**, 110). The resulting magnetic electron density is: 25% of the magnetic electron on each chlorine, 50% on copper, less than 1% on oxygen. The magnetic electron is, therefore, in an antibonding molecular orbital.

S1·9. R. Mason. *Diamagnetic anisotropy, electron distribution and crystal structure of aromatic compounds.*

Quantum mechanical models of the electron distribution in aromatic molecules are examined in relation to their diamagnetic anisotropies, as deduced from crystal measurements, with special reference to naphthalene and anthracene at 95 and 290° K.

S1·10. C. Dean. *Crystallographic applications of the magnetic splitting of nuclear quadrupole resonances.*

A nucleus with spin $I \geq 1$ is distorted from spherical shape, the amount being described by its electric quadrupole moment. Therefore an unsymmetrical electron density around such a nucleus can exert a torque on it, an interaction involving the gradient of the electric field, the tensor ∇E. The quantized states of orientation of the nucleus (m_I) therefore have different energies, and transitions between the levels correspond to spectra in the radio-frequency range. In covalent compounds ∇E at a nucleus is due principally to the electron distribution on that atom, so that the tensor quantities are related quite directly to the bonds formed by that atom.

Such a nucleus also has a magnetic dipole moment that will interact with a laboratory magnetic field and split the r.f. absorption line, the details depending on the orientation of the field with respect to ∇E. Thus, with a single crystal the observed splittings as a function of magnetic-field orientation determine the orientation of ∇E for each such atom in the cell. For a single covalent bond, ∇E has approximately cylindrical symmetry around the bond direction, and the bond direction can be found from just this symmetry. Fractional double-bonding causes a deviation from this symmetry, and further information can be obtained (e.g., direction of a halogen π orbital).

Applications to be discussed concern molecules with halogen atoms. They include the detection of polymorphic phase transitions, the use of the directional data as an aid in crystal-structure analysis, and the study of the question of steric strains within the molecules.

S1·11. G. M. Volkoff. *Crystallographic applications of the quadrupole splitting of nuclear magnetic resonances.*

Non-spherical nuclei (of spin $I > \frac{1}{2}$) situated at sites within a crystal at which the gradient of the crystalline electric field is not zero have their electric quadrupole moment eQ coupled to the field gradient with an energy which depends on the allowed quantized orientations of the nuclei with respect to the crystalline field. Observation of resonances with an externally applied weak radio-frequency magnetic field which correspond to induced reorientations of nuclei between the above discrete 'pure quadrupole' levels can provide a tool for the study of crystalline electric fields at nuclear sites.

In some cases (covalent bonds and large eQ) strong quadrupole coupling gives 'pure quadrupole' lines of hundreds of megacycles/sec., frequency. But in other cases (ionic crystals or small eQ) the quadrupole coupling may be so weak that the 'pure quadrupole' transitions would have frequencies of a megacycle/sec. or less. For experimental reasons, resonances with frequencies below several hundred kilocycles/sec. are practically impossible to observe in crystals.

However, a weak crystalline electric field gradient can still be studied by placing the crystal in a uniform external magnetic field H_0. This provides an additional coupling between the nuclear magnetic moment μ and H_0 which depends on the orientation of the nucleus with respect to H_0. By varying H_0 from 0 up to 10000 gauss, frequencies corresponding to nuclear magnetic resonance transitions between adjacent Zeeman levels are obtained varying from 0 up to $1-10$ megacycles/sec., depending on the value of μ. In contrast to the preceding paper by Dean, in which such a magnetic coupling is treated as a small perturbation on the main strong quadrupole effect, we consider situations where by increasing H_0 to several thousand gauss we can continuously pass over from the 'pure quadrupole' case to the opposite limiting case in which a weak quadrupole coupling of a few hundred kilocycles/sec. or less can be treated as a small perturbation

on a nuclear magnetic resonance Zeeman line of several megacycles/sec. frequency. In our work we have also observed intermediate spectra when the two couplings are of comparable magnitude.

By studying the first- and second-order quadrupole splittings of the Zeeman line as a function of crystal orientation in a strong magnetic field H_0 it is possible to determine: (1) the orientation with respect to the crystallographic axes of the principal axes x, y, z of a weak electric field gradient tensor $\varphi_{ij} \equiv \partial^2\varphi/\partial x_i \partial x_j$ at the nuclear sites; (2) the asymmetry parameter $\eta \equiv (\varphi_{xx}-\varphi_{yy})/\varphi_{zz}$ for the tensor; (3) the absolute value of the quadrupole coupling constant $|eQ\varphi_{zz}/h|$ at each site; and (4) the number of essentially different kinds of sites for each nuclear species in a given crystal.

Applications of such methods to the study of Li and Al sites in spodumene, B and Na in kernite, Al in euclase, corundum, etc. will be described.

*S*1·12. R. Bersohn. *The electric field gradient in ionic crystals.*

For an idealized model of an ionic crystal, the interaction energy of the gradient of the electric field ∇E with an ion whose nucleus has a quadrupole moment Q is $(1-\gamma_\infty)Q\nabla E$, where γ_∞ is a measure of the quadrupole polarizability of the ion. The interaction of a paramagnetic ion (whose electronic ground state in the crystal is far below the first excited state) with ∇E is $\beta_\infty e(h/mc)^2\nabla E$, where β_∞ is a measure of the quadrupolar polarizability of the unpaired electrons. γ_∞ and β_∞ are numerical constants for each ion which have been determined theoretically and experimentally. With their help one can discuss the field gradient in crystals; in ionic crystals including Al_2O_3 and Cu_2O the experimental field gradient agrees well with naive calculations. A survey of experimental field gradients will be presented.

*S*1·13. H. E. Petch & F. Holuj. *An investigation of the B^{11} nuclear magnetic resonance spectrum in colemanite.*

As a first step in an investigation of the part the boron atoms play in the ferroelectric behaviour of colemanite we have studied the B^{11} nuclear magnetic resonance spectrum in a single crystal of colemanite at room temperature. A total of 14 resolved lines, whose frequencies depend on the crystal orientation with respect to the magnetic field, have been observed centered about a much stronger line which remained fixed at about 11·98 mc./sec. (H_0 = 8·75 kilogauss). Eight of the lines remain within 150 kc./sec. of the central line. These eight lines appear in pairs with the members of each pair symmetrically situated on either side of the strong central line. Two other lines remain within 40 kc/sec. of the central line but they are not symmetrically situated with respect to it. The remaining four lines are approximately symmetrically situated in pairs about the central line but each is separated from the central line by sometimes as much as 1400 kc./sec. When the *b* crystallographic axis was placed either perpendicular or parallel to the magnetic field a number of the lines coincided, so that the spectrum consisted of seven lines in addition to the strong central line.

The observed spectrum of 15 lines can be explained in complete detail if one assumes that the twelve boron sites in colemanite, at room temperature, are derived from the operation of the symmetry elements $2/m$ on three uniquely different sites. At one of these three sites the electric field gradient is large, indicating that the chemical bonding at this site has a strongly covalent character; whereas at the other two sites the electric field gradients are much smaller, suggesting that the bonding has a high degree of ionicity. The electric quadrupole coupling constant, the asymmetry parameter, and the directions of the principal axes of the electric field gradient tensor have been calculated for each non-equivalent boron site.

Symposium 2: Electron diffraction

*S*2·1. Z. G. Pinsker & B. K. Vajnštejn. *Structure analysis by electron diffraction.*

The progress of studies in the field of electron diffraction during the last thirty years is reviewed. The development of structure analysis by electron diffraction has been the most important trend of investigation, promoting the advance of the theory of electron scattering and of the experimental technique.

In establishing the limit of applicability of the kinematical theory, it is necessary to consider in addition to the crystal dimensions and ordinal numbers of components forming a given phase, also the degree of complexity of the structure and its symmetry. Various experimental data are considered which refer to revealing dynamic effects in examining experimental scattering curves, in measuring the banded structure on patterns obtained in a divergent beam and in measuring the effects of dynamic birefringence. The possibility of using the Kikuchi lines and Kikuchi bands for structure analysis is considered.

The general course of structure determination by the electron-diffraction method is given. A discussion is presented of the Fourier synthesis as well as of the advantages and peculiar features of the electron-diffraction structure analysis as compared to the X-ray and the neutron-diffraction method.

A description is given of the camera used in electron-diffraction analysis at the Institute of Crystallography. This is followed by a brief presentation of the results of the electron-diffraction studies carried out on hydrates of chlorides of some metals, clay minerals (seladonite); of the investigations of the position of hydrogen atoms in some inorganic and organic structures; of the studies of semi-conducting alloys of Bi, Cd, Tl, Sb, Se, Te and some other elements, including investigations of the amorphous structure of some phases of this kind. In connexion with the discussion of the studies enumerated, many important peculiar features and possibilities of the electron-diffraction method are indicated, namely: precision of locating light atoms, study of the ionization state of some atoms, a more precise determination of the composition of phases by the structure method, etc.

*S*2·2. S. Miyake. *Some problems in dynamical scattering of electrons by crystals and its transition to kinematical scattering.*

The dynamical theory of diffraction plays a much more important role in electron diffraction than in X-ray diffraction. The dynamical process gives rise to many diffraction effects which cannot be explained by the kinematical theory. In particular, direct influence of the

phase of the structure amplitude can appear only in dynamical diffraction patterns. S. Miyake & K. Kambe (1954) and K. Kambe (1957) showed that the phase determination is practically feasible by analysing patterns due to simultaneous reflexion by two lattice planes. Failure of Friedel's law observed by S. Miyake & R. Uyeda (1950) in zincblende, and an asymmetric pattern observed by R. Uyeda & S. Miyake (1957) in molybdenite are other examples revealing the phase effect.

However, many of the difficulties in the crystal-structure determination by electron diffraction come from the dynamical effects. For large crystals for which the dynamical theory applies, the relation between diffracted intensity and crystal structure is in general fairly complicated. Even for the simplest case we cannot avoid the effect due to the 'systematic correlations' of diffracted waves, as discussed by J. A. Hoerni (1956). Moreover, back-effects of inelastic scattering on elastic scattering should also be taken into account. Very recently J. Yosioka (1957), who formulated quantum-mechanically the imaginary components of Fourier terms of crystal potential introduced previously by Molière on a phenomenological basis, showed that the values of Fourier terms for the static potential are effectively subjected to corrections of several percent by the influence of inelastic scattering.

For crystals of finite sizes, the kinematical theory, or at least the pseudo-kinematical theory, is expected to apply when the wave length of the electrons is sufficiently short. Honjo & Kitamura have recently shown, by utilizing 30–300 kV. electrons, that the kinematical values of the intensities of Bragg reflexions can be experimentally obtained by extrapolation when the intensities are measured as functions of wave-length. Nagakura's procedure (which is reported by Honjo & Miyake in this Symposium) also gives a practical method of deducing the kinematical intensity.

*S*2·3. M. J. Whelan & P. B. Hirsch. *Electron diffraction from crystals containing stacking faults.*

The solution of Schrödinger's wave equation for an electron in a periodic crystal field gives the well known dynamical equations of electron diffraction in the approximation of one strong diffracted beam. By considering the case of overlapping crystals, the theory has been extended to include the diffraction of electrons from crystals containing imperfections, such as grain boundaries and stacking faults. The theory is developed in detail for the case of a single stacking fault traversing a thin parallel-sided metal foil. In this problem there is a phase difference in the electron waves scattered by atoms on opposite sides of the fault. This phase difference arises from the fact that the shear displacement at the fault is not a lattice translation vector. For stacking faults in a face-centred cubic lattice the phase difference vanishes for certain reflexions. By including the effects of this phase difference in the dynamical equations, an expression is derived for the electron wave function at the exit surface of the crystal in the region of overlap. The theory shows that the intensity variation at the exit surface is a result of the interference of three coherent electron waves. Interference fringes, analogous to those observed in wedge-shaped crystals, are predicted. Close to the Bragg reflexion, the periodicity of the fringes is half that of the corresponding thickness fringes expected if one half of the faulted crystal is removed. At large deviations from the Bragg reflexion, the dynamical theory is asymptotic to the kinematic theory. The theory can also be applied to the case of overlapping stacking faults on neighbouring crystal planes. The predicted contrast variations are observed directly on transmission electron micrographs of metals of low stacking-fault energy, where stacking faults are produced as a result of splitting of dislocations into partial dislocations.

*S*2·4. K. Molière. *Dynamische Beugungseffekte von durchstrahlten Mikrokristallen.*

Die Arbeiten, über die hier zusammenfassend berichtet wird, beschäftigen sich mit dem dynamischen Effekt der Interferenz-Doppelbrechung. Dieser Effekt kommt in einer Feinstruktur der Laue-Punkte zum Ausdruck, welche beobachtbar ist, wenn kleine Kristall-Polyeder von idealer Struktur (z. B. würfelförmige Rauch-Partikel von MgO oder CdO) mit einem Elektronenbündel von sehr geringer Apertur durchstrahlt werden. Der Effekt ist vor etwa 10 Jahren von Cowley & Rees, sowie von Honjo beobachtet und von Sturkey gedeutet worden. Gründliche Untersuchungen, die inzwischen durchgeführt wurden, ermöglichten eine sehr direkte, quantitative Prüfung der dynamischen Theorie der Elektronen-Interferenzen.

Nach der dynamischen Theorie setzen sich die im Kristall erregten Wellenfelder je nach der Orientierung der Fläche, durch welche die Elektronen in den Kristall eintreten, aus einigen starken, ebenen Partialwellen mit verschiedenen Amplituden $u_0, u_g, \ldots$ und verschiedenen Ausbreitungsvektoren $k_0, k_0+b_g, \ldots$, zusammen. Sind mit einer gewissen Annäherung die Laue-Bedingungen für n Indextripel erfüllt, so gibt es im Kristall höchstens $n+1$ starke Wellenfelder, deren jedes aus maximal $n+1$ starken Partialwellen besteht. Ist die Fläche, durch welche die Elektronen den Kristall verlassen (Austrittsfläche) nicht parallel zur Eintrittsfläche, so garantieren die Grenzbedingungen ein getrenntes Austreten der einzelnen Partialwellen. Das ist der Fall bei Durchstrahlung einer keilförmigen Kristallpartie, welche einer Kante benachbart ist. Die Ausbreitungsvektoren der aus den Partialwellen hervorgehenden Vakuumstrahlen eines Reflexes liegen in einer Ebene senkrecht zu der Kante des keilförmigen Kristallbereiches. Die zugehörigen Feinstruktur-Maxima markieren sich also auf der photographischen Platte längs einer auf dieser Kante senkrecht stehenden geraden Linie. Die Winkeltrennung der Maxima kann die Grössenordnung 10^{-3} erreichen. Ihre Lage hängt ab: (i) Von den Anregungsfehlern ϱ_g (proportional zu den Abweichungen von den Bragg'schen Winkeln); (ii) Vom Brechungspotential φ_0 (nicht ganz identisch mit dem mittleren Kristall-Potential); (iii) Von den Strukturpotentialen φ_g (Fourierkoeffizienten des periodischen Potentials). Da bei einem Parallelepiped oder speziell bei einem würfelförmigen Kristall drei Paare von einander gegenüberliegenden, keilförmigen Kantenbereichen durchstrahlbar sind, erscheinen hier alle Maxima einer Feinstrukturfigur auf die drei Seiten eines Dreiecks verteilt. Die Fläche des Dreiecks ist proportional dem Quadrat des Anregungsfehlers der betreffenden Interferenz.

Ist nur eine Interferenz stark angeregt, so besteht auf Grund dieser Zusammenhänge die Möglichkeit, allein aus der Geometrie der Aufspaltungsfiguren der Lauepunkte die Kristall-Orientierung, das Brechungspotential und das zugehörige Interferenzpotential zu ermitteln. Es wird

so im Prinzip eine Bestimmung von Strukturfaktoren ohne Intensitätsmessung ermöglicht. Hervorzuheben ist, dass einzelne Mikrokristalle (z. B. MgO-Würfel von 500–1000 Å Kantenlänge) individuell analysiert werden können. Hierzu hat sich ein Verfahren als zweckmässig erwiesen, bei feststehendem Objekt Aufnahmereihen mit jeweils verschiedenen Elektronengeschwindigkeiten herzustellen (z. B. zwischen 30 und 60 kV.).

Wegen der starken Wechselwirkung tritt bei der Elektronenbeugung an Kristallen fast immer der Fall einer simultanen Anregung mehrerer Interferenzen auf. Bei der Bestimmung von Strukturfaktoren lässt sich der Einfluss von schwach angeregten Neben-Interferenzen bei Auswertung einer grösseren Anzahl von unter verschiedenen Bedingungen angestellten Experimenten durch Mittelwertsbildung eliminieren. Bei gleichzeitiger, starker Anregung mehrerer Interferenzen zeigen die Experimente, dass meistens jedes Wellenfeld nur zwei starke Partialwellen enthält. Das liess sich auch durch die Theorie in einer Anzahl von genauer analysierten Fällen bestätigen.

Von besonderem Interesse ist es, dass die Analyse der Interferenzbrechung Möglichkeiten zur Bestimmung des Absorptionskoeffizienten der Elektronen im Kristallgitter bietet. Die Halbwertsbreite eines Intensitätsmaximums längs der Feinstruktur-Geraden ist dem Absorptionskoeffizienten proportional. Dieser erweist sich im Interferenzfall als eine extrem richtungsabhängige Grösse.

*S*2·5. H. Wilman. *A stationary-crystal method of determining the mean inner potential of a single crystal.*

When a crystal possesses two smooth faces meeting at an edge, electron-diffraction photographs can be obtained with the beam passing along the edge so as to graze simultaneously the two faces (G. I. Finch & H. Wilman, 1937). It is shown that by adjusting the angle of grazing incidence so as to make the intensity of a suitable diffraction spot a maximum (a Bragg reflexion), as observed on the fluorescent screen, photographs can be obtained which allow the estimation of the inner potential of the crystal with good accuracy. The intersection of the elongated diffraction spots of a pair having given indices *hkl*, displaced by refraction at the two surfaces, determines the position corresponding to absence of refraction, and hence the displacement of the Bragg reflexion can be calculated.

The method is exemplified by results from pyrites natural crystal faces of (100) type. With the beam along either of the cube edges in the face, the inner potential was found to be 12·9 V. (mean of 12·5, 13·0 and 13·1 V.) accurate to within about 0·5 V. Two other crystals bounded by (650) and (100), and by (213) faces respectively, gave much lower values in the region of 6–8 V., accurate to within about 1 V. since the conditions were rather less favourable than on the cube face of the first crystal.

*S*2·6. L. Marton. *Energy losses of electrons passing through solids: importance and influence on the interpretation of electron-diffraction diagrams.*

In the last ten years a vast store of knowledge has been accumulated on the energy losses suffered by electrons when passing through solids. It has been found that any solid, without exception, will produce a spectrum of characteristic energy losses. The spectra can be characterised as consisting of narrow lines, diffused lines, and of wide bands. The characteristic losses can be observed both in transmission through very thin layers or in a reflection on bulk material. These losses are independent, in first approximation at least, of the primary energy, of the temperature of the solid, and of the angle of observation. The absolute cross-sections for these events depend, apparently, on the grain structure of the solid. There is some indication that with a varying degree of crystallinity the ratio of inelastically scattered electrons to the elastically scattered ones may vary. The interpretation of electron-diffraction diagrams can depend, therefore, in extreme cases on a precise knowledge of the inelastic scattering cross-section of the material to be investigated.

*S*2·7. D. A. Swick. *An energy analyzer for electron diffraction by gases.*

An electron velocity analyzer of the Mollenstedt type has been constructed for use in diffraction by gases as well as solids. Several features for facilitating experiments at wide scattering angles have been incorporated.

An auxiliary magnetic lens, with a wide aperture has been placed just below the point of diffraction. By compressing the diffraction pattern, i.e., by reducing the apparent scattering angle associated with a given s value, this lens permits more of the diffracted electrons to enter the analyzer. This lens can be rotated several degrees about an axis perpendicular to the beam and to the longitudinal axis of the analyzer. This adjustment permits focusing of electrons scattered at wide angles, with a minimum of spherical aberration. The aberrations of this lens must be considered in the calibration of the instrument.

The velocity analyzer itself consists of a fine slit above an electrostatic cylindrical lens. The slit is about 5 cm. in length; its width is of the order of a few microns, and can be adjusted externally. External adjustments are also provided for the angle of the slit with respect to the cylindrical lens, and for its lateral position with respect to the electron beam. The cylindrical lens consists of two grounded electrodes parallel to and on opposite sides of an electrode at or near cathode potential. All three electrodes have slit-like apertures, approximately 1×5 cm. The lateral position of this lens can also be adjusted externally, independently of the adjustments of the slit.

If the slit is displaced off of the optical axis, its image is sensitive to small changes in the energy of the electrons. The 5 cm. length of the apertures permits analysis of electrons scattered at fairly wide angles.

*S*2·8. V. Schomaker. *Electron-diffraction studies on gas molecules containing both heavy and light atoms.*

New electron-diffraction results obtained in Pasadena on trifluoroiodo methane, lead tetramethyl, and the hexafluorides of tungsten, osmium, iridium, uranium, neptunium, and plutonium will be presented along with a review of earlier results (V. Schomaker & R. Glauber, *Nature, Lond.* (1952), **170**, 290) on heavy-atom–light-atom molecules. The apparent amplitudes and phases of scattering of electrons (11–46 keV., but mainly of about 40 keV.) by the several kinds of atoms will be compared

with the theoretical values of J. A. Hoerni & J. A. Ibers (*Phys.Rev.* (1953), **91**, 1182; *Acta Cryst.* (1954), **7**, 405), and the structural results for all the molecules will be summarized.

*S*2·9. J. A. IBERS. *Some values of the scattering factors for electrons at zero scattering angle.*

Values of $f_{\text{el.}}(0)$ play approximately the same role in structure determinations of solids by electron diffraction that values of $f_{\text{X-ray}}(0) = Z$ do in such determinations by X-ray techniques. The usual method for the calculation of $f_{\text{el.}}(0)$ is to assume the Born approximation and write

$$f_{\text{el.}}(0) = \lim_{s\to 0} \frac{2}{a_0}\left[\frac{Z - f_{\text{X-ray}}(s)}{s^2}\right]; \quad s = (4\pi/\lambda)\sin\theta\,. \qquad (1)$$

This method, which was used by B. K. Vainshtein (*Zh. eksper. teor. Fiz.* (1953), **25**, 157) is somewhat unreliable because of the difficulty of successful extrapolation. It will be shown that within the limits of the Born approximation one may write

$$f_{\text{el.}}(0) = kZ\overline{r^2}\,, \qquad (2)$$

where k is a known constant, and where $\overline{r^2}$ is the mean-square atomic radius. The calculation of $f_{\text{el.}}(0)$ from (2) requires no extrapolation. Since $f_{\text{el.}}(0)$ is by (2) proportional to the mean-square atomic radius it is evident that even for heavy atoms the Thomas–Fermi potential, since it averages out the effects of shell structure, is a poor potential to use for such calculations. Values of $f_{\text{el.}}(0)$ have been obtained here using (2) for those atoms for which Hartree–Fock or Hartree wave functions are available. There are some large differences between these values and those obtained by Vainshtein from (1) for atoms below argon, and from the Thomas–Fermi potential for heavier atoms.

Some remarks will be made on the possibility of obtaining $f_{\text{el.}}(0)$ experimentally from single-electron impact experiments in gases.

*S*2·10. J. A. HOERNI. *Electron diffraction by crystals containing heavy atoms.*

In the case of crystals containing heavy atoms, it is possible to formulate a pseudo-kinematic theory of electron diffraction, in which the Born approximation is made to evaluate the total scattering from the contributions of the various atoms, but rigorous solutions to each single-atom scattering problem are used. On the basis of this theory, intensity anomalies equivalent to those observed in molecules containing both heavy and light atoms should occur at high scattering angles. Powder diagrams from thorium oxide have been recorded photographically. In agreement with the pseudo-kinematic theory, the contribution of oxygen atoms is found to be unimportant at the highest observable scattering angles, for which the phase difference between the complex scattering amplitudes of thorium and oxygen is about 90°. The general variation of diffracted intensity is found to be closer to the first power, rather than to the square of the structure factor. This indicates that, in addition to the multiple intra-atomic scattering taken into account by the pseudo-kinematic theory, dynamic effects due to multiple interatomic scattering also take place.

*S*2·11. L. STURKEY. *The use of electron-diffraction intensities in structure determination.*

I. *'Cross-grating' patterns*

Before a structure determination can be reliably performed using the intensities of the spots in a cross-grating pattern, a theoretical investigation must be made to verify that the intensity of each spot is proportional to the square of the structure factor for the corresponding plane and to ascertain the limits of validity of this so-called 'kinematical' approximation.

The only convenient scheme at present available for calculating the intensities in a cross-grating pattern accurately without neglecting interactions appears to be the 'scattering-matrix' method. With this method any number of simultaneous reflections may be treated, and the effects of extinction and '*Aufhellung*' are automatically included. For the Laue case, the amplitudes of the various diffracted waves after traversing a thickness t may be computed from the incident wave $\varphi_0(0)$ by:

$$\begin{pmatrix}\varphi_0(t)\\ \varphi_1(t)\\ \varphi_2(t)\\ .\\ .\\ .\end{pmatrix} = \exp(i\mathscr{R}t)\begin{pmatrix}\varphi_0(0)\\ 0\\ 0\\ 0\\ 0\\ .\\ .\\ .\end{pmatrix},$$

where $\mathscr{R}$ is the scattering matrix

$$\mathscr{R} = \begin{pmatrix} 0 & r_{01} & r_{02} & . & . & . & .\\ r_{10} & 0 & r_{12} & . & . & . & .\\ r_{20} & r_{21} & 0 & . & . & . & .\\ . & . & . & & & & \\ . & . & . & & & & \\ . & . & . & & & & \end{pmatrix}.$$

The r_{uv} values may be computed from

$$r_{uv} = \frac{2\pi/\lambda}{\text{Vol. of crystal}} \times \oint \exp(-i\mathbf{K}(u).\mathbf{s})N\exp(i\mathbf{K}(v).\mathbf{s})dV\,.$$

N is the index of refraction of the crystal for the particular scalar wave considered expressed as a Fourier series in terms of the reciprocal lattice. For electrons, N will be expressed in terms of the Fourier coefficients V_{hkl} of the potential.

The quantity r_{uv} is an amplitude reflection coefficient for the reflection of a wave in the direction $\mathbf{K}(v)$ to the direction $\mathbf{K}(u)$. For electrons incident on the (x, y) surface of a thin plate-like crystal:

$$r_{uv} = \frac{\pi V_{hkl}}{\lambda E}\left(\frac{\sin\frac{1}{2}\Delta K_z t}{\frac{1}{2}\Delta K_z t}\right).$$

This method has been used to calculate the intensities of the spots in a cross-grating pattern from a thin plate of a Mg crystal, with the electrons incident perpendicular to the surface of the flake and along the [100] direction. Twenty reflections are considered, and two computations have been performed, one assuming a thickness of 125 Å and another a thickness of 42 Å. Even in these fairly ideal cases it is shown that the resulting computed inten-

sities are unsuitable for use in accurate structure determinations, and if used could result in the postulation of very peculiar structural details. An actual diffraction pattern demonstrates the reliability of the calculated intensities.

The criterion for the validity of the small-scattering approximation—and consequently for the reliability of a structure determination from the electron-diffraction data—is shown to be:

$$\mathscr{I}+i\mathscr{R}t \fallingdotseq \exp(i\mathscr{R}t),$$

which means that for every r_{uv}

$$|r_{uv}t|^2 \gg |\sum_k (r_{vk}t)(r_{kv}t)|^2 .$$

Since the number of terms in $\Sigma r_{uk}r_{kv}$ increases as the thickness t decreases—i.e. the number of cross-grating spots increases—there is no obvious reliable upper limit for the thickness. The errors are most serious for the weaker reflections, and deductions about structural details principally determined by the weak reflections will usually be incorrect. Thus the appearance of forbidden reflections may lead to the assumption of an order or of a disorder that does not actually occur.

II. *Phase determination*

Since double or simultaneous reflections usually occur in electron-diffraction patterns, it might be suspected that phase information is contained in the diffraction pattern. By using the scattering-matrix method, it is shown that it is not possible to obtain direct phase information if the phases are real, even if double reflection occurs. It is also shown that even when the phases are complex the phase information is ambiguous. For if $|F(hkl)| = |F(\bar{h}\bar{k}l)|$ and an electron-diffraction pattern shows that $I(hkl) < I(\bar{h}\bar{k}l)$ then

$$F(2h) = -|F|\exp(+i\varphi) \quad \text{or} \quad F(2h) = +|F|\exp(-i\varphi),$$

and it is not possible to decide between the two cases.

These results can be extended to the X-ray Laue case of several simultaneous reflections if polarization is neglected, and no phase information appears likely in such a case. In each case studied, the structure factors appear only as squared terms in the intensity formulae.

*S*2·12. J. M. Cowley & A. F. Moodie. *A new approach to electron-diffraction theory, with applications to structure analysis.*

A new formulation of physical optics, equally applicable to light and electrons, recently given by the authors, has been applied to the scattering of electrons by atoms and crystals, thereby allowing a new approach to problems of dynamic scattering, particularly in relatively thin crystals. In the present communication we consider some of the simpler results obtained and discuss their significance with respect to the use of the intensities of spots in single-crystal electron-diffraction patterns for structure analysis.

Fundamental to the theory is the idea of approximating to a three-dimensional potential distribution by a sufficiently large number of essentially two-dimensional potential distributions. The effect of such a planar potential distribution on an incident electron wave function is given by multiplication by a real, complex or imaginary function. Propagation from one plane to another has the effect of convoluting the wave function with a unit propagation function of the form $\exp\{i\alpha x^2\}$. It can be shown that the diffraction pattern of an object is given by the Fourier transform of the wave function at the exit face of the object.

The principal effect of an atom on an electron beam is to change the phase of the electron waves. The atomic scattering factor is the Fourier transform of a phase distribution corresponding to the potential distribution in the atom, and is therefore complex. The dependence of the phase angle of the atomic scattering factor on the atomic number, angle of scattering and electron velocity is readily demonstrated.

If a crystal is thin enough to be regarded as a two-dimensional potential distribution, $\varphi(x, y)$, the diffraction pattern will be given by the Fourier transform of the phase distribution function $\exp\{ic\varphi(x, y)\}$ and not, as is usually assumed, by the Fourier transform of the amplitude distribution function $c\varphi(x, y)$. If the spot intensities are used to calculate a Patterson projection of the crystal lattice, the peaks will decrease in height and in diameter by an amount increasing with the atomic numbers of the atoms concerned and the thickness of the crystal, but their positions will be unaltered. By obtaining patterns from crystals of several different known thicknesses, it should be possible to distinguish between Patterson peaks corresponding to different types of interatomic vector. This makes possible a method of structure analysis similar to that of using anomalous scatterers in X-ray diffraction work.

In this approximation, dynamic scattering can give rise to the appearance of no 'forbidden' reflexions provided that the crystal is perfect. However 'forbidden' reflexions can occur with considerable intensity if the crystal lattice contains only one stacking fault. It would appear that most 'forbidden' reflexions in spot patterns are produced in this way. A single scattering fault can reduce the maximum phase shift produced by a crystal by a factor of up to 2.

In most crystals used for purposes of structure analysis the number of stacking faults will be appreciable, but not great enough to make the statistical treatments of disordered crystals used in X-ray diffraction valid. Structure analysis may then be carried out by use of the distribution-function techniques recently described by one of the authors (J. M. Cowley, *Acta Cryst.* (1957), **10**, 141).

*S*2·13. B. K. Vainštejn. *Reflexion intensities of electron-diffraction patterns.*

The specimens to be used for structure analysis by electron diffraction are aggregates of a very large number of single small crystals (blocks). Hence, to compute the intensity one needs to consider, first, the law of scattering in a single block, and second, the structure of a specimen made up by these blocks.

For specimens used in structure analysis by electron diffraction, in most cases such conditions are satisfied when the kinematic theory is applicable, i.e. the blocks are of a small size. There are, however, cases when dynamic scattering is observed. Cases of scattering intermediate between the kinematic and the dynamic are also of interest; these so far have not been explained.

In solving the problem for the general case of the specimen consisting of blocks having any (various)

thickness, in the first place the integral intensity of reflexion by a single crystal is calculated. Subsequently, the structure of the specimen is taken into consideration; it is described by introducing the function of crystal distribution among angles $f(\alpha)$, as well as the function of their distribution according to their dimensions $p(A)$. A concrete consideration of the form $f(\alpha)$ for specimens of different types (mosaic monocrystals, textures, polycrystals) leads to the introduction into the intensity formulae of L, a factor analogous to the Lorentz factor in X-ray analysis. The form of this factor L has been previously found by the author. The final formula includes also the function $p(A)$. If all the crystals (blocks) in the specimen are small, the general formula is reduced to a purely kinematic case, and the squares of structure factors enter into it. If the size of all the blocks exceeds the critical one, formulae of the dynamic theory are obtained, into which the structure factor enters in the first power. A general case may be also described, when the distribution function $p(A)$ is such that the specimen contains blocks the dimensions of which are both greater and smaller than the critical size. The intensity of reflexion from such specimens can be described in sufficient approximation by a formula comprising both the first and the second power of the structure factor.

For the sake of comparison with experiment, precision data of Lennander, a Swedish author, have been used. He measured the intensities of electron scattering from polycrystalline specimens of aluminium, silver and gold. From the line profiles characteristic of each specimen the function $p(A)$ has been obtained, followed by a calculation of the intensities. The values obtained are in good agreement with the experimental ones. In particular, an explanation of the deviations from the kinematic law f^2 for gold and silver is explained. The scattering in aluminium is practically completely kinematic, which fact is quite natural since aluminium is the lightest of the elements investigated.

S2·14. G. Honjo & S. Miyake. *Electron-diffraction structure analysis of some inorganic substances.*

Two examples of the electron-diffraction structure analysis performed in Japan will be reported. One is the study of cubic ice by Honjo & Shimaoka and the other is the study of nickel carbide by Nagakura. These are the cases where the electron-diffraction method is especially advantageous, since the light atoms (H and C) contribute very considerably to the diffraction intensity, the structures are fairly simple and their samples for X-ray and neutron diffraction studies are very difficult to prepare.

(i) *Cubic ice*

Debye patterns of no preferred orientation were obtained from cubic ice prepared by condensing water vapour on thin collodion films at $-150°$ C. by means of a low-temperature specimen method and were photographed by a s^1-sector camera. The radial distribution and two-dimensional Fourier analyses of the patterns showed that there are two half hydrogens on each O–O bond (2·75 Å) at positions of about 1 Å, indicating the fact that Pauling's half hydrogen model is valid also in the low-temperature modification of ice.

(ii) *Nickel carbide*

Debye patterns and single crystalline patterns were observed for nickel carbide (Ni_3C) prepared by carburizing evaporated nickel films. The patterns showed reflexions due to a lattice which is a superlattice ($a = \sqrt{3}.a_h$, $c = 3c_h$) of the hexagonal lattice ($a_h = 2{\cdot}464$, $c_h = 4{\cdot}329$ Å) proposed for this substance by Jacobson & Westgren from X-ray study. The two-dimensional Fourier analysis of the diffraction data from the Debye patterns showed that carbon atoms occupy regularly one third of the octahedral interstices of nickel atoms. The structure can be represented by a scheme,

$$A(C_A)B(C_B)A(C_C)B(C_A)A(C_B)B(C_C)A\ldots,$$

where A and B mean hexagonal layers of nickel atoms stacked with the hexagonal sequence and C_A, C_B and C_C hexagonal layers of carbon atoms stacked with the rhombohedral sequence. In this study a method to eliminate the primary extinction effect in the diffraction intensity on the basis of Wilson's intensity statistics was utilized. This method can be applied in general in electron-diffraction structure analysis.

S2·15. S. Ogawa & D. Watanabe. *The structure analysis of the ordered alloys with long period.*

According to the electron-diffraction work so far carried out in our laboratory, ordered alloys such as CuAu(II), Cu_3Pt, Ag_3Mg and Cu_3Pd have superlattices consisting of anti-phase domains of definite size in a stable state. For example, CuAu(II) has a one-dimensional anti-phase domain structure characterized by the first kind of out-of-step, while Cu_3Pd has a two-dimensional anti-phase domain structure characterized by combination of the first kind and the second kind of out-of-step.

In the present work the ordered alloy Au_3Mn was studied in thin evaporated films. Well oriented films were formed by the usual method and, after thermal treatments, examined by electron diffraction. From fine splits of normal reflexions the fundamental lattice was known to be orthorhombic, while from marked splits of superlattice reflexions an anti-phase domain structure of a new type was deduced to occur in the alloy. It is a two-dimensional one in which the first kind of out-of-step occurs with different periods along the x and y direction. In some cases the periods were $1{\cdot}2a_1$ and $2{\cdot}2a_2$ respectively, where $a_1 = 4{\cdot}08$ Å, $a_2 = 4{\cdot}05$ Å and $a_3 = 4{\cdot}03$ Å are the lattice constants of the fundamental lattice. This anti-phase domain structure belongs to the space group *Pnnm*.

In order to obtain more information about the origin of satellites around normal reflexions which were observed also in the case of CuAu(II) as well as Cu_3Pd and were deduced to occur from lattice modulations with periods of out-of-steps, the Fourier analysis was carried out. From this analysis the amount of a periodic change of the atomic distance along the x direction was estimated, which change caused one of the two kinds of the satellites to be formed. A lattice modulation along the y direction causing the other kind of satellites to be formed may consist not only of a periodic change of the atomic distance but also of a periodic change of the scattering factor.

*S*2·16. M. Blackman & E. Grunbaum. *Electron-diffraction patterns from cobalt.*

The diffraction patterns from an unmagnetized single crystal of hexagonal cobalt show, under certain circumstances, an abnormal character due to the magnetic leakage field at the surface of the crystal. This field is associated with the arrangement of the magnetic domains; it is particularly marked in cobalt at ordinary temperatures owing to the high magnetic anisotropy and to the fact that the hexagonal axis is the axis of easy magnetization.

A single crystal of cobalt, cut to the prism face and electrolytically polished, produces a diffraction pattern consisting of spiral-like curves when an electron beam, of normal width at the specimen level, is directed along the hexagonal axis. The centres of gravity of these spirals form the hexagonal array expected from the crystal structure. Patterns taken with the beam perpendicular to the hexagonal axis do not show any such abnormality.

If the primary beam is limited by apertures of diameter 50–12μ, the spirals are replaced by a system of arcs. These are displaced from, and are concave towards, the position where an electron-diffraction spot would have been expected. When the aperture is moved parallel to the edge of the crystal a continuous rotation of the arcs is observed, these describing almost closed curves. The spirals observed with the unrestricted beam are superpositions of such arcs.

A fairly detailed study has been made of the features of the magnetic field, using a fine electron beam as a probe. From these and other observations, it has been possible to form a picture of the form of the magnetic field which allows the above, and other observations, to be explained.

In general no diffraction patterns were observed when an electrolytically polished hexagonal face was studied. It appears that the local magnetic fields, associated with the randomly arranged secondary domains on the hexagonal face, are sufficiently strong and so arranged as to blur the diffraction pattern completely. Patterns are, however, obtained when the crystal is heated to about 250° C. Probe measurements have established that the surface magnetic fields decrease rapidly with temperature. This is associated with the approach to magnetic isotropy, which is found to occur in hexagonal cobalt when the temperature is raised towards 250° C.

*S*2·17. O. Bastiansen. *Recent advances in electron-diffraction gas work in Norway.*

New improvements in the electron-diffraction sector method for gas work have justified re-investigations of substances earlier studied. One of the substances that naturally suggests itself is benzene, not primarily because of its attractive structure but first of all because it appears to be a well suited test compound for the method. If the hexagonal structure is assumed for the benzene molecule, there are only two structure parameters to be determined, namely the C–H and the C–C bond distances. In the radial distribution curve of benzene three C–C and four C–H peaks should be expected. Theoretically three H–H distances should also exist, though their real appearance in an experimental distribution curve seems from chemical experiences rather doubtful. In any case the electron-diffraction radial distribution curve should support us with at least seven single distances, i.e. at least seven equations for the determination of the two unknowns. We should, therefore, in this way obtain a highly over-determined system of equations, which should provide us with an excellent possibility to test the self-consistency of the method.

The essential improvements consist first of all in a considerable enlargement of the measurable diffraction angles. In favourable cases reproducible intensity data are obtained up to $s = 60$ Å^{-1} ($s = 4\pi/\lambda \sin\theta$, θ being half the diffraction angle). The classical range of the sector method ended at about $s = 25$ Å^{-1}. Beside this, considerable improvements have been made also by increasing the accuracy of the intensity measurements in the classical s range. These improvements have been possible by a careful construction of the diffraction unit. Particular care has been taken to avoid extraneous scattering from the pinhole system. The gas nozzle and the sector were constructed with high precision, and the liquid-air trap was made as efficient as possible to avoid gas spread all over the apparatus.

A critical test of cleanness of the exposed plates is the fitting in of the theoretical background. Practice shows that it is extremely difficult to get the theoretical background to fit to the observed intensity curve for the whole s range of the plate. In the case of benzene, and also for other hydrocarbons, we have been able to get the observed and corrected intensity curve to follow the background very nicely. However, to be able to do this we have to abandon the zero line determined by the photometer readings and adopt a new zero line. This procedure does not seem to work satisfactorily for substances containing heavier atoms, as for instance bromine. This is probably not due to extraneous scattering but is perhaps more naturally explained by a kind of 'shadow effect'.

Two independent sets of diagrams of benzene have been studied to get information concerning the self-consistency and reproducibility of the method. The C–C distance found to be 1·397 Å is reproduced better than 0·001 Å. The C–C bond-distance values obtained from the various peaks differ on the average by less than 0·05% from the mean value. High accuracy is also obtained in the C–H bond-distance determination, though the C–H bond distance is for obvious reasons less accurate than the corresponding C–C distance.

A study of the outer part of the radial distribution curve shows that H–H peaks can be identified and reproduced. The H_1–H_3 and H_1–H_4 distances can be measured. The H_1–H_2 distance, however, is too close to the C_1–C_3 distance to leave any hope of being observed.

The areas under the peaks have also been measured and compared with the theoretical values. These values also are reproducible and check well with theory.

Finally, measurements of the root-mean-square deviations from the most probable value for the various distances have been calculated; also these values are satisfactorily reproduced. Attempts are being made to calculate these values from the spectroscopically observed vibration for comparison with electron-diffraction data.

*S*2·18. B. M. Siegel, C. C. Peterson & M. Cohen. *An electron-diffraction camera for studies in ultra-high vacua.*

An electron-diffraction camera has been developed which makes possible the study of 'clean' surfaces free

of adsorbed gases. The glass column containing the specimen, electron gun, apertures and fluorescent screen can be baked out and evacuated to the 1×10^{-9} mm. of Hg range. The accelerating voltages employed are 40–60 kV. There are two removable magnetic lenses external to the column: the first is a short-focal-length lens used to produce a reduced image of the source; the second lens, placed just before the specimen, focuses the beam on the final screen. The diffraction pattern is recorded by photographing the fluorescent screen. The various factors determining the performance of the instrument will be discussed.

Specimen chambers are designed for observation by both transmission and reflection diffraction. Thin films can be deposited by evaporation techniques in the camera under ultra-high vacuum conditions. Carefully controlled atmospheres can be admitted to the specimen chamber and the specimen can be subjected to surface reactions over a range of temperatures. The present applications and potentialities of this apparatus will be discussed.

S2·19. K. Tanaka & H. Hashimoto. *Electron microscopic and diffraction photographs taken at temperatures between 700 and 2000° C.*

In order to observe the phenomena which occur at the surface of a specimen at a high temperature above 1000° C., we designed a new type of specimen holder attached to our universal electron-diffraction microscope and, as an example, a continuous variation of the structure of the surface of a tungsten filament at 700 ~ 2300° C. was observed.

One of the most difficult points of the experiment at such high temperature is to protect the photographic plate against the light which comes from the specimen. For this purpose, we set the specimen in the chamber of our microscope so that the light was screened by a small aperture in the lens and only the electron beam was allowed to pass. In this case, as the specimen has to be set near the objective lens, precautions for protecting the lens from heating and contamination caused by the high temperature were taken.

We will show the mechanism of the device and some photographs taken at such high temperatures.

S2·20. J. Kakinoki, T. Ino & K. Katada. *Refinements of the radial distribution method.*

(1) How small should we make the spacing Δs when we perform the numerical integration? When we calculate the radial distribution function

$$rD(r)=\frac{1}{2\pi^2}\int_0^\infty sI(s)\sin sr\,ds\,,$$

we usually approximate the integral by a summation. If we can estimate the non-zero region R_0 beyond which $D(r)$ is practically zero, the interval Δs should be so chosen as to satisfy the condition

$$\Delta s<\pi/R_0\quad\text{or}\quad \Delta q<10/R_0\quad(q=(10/\pi)s)\,. \tag{1}$$

(2) How to treat the unknown intensity in the region of small angles? In the region of the small scattering angle, for example, less than $s_0\fallingdotseq 3$ Å^{-1}, the scattering intensity is not available or not observable. This unknown part of the intensity curve is expanded as

$$sI(s)=\sqrt{\frac{\pi}{2}}\cdot\sum_{k=0}^{\infty}(-1)^k a_{2k+1}P_{2k+1}(x)\,,\quad x=\frac{s}{s_0}\,, \tag{2}$$

where P_{2k+1} is the Legendre polynomial of the $(2k+1)$th order. When the intensity curve in the region $0<s<s_0$ is not so much complicated that it can be practically expanded by several terms, the coefficient of each term may be determined by several relations which are obtained by the values of the derivatives at $s=0$ and $s=s_0$ of the intensity curve and by those at $r=0$ of the uncorrected radial distribution function as

$$rD(r)=\frac{1}{2\pi^2}\int_{s_0}^{\infty}sI(s)\sin sr\,dr\,. \tag{3}$$

(3) How to correct the error due to the different behaviours of the atomic scattering factors of different atoms? The following function $M^{(ij)}(s)$ for each pair (ij)

$$M^{(ij)}(s)=\left\{\left(1-\frac{f_i}{Z_i}\right)\left(1-\frac{f_j}{Z_j}\right)\frac{\sum_i Z_i^2}{\sum_i (Z_i-f_i)^2}-1\right\}\exp\left[-as^2\right] \tag{4}$$

may be approximated as

$$M^{(ij)}(s)=\sum_{k=1}A_k^{(ij)}\exp\left[-h_k^{(ij)}s^2\right]\,. \tag{5}$$

With these $A_k^{(ij)}$ and $h_k^{(ij)}$, the radial distribution function corresponding to each pair, $rD^{(ij)}(r)$, can be expressed as

$$rD^{(ij)}(r)=\frac{1}{8\pi^{\frac{3}{2}}}\frac{Z_iZ_j}{r_{ij}\sum_i Z_i^2}\left\{\frac{1}{\sqrt{(a+\frac{1}{2}\Delta_{ij})}}\exp\left[-\frac{(r-r_{ij})^2}{2(2a+\Delta_{ij}^2)}\right]\right.$$
$$\left.+\sum_{k=1}\frac{A_k^{(ij)}}{\sqrt{(h_k^{(ij)}+\frac{1}{2}\Delta_{ij}^2)}}\exp\left[-\frac{(r-r_{ij})^2}{2(2h_k^{(ij)}+\Delta_{ij}^2)}\right]\right\}, \tag{6}$$

where Δ_{ij}^2 is the mean square deviation for each pair and the terms containing $(r+r_{ij})$ are omitted.

(4) How to decompose the peaks on the radial distribution curve into the components? When a peak on the radial distribution curve consists of two or three peaks, unknown two or three sets of r_{ij} and Δ_{ij} can be solved from a simultaneous equation of μ_n's, where

$$\mu_n=\int_{-\infty}^{\infty}r^n rD(r)\,dr\,. \tag{7}$$

S2·21. R. Uyeda. *Electron-diffraction techniques for structure determination.*

A survey is given of electron-diffraction techniques which have been developed since World War II. The talk is designed mainly for the general crystallographer but it may be useful for specialists on electron diffraction.

Before the war, electron diffraction and electron microscopy were two separate fields in electron optics. They were, however, unified after the war, resulting in the techniques of selected-area diffraction and high-resolution diffraction. By the former technique, we can obtain diffraction patterns from a crystal as small as 1μ diameter, the shape of which can be observed by electron microscope. By the latter technique, we can determine lattice parameters with an accuracy as high as 1/10,000 and can observe fine structure in diffraction patterns. Very recently, crystal lattices were directly observed by electron microscope and it is our hope that this technique will be of practical use to crystallographers. At the present

stage, all these techniques are restricted to the determination of lattice parameters.

Crystal analysis by electron diffraction is mainly carried out by using Debye–Scherrer rings. The intensity of the rings is usually measured photographically, but a few researchers are developing methods of direct measurement. It is not yet clear which method is the most promising. In the photographical method, the steep variation of intensity, very high near the centre and very low toward the periphery, affects the accuracy of measurement. To flatten the variation, we use diffraction cameras provided with a rotating sector originally developed for electron diffraction by gas. By this technique, accurate crystal analyses are possible provided specimens are adequate. Crystal analysis using single crystals is a technique still in its infancy and we have only a few examples. It may be a subject for ambitious researchers, particularly for crystals which are so small that they need selected-area diffraction.

S2·22. J. J. Trillat. *Étude par diffraction électronique de la nitruration du nickel.*

Par chauffage dans un courant de gaz ammoniac, les atomes d'azote s'insèrent d'abord dans le réseau c.f.c. du nickel et le dilatent considérablement, puis, vers 175° C., le réseau dilaté se transforme en un réseau hexagonal correspondant à la formation d'un composé d'insertion Ni_3N. Ce dernier, chauffé dans le vide, est dédruit et par dénitruration, redonne le nickel ordinaire.

Par bombardement ionique de nickel au moyen d'ions provenant de l'air, des résultats analogues sont obtenus.

Tous ces phénomènes ont été étudiés par diffraction électronique, grâce à des techniques permettant de suivre d'une façon continue les modifications obtenues et d'effectuer le bombardement ionique dans le corps même de l'appareil.

S2·23. A. Laberrigue. *Diffraction des électrons par des monocristaux: influence de la température.*

Des expériences en cours révèlent que le flux des électrons diffractés par un cristal varie avec la température donc avec l'amplitude de l'agitation thermique, non seulement suivant les directions des réflexions sélectives conformes à la loi de Bragg mais suivant toutes les directions.

S2·24. H. Raether. *Elektroneninterferenzen hoher Auflösung.*

Eine Interferenzapparatur hoher Auflösung wird erhalten durch Elektronenstrahlen mit sehr kleinem Durchmesser auf der photographischen Platte. Hierzu gibt es zwei Möglichkeiten: 1. Objekt im nahezu parallelen Strahl. Die Kleinheit des Fleckes wird bedingt durch die Kleinheit des Objektes (Objekt = Blende). 2. Herstellung eines kleinen Fleckdurchmessers durch verkleinernde Abbildung der Elektronenquelle mit Hilfe von Linsen.

Die Grenze der Auflösung ist durch das Korn der photographischen Platte gegeben. Notwendig ist gute Spannungskonstanz, da die Durchmesser der gebeugten Strahlen hierauf besonders empfindlich sind. In den Experimenten wurde einige μ Fleckdurchmesser erreicht (H. Ehlers, *Z. Naturforsch.* (1956), **11***a*, 359).

Die bisherige Hauptanwendung lag in der Untersuchung der Feinstruktur der Reflexe bedingt durch die dynamische Theorie (Interferenzdoppelbrechung) (H. Raether, *Handbuch der Physik*, Bd. 32, S. 485). Im folgenden wird die Anwendung auf Fragen der Messung von Gitterkonstanten behandelt, für die die erste Methode unbrauchbar ist.

1. Änderung der Gitterkonstanten durch thermische Wirkung: Die Verschiebung der Reflexe an Al-Folien (Aufdampfschichten) von verschiedener Temperatur (20° C. und 300° C.) ergibt einen Ausdehnungskoeffizienten von $(27 \pm 0{,}5) \times 10^{-6}$ pro °C. in Übereinstimmung mit den Daten am kompakten Kristall.
2. Für Präzisionsbestimmungen von Gitterkonstanten sind Eichsubstanzen notwendig, die, vor allem in dünner Schicht, durch eine hohe Konstanz der Gitterkonstanten (z. B. unabhängig vom Herstellungsverfahren usw.) charakterisiert sind. Eine Reihe von Substanzen wird auf diese Eignung untersucht (R. E. Meyerhoff, *Z. Naturforsch.* **12***a*, 23 (1957)):

TlCl ist am besten geeignet, (Aufdampfschichten ergeben grosse Kristalle (500 Å)), Gitterkonstante ist unabhängig vom Aufdampfverfahren und auf 0,01% constant. LiF ist ungeeignet, da sowohl aus Lösungen kristallisierte wie aufgedampfte Schichten schwankende Gitterkonstanten (0,1–0,2%) zeigen (bei Aufdampfschichten durch Einbau von W Atomen des Schiffchens bedingt). KCl zeigt eine Gitteraufweitung bis 0,2%, durch Einbau von Fremdatomen verursacht. Al zeigt Schwankungen der Gitterkonstante bis 0,3%, bedingt durch Einbau von Sauerstoff. Ag getempert, liefert Gitterkonstanten, die auf 0,01% konstant sind.